Numerical Analysis of Lithium-ion Battery Thermal Management System Towards Fire Safety Improvement

Author:
Li, Ao

Publication Date:
2023

DOI:
https://doi.org/10.26190/unsworks/25121

Numerical Analysis of Lithium-ion Battery Thermal Management System Towards Fire Safety Improvement

Ao Li

A thesis in fulfilment of the requirements for the degree of

Doctor of Philosophy

School of Mechanical and Manufacturing Engineering

Faculty of Engineering

The University of New South Wales

February 2023

The University of New South Wales

Thesis/Dissertation Sheet

Surname or Family name: **LI**

First name: **AO** Other name/s:

Abbreviation for degree as given in the University calendar: **PHD**

School: **School of Mechanical and Manufacturing Engineering**

Faculty: **Faculty of Engineering**

Title: **Numerical Analysis of Lithium-ion Battery Thermal Management System Towards Fire Safety Improvement**

Abstract

The development of alternative energy sources aims to tackle the energy crisis and climate change. Due to the intermittent nature of renewable energy, energy storage systems find antidotes to the current flaws for ensuring a stable and consistent power supply and reducing our reliance on fossil fuels. Lithium-ion batteries are the most used energy storage unit and have been applied in many fields, such as portable devices, building infrastructure, automotive industries, etc. Nevertheless, there remain significant safety concerns and fire risks. Thus, this has created much interest particularly in developing a comprehensive numerical tool to effectively assess the thermal behaviour and safety performance of battery thermal management systems (BTMs).

In this thesis, a modelling framework was built by integrating the artificial neural network model with the computational fluid dynamics analysis. This includes (i) a comparison of natural ventilation and forced air cooling under various ambient pressures; (ii) an analysis of thermal behaviour and cooling performance with different ambient temperatures and ventilation velocities; and (iii) optimisation of battery pack layout for enhancing the cooling efficiency and reducing the risks of thermal runaway and fire outbreak. The optimal battery design achieved a 1.9% decrease in maximum temperature and a 4.5% drop in temperature difference. Moreover, this thesis delivered an overall review of BTMs employing machine learning (ML) techniques and the application of various ML models in battery fire diagnosis and early warning, which brings new insights into BTMs design and anticipates further smart battery systems. In addition, the battery thermal propagation effect under various abnormal heat generation locations was demonstrated to investigate several stipulating thermal propagation scenarios for enhancing battery thermal performances. The results indicated that various abnormal heat locations disperse heat to the surrounding coolant and other cells, affecting the cooling performance of the battery pack.

The feasibility of compiling all pertinent information, including battery parameters and operation conditions, was studied in this thesis since ML models can build non-related factors relationships. The integrated numerical model offers a promising and efficient tool for simultaneously optimising multiple factors in battery design and facilitates a constructive understanding of battery performance and potential risks.

Originality Statement

DECLARATIONS

ORIGINALITY STATEMENT

☑ I hereby declare that this submission is my own work and to the best of my knowledge it contains no materials previously published or written by another person, or substantial proportions of material which have been accepted for the award of any other degree or diploma at UNSW or any other educational institution, except where due acknowledgement is made in the thesis. Any contribution made to the research by others, with whom I have worked at UNSW or elsewhere, is explicitly acknowledged in the thesis. I also declare that the intellectual content of this thesis is the product of my own work, except to the extent that assistance from others in the project's design and conception or in style, presentation and linguistic expression is acknowledged.

COPYRIGHT STATEMENT

AUTHENTICITY STATEMENT

☑ I certify that the Library deposit digital copy is a direct equivalent of the final officially approved version of my thesis.

Copyright Statement

PUBLICATIONS STATEMENT

UNSW is supportive of candidates publishing their research results during their candidature as detailed in the UNSW Thesis Examination Procedure.

Publications can be used in the candidate's thesis in lieu of a Chapter provided:

- The candidate contributed **greater than 50%** of the content in the publication and are the "primary author", i.e. they were responsible primarily for the planning, execution and preparation of the work for publication.
- The candidate has obtained approval to include the publication in their thesis in lieu of a Chapter from their Supervisor and Postgraduate Coordinator.
- The publication is not subject to any obligations or contractual agreements with a third party that would constrain its inclusion in the thesis.

☑ The candidate has declared that **some of the work described in their thesis has been published and has been documented in the relevant Chapters with acknowledgement**.

A short statement on where this work appears in the thesis and how this work is acknowledged within chapter/s:

> Chapter 2 includes the contents from two published journal articles: Li, A., Yuen, A. C. Y., Wang, W., De Cachinho Cordeiro, I. M., Wang, C., Chen, T. B. Y., Zhang, J., Chan, Q. N., & Yeoh, G. H. (2021) "A Review on Lithium-Ion Battery Separators towards Enhanced Safety Performances and Modelling Approaches," Molecules, 26(2), 478. and Li, A., Weng, J., Yuen, A. C. Y., Wang, W., Liu, H., Lee, E. W. M., Wang, J., Kook, S., & Yeoh, G. H. (2023) "Machine Learning Assisted Advanced Battery Thermal Management System: A State-of-the-art Review," Journal of Energy Storage, 60, 106688. with modifications and reorders to better fit the structure of this thesis.
> Chapter 4 includes the contents from a published journal article: Li, A., Yuen, A. C. Y., Wang, W., Weng, J., & Yeoh, G. H. (2022). Numerical investigation on the thermal management of lithium-ion battery system and cooling effect optimisation. Applied Thermal Engineering, 215, 118966. with modifications and reorders to better fit the structure of this thesis.
> Chapter 5 includes the contents from a published journal article: Li, A., Yuen, A. C. Y., Wang, W., Chen, T. B. Y., Lai, C. S., Yang, W., Wu, W., Chan, Q. N., Kook, S. & Yeoh, G. H. (2022). Integration of Computational Fluid Dynamics and Artificial Neural Network for Optimization Design of Battery Thermal Management System. Batteries, 8(7), 69. with modifications and reorders to better fit the structure of this thesis.
> Chapter 6 includes the contents from a published journal article: Li, A., Yuen, A. C. Y., Wang, W., Weng, J., Lai, C. S., Kook, S. & Yeoh, G. H. (2022). Thermal Propagation Modelling of Abnormal Heat Generation in Various Battery Cell Locations. Batteries, 8(11), 216. with modifications and reorders to better fit the structure of this thesis.

Candidate's Declaration

I declare that I have complied with the Thesis Examination Procedure.

Abstract

The development of alternative energy sources aims to tackle the energy crisis and climate change. Due to the intermittent nature of renewable energy, energy storage systems find antidotes to the current flaws for ensuring a stable and consistent power supply and reducing our reliance on fossil fuels. Lithium-ion batteries are the most used energy storage unit and have been applied in many fields, such as portable devices, building infrastructure, automotive industries, etc. Nevertheless, there remain significant safety concerns and fire risks. Thus, this has created much interest particularly in developing a comprehensive numerical tool to effectively assess the thermal behaviour and safety performance of battery thermal management systems (BTMs).

In this thesis, a modelling framework was built by integrating the artificial neural network model with the computational fluid dynamics analysis. This includes (i) a comparison of natural ventilation and forced air cooling under various ambient pressures; (ii) an analysis of thermal behaviour and cooling performance with different ambient temperatures and ventilation velocities; and (iii) optimisation of battery pack layout for enhancing the cooling efficiency and reducing the risks of thermal runaway and fire outbreak. The optimal battery design achieved a 1.9% decrease in maximum temperature and a 4.5% drop in temperature difference. Moreover, this thesis delivered an overall review of BTMs employing machine learning (ML) techniques and the application of various ML models

in battery fire diagnosis and early warning, which brings new insights into BTMs design and anticipates further smart battery systems. In addition, the battery thermal propagation effect under various abnormal heat generation locations was demonstrated to investigate several stipulating thermal propagation scenarios for enhancing battery thermal performances. The results indicated that various abnormal heat locations disperse heat to the surrounding coolant and other cells, affecting the cooling performance of the battery pack.

The feasibility of compiling all pertinent information, including battery parameters and operation conditions, was studied in this thesis since ML models can build non-related factors relationships. The integrated numerical model offers a promising and efficient tool for simultaneously optimising multiple factors in battery design and facilitates a constructive understanding of battery performance and potential risks.

Acknowledgement

Standing at this particular point and looking back to the past four years of PhD journey, my most profound feeling is gratitude beyond description. Since I have met these excellent people who continuously guided, accompanied, and conformed me to overcome innumerable hurdles throughout my PhD candidature, I would like to express my sincere gratitude to them for their valuable advice and endless support.

First and foremost, the most heartfelt thanks go to my supervisors, Prof. Guan Heng Yeoh, Dr Anthony Chun Yin Yuen, and Dr Wei Wang, for their devoted guidance and immeasurable support. Thank you, Guan, you have completely changed my life. Thank you for being willing to be my PhD supervisor and mentoring me for my whole PhD life. Thank you for dedicating enormous insightful suggestions that inspired my way of thinking and solving problems. Your scrupulous care made me feel confident and stressless so that I could go beyond myself. Your top-up scholarship made my life easier and provided me with the opportunity to devote my time to this research fully. What I learnt from your innovative comments and inspirations will be a precious treasure for the rest of my career and life. Thank you, Anthony, for your patience, time and constructive academic advice. Thank you for always helping me tackle those tedious numerical issues and keeping me on the right track. Thank you for introducing me to the multi-sports team,

which built my healthy body and released my study pressure. Your professional experience and knowledge helped me complete this PhD journey steadily and gradually. Also, thank you, Wei, for your selfless sharing of your knowledge and ideas, which encouraged me to achieve fruitful research.

Great gratitude also goes to my academic panels, A/Prof. Chris Menictas, Prof. Zhongxiao Peng and Dr Shaun Chan. Your constructive advice amended lots of my research gaps.

I am very thankful for many senior academics, Dr Wei Yang and Dr Imrana Kabir, and PhD colleagues from the ARC Training Centre for Fire Retardant Material and Safety Technologies – Dr Cheng Wang, Dr Timothy Bo Yuan Chen, Dr Ruifeng Cao, Dr Hengrui Liu, Dr Bo Lin, Luzhe Liu, Ivan Miguel De Cachinho Cordeiro, Sarah, Preety and Enzo. Thank you all for your generous support and company during the long hours at the office. Special thanks to Prof. Richard Yuen and Prof. Eric Lee from the City University of Hong Kong for their guidance and for sharing their knowledge on machine learning and fire safety science.

I would also thank the Australian Government for providing financial support for my PhD. This research has been supported by an Australian Government Research Training Program (RTP) Scholarship.

A special thank you goes to my wife, Dr Xu Wang. Thank you for entering my life and staying by my side. Thank you for your caring and encouragement when I felt pressured in the research and daily life.

Acknowledgement

Finally, I would like to express my enormous gratitude to my parents and my parents-in-law. Your unconditional love and support make me the happiest person on earth. You are the reasons that keep me persevering. I hope this thesis could let you feel proud.

Table of Content

DECLARATIONS **5**

PUBLICATIONS STATEMENT **7**

Abstract ..... **I**

Acknowledgement ..... **III**

Table of Content ..... **VI**

List of Figures ..... **IX**

List of Tables ..... **XIV**

List of Publications ..... **XV**

List of Abbreviations ..... **XIX**

List of Symbols ..... **XXI**

Chapter 1 Introduction **1**

1.1 General Background 1

1.2 Aim and Scope 7

1.3 Thesis Outline 10

Chapter 2 Literature Review **13**

2.1 General Description 13

2.2 Introduction 15

2.2.1 Overview of battery research 15

2.2.2 Numerical techniques and research gap 17

2.2.3 Contribution and structure 19

2.3 LIB Numerical Model 21

2.3.1 Battery cell models 22

2.3.2 Battery module and pack models 24

2.3.3 Other models 25

2.4 Machine Learning Overview 26

2.4.1 Artificial neural network (ANN) 28

2.4.2 Deep learning (DL) 31
2.4.3 Other machine learning methods 34
2.5 Machine Learning and Battery Thermal Management 36
2.5.1 Heat generation and temperature prediction/Thermal data prediction 37
2.5.2 System optimisation with machine learning 41
2.6 Battery Safety and Machine Learning 48
2.6.1 Battery safety 49
2.6.2 Hazard prediction 54
2.6.3 Hazard mitigation and safety control 60
2.7 Chapter Summary 62
Chapter 3 Methodology 65
3.1 General Description 65
3.2 CFD Model 66
3.2.1 Electrochemical battery model 70
3.2.2 Thermal battery model 75
3.3 ANN Model 79
3.4 Chapter Summary 86
Chapter 4 Lithium-ion Battery Thermal Management Systems and Cooling Systems 87
4.1 General Description 87
4.2 Introduction 88
4.3 Results and Discussions 93
4.3.1 Thermo-electrochemical model setups 93
4.3.2 Model validation 96
4.3.3 Simulation results under various pressure conditions 99
4.3.4 Simulation results under various air cooling directions 103
4.3.5 Optimum results coupled MLP model 108
4.4 Chapter Summary 116
Chapter 5 Coupling ANN with CFD for Optimisation Design of Battery Thermal Management Systems 118
5.1 General Description 118
5.2 Introduction 119

Table of Content

5.3 Results and Discussions 124
5.3.1 Numerical simulation results 125
5.3.2 Training and results analysis 134
5.3.3 Optimisation analysis and discussions 138
5.3.4 Verification of the optimal spacing combination 141
5.4 Chapter Summary 142
Chapter 6 Thermal Propagation Modelling of Abnormal Heat Generation in Various Battery Cell Locations 144
6.1 General Description 144
6.2 Introduction 145
6.3 Model Configuration 150
6.3.1 Model description 150
6.3.2 Model verification and validation 152
6.4 Results and Discussions 157
6.4.1 Applied extreme heat to the model 157
6.4.2 Different abnormal heat generation locations 162
6.4.3 Further discussions 170
6.5 Chapter Summary 170
Chapter 7 Conclusions and Future Works 172
7.1 Conclusions 172
7.2 Suggestions for Future Works 176
References 179

List of Figures

Figure 1.1 Tesla Model S crashed and started a fire in Australia [7]; (b) - (d) FM Global battery-related losses from 2000-2019 [8]: (b) Overall details of numbers, (c) Percentage distribution for number of loss, (d) Percentage distribution for total gross. 3

Figure 1.2 The framework of this thesis. 9

Figure 2.1 Domino effect of battery TR and the corresponding temperature profile along different stages. 16

Figure 2.2 LIB battery types and numerical models. 22

Figure 2.3 The synthetic route of DMOP. 27

Figure 2.4 Major types of ML techniques [119]. 27

Figure 2.5 The soft margin loss setting for a linear SVM [123]. 31

Figure 2.6 Relationship among AI, ML and DL [124]. 32

Figure 2.7 The architecture of a typical vanilla LSTM block [125]. 33

Figure 2.8 Publication amount trend of ML applied in battery in recent years. 36

Figure 2.9 Schematic figures of the ANN model structure [142] (a) single hidden later NN, (b) deep hidden layer NN. 38

Figure 2.10 (a) the developed modelling strategy for creating the dataset of CPCMs, (b) two CPCM samples with their cross-section images and time evolution of surface

temperature [145]. 40

Figure 2.11 (a) 3 D and (b) 2 D diagrams of the BTMs, (c) computational domain of the conjugate problem, (d) MBP 1, (e) MBP 2, and (f) MBP 3 [150]. 42

Figure 2.12 Section views of (a) serpentine tube cold plate (STCP) and (b) mini channel cold plate (MCCP) [81]. 43

Figure 2.13 Illustration of the GP process [153]. 45

Figure 2.14 Diagram of (a) LC-based BTMs (b) mini-channel-based cooling plate, (c) proposed NN model [156]. 47

Figure 2.15 (a) Accidents related to LIB failure and correlated abuse conditions [61]; (b) Thermal digraph of a reaction and heat loss from a vessel at three ambient temperatures, where B is at the critical temperature [174]. 50

Figure 2.16 Flowchart of the Data-Driven Safety Envelope Using ML Algorithm [176]. 53

Figure 2.17 Record-keeping the related data of LIB for data-driven prediction and physical interpretations [179]. 55

Figure 2.18 Schematic diagram explaining artificial neural network enhanced by likelihood mapping approach [180]. 56

Figure 2.19 Configuration of the proposed battery TR prognosis method based on the CNN-LSTM [184]. 58

Figure 2.20 TR states of LIB pack and correlated mitigation strategies [186]. 61

Figure 2.21 Summary of ML techniques potential applications. 63

List of Figures

Figure 3.1 The principle of operation for a typical LIB and its structure. 72

Figure 3.2 Configuration of the applied thermal model for a cylindrical LIB..... 76

Figure 3.3 Coupling between the cell and thermal model. 79

Figure 3.4 A typical multilayer perceptron neural network architecture. 81

Figure 3.5 Neural network training procedure. 83

Figure 3.6 The flowchart of MLP optimisation algorithm. 85

Figure 4.1 Schematic of the proposed approach with coupling thermo-electrochemical model and ANN model..... 92

Figure 4.2 Schematic of the LIB pack configuration. 95

Figure 4.3 Comparison results of working voltage during 1C discharge under natural convection conditions..... 98

Figure 4.4 (a) Temperature contour of battery cell with velocity streamline at t=1500s; (b) Temperature contour of the whole flow domain. 99

Figure 4.5 Comparison results of maximum temperature and temperature difference under various operation conditions. 101

Figure 4.6 Maximum temperature and temperature difference plots of 63 cases. 103

Figure 4.7 Simulation results of temperature distribution contour and temperature gradient streamline for natural ventilation (a) & (c) and forced air cooling (b) & (d). 104

Figure 4.8 Comparison results of maximum temperature and temperature difference for natural ventilation (a) & (c) and forced air cooling (b) & (d). 105

Figure 4.9 Comparison results of maximum temperature and temperature difference under

different ambient pressures for natural ventilation (a) & (c) and forced air cooling (b) & (d). 108

Figure 4.10 (a) Error histogram of the ANN model; (b-e) Regression analysis of the ANN model. 111

Figure 4.11 Validation performance of the ANN model. 112

Figure 4.12 Training states of the ANN model. 113

Figure 4.13 Numerical results of various operation parameter combination groups (a) Maximum temperature; (b) Temperature difference. 115

Figure 5.1 Schematic of the proposed CFD-ANN model. 123

Figure 5.2 Comparison of numerical results of (a) working voltage and (b) temperature with experimental results [93] during 1C galvanostatic discharge under natural convection conditions 129

Figure 5.3 Temperature contours of different battery pack configurations. 131

Figure 5.4 The profile of maximum temperature (a, b) and temperature difference (c) under various operation conditions. 134

Figure 5.5 The configuration structure of the proposed ANN model. 137

Figure 5.6 Regression results of ANN model. 137

Figure 5.7 RMS error histogram of the ANN model predictions. 138

Figure 5.8 (a) Maximum temperature and (b) temperature difference of the battery pack for different input combinations 140

Figure 6.1 Schematic picture of the structure of this chapter. 150

List of Figures

Figure 6.2 Schematic figure of the battery pack with 24 18,650 cells. 152

Figure 6.3 Schematic figure of thermocouple testing point. 153

Figure 6.4 (a) Schematic of the computational domain and mesh; (b) Mesh independence analysis. 155

Figure 6.5 (a) Numerical model validation, the error bar is 0.3%; (b) Temperature distribution in the cross-section plane. 157

Figure 6.6 (a) Schematic figure of the battery with a thermal runaway cell; (b) Temperature distribution in the cross-section plane under this scenario. 159

Figure 6.7 The temperature distribution of the different rows' vertical cross-section under C6 conditions, (a) The whole pack; (b) Row 2. 160

Figure 6.8 Comparison between the numerical and experimental data for a temperature change of the neighbouring cell. The error bar is 2.5%. 161

Figure 6.9 Comparison of the temperature distributions among the applied abnormal heat generation on different cells in Row 2. 166

Figure 6.10 Temperature changes of cell 15 among the applied abnormal heat generation on different cells in Row 2. 167

Figure 6.11 Comparison of the temperature distributions among the applied abnormal heat generation on different cells in Row 1. 169

List of Tables

Table 2.1 Summary of the ML applied in the battery thermal management design and thermal data prediction.....47

Table 2.2 Summary of the ML applied in battery fire safety research.....59

Table 4.1 Parameters of the single cell applied in the LIB pack.....94

Table 4.2 Parameter details of the ANN dataset. 109

Table 5.1 Table of mesh independence analysis. 125

Table 5.2 Geometry dimension and electrochemical parameters of the battery cell. ...127

Table 5.3 Details of the inputs and outputs for the ANN model. 135

Table 6.1 Parameters and properties of the battery cell, ventilation fan and outer case. 151

List of Publications

In total, during my PhD candidature, I have published ten journal papers and presented once at a conference. Four journal papers (No. 1 to 3, and 5) are included in this thesis as the main components of some chapters (Chapters 2 to 5).

Journal Publications

1. **A. Li**, J. Weng, A. C. Y. Yuen, W. Wang, H. Liu, E. W. M. Lee, J. Wang, S. Kook, and G. H. Yeoh, "Machine learning assisted advanced battery thermal management system: A state-of-the-art review," *Journal of Energy Storage,* vol. 60, p. 106688, 2023/04/01/ 2023.
2. **A. Li**, A. C. Y. Yuen, W. Wang, J. Weng, and G. H. Yeoh, "Numerical investigation on the thermal management of lithium-ion battery system and cooling effect optimization," *Applied Thermal Engineering,* vol. 215, p. 118966, 2022.
3. **A. Li**, A. C. Y. Yuen, W. Wang, T. B. Y. Chen, C. S. Lai, W. Yang, W. Wu, Q. N. Chan, S. Kook, and G. H. Yeoh, "Integration of Computational Fluid Dynamics and Artificial Neural Network for Optimization Design of Battery Thermal Management System," *Batteries,* vol. 8, no. 7, p. 69, 2022.
4. **A. Li**, A. C. Y. Yuen, W. Wang, J. Weng, C. S. Lai, S. Kook, and G. H. Yeoh, "Thermal Propagation Modelling of Abnormal Heat Generation in Various Battery Cell

Locations," *Batteries,* vol. 8, no. 11, p. 216, 2022.

5. **A. Li**, A. C. Y. Yuen, W. Wang, I. M. De Cachinho Cordeiro, C. Wang, T. B. Y. Chen, J. Zhang, Q. N. Chan, and G. H. Yeoh, "A Review on Lithium-Ion Battery Separators towards Enhanced Safety Performances and Modelling Approaches," *Molecules,* vol. 26, no. 2, p. 478, 2021.

As a co-author:

6. B. Lin, A. C. Y. Yuen, **A. Li**, Y. Zhang, T. B. Y. Chen, B. Yu, E. W. M. Lee, S. Peng, W. Yang, and H.-D. Lu, "MXene/chitosan nanocoating for flexible polyurethane foam towards remarkable fire hazards reductions," *Journal of hazardous materials,* vol. 381, p. 120952, 2020.
7. Y. Han, X. Wang, A. C. Y. Yuen, **A. Li**, L. Guo, G. H. Yeoh, and J. Tu, "Characterization of choking flow behaviors inside steam ejectors based on the ejector refrigeration system," International Journal of Refrigeration, vol. 113, pp. 296-307, 2020.
8. A. C. Y. Yuen, T. B. Y. Chen, **A. Li**, I. M. De Cachinho Cordeiro, L. Liu, H. Liu, A. L. P. Lo, Q. N. Chan, and G. H. Yeoh, "Evaluating the fire risk associated with cladding panels: An overview of fire incidents, policies, and future perspective in fire standards," Fire and Materials, 2021.
9. I. M. D. C. Cordeiro, H. Liu, A. C. Y. Yuen, T. B. Y. Chen, **A. Li**, R. F. Cao, and G. H. Yeoh, "Numerical investigation of expandable graphite suppression on metal-based fire," Heat and Mass Transfer, pp. 1-17, 2021.

10. W. Wang, A. C. Y. Yuen, H. Long, W. Yang, **A. Li**, L. Song, Y. Hu, and G. H. Yeoh, "Random nano-structuring of PVA/MXene membranes for outstanding flammability resistance and electromagnetic interference shielding performances," Composites Part B: Engineering, p. 109174, 2021.
11. A. C. Y. Yuen, T. B. Y. Chen, I. M. D. C. Cordero, H. Liu, **A. Li**, W. Yang, S. C. P. Cheung, Q. N. Chan, S. Kook, and G. H. Yeoh, "Developing a solid decomposition kinetics extraction framework for detailed chemistry pyrolysis and combustion modelling of building polymer composites," Journal of Analytical and Applied Pyrolysis, vol. 163, p. 105500, 2022.
12. H. Li, X. Wang, H. Huang, J. Ning, **A. Li**, and J. Tu, "Numerical study on the effect of superheat on the steam ejector internal flow and entropy generation for MED-TVC desalination system," Desalination, vol. 537, p. 115874, 2022.
13. J. Weng, Q. Huang, X. Li, G. Zhang, D. Ouyang, M. Chen, A. C. Y. Yuen, **A. Li**, E. W. M. Lee, and W. Yang, "Safety Issue on PCM-based Battery Thermal Management: Material Thermal Stability and System Hazard Mitigation," Energy Storage Materials, 2022.
14. W. Wang, A. C. Y. Yuen, Y. Yuan, C. Liao, **A. Li**, I. I. Kabir, Y. Kan, Y. Hu, and G. H. Yeoh, "Nano architectured halloysite nanotubes enable advanced composite separator for safe lithium metal batteries," Chemical Engineering Journal, vol. 451, p. 138496, 2023.

Conference Presentations

1. **A. Li.**, A. C. Y. Yuen, W. Wang and G. H. Yeoh, Numerical investigation of the thermal propagation and cooling effect of a lithium-ion battery system, *The 15th International Conference on Heat Transfer, Fluid Mechanics and Thermodynamics (ATE-HEFAT2021)*, Online, (26-28 July 2021).

List of Abbreviations

AI	Artificial intelligence
ANN	Artificial neural network
BESS	Battery energy storage system
BTMs	Battery thermal management system
CFD	Computational fluid dynamics
CNN	Convolutional neural network
COP	Coefficient of performance
DL	Deep learning
DT	Digital Twin
DEC	Diethyl carbonate
DMC	Dimethyl carbonate
DOD	Depth of discharge
DRL	Deep reinforcement learning
EC	Ethylene carbonate
EV	Electric vehicle
FEM	Finite element method
FF	Feed-forward

List of Abbreviations

LIB	Lithium-ion battery
LM	Levenverg-Marquardt
LSTM	Long short-term memory
ML	Machine learning
MLP	Multi-Layer Perceptron
MSE	Mean square error
NN	Neural network
OVC	Open circuit voltage
SEI	Solid electrolyte interphase
SOC	State of charge
SOH	State of health
SVR	Support vector regression
TR	Thermal runaway
1D	One-dimension(al)
2D	Two-dimension(al)
3D	Three-dimension(al)

List of Symbols

C_p	Heat capacity
d	Dimension number
E	Voltage
e	Errors
F	Faraday's constant
g	Gradient
H	Heat
I	Current
J	Jacobian matrix
J_0	Dimensionless charge exchange current
k	Turbulence kinetic energy
N	Number
Q	Battery capacity
R	Resistance
r	Molar gas constant

List of Symbols

S	Source term
T	Temperature
v	Velocity vector
X	Vector of weights and biases

Greek symbols

α	Scaling factor
β	Learning rate
Γ	Diffusion coefficient
η	Overpotential
κ	Thermal conductivity
μ	Scalar
ξ	Property
ρ	Density
σ	Electric conductivity
τ	Diffusion time constant
φ	Electric potential
ω	Specific dissipation rate

Subscripts

Ech	Electrochemical reaction heat
short	Internal short-circuit heat
abuse	TR reaction heat under thermal abuse conditions
act	Activation overpotential
cell	Battery cell
ohm	Ohmic overpotential
aver	Average
surf	Surface
conc	Concentration
0	Initial state
1C	1C rate, the discharge of the entire battery in 1 hour
h	Number of hidden neurons
s	Number of samples
i	Number of inputs
o	Number of outputs
1D	One-dimension(al)

List of Symbols

2D	Two-dimension(al)
3D	Three-dimension(al)

Chapter 1 Introduction

1.1 General Background

The global energy crisis and climate change have come to a historic turning point, and people have already been influenced by and felt the changes in our daily lives. Net zero and energy security are two sides of the same coin for developing clean-energy innovations. Nowadays, advanced technology can convert nuclear, wind or solar energy into electric energy with cleaner processes and higher efficiency [1], where the energy storage system is an essential component of the energy transition. Lithium-ion battery (LIB) is one of the most commonly used energy storage devices in the current market [2], which Yoshino first proposed in 1985 [3]. LIBs as a source of alternative energy respecting the environment through the use of renewable energies have been proposed in industries for innovative applications. LIBs are the batteries of choice for portable consumer electronic devices, including cell phones, tablets, laptop computers, digital cameras, power tools, and toys, due primarily to their durability, high specific energy (100 to 200 Wh/kg), and ability to operate at reasonably high power [4]. Subsequently, the discovery and development of each battery component have been carried out,

including the positive/negative electrode, the electrolyte, and the separator [5, 6]. Recently, LIBs have begun to enter the automotive market as power packs for electric vehicles (EVs), such as fully EVs, hybrid EVs, plug-in hybrid EVs, mild hybrid EVs, fuel cell EVs, etc. In addition to the high specific energy, the automotive market also benefits from this chemistry's high power, efficiency, and long cycle life capability. As the automotive market drives the expansion of lithium-ion production, these batteries may also enter stationary service as well, facilitating the implementation of renewable energy technologies such as solar and wind.

Nevertheless, although these batteries have become quite common for consumer market applications like cell phones, laptops, or EVs, the widespread use of this technology for emerging markets like electromobility or smart grids requiring stronger energy and power capacities must be examined from a safety point of view. Compared to many other battery technologies, LIB is less thermally stable, and many accidents happened before. For example, Figure 1.1 (a) shows an EV fire incident in Australia [7]. If the cell temperature is increased beyond a certain threshold, a thermal runaway (TR) can occur, resulting in a rapid temperature increase and possibly other related adverse effects such as the release of gas and smoke, fire, and rupture/explosion. Figure 1.1 (b) - (d) shows FM Global client losses involving batteries over a recent 20-year period [8]. The majority of the battery incidents are due to battery fire and mechanical breakdown, and these two issues lead to over third quarters of the total gross. Numerous types of abuse situations can result in an overtemperature inducing a TR, such as over-heating [9-12], over-charged [13], short

circuit [14], and mechanical shock [15]. On the cell level, the TR response during abuse conditions depends on cell chemistry, cell design, size of battery and abuse type. It is vital to alleviate the TR propagation from the single cell to several modules or a complete battery pack to avoid severe consequences. Thus, the temperature of the battery cell itself and the whole ambient environment become a key parameter of battery working and safety performances.

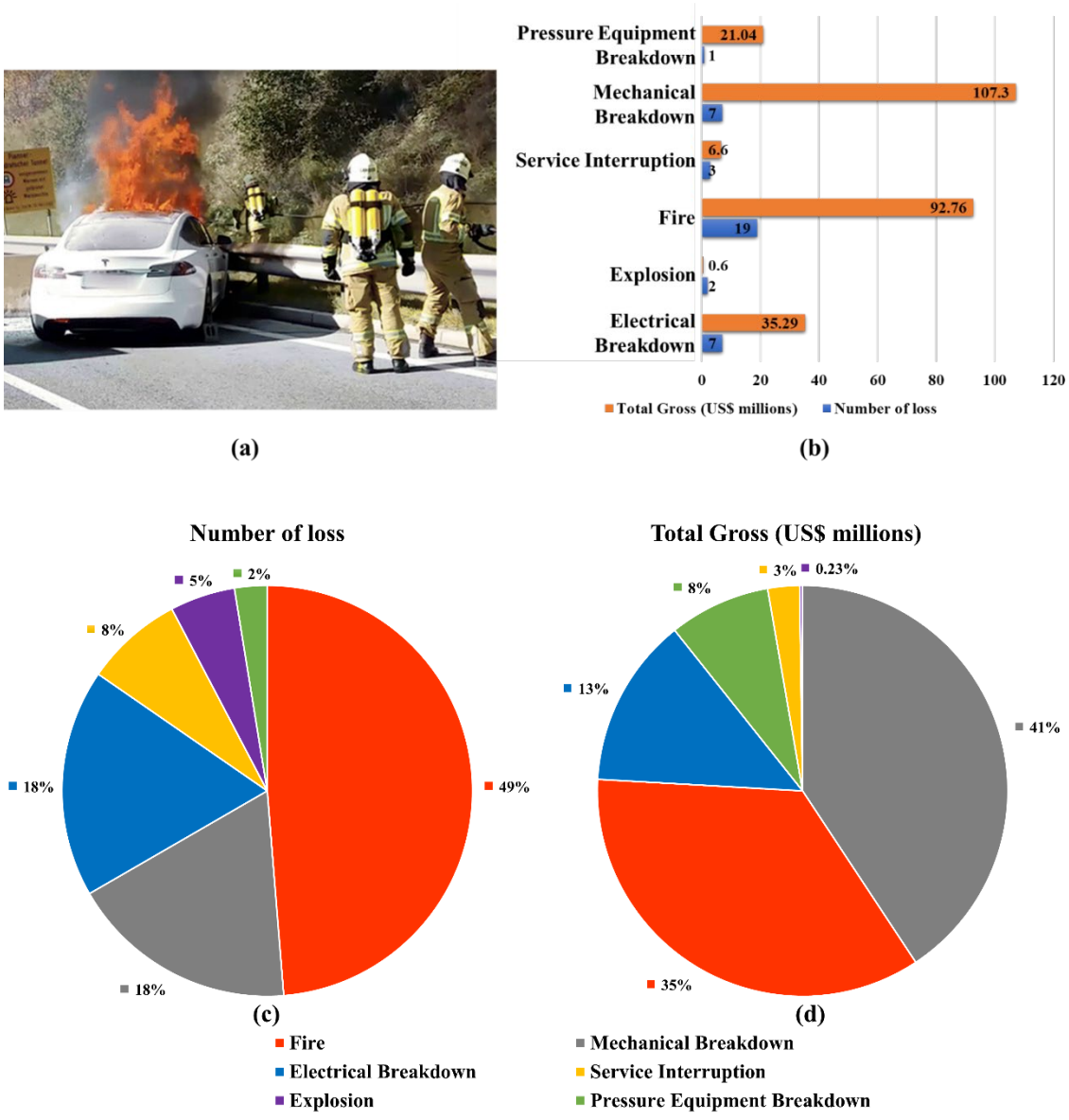

Figure 1.1 Tesla Model S crashed and started a fire in Australia [7]; (b) - (d) FM Global battery-related losses from 2000-2019 [8]: (b) Overall details of numbers, (c) Percentage distribution for number of loss,

(d) Percentage distribution for total gross.

Furthermore, an efficient cooling battery thermal management system (BTMs) is crucial to maintain battery cell temperature within the proper range and to balance the temperature variance among the whole battery system. The previous studies demonstrated two main criteria to evaluate the performance of the BTMs, which are the maximum temperature and the temperature difference. Also, the temperature range between 20℃ and 40℃ maintains the optimal battery performance and prolongs the battery lifespan, and the temperature difference among all the cells controls less than 5℃ [16]. Based on the cooling medium, BTMs are divided into five main types, which are air-based cooling [17-19], liquid-based cooling [20-23], heat pipe-based cooling [24-26], phase change material (PCM)-based cooling [27-32] and hybrid cooling with the combination of the above methods [33-36]. Liquid-based cooling BTMs can be further divided into direct and indirect systems. For the direct type of cooling systems, the whole battery is submerged in the liquid coolant, while in the indirect style, the cooling medium is circulated on the battery cell surfaces via cold plate, heat pipe, etc. PCM-based cooling applies passive strategies for heat dissipation. Based on different types of phase transition (i.e., solid-liquid, liquid-vapour, and solid-vapour) and the material composition, including organic, inorganic, etc., the PCM-based cooling BTMs can be further classified. Air-based cooling BTMs performed many advantages over the other BTMs applied in electric vehicles [37], such as relatively low cost, simple structure, easy maintenance, no

liquid leakage, no additional weight, etc. Therefore, air-based cooling BTMs have been applied in many commercial EVs due to the advantages mentioned above. On the contrary, there are also some shortcomings for air-based cooling BTMs, namely, the low heat capacity of air and the requirement for a massive volumetric flow rate. The optimisation and development of air-based cooling BTMs are still to be carried out to provide EVs with a safer BTMs solution.

Characterising the detailed temperature distribution of the battery cell and the whole fluid domain of the battery system is essential for analysing, optimising and predicting the thermal behaviour, cooling performance and safeness of the battery energy storage system. Additionally, numerical models, especially the computational fluid dynamics (CFD) model, applied mathematical techniques for solving complex thermal problems, have been used in analysing battery thermal performance and fire safety in the recent decades. As a solution to the limitations of battery thermal and fire experiments, numerous models at various length scales have been developed to investigate the internal and external thermal behaviour of battery cell or systems [38-41]. The detailed temperature distribution of both the inside and outside of the battery can be represented by the CFD models efficiently and cost-effectively compared to the experiments. Mainly, it is very competitive in changing different battery properties and operation parameters. On the same note, the development of machine learning techniques has profoundly influenced the engineering system design. For example, the artificial neuron network (ANN) technique is able to learn and adapt to find potential correlations among different

properties, which has been applied in battery optimisation design by evaluating multiple factors simultaneously [42-44]. Furthermore, ANN can also optimise on multi-parameters simultaneously, balancing many factors and providing rational solutions. For optimal battery modelling and thermal safety, many operating parameters and ambient boundary conditions need to be assessed and balanced at the same time. Therefore, it is crucial to investigate the LIB thermal runaway process by accurately monitoring and predicting temperature dynamics during thermal propagation and implementing some effective methods during the LIB fire to improve its fire safety.

Understanding thermal propagation and heat transfer mechanism among battery cell to cell and battery cell to ambient coolant or environment is also crucial for accurately predicting the thermal runaway and optimising the BTMs. The key points that need to be addressed include (i) the heat generation from multiple mechanisms, such as joule heat, polarization heat, reaction heat, and side reaction heat, etc., (ii) the heat exchange of different parts in the battery system due to convection, conduction and radiation from the generated heat, (iii) the different external conditions, such as normal conditions and extreme conditions (e.g., abnormal heat generation, thermal runaway, etc.). Most of the research work relies on the thermal model which predicted the average temperature for a LIB [45] and many experimental studies on the thermal propagation, which are hard to capture more detailed information, have been done [46-48]. These assumptions limit the safety margin of the battery numerical model.

The establishment of the integrated battery thermal system firstly provides a risk assessment methodology stemming from unforeseen thermal hazards; secondly, delivers a solution to capture the critical information from challenging physical environments, even real-time environment changes, for monitoring the performance of the whole system; thirdly, prevents the potential loss of fortune and injury of people from battery fire risk. For the first time, integrate the multi-scale multi-physics model, including CFD and ANN, and study the all-inclusive coupled internal/external phenomena of LIB thermal risks and fires. These contribute to improving the fire resilience of our energy storage system and responding to the energy crisis.

1.2 Aim and Scope

This thesis aims to develop an integrated CFD-ANN framework that simultaneously evaluates and optimises system performance. More specifically, a three-dimensional thermo-electrochemical model to effectively assess the thermal behaviours and detailed temperature distribution of the battery energy storage system. Moreover, the ANN techniques will be coupled with the proposed model. The generated CFD simulation results will be established as a dataset to train the ANN model, and the ANN model will generate a massive number of different combinations with all the parameters staying at a specific range in a short time. Ultimately, this framework will provide an optimised combination by evaluating the multiple operating and ambient conditions. Additionally, the thermal behaviour during the battery working process will be further investigated,

considering both normal working conditions and abnormal heat generation scenarios. The entire framework of this thesis is presented in Figure 1.2.

To address the challenges mentioned above, the following objectives are derived:

(i) To capture and replicate the whole temperature distribution and thermal behaviour during the battery charging/discharging cycles via the proposed thermo-electrochemical model.

(ii) To consider the cooling performance and thermal behaviour under different operating parameters and ambient environment conditions with the proposed model from (i).

(iii) To apply the numerical data from (ii) into an ANN model as a training dataset, generating more scenarios and optimizing the performance with different combinations of all the operating parameters and ambient conditions.

(iv) To investigate the effect of various abnormal heat generation locations on the thermal behaviour and cooling performance of the battery pack. Based on the results of (iii), predict the potential thermal hazards of the battery pack.

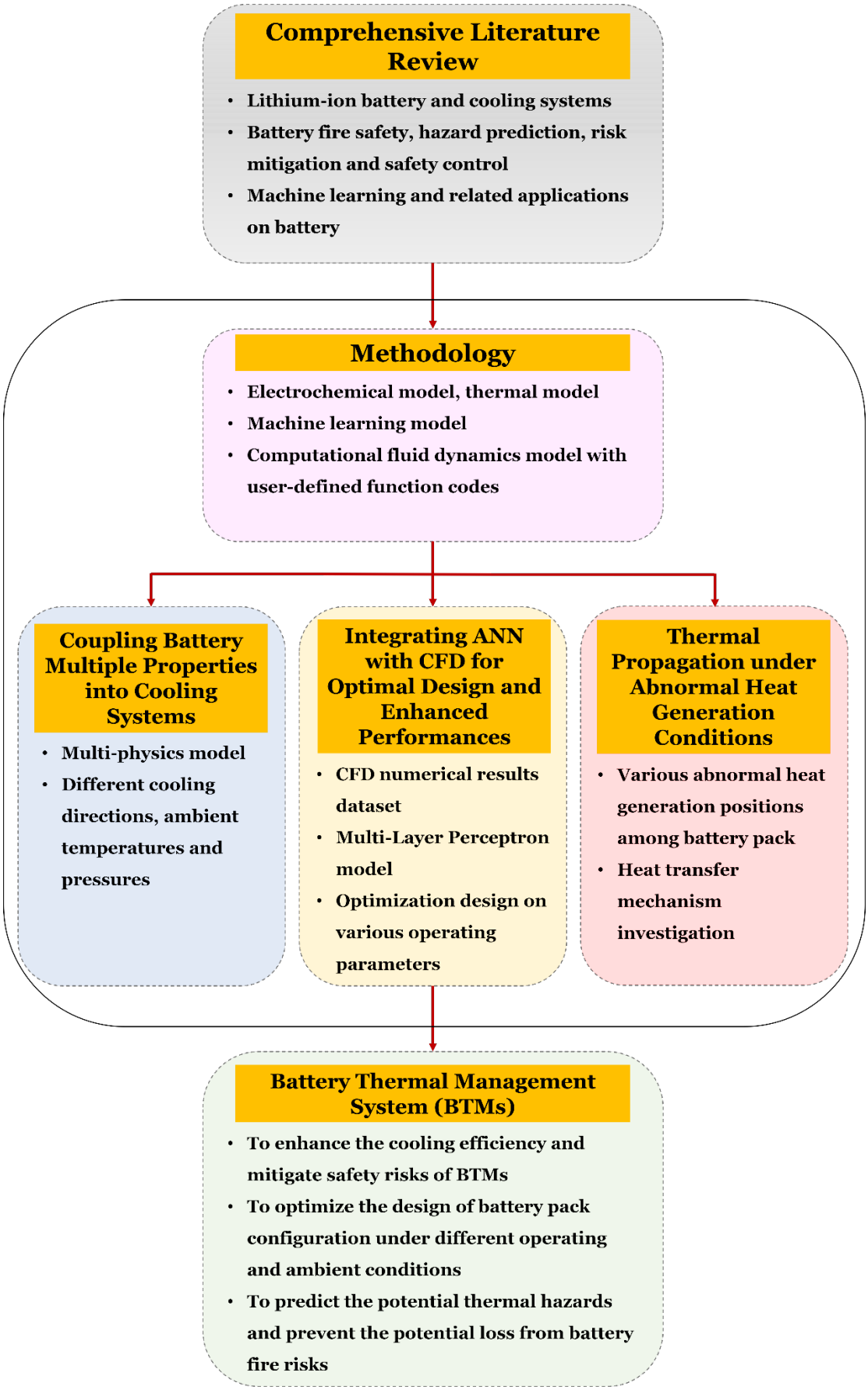

Figure 1.2 The framework of this thesis.

1.3 Thesis Outline

This thesis is sub-divided into six chapters in total with a structured, logical flow, including background, motivation and knowledge gap, research aim and objectives, literature reviews, methodology, results, and conclusions. The summary of each chapter is briefly outlined in this section. Firstly, this chapter presents the background and current research stage about alternative and renewable energy technologies, mainly LIB, as well as their advantages and disadvantages. The applications of LIB have been presented in this chapter, accompanied by potential fire safety issues. Concurrently, the TR process of LIB and the various BTMs have been mentioned. Moreover, the aim and scope of this research are elaborated in this chapter before the description of the thesis outline.

Chapter 2 presents a comprehensive literature review on the subjects of BTMs employing machine learning (ML) models. Some typical ML models have been introduced with samples and applications in section 2.3. Moreover, the potential applications of ML techniques applied to analysing the thermal behaviour of battery systems, enhancing the performance of BTMs, predicting battery hazards, and controlling battery safety have been reviewed and discussed in sections 2.4 and 2.5, respectively. Lastly, the overview of the ML application on BTMs is summarised in section 2.6.

The methodology of this thesis is introduced in Chapter 3. Section 3.2 demonstrated the CFD models applied in this work including electrochemical model and thermal model. The machine learning model, especially multi-layer perceptron model, is presented in

section 3.3, followed by section 3.4 with the description of the user-defined function applied in Chapter 6.

In Chapter 4, section 4.3 describes a novel approach to characterise the temperature distribution of a battery pack based on the three-dimensional thermo-electrochemical model, and the application of the CFD-ANN framework. The different forced air-cooling directions (axial and radial of the battery cell) and various ambient environment pressures are investigated. Also, the optimal configuration design is proposed in this section by the numerical analysis of the CFD-ANN framework comparing the maximum temperature and temperature difference among the battery pack.

On top of the work conducted in Chapter 4, to further study the operating setups and ambient environment conditions, more parameters natural ventilation scenarios are demonstrated and analysed in Chapter 5. Section 5.3 sheds light on the detailed numerical model descriptions and validation. In this section, various parameters are investigated related to the battery cooling performance, including the gap between each cell along different directions, the ambient temperatures, and the natural ventilation velocities. The integrated CFD-ANN model delivers the optimisation of the battery pack layout with the balancing of the mentioned parameters.

After the investigation of the normal working environment for the battery pack in Chapters 4 and 5, Chapter 6 conducts the study of the battery pack thermal behaviour under extreme conditions. The section 6.2 highlights the extreme conditions that cause a detrimental effect on the battery cooling performance. The abnormal heat generation has

been adopted into the thermal propagation model to analyse the battery thermal behaviour. Furthermore, the different abnormal heat generation locations have been studied and the heat exchange mechanism has been investigated in section 6.3.

Finally, Chapter 7 concludes the results and summarises the key findings of this thesis, and the highlighted contributions have been put forward in section 7.2. Additionally, the limitations of the current works are clarified with the suggested recommendations for future works in section 7.3.

It should be noted that the main contents in Chapters 4 to 6 are constructed from the published journal articles with modifications and reorders (shown in the List of Publications), and the main contents of Chapter 2 are based on a submitted draft, which is currently under major revision. These mentioned drafts and articles are specified at the beginning of each chapter.

Chapter 2 Literature Review

This chapter includes the contents from two published journal articles [49, 50]: **Li, A.**, Yuen, A. C. Y., Wang, W., De Cachinho Cordeiro, I. M., Wang, C., Chen, T. B. Y., Zhang, J., Chan, Q. N., & Yeoh, G. H. (2021) "A Review on Lithium-Ion Battery Separators towards Enhanced Safety Performances and Modelling Approaches," *Molecules,* 26(2), 478. and **Li, A.**, Weng, J., Yuen, A. C. Y., Wang, W., Liu, H., Lee, E. W. M., Wang, J., Kook, S., & Yeoh, G. H. (2023) "Machine Learning Assisted Advanced Battery Thermal Management System: A State-of-the-art Review," *Journal of Energy Storage*, 60, 106688. with modifications and reorders to better fit the structure of this thesis.

2.1 General Description

With an increasingly wider application of the LIB, specifically the drastic increase of electric vehicles in cosmopolitan cities, improving the thermal and fire resilience of LIB systems is inevitable. Thus, in-depth analysis and performance-based study on BTMs design have arisen as a popular research topic in energy storage systems. Amongst the LIB system parameters, such as battery temperature distribution, battery heat generation rate, cooling medium properties, electrical properties, physical dimension design, etc.,

multi-factor design optimisation is one of the most difficult experimental tasks. Computational simulations deliver a holistic solution to the BTMs design, yet it demands an immense amount of computational power and time, which is often not practical for the design optimisation process. To summarise the state-of-the-art numerical models used in battery research, a review of multi-scale multi-physics models is needed. Meanwhile, the battery numerical simulations involved a large number of parameters, such as electrical properties, thermal properties, operating conditions, physical configurations, etc.; ML techniques are able to find not only the connection among various factors but also improve the efficiency of simulations. Therefore, ML models play a non-substitute role in the safety management of battery systems. They also aid in temperature prediction and safety diagnosis, thereby assisting in the early warning of battery fire and its mitigation.

In this chapter, extensive lists of literature on BTMs employing ML models and identifying the current state-of-the-art research are summarised, which is expected to serve as a much-needed guideline and reference for future design optimisation. Following that, the application of various ML models in battery fire diagnosis and early warning is illustrated. Finally, improved approaches are proposed to advanced battery safety management with ML. This review chapter aims to bring new insights into the application of ML in the LIB thermal safety issue and BTMs design and anticipate boosting further advanced battery system design not limited to the thermal management system, as well as proposing potential digital twin modelling for BTMs.

2.2 Introduction

2.2.1 Overview of battery research

As mentioned in Chapter 1, greenhouse gas emissions and global warming remain the utmost concerning issues around the globe, countries worldwide have taken proactive countermeasures attempting to mitigate waste emissions to advocate a cleaner future [51]. As accordingly, there is a seek for a secondary energy source for public transportation and logistic purposes. One example is the uprising blooming application of EVs, which are powered by cleaner fuel sources. Rechargeable batteries, particularly LIBs with high energy density, long life-span and high efficiency, have been used extensively in EVs and other energy storage solutions [52, 53]. Lithium-ion based battery energy storage systems also have become the most competitive choice for various applications [54-57]. Nonetheless, the high energy density and thermal instability of LIBs bring key challenges to battery thermal safety, such as thermal management [58]. Furthermore, it is worth mentioning an extreme condition called battery TR, which is a potential risk in the battery pack [59, 60]. In addition, battery TR propagation has become one of the greatest challenges for battery safety and often aggravates the thermal hazards through the domino effect during TR propagation [61]. Many experimental studies have characterised the battery TR, including initial conditions, materials, and configurations [62, 63]. The majority of TR initiates with the solid-electrolyte interphase (SEI) layer decomposition. With this trigger point, other exothermic reactions and an internal short circuit start, followed by the accumulated heat and gases. The whole process looks like a domino effect,

and once it starts, it will not go back. Due to the increasing temperature and pressure, TR and battery fire hazards occur. Figure 2.1 shows a series of chain reactions corresponding to the battery TR process, and the three-stage profile was presented by Wu et al. [64]. Researchers have conducted studies for the module design concerning fire protection and thermal insulation functions.

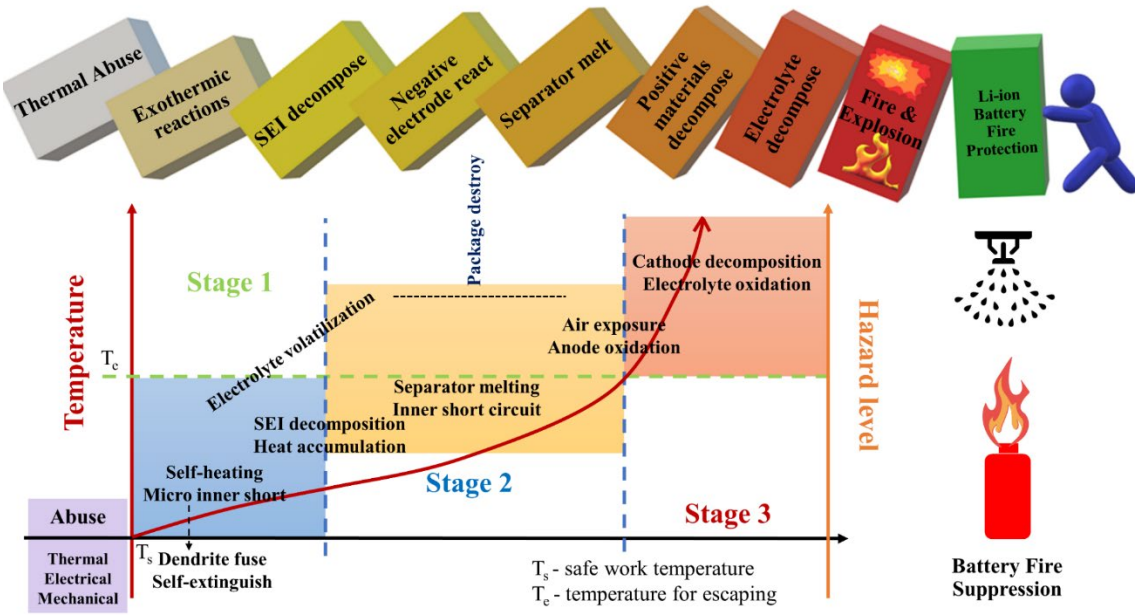

Figure 2.1 Domino effect of battery TR and the corresponding temperature profile along different stages.

Given that LIBs are sensitive to working temperature [16, 65, 66], it is essential to ensure the battery works in a suitable temperature range to guarantee working efficiency and thermal safety [67]. Therefore, it is imperative to develop effective BTMs, which require a comprehensive system design with multi-factors considered.

2.2.2 Numerical techniques and research gap

With the development of computer science, numerical simulations are gradually applied in many assessments for battery performance evaluation and safety designs. Numerical simulation validates experiment results with fewer physical resources than standard experiments and reveals in-depth key performance parameters, including temperature, pressure, and electrochemical properties. Furthermore, simulation results visualize the battery system internally to effectively diagnose the problems that may lead to potential battery failures. The development of numerical battery models has facilitated a better understanding of the underlying principles of the battery circuit and its associated influence towards the ambient environment.

Benefiting from the rapid development of numerical algorithms alongside data acquisition, ML has become more versatile and efficient with wide applications including electronic devices [68, 69], machinery [70, 71], and advanced materials [72-74]. The ML technique plays a substitutable role in system design and optimisation since it has strong functions in figuring out an optimal solution among multi-factors within a quite limited time [75]. This undoubtedly is not an easy task to fulfil via experiments and numerical simulation. Usually, the experiments can only aid in determining the optimal solution among some limited previous settings. Meanwhile, numerical simulations, such as CFD simulations, demand intense computational power and time to deliver a single solution for one case scenario. Therefore, the implementation of ML techniques in the BTMs, to some extent, addresses this issue by being able to almost instantly provide an optimised

parameter value provided with sufficient training of data. In addition, ML is expected to assist the temperature prediction at a certain time, enhancing the BTMs' function and giving an early warning before battery TR. For instance, according to time series data, the temperature change during the battery operation can be distinguished by the reversible heat and the irreversible heat, which is also linked to the charge/discharge current. To understand this, researchers attempted to implement ML models, such as artificial neural networks (ANN) [76], convolutional neural networks (CNN) [77], long short term memory (LSTM) [78], deep reinforcement learning (DRL) [79], etc., to assist the BTM system for enhanced battery thermal safety and resilience. For example, Jaliliantabar et al. [80] developed an ANN model for the prediction of LIB temperature equipped with BTMs and proved the capability of ANN to predict battery temperature in various operating conditions of BTMs. Kalkan et al. [81] built an ANN model, whose inputs involve the coolant flow rate, discharge rate, and coolant inlet temperature, for designing a novel serpentine tube cold late and mini channelled one. Jiang et al. [82] proposed a novel data-driven method for LIB fault diagnosis and TR warning based on state representation methodology.

Nevertheless, ML algorithms for BTMs remain an ongoing development and comprehensive studies with a vast amount of training database are both required to empower their industry applications. Furthermore, to the best of our knowledge, there are few relevant review articles summarizing the state-of-the-art literature using ML in the BTMs and battery fire prediction, which leads to a research gap in classifying ML models

in thermal safety issues applications. At the same time, considering the complicated battery properties, operation parameters and different types of battery cells, a numerical dataset for battery and BTMs performance is lacking. This review section summarises the current ML techniques applied in battery safety studies and demonstrates a potential solution for battery optimisation design. In this section, by revealing past and current research works on ML-assisted battery systems, we aim to develop insights and future perspectives on the development of both intelligent BTMs optimisation and safety design.

2.2.3 Contribution and structure

On the basis of the aforementioned research gap, this section summarizes the numerical models of battery thermal studies and the state-of-the-art publications regarding the ML application in the battery thermal safety issue, including battery thermal management and battery fire. Also, the potential improvement directions with ML models applied in the battery are highlighted in the graphical abstract, including building and infrastructure, EVs and power stations, electrical transportation systems, portable devices, and rural region power supply hubs. In addition to the literature review, this review section has proposed some critical thinking in the potential combination of ML techniques with the battery system, particularly from the thermal safety perspective. The structure of this section is summarized as follows:

Section 2.3 reviews CFD modelling developments for LIBs. The basics of CFD models that contribute towards the establishment of battery thermal propagation modelling are introduced. Also, how electrochemistry is being studied eventually in a numerical way is demonstrated.

Section 2.4 briefly introduces ML, where most ML models (such as ANN, CNN, and LSTM) used in the current related works are demonstrated in a certain category.

Section 2.5 summarizes the related literature using ML to solve problems, where the applications are generally divided into section 2.5.1 Heat generation and temperature prediction/Thermal data prediction and section 2.5.2 System optimisation with machine learning.

Following that, Section 2.6 lists the previous publications about battery fire (treated as the extreme state of thermal hazards) and ML applied in battery fire prediction. Compared to section 2.5, which focuses on the thermal behaviour and cooling performance, this section concentrates on the battery hazards and fire. These two sections cover the normal working conditions of battery systems and the extreme scenarios of battery fires, respectively.

Finally, in the section 2.7, conclusions and potential contributions of this chapter are summarised based on the current development. Besides, some novel ideas on the way forward for future applications are proposed, hoping to give guidance and references for further probe into this field. Last but not least, this review chapter can give more

references for researchers in designing and/or optimizing future BTMs. The booming artificial intelligence technology can further boost the development of BTMs.

2.3 LIB Numerical Model

Mathematical models have been widely used in the battery property investigation and battery working procedure [83-85]. The development of a detailed mathematical model is important to design and optimise the batteries. Simulation results provide intuitive data on the performance of the battery. A suitable mathematical model can describe a few parameters which are not known experimentally and regulate parameter adjustment. For example, the direct experimental data for tortuosity or liquid-phase transport resistance is lacking, which can be simulated from mathematical models [86, 87].

CFD is a practical tool to study different thermal fluid dynamic parameters and simulate multiple physics fields [88], and CFD makes it possible to use the equations governing a fluid motion for an extensive range of complex situations, providing both insight and quantitative predictions. CFD simulation can provide detailed information about the electrical and thermal field inside the battery that is often difficult to be assessed by experimental means. Model-based investigations promote theoretical understanding of battery physics beyond what is possible from experiments only. In this section, the LIB numerical models are reviewed by different battery scales, as shown in Figure 2.2.

By considering specific equations and processes, complex fluid mechanics and electrochemical reactions can be simulated. The significant advances compared to experiments are expressed with the development of multi-scale multi-domain models. Meanwhile, the escalating trend of fast computing makes the CFD models a reliable and efficient tool to reveal complicated phenomena and analyse the mechanisms. For various scales of battery setup, CFD models allow engineers and researchers to predict and assess the LIB performance through the design process.

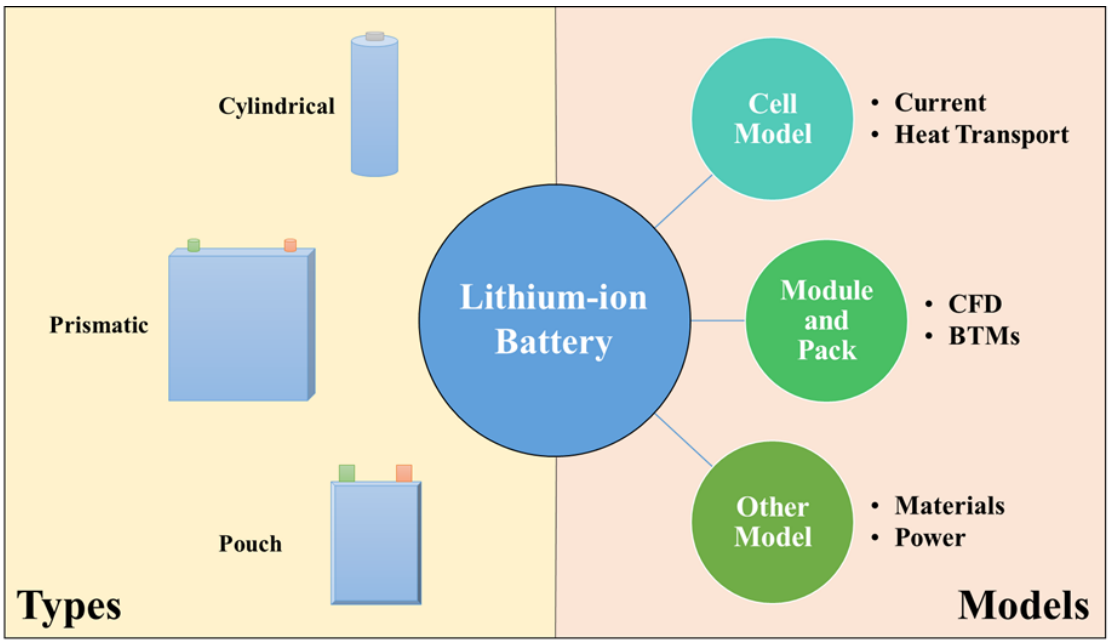

Figure 2.2 LIB battery types and numerical models.

2.3.1 Battery cell models

In the early 1990s, Newman and his colleagues suggested a LIB model utilizing porous electrode theory [84]. The model solves lithium diffusion dynamics and charges transfer kinetics to predict the electrical response of a cell in a paired intercalation electrode

system. This model has been widely used in academia and industry to describe the performance of a LIB based on material properties and electrode design. With the application of a two-dimensional battery cell model, Kim et al. [89-92] investigated thermal behaviour of LIB under various electrode configurations, as well as during discharge and charge. The potential, current density distribution and temperature distribution were predicted. Also, the scale-up battery and low environment temperature were considered. Xu et al. [93] developed a two-dimensional electrochemical-thermal model, considering the effect of current collecting tabs on cell performance. Cheng et al. [94] built a thermo-electrical model to investigate the surface temperature distribution of a LIB cell. Larsson et al. [95] presented a thermal model to allow a fast evaluation of several different preventive means of thermal insulation and predict the propagation of a thermal runaway in a cell to neighbouring. In order to study the thermal abuse behaviour of large format LIBs, Kim et al. [96] studied a three-dimensional model based on a one-dimensional model formulated by Hatchard et al. [97]. Their model demonstrates multidimensional behaviours of thermally abused cell. Kim and his colleagues developed a Multi-Scale Multi-Dimensional model, which addresses the interplay among the physics in varied scales [98], and this model is applied to resolve electrochemical-, electrical-, and thermal-coupled physics in large-format stacked prismatic cell designs.

2.3.2 Battery module and pack models

Based on different shapes and forms, there are three most common ones for LIB cells, which are prismatic, pouch and cylindrical. Multiple battery cell arranged in modules to achieve serviceable units. Yi et al. [99] demonstrated a three-dimensional model for LIB module, the potential, current density distribution were predicted as a function of discharge time. Cicconi et al. [45] proposed thermal simulation of one battery cell, and the CFD analysis of a battery module. The air-cooling system has been evaluated. However, each battery cell was simulated as an average temperature, which can be further investigated.

Moreover, battery cells are connected in series and in parallel into battery packs to achieve the desired voltage and energy capacity. Feng et al. [100] studied and designed substantial quantified solutions to prevent thermal runaway propagation via applying battery pack. They predicted that inserting thermal resistant layer between adjacent batteries can be helpful. Chen et al. built a detailed three-dimensional thermal model to examine the thermal behaviour of the LIB, and it precisely considered the layered-structure of the cell stacks, the case of a battery pack, and the gap between both elements [101]. Lin et al. [102] developed a three-dimensional model of battery pack with the passive thermal management system, and the temperature rising curves of this model matched very well with the experimental results.

2.3.3 Other models

Abada et al. developed a 3D physical model of electro-thermal behaviour at thermal runaway conditions, which also provides a better understanding of the ageing influence on the thermal runaway process [103]. Cai et al. [104] studied a mathematical model on the thermal behaviour of LIB during the galvanostatic discharge process with and without a pulse. Xie et al. [105] developed a resistance-based thermal model to simulate the ohmic resistance, polarization resistance, and entropy change, considering effects of the state of charge (SOC) and temperature on heat generation. Fang et al. [106] proposed a prediction model based on artificial neural network for surface temperature simulation of nickel–metal hydride battery. With a good agreement to experimental data, battery surface temperature is calculated with various ambient temperature and charging rates.

In this section, numerous studies related to LIB numerical modelling have been reviewed. From the safety perspective, most of the research work relies on the thermal model, which predicted the average temperature for a LIB cell [45, 93, 95], and many experimental studies on the thermal propagation have been done [107, 108]. The battery fire risks and potential hazards demonstrated a close relationship with the temperature. However, the non-uniform temperature distribution in the LIBs leads to an electrical imbalance, lower battery performance and shorter battery life. The models that can replicate the comprehensive battery temperature distribution should be further addressed.

2.4 Machine Learning Overview

Based on the prementioned LIB numerical models, the various battery properties and operating conditions were adopted for the CFD approaches. Achieving an optimal balance among these parameters is crucial from an optimization standpoint. Furthermore, most of these parameters lack a clear relationship, so employing a methodology to establish connections between them is required. As the world is rapidly transiting towards electrification and automation, artificial intelligence (AI) systems are increasingly integrated into our daily lives (telecommunication networks, infrastructures, transportation systems, etc.). Concurrently, our current age is deemed a digital world, and various data types are ubiquitous. Implementing AI, particularly ML approaches, is the key to intelligently analysing the data and constructing correlative smart applications. With the revolutionary developments of computer science and processing power over the last decades, ML algorithms have been widely applied in different fields, such as building [109, 110], chemistry [111], manufacturing [112], agriculture [113, 114], etc. ML is a computer program that learns from experiences concerning some class of tasks and performance measures if its performance at tasks improves with the experiences [115]. Figure 2.3 shows the schematic of ML. Samples train the machine, and then when input comes to the machine, the machine's structure and/or parameters are updated by the new samples. The approximated output will be generated afterwards.

Also, many previous reviews of ML have been done [116-118]. Normally, ML techniques are categorised into four major types: Supervised learning, Unsupervised learning, Semi-

supervised learning, and Reinforcement learning [119], shown in Figure 2.4. Supervised and unsupervised learning depends on whether the data is labelled. The semi-supervised learning is a hybridisation of the first two types, while reinforcement learning enables machines to evaluate the behaviour or environment to improve efficiency.

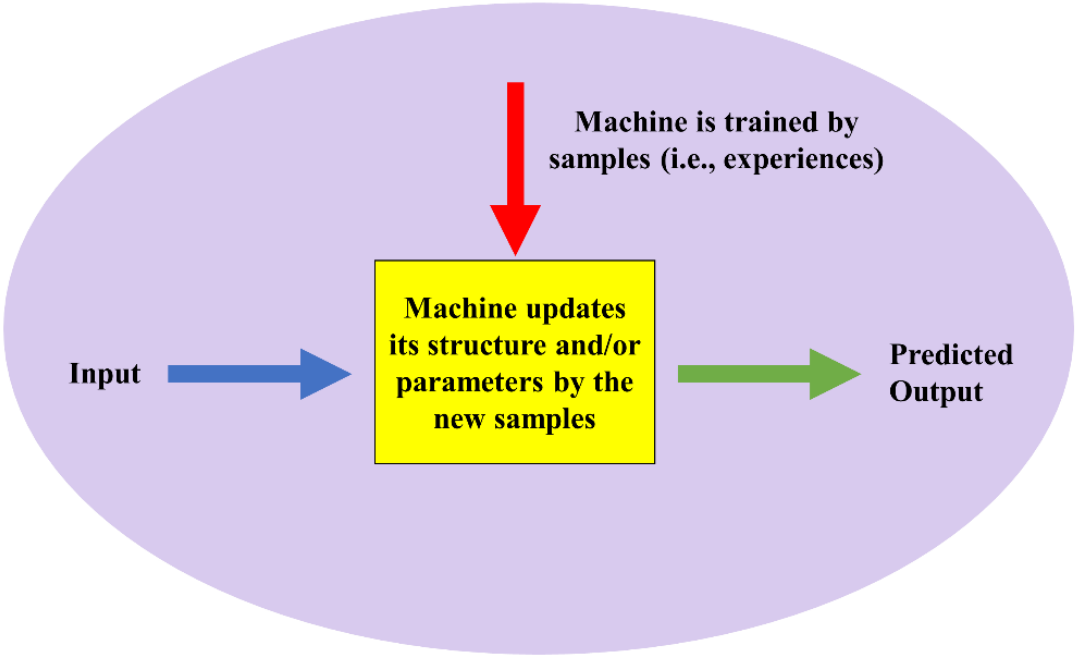

Figure 2.3 The synthetic route of DMOP.

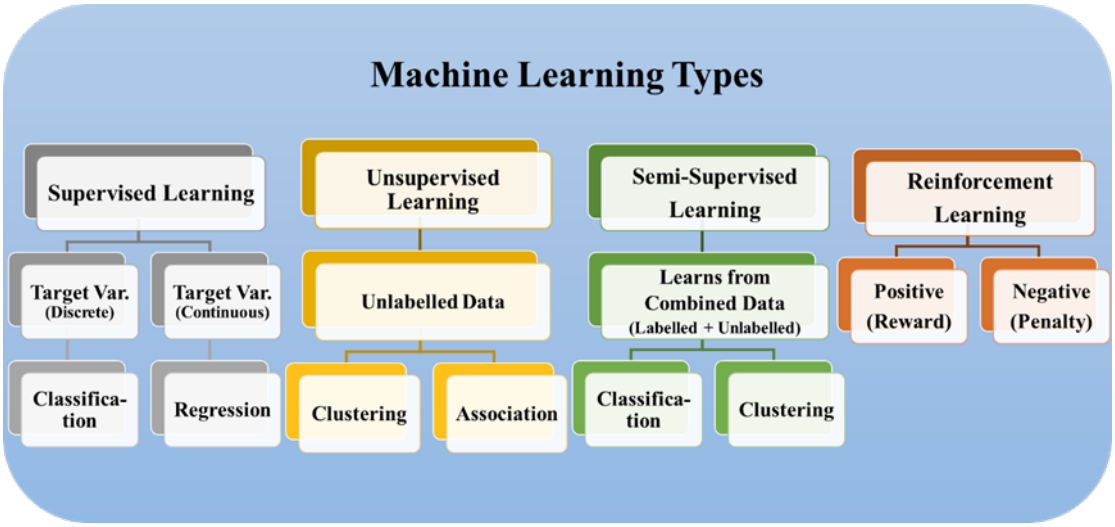

Figure 2.4 Major types of ML techniques [119].

This review mainly focuses on the ML applied in the battery thermal safety issues field. The applied algorithm depends on many factors, including the problem to be addressed, the number of variables, the chosen model, and so force. In line with the overall reviewed papers, the ML algorithms in this review are summarised in three components: ANN, deep learning (DL) and other methods. In this section, we briefly outline the ML algorithms used in the battery thermal safety issues and provide the potential of the applied ML models to improve the intelligence and capabilities of BTMS applications.

2.4.1 Artificial neural network (ANN)

Artificial neural networks, normally called neural networks (NNs), are computing systems inspired by the biological neural networks that form animal brains. ANN has rapidly developed as a common tool to model a broad range of engineering systems due to its capability to learn and adapt to find potential correlations among different properties. ANN-based models are empirical. However, they can contribute to practical, accurate solutions for accurately or imprecisely formulated problems and phenomena only identified with experimental data and field observations. ANNs have been used in various applications, including modelling, classification, pattern recognition, multivariate data analysis, etc. Owing to the high precision and outstanding data noisy tolerance, ANN has been successfully utilised in studying battery-related topics, such as the state of charge

estimation, state of health assessment, battery temperature prediction, BTMs optimisation, etc.

ANN is a non-program, adaptive, brain-style information processing that functions through network transformation and dynamic behaviour [120]. An ANN model has five main components: inputs, summation functions, weights, activation functions, and outputs, which the early researchers propose to model the operation of the artificial neurons. The working process of a typical ANN model is straightforward. Inputs of ANN were received by an artificial processing neuron and were combined to generate a net input. The neuron passes that through a threshold gate and transmits the output to another neuron or the environment.

The artificial neuron in the hidden layer works as a biological neuron in the brain. To form a directed and weighted graph, the network is shaped by linking the output of specific neurons to the input of other neurons. A learning process can adapt the activation functions and weights. The learning rule or training approach controls the certain learning process. The activation function of a node governs the output of that node, or "neuron," provided input or set of inputs. The activation function presents a functional relationship between the input and output layers. Step activation, threshold, sigmoid, and hyperbolic tangent are frequently applied activation functions.

ANN approaches are applied in the control or modelling of systems with unknown or complex internal structures by achieving the advantage of learning and the stability of

facing minor disturbances. This section focuses on multilayer perceptron and support vector regression applied for BTMs.

2.4.1.1 Multilayer perceptron (MLP)

Multilayer Perceptron (MLP) is known by its architecture, which is also a feed-forward ANN [119]. A typical MLP contains at least three layers of nodes: an input layer, a hidden layer and an output layer. Except for the input layer, each node of other layers is a neuron that utilises a nonlinear activation function to connect. MLP utilises a supervised learning technique called back-propagation for training. Its multiple layers and nonlinear activation separate MLP with a linear perceptron, which can distinguish data that is not linearly separable. A hidden layer is a layer located between the input and output of the ANN model, in which artificial neurons apply a set of weights to the inputs and direct them through an activation function as the output. Hidden layers of ANN allow for a neural network's function to be taken apart for specific data transformations. For example, images and documents are treated as initial inputs from external data. The ultimate outcomes, such as recognizing objects in a snap, complete the task.

2.4.1.2 Support vector regression (SVR)

Support Vector Regression (SVR) is popularly and widely applied for classification problems in ML. SVR is an analytical approach to investigating the relationship between one or more predictor parameters and a real-valued (continuous) dependent variable [121]. As a significant branch of support vector machine (SVM), SVR only has one kind of

sample point [122]. Compared to SVM, SVR is less popular, but it is an effective tool for estimating real-value functions. SVR uses kernel functions to outline the nonlinear regression problem for nonlinear problems. The optimal hyperplane it pursues is not to maximize the separation length between two or more types of sample points like SVM but to minimize the total variation between sample points and hyperplane. And the sample points can be separated by an optimal hyperplane in high-dimensional spaces. For example, for a linear situation of SVM, the points outside the middle shaded tube region affect the cost insofar as the deviations are penalized linearly [123], shown in Figure 2.5.

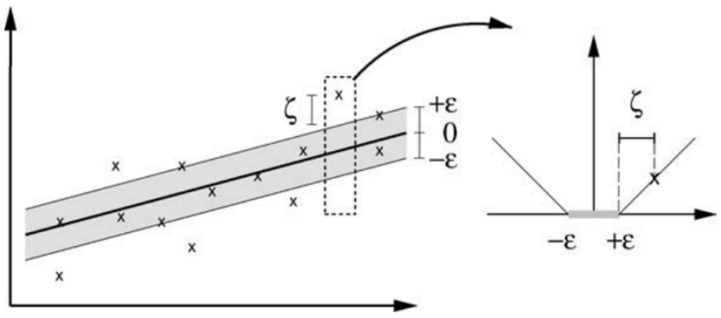

Figure 2.5 The soft margin loss setting for a linear SVM [123].

2.4.2 Deep learning (DL)

Deep learning (DL) is a subfield of ML, typically a neural network with three or more layers of neurons, as shown in Figure 2.6. DL attempts to replicate the behaviour of the human brain, allowing numerical models with multiple layers to learn multiple levels of large amounts of data. While a neural network with a single layer can still make

approximate predictions, additional hidden layers contribute to optimising and refining accuracy.

Compared to traditional neural networks, DL shows a better performance in everyday products and service cases with large datasets, such as voice-enabled TV remotes and credit card fraud detection. Observing patterns in the data allows a DL model to cluster inputs appropriately. Therefore, a DL model would require more data points to improve its accuracy. Furthermore, DL has some limitations: data amount, computational power, and training time. Typical types of DL related to BTMs in this section are listed as follows.

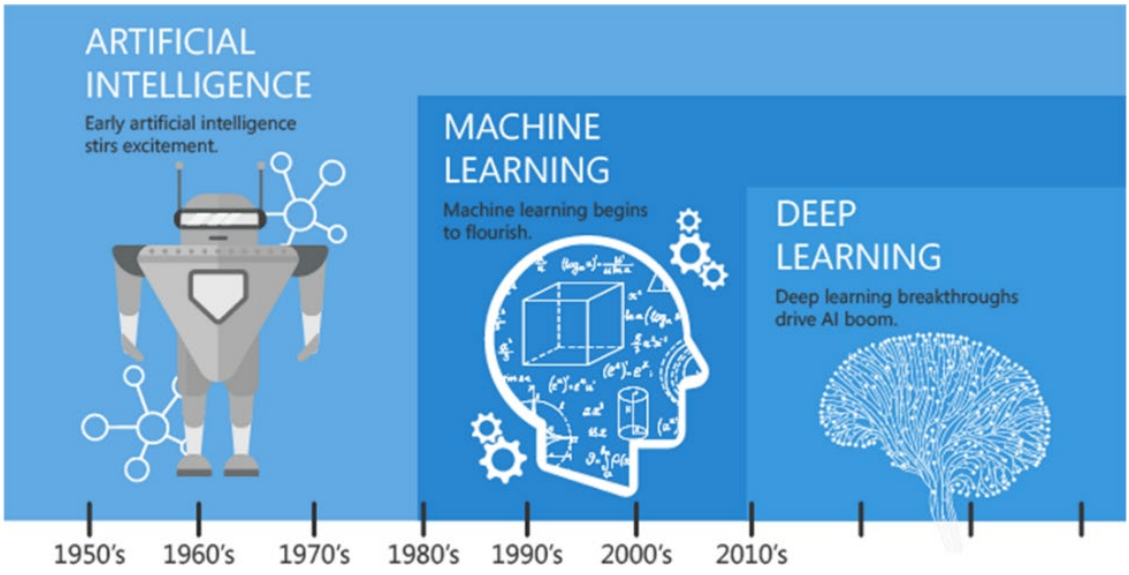

Figure 2.6 Relationship among AI, ML and DL [124].

2.4.2.1 Convolutional neural networks (CNNs)

Convolutional neural networks (CNNs) are applied primarily in image and video recognition, classification, natural language processing, etc. CNN can take advantage of the two-dimensional structure of the input data for detecting features and patterns and

achieving tasks like object detection or recognition. Many successful applications of CNN models in the field. For example, CNN first bested a human in an object recognition challenge in 2015.

2.4.2.2 Long short-term memory (LSTM)

Long short-term memory (LSTM) is a recurrent neural networks (RNNs) architecture, which is typically applied in natural language and speech recognition as it leverages sequential or time-series data. LSTM can overcome the training difficulty caused by the exploding/vanishing gradient problem. The learning advantage of LSTM impacted several fields from both a practical and theoretical viewpoint, so it became a state-of-the-art model [125]. Figure 2.7 shows the architecture of a typical LSTM block, including gates, inputs and outputs. The output of the block will be connected back to the block input and all of the gates for the calculation. Also, researchers keep studying the possibilities to improve the performance of the typical LSTM.

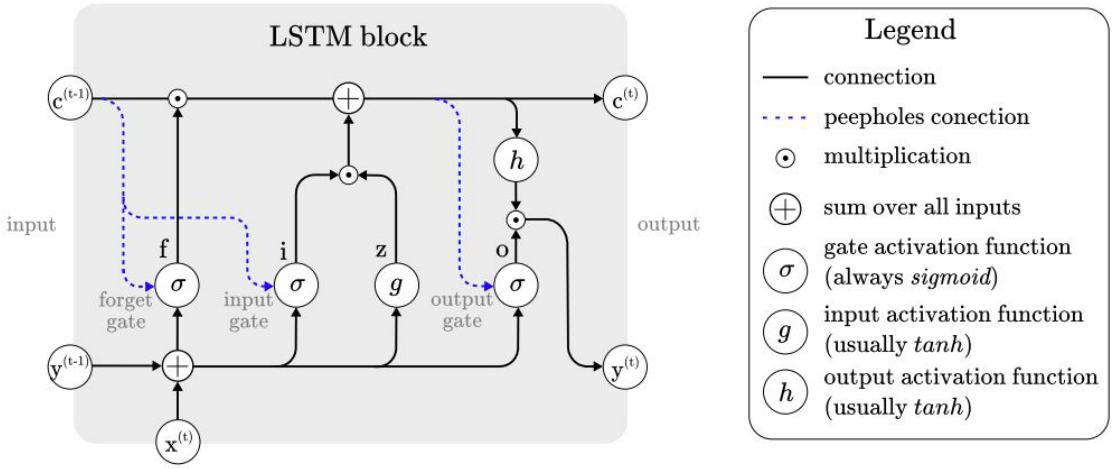

Figure 2.7 The architecture of a typical vanilla LSTM block [125].

2.4.3 Other machine learning methods

Due to the battery itself combining electrical, chemical and mechanical parameters, many different perspectives should be involved, such as voltage, temperature, State of Charge (SOC), Depth of Discharge (DOD), resistance, cycle life, State of Health (SOH), etc. Therefore, besides the prementioned ML techniques, some other ML algorithms are still applied in battery thermal and safety research. In addition, the combined ML methods will be listed in the next section.

2.4.3.1 k-nearest neighbours algorithm (KNN)

k-Nearest neighbours (KNN) is an uncomplicated algorithm that allocates new data based on a similarity measure (e.g., distance functions) with the input data, also known as a 'lazy' learning model. KNN has been applied in some analysis fields, such as statistical estimation and pattern recognition. The concept behind nearest neighbour methods is to catch a pre-determined number of training objects closest to the new point and utilise them to predict its label. KNN is quite robust to noisy training data, and accuracy depends on the data quality. The number of cases can be a user-defined constant, which can also vary locally depending on the density of points.

2.4.3.2 Gaussian process regression (GPR)

Gaussian process defines a distribution over functions and inferences taking place directly in the space of functions. Gaussian processes often have characteristics that can be changed by setting certain parameters. The algorithm is applied to estimate the SOH and

SOC of LIBs. Also, the GPR model has a straightforward parameterization. The model parameters can be computed by maximizing a marginal loglikelihood function, which is easy to implement and flexible to use, in contrast to commonly used grid-searching trial-and-error methods used to optimise the SVM [126].

2.4.3.3 Digital twin (DT)

With the wave of the digital economy, the application of the Internet of Things (IoT), cloud computing, big data and other technologies have become a future trend in battery management and production [127]. To overcome the increase in battery cell number, algorithm complexity, and new functionalities, a digital twin (DT) was built to improve the computation and data storage capabilities. All battery-relevant data can be measured and transmitted seamlessly to the cloud platform at a DT [128]. DT uses massive twin data and real-time coupling to achieve simulation, prediction, diagnosis, etc., while ML can be matched with intelligent algorithms for multiple needs [129]. DT can improve the accuracy and responsiveness of different functions with ML algorithms.

To sum up, in the field of battery research, ML has emerged as a potential modelling method and has already been applied in many perspectives of this area. Figure 2.8 shows the trend of applying ML methods in battery research continually increases. The number of publications on battery fire (BF) and BTMs in 2021 is double that in 2020, demonstrating that ML has great potential in the application on BF and BTMs. Meanwhile, it has specific advantages in fast and accurate real-time battery state predictions. In this section, we summarise the most used ML methods for battery thermal and safety issue.

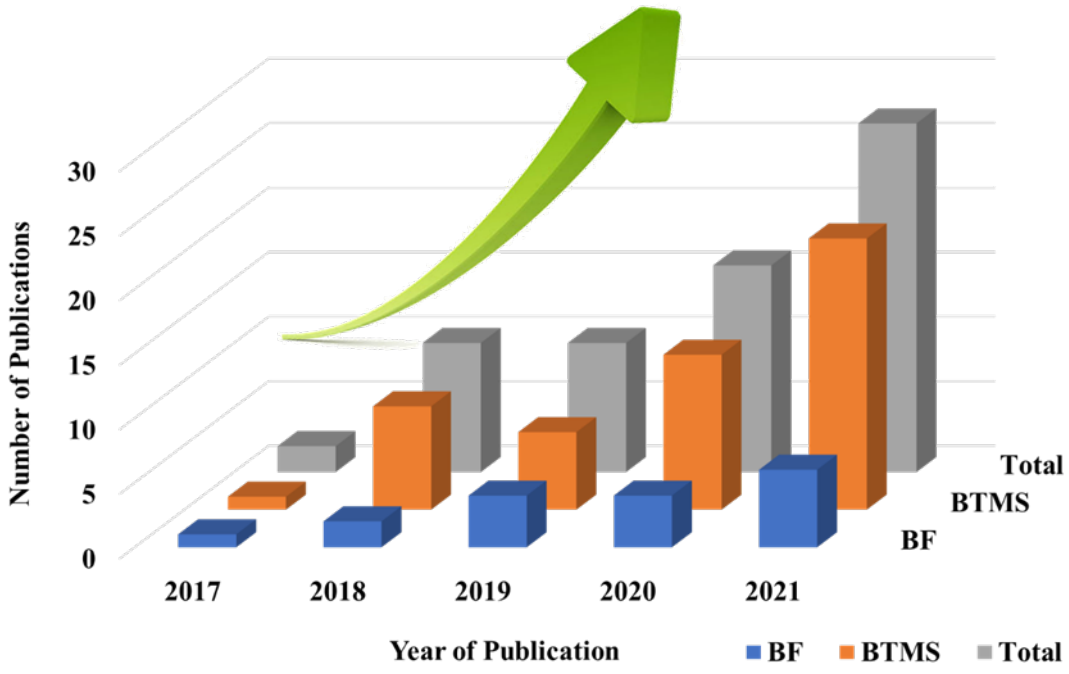

Figure 2.8 Publication amount trend of ML applied in battery in recent years.

2.5 Machine Learning and Battery Thermal Management

As mentioned in Section 1, it is imperative to design ideal BTMs due to the strict temperature requirement of LIBs. Currently, there are numerous studies concerning BTMs emerging fast, which employ air cooling, liquid cooling, phase change material (PCM) cooling, etc. Among them, many parameters must be determined or optimised before establishing effective BTMs. These parameters optimisation include air velocity in the forced air cooling [130, 131], the ambient temperature in the forced air cooling [132], the flow rate of the liquid [133, 134] and cooling liquid temperature [135, 136]. However, it is not an easy task to optimise so many parameters via experiments or simulations only. For one thing, most experimental studies adopt the method of

determining the most optimum one among many options. For another, even though the numerical studies mostly follow this pattern, whose results are indeed superior but operated under a recommended range. Rare studies proposed the most optimum values applying the optimisation progress with ML methods [137], which are considered a superior tool in optimizing and predicting parameters [138-140].

2.5.1 Heat generation and temperature prediction/Thermal data prediction

Kleiner et al. [141] developed a lumped thermal model with a novel neural network and proposed a direct comparison of a physics-based and a data-driven thermal battery module for the first time. In their study, the temperature estimation of both modelling approaches is in good agreement with the reference temperatures for multiple locations.

Afzal et al. [142] compared single layer NN with deep NN to figure out an optimised number of hidden layers to predict Nu coupling with neurons and activations functions (See Figure 2.9). They concluded that the deep NN provided a much better prediction than the single layer NN model.

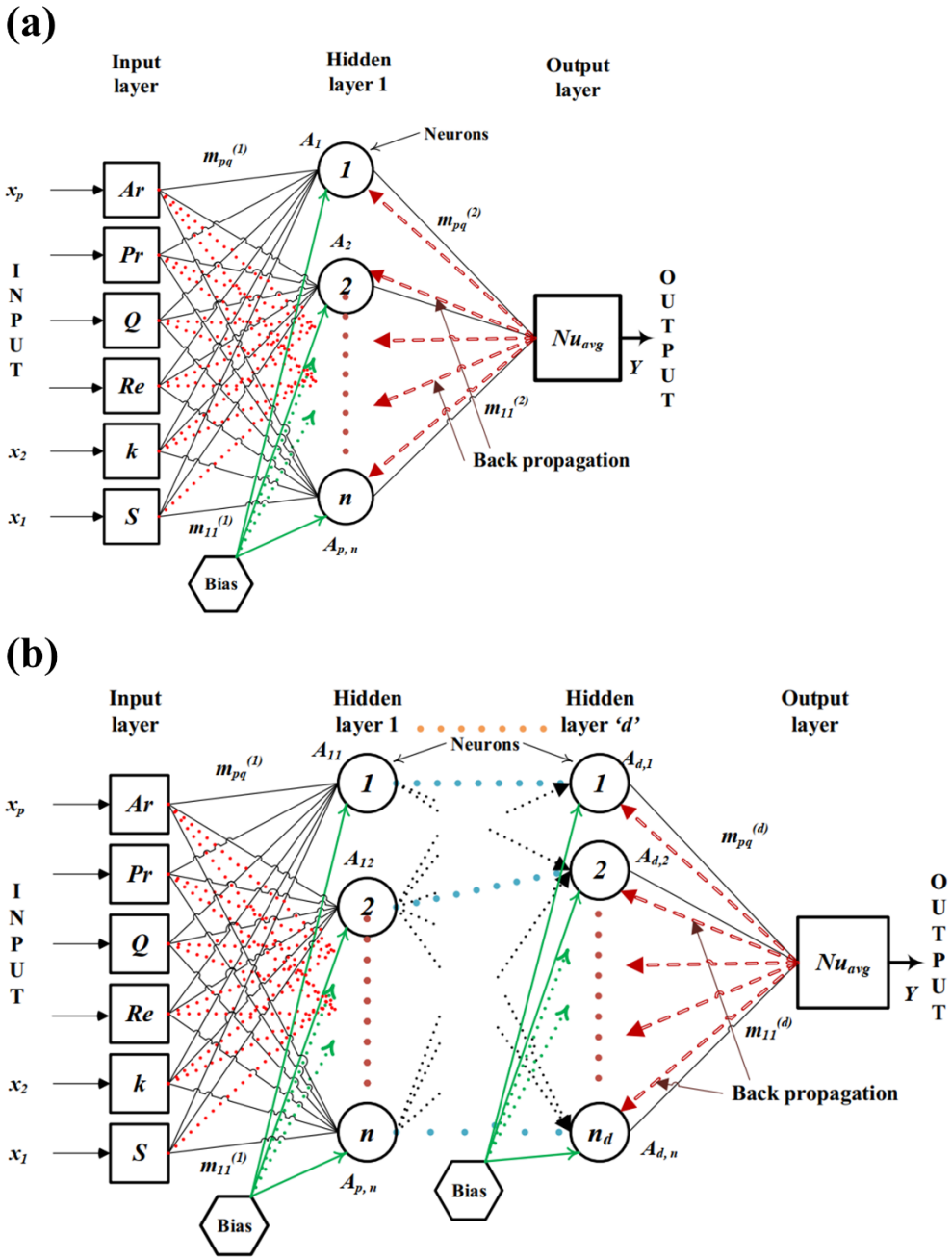

Figure 2.9 Schematic figures of the ANN model structure [142] (a) single hidden later NN, (b) deep hidden layer NN.

Kleiner et al. [143] proposed a novel simplified modelling approach for predicting the jelly roll temperature of large format prismatic cells based on ANN. Arora et al. [144]

also proposed a new computational model based on ANN for estimating battery heat generation rate with cell nominal capacity as one of its key inputs, along with ambient temperature, discharge rate and depth of discharge. Their trained ANN accurately simulates the thermal behaviour of LiFePO4 pouch cells of the nominal capacities from 8 to 20 Ah under varied conditions.

Except for ANN, CNN and LSTM are also popular ML models for evaluating the effectiveness of the BTMs. To highlight the accuracy and application prospect of CNNs to substitute complex, time-consuming finite element method (FEM) modelling, Kolodziejczyk et al. [145] first modelled composited phase change material (CPCM) microstructures with FEM, whose image dataset is subsequently used to train CNN models. After that, the CNN was used to predict the temperature evolution of the CPCM-based BTMs during charging/discharging currents, as shown in Figure 2.10. Wang et al. [146] applied CNN and virtual thermal sensors to predict a ternary battery's internal temperature and highlighted this method needs no knowledge of battery thermal properties, heat generation or thermal boundary conditions. Besides, Zhu et al. [147] used time-series data to train the LSTM model and found that battery temperature fluctuation can be efficiently predicted over a long period, serving as a battery temperature prognostic. Huang et al. [148] propose a deep reinforcement learning model to optimise the battery energy management strategy considering battery thermal effects. By comparing the numerical results to two conventional reinforcement learning algorithms, the proposed

method demonstrates a more than 6.7% energy reduction, which saves the cost for training and makes the data sets close to the practical scenario.

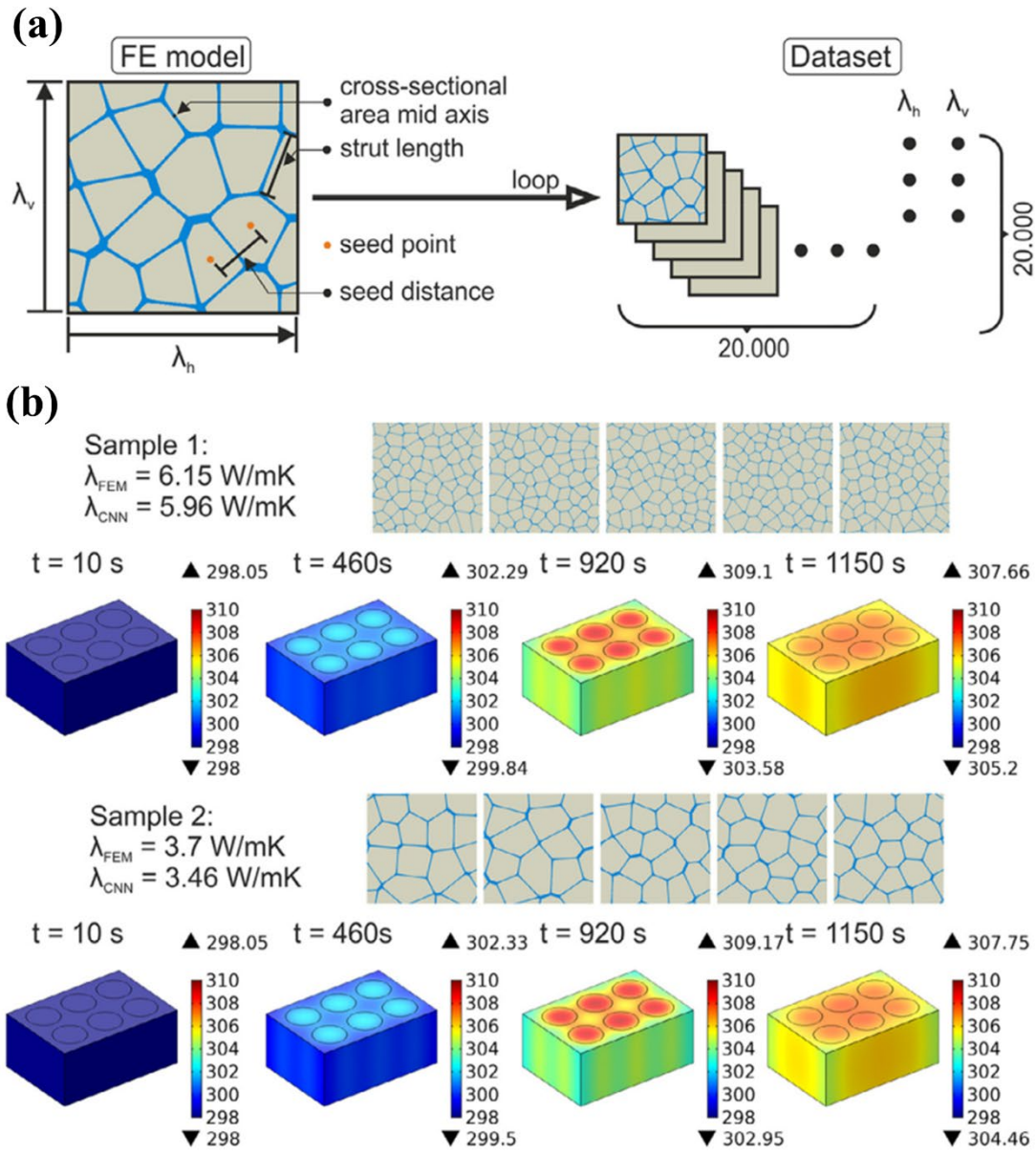

Figure 2.10 (a) the developed modelling strategy for creating the dataset of CPCMs, (b) two CPCM samples with their cross-section images and time evolution of surface temperature [145].

2.5.2 System optimisation with machine learning

ML is a smart tool to assist multi-factor design. For example, ANN can be applied to describe the relationship between BTMs parameters [149] and provides a time-saving and efficient method for optimal design.

2.5.2.1 Multi-factor design

Mokashi et al. [150] applied ANN model to analyse the heat removal from the battery pack using a different flowing fluid with an average Nusselt number. In their work, three different types of multi-layered feed-forward (FF) networks with back-propagation were developed, i.e., the multiple back propagation (MBP) 1-3 (Figure 2.11 (d-f)). The multiple back-propagation algorithms assist the regression analysis of the average Nusselt number.

Lin et al. [149] utilise an ANN network combined with a genetic algorithm to optimise the thermal performance of air-PCM BTMs regarding the inlet air velocity, inlet air temperature, PCM thickness, and battery unit spacing and discharge rate. Their results showed that the PCM thickness and battery unit spacing affect the battery temperature. The optimal parameter combinations help slow the temperature rise and delay the PCM phase transition.

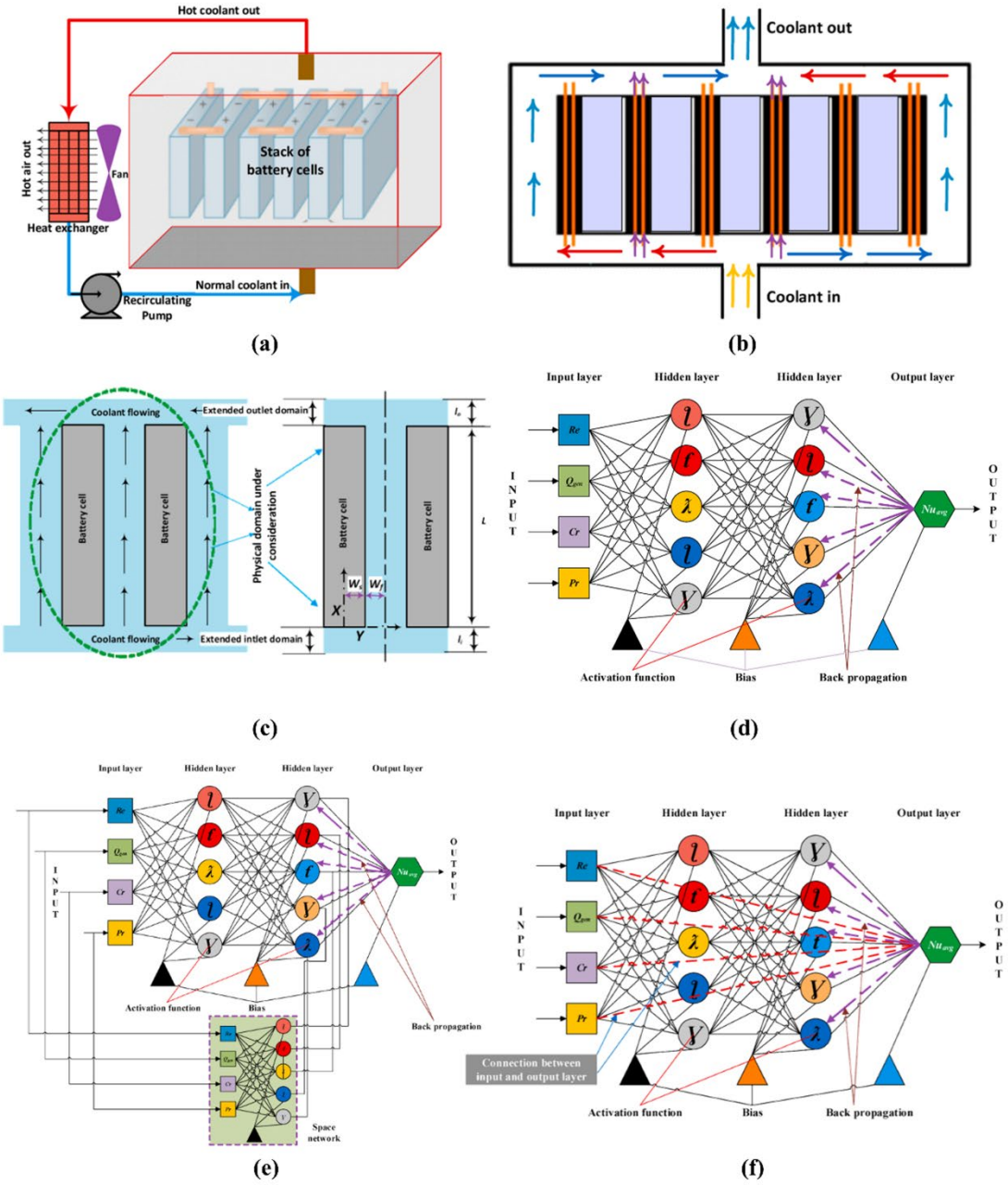

Figure 2.11 (a) 3 D and (b) 2 D diagrams of the BTMs, (c) computational domain of the conjugate problem, (d) MBP 1, (e) MBP 2, and (f) MBP 3 [150].

Xu et al. [151] proposed a novel digital twin virtual model-based BTMs parameter optimisation (including microchannel plate width or cell internal spacing d1, side spacing d2, microchannel height l and coolant flow rate V). Finally, they developed a new type

of microchannel liquid cooling BTMs, which has a better cooling effect but smaller volume. Similarly, Talele et al. [152] applied ANN to investigate the delay effect caused by the battery pack to resist the set limit of the threshold temperature range, where a multi-objective optimisation strategy is proposed between the battery pack delay effect for selected paraffin wax and RT-18 PCM against its given C-rate. Kalkan et al. [81] applied the ANN model to study the thermal performance when developing a cold plate (Figure 2.12), including some key parameters like coolant flow rate, the inlet temperature of coolant and discharge rate. By considering 270 data sets, the average temperature and maximum temperature difference are evaluated and predicted accurately.

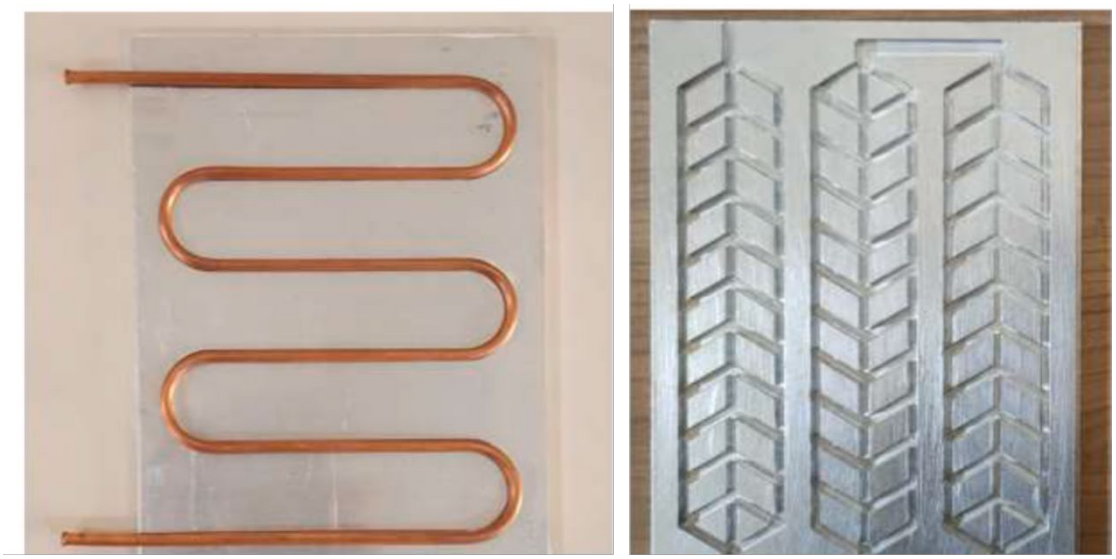

(a) **(b)**

Figure 2.12 Section views of (a) serpentine tube cold plate (STCP) and (b) mini channel cold plate (MCCP) [81].

Genetic programming (GP) models are also popular in system optimisation. For example, Su et al. [153] applied genetic programming (GP) when optimizing the inlet coolant

temperature in the BTMs. The GP model process is illustrated in Figure 2.13, and the iterative optimisation is demonstrated as well, including model generation, evaluation, selection, and modification. This process aims to minimise the objective function value of the model to optimise the predictive performance.

There are also some newly developed models by the researchers to investigate the specific scenarios. Shi et al. [154] developed a fully connected deep network to optimise the air cooling model regarding different shell structure features, including various numbers, positions, and sizes of the additional outlet in the U-type cooling BTMs.

Besides, SVR models can also be applied to predict battery temperature changes. For example, Tang et al. [155] used the system coefficient performance-support vector regression (PSO-SVR) model to investigate the influence of ambient temperature, air flow rate of the external heat exchanger and compressor speed on performances of the liquid-cooled BTMs and proved the PSO-SVR model can be used as a new method to fit the complex nonlinear relationship among the system coefficient of performance (COP).

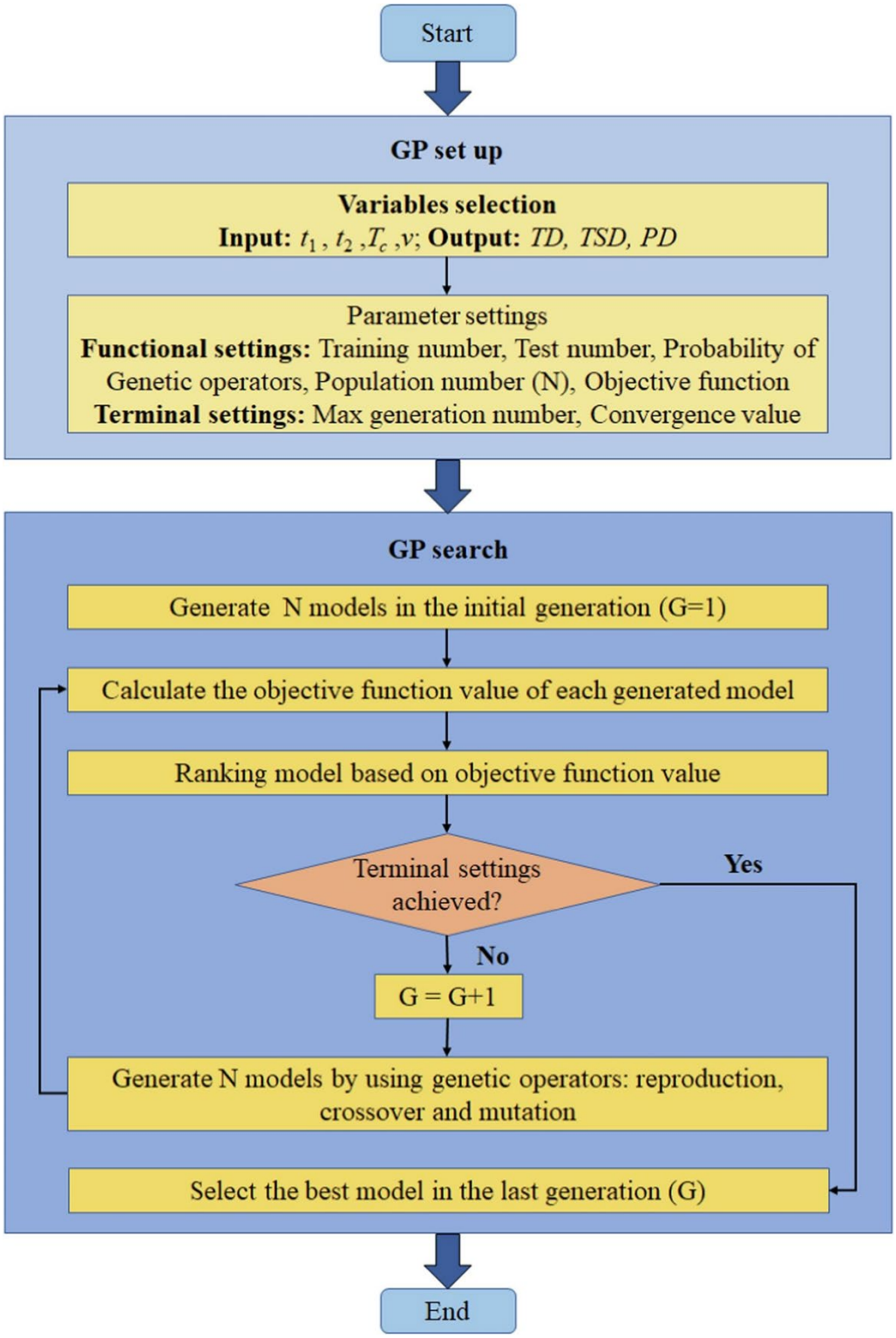

Figure 2.13 Illustration of the GP process [153].

2.5.2.2 Cooling efficiency determination

Except for the simultaneous design of multi-factor optimisation in the BTMs, there is also an important but seldom investigated issue, namely the coordination among (fast) charging, effective cooling and energy efficiency. This task can be extremely tough to realize via limited experiments, while machining learning models can help. Chen et al. [156] proposed the NN model to assist in combining fast-charging process scheduling with thermal management and figure out a trade between the charging speed, cooling efficiency and energy consumption, as shown in Figure 2.14. In their study, the regression model could predict three target values for all of the combinations among a wide range of charging current rates (0.5C, 1C, 1.5C, 2C and 2.5 C) at three different charging stages and a range of coolant rates (0.0006, 0.0012 and 0.0018 kgs^{-1}). The maximum temperature and temperature standard deviation (TSD) were lower than 33.35 and 0.8 °C. Similarly, Park et al. [157] first proposed an optimal TM strategy and then used an ANN-based model to reduce the total energy consumption while maintaining the battery temperature within an acceptable range.

In this section, the related literature with the applications of ML techniques to solve problems of battery thermal prediction and system optimisation are reviewed. Table 2.1 summarises the reviewed research works that applied ML techniques for BTMs, and it is concluded that ANN is applied the most in this area. At the same time, other methods, including CNN, SVR, and LSTM, also have the potential to enhance BTMs.

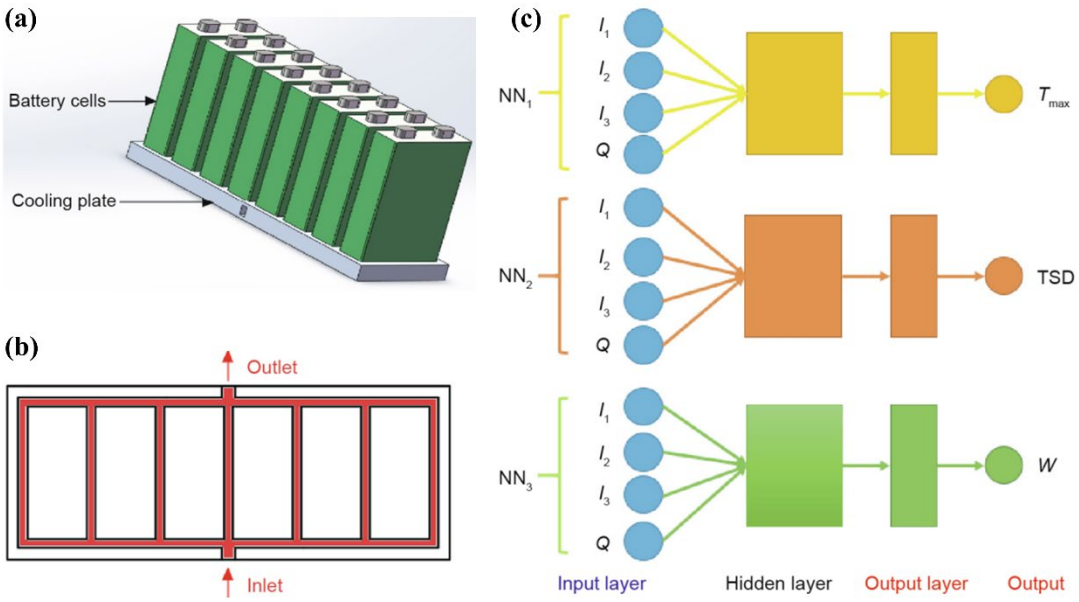

Figure 2.14 Diagram of (a) LC-based BTMs (b) mini-channel-based cooling plate, (c) proposed NN model [156].

Table 2.1 Summary of the ML applied in the battery thermal management design and thermal data prediction.

ML approach	Target object	Reference
ANN	PCM design	[80]
	Cold-plate design	[81]
	Optimisation of battery pack enclosure	[138]
	Battery pack configuration	[139]
	Temperature prediction	[143]
	PCM-based BTMs design	[149]
	PCM delay	[152]

	BTMs design	[157]
	Energy efficiency optimisation	[158]
	Surface temperature	[159]
	Liquid cooling based BTMs	[160]
	Thermal coupled equivalent circuit model	[161]
	Heat generation rates	[162]
MLP	Liquid cooling	[156]
CNN	PCM design in thermal management	[145]
LSTM	Thermal effects and temperature changes	[147]
DRL	Battery temperature and energy consumption	[148]
SVR	Liquid-cooled battery thermal management	[155]

2.6 Battery Safety and Machine Learning

Batteries, as complex materials systems, pose unique challenges for the application of ML [163]. In recent decades, LIBs have been widely used in our daily life, such as electric vehicles (EVs), battery energy storage systems (BESSs), and small portable devices. Many battery fire accidents happen now and then, even some explosions leading to people injured and fortune lost [164, 165]. Ghiji et al. [166] demonstrated more than 300 fires or

fire-related incidents with 40 fatalities reported over the past two decades. Although a shift to data-driven, ML-based battery safety research has started, new initiatives in academia and industry are still needed to exploit its potential fully.

2.6.1 Battery safety

LIBs with high energy density materials are sensitive to abusive conditions whose thermal stability is low, and some inside chemical reactions are prone to happen when the internal temperature is high, including the chemical reactions between electrolyte and electrode materials [167-169], and safety problems like TR and its propagation [170, 171]. These papers have reviewed and summarised many representative incidents of LIBs failure accidents [172, 173]. Due to the typical explosive components of a battery, such as plastic packing, separator and electrolyte, LIB accidents happen in various applications, from mobile telephones to EVs and even aeroplanes. Based on these reviews, the various abusive conditions, such as over-heating, over-charged, short circuit and mechanical shock, have been studied, and it is easy to conclude that thermal abuse is the root cause of battery TR [61]. Moreover, the abuse conditions can be categorized into three sections: mechanical abuse, electrical abuse and thermal abuse, whose common features are smoke, fire and explosion, as shown in Figure 2.15 (a).

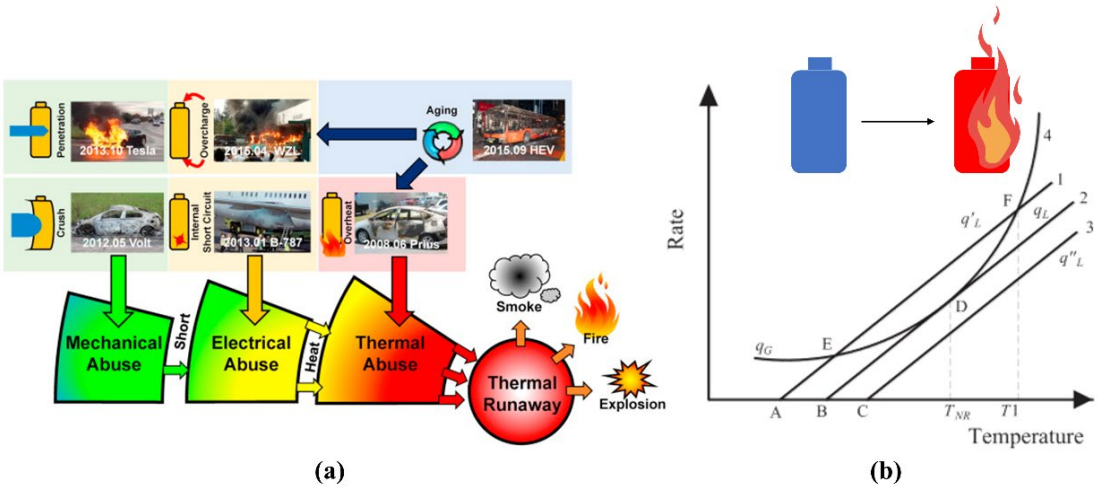

Figure 2.15 (a) Accidents related to LIB failure and correlated abuse conditions [61]; (b) Thermal digraph of a reaction and heat loss from a vessel at three ambient temperatures, where B is at the critical temperature [174].

As for the necessary components of combustion, fuel, oxygen, and an ignition source consist of the combustion triangle. For LIB fire, these three parts are also necessary. The main fuel is the electrolyte, which is made of organic solvent and inorganic salt. Furthermore, LIBs are separated from the air in a normal situation without an explosion or fire danger as a closed system. However, due to the TR, the positive electrode decomposes and releases O_2, which is one of the contributions to the combustion triangle and chemical reactions at the negative electrode. Meanwhile, all these decompositions are exothermic processes that serve as the ignition source. Consequently, the LIB is under fire hazard risks.

As shown in Figure 2.15 (b), the TR process can be described as follows: with the increase of the battery temperature and more exothermic chemical reactions happening, more heat

was generated. The curved line 4 stands for the generated heat owing to an exothermic reaction, while the straight lines stand for heat removal, which is a linear function at various coolant temperatures. Straight line 2 has one tangent point D with curved line 4. This point is a critical point, as heat removal equals heat generation; thus, this critical equilibrium temperature is named the “Temperature of No Return”. The temperature B is called the self-accelerating decomposition temperature. If the TR happens, once the temperature is over the critical point, all the exothermic chemical reactions will contribute to the self-heating and will not return. Then the temperature and pressure in the LIB are cumulated until it exceeds the battery endurance. The fire and explosion are inescapable, and the whole process can be described as the Domino effect of the reaction chain. For the sake of fire protection, it is important to take measures to break the Domino chain to avoid TR and fire hazards.

The battery TR is similar to a series of chain reactions, which can be described as the domino effect, shown in Figure 2.1. The battery TR process can be generally divided into three stages, summarised as follows. Stage 1: In this stage, self-heating and micro inner short circuits happen, during which period the SEI decomposes. Stage 2: With the heat generated in Stage 1, the separator melts coupled with an internal short-circuit, followed by anode oxidation. Stage 3: Because of the increasing heat accumulated inside the battery, more chemical reactions, including cathode decomposition and electrolyte oxidation, happen. Consequently, battery fire hazards arise with fire ejection and a large amount of heat released, which is difficult to be extinguished. Under the common battery

working conditions, the battery temperature is no more than 40 °C, which is relatively low. Still, the abuse situations, such as short circuit, overcharge, applying reverse polarity or exposure to extreme temperature, will lead to a sharp increase in the temperature. In a situation with a temperature exceeding 66.5 °C, more reactions trigger, generating more heat to quicken up self-heating reactions. After that, the reaction will not return when the temperature is over 75 °C. Along with more chain reactions, the generated gas and heat are cumulated. Once the inner environment pressure exceeds the battery endurance, the explosion is inevitable, and the battery components are easily ignited and thus leading to a LIB fire. The BTMs control and maintain the battery pack under the usual conditions. When the TR happens, it may not cool down the battery temperature. Therefore, it is essential to monitor the battery temperature with early detection of abnormal heat generation or predict the battery fire risks by applying ML techniques to mitigate them.

Kriston et al. [175] investigated the impact of TR initiation conditions on the severity of TR of Graphite-NMC (111) cells, which comprises graphite anodes and lithium Nickel-Manganese-Cobalt oxide cathodes (written as NMC(111)). Seven hundred eighty various TR events are simulated, and the output is studied by ML techniques such as principal component analysis and clustering.

Similarly, Li et al. [176] employed a high-accuracy finite element model of a pouch cell to generate over 2,500 simulations and analysed the data with ML methods, shown in Figure 2.16. The safety envelope was visualized with two types of phase diagrams, a classifier that predicts a fast speed on the short circuit or safe to a given loading condition

and a regressor that quantitatively tells the amount of deformation needed to develop a short. The safety envelope provides important guidelines for the design of EVs and batteries. The regression model provided the ranges of the safe and electric short circuit ranges, and also predict the quantity of intrusion, force, and energy absorption to which the short circuit happens.

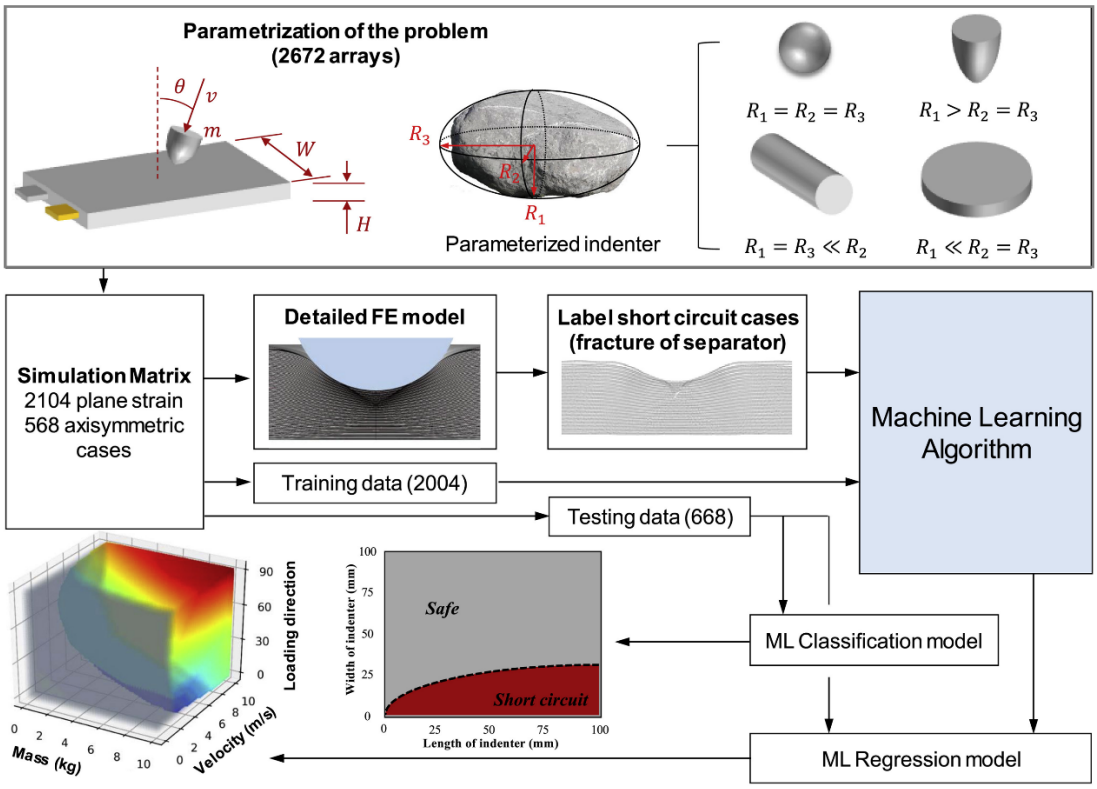

Figure 2.16 Flowchart of the Data-Driven Safety Envelope Using ML Algorithm [176].

From the electrochemical perspective, Seo et al. [177] demonstrated a method for detecting the internal short circuit in the LIB using CNN, which is used to classify the degree of the internal short circuit faults. The proposed method shows classification

results with high accuracy of 96.0% and consequently contributes to detecting the internal short circuit in the early battery state.

Furthermore, Petrich et al. [178] used MLP to detect cracks in the anode of a LIB after the TR. The classifier studies pairs of particles and distinguishes three causes for their separation: breakage during the TR, image segmentation and disjointness in the pristine cell. For the dataset of the hand-labelled data from a real electrode, an overall accuracy of 73% is achieved.

2.6.2 Hazard prediction

Due to the wide applications of LIBs, the safety and reliability of LIBs are crucial for people's lives. Yet, our capability to predict failure through online and offline diagnostics still has space to improve [72]. LIBs hazardous failure is rare, but the consequences are relatively severe. LIBs can be treated as highly complex and nonlinear systems. Worse, similar battery cells or packs may perform differently towards identical mechanical, electrical, or thermal stimuli, limiting the performance of classical deterministic numerical approaches. For supporting decisions in design and control, a probabilistic method can be applied to quantify uncertainty. For example, Figure 2.17 demonstrates an overview of data from battery cells can be applied to interpret and perhaps to enhance the prediction accuracy by data-driven techniques, where spatial surface temperature profiles can also be monitored as a thermal data input.

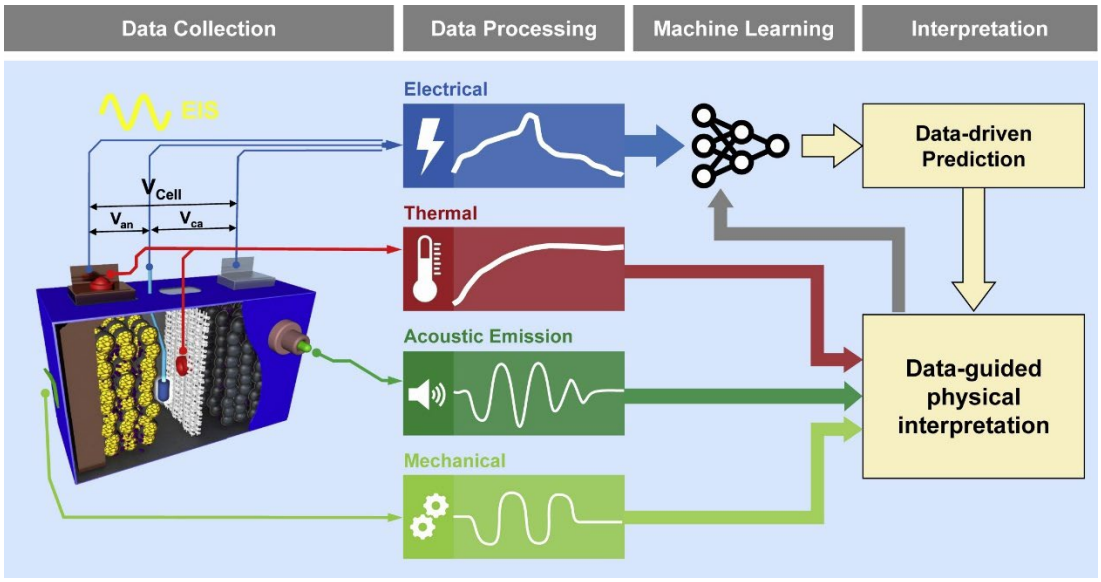

Figure 2.17 Record-keeping the related data of LIB for data-driven prediction and physical interpretations [179].

ML algorithms are well fitted for predicting nonlinear systems like lithium-ion cells. ML is typically agnostic to underlying physics even if the algorithms predict accurately. It thus demonstrates limited value in informing researchers and engineers on design opportunities to improve the cells' performance. Still, training and validation of models are challenging for safety applications since large amounts of failure data are essential. Battery researchers have a high interest in conquering these challenges. This perspective offers suggestions on the potential ways of study to manage precise predictions of the hazards of cell failure while obtaining some physical insights into the predicted behaviours.

Lee et al. [180] mapped partial charging data into a distinct statistical entity called the likelihood vector, as shown in Figure 2.18. Then the likelihood vectors are computed by

referring to possibility distribution functions of experimental voltage and current simulating different degradation/abuse conditions for LIBs. Compared with the brute-force training method utilizing partial charging curves to train MLP classifier models, training assisted by likelihood vectors leads to improvements in test set classification accuracy by 26-85%, according to the size of neural networks. Furthermore, by monitoring the failure index calculated from the cumulated list of detections made, it is experimentally presented that the TR and resultant fatal explosion event of lithium pouch cell under operando dent test can be predicted before the event occurs.

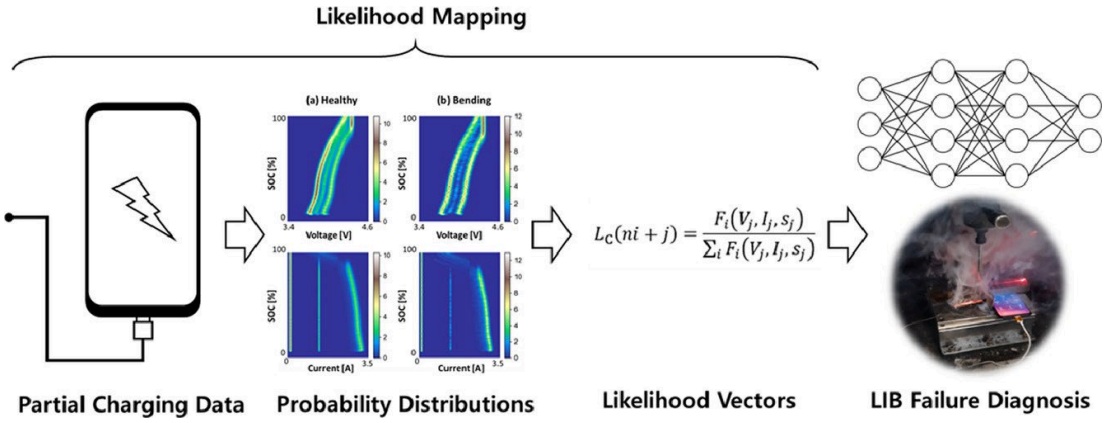

Figure 2.18 Schematic diagram explaining artificial neural network enhanced by likelihood mapping approach [180].

Besides, Jiang et al. [82] propose a novel data-driven method for LIB pack fault diagnosis and TR warning based on state representation methodology. The results show that the proposed method can perform not only the accurate identification of the faulty cells and accurate determination of the voltage fault type but also the early detection of faults and early warning of TR. Also, Ding et al. [181] proposed a novel data-driven approach to

perform multistep ahead forecast accurately for battery TR state at cell-level by applying meta TR forecasting neural network (Meta-TRFNN). Both simulated and real-world samples were tested, demonstrating the forecasting ability of Meta-TRFNN, the benefit of embracing high-dimensional thermal images, and the efficacy of the meta-learning framework.

Additionally, Yang et al. [182] applied an extreme learning machine (ELM)-based thermal (ELMT) model to depict battery temperature behaviour under an external short circuit, where a lumped-state thermal model was chosen to replace the activation function of conventional ELMs. Compared the ELMT model with a multi-lumped-state thermal (MLT) model parameterized by the genetic algorithm using the experimental data from various sets of battery cells, it is demonstrated that the ELMT model can achieve higher computational efficiency than the MLT model and better fitting and prediction accuracy.

Moreover, Ojo et al. [183] introduced an LSTM-based NN model in conjunction with the newly developed stretch-forward technique and residual monitor to detect these faults. The experimental results showed that this approach could estimate the surface temperature of the cell, which means that it achieved a good predictive accuracy and fault detection performance. Da Li et al. [184] proposed an enabling TR prognosis model based on abnormal heat generation, which combines the long short-term memory neural network (LSTM) and the convolutional neural network (CNN), shown in Figure 2.19. The verification results conclude that the presented scheme exhibits accurate 48-time-step battery temperature prediction with a mean-relative error of 0.28% for all four

seasons, which verifies its robustness and adaptability. Also, the proposed model can realize a 27-min-ahead TR prognosis, including 19 mins ahead by abnormal heat generation (AHG) diagnosis method and 8 mins in advance by CNN-LSTM.

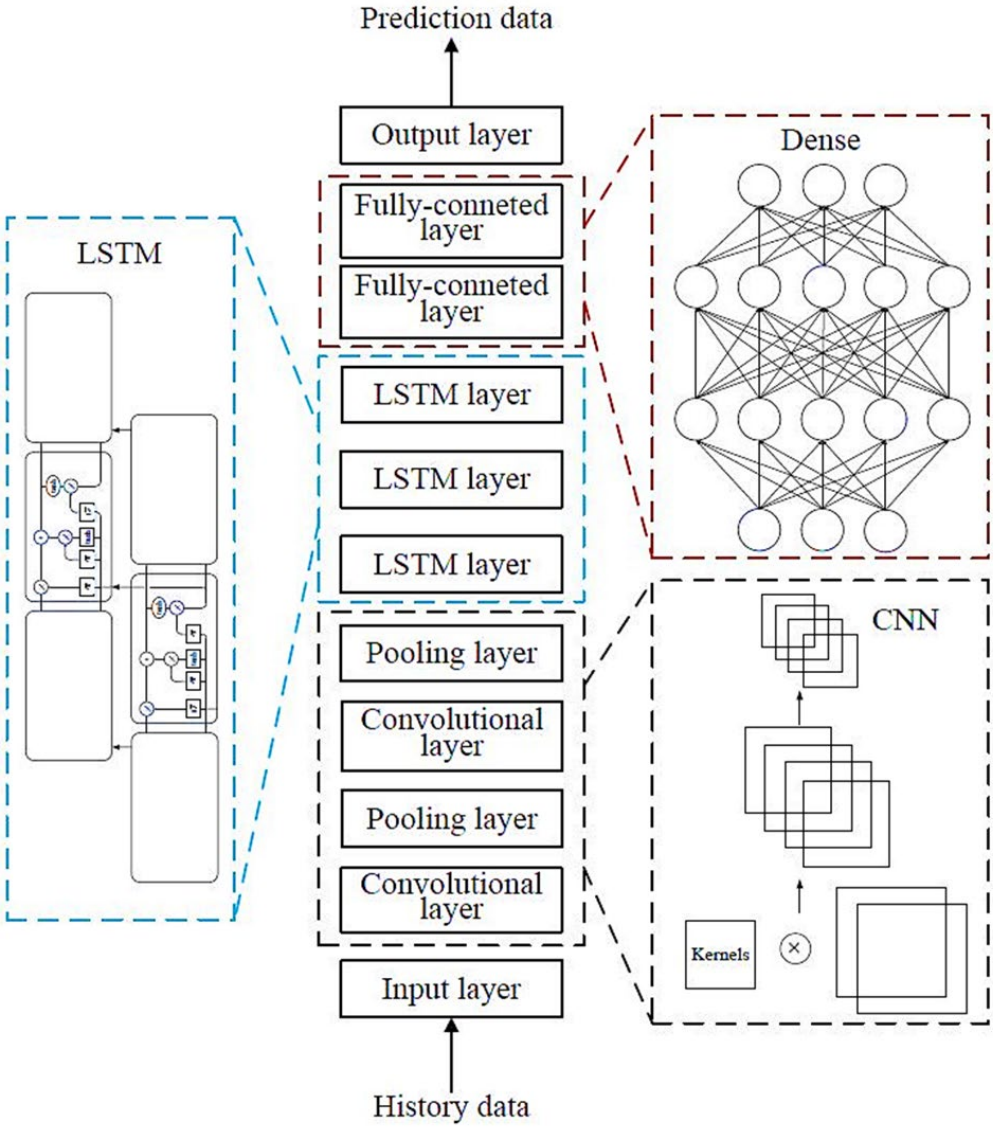

Figure 2.19 Configuration of the proposed battery TR prognosis method based on the CNN-LSTM [184].

Furthermore, Garg et al. [185] proposed an intelligent system framework based on DT to provide access to real-time big data cloud storage and address some serious issues, such

as switching malfunction, heat generation, changing temperature rise, SOC/SOH estimation, etc. Based on the proposed system, the hardware and software design for the reconfiguration battery system can be further integrated.

This section lists previous publications about battery fire and ML applied in battery fire prediction. It can be concluded that increasing ML methods are applied and developed in battery safety issues from many perspectives, such as TR, internal or external short circuits, temperature prediction, failure diagnosis, etc. Table 2.2 summarises the related research works that applied ML to improve battery thermal performance and enhance battery fire safety.

Table 2.2 Summary of the ML applied in battery fire safety research.

ML approach	Achievement	Reference
K-means clustering	TR initiation conditions	[175]
Decision tree; SVM; ANN	Mechanical loading conditions	[176]
CNN	Internal short circuit	[177]
MLP	Crack detection	[178]
MLP	Failures diagnose	[180]
Meta-TRFNN	Forecast TR	[181]
ANN	External short circuit	[182]

LSTM	Temperature prediction	[183]
LSTM & CNN	Temperature prediction; TR prognosis	[184]
DT	Heat generation; charging temperature	[185]

2.6.3 Hazard mitigation and safety control

Safety is the utmost priority in LIB applications in energy storage systems. Recent accidents with different failure mechanisms undermine the industry's confidence in using LIBs. To our knowledge, the TR mechanism has been studied using a time sequence map. The state transition in the time sequence map explains the potential mechanisms for all types of observations in TR tests. Effective hazard mitigation approaches have been investigated by understanding the TR mechanisms. Battery failures and TR hazards can be properly alleviated by researchers applying safety control actions under various practical scenarios, such as material, cell and system levels.

Mitigation strategies are fulfilled by cutting off a specific transformation flow between the states in the time sequence map. Figure 2.20 outlines the battery TR mechanisms and the thought of time sequence regulation. The safety design of battery systems aims to lower the possibility of abuse, eliminate abuse once it happens, and build TR alert systems at the earliest stage. A competent mitigation strategy that helps avoid the occurrence of TR is founded on the mechanisms of abuse conditions. Charging and temperature control are critical for battery safety and the TR system. The mitigation strategies work at

different levels and guarantee the global safety of an electric energy storage system using LIBs.

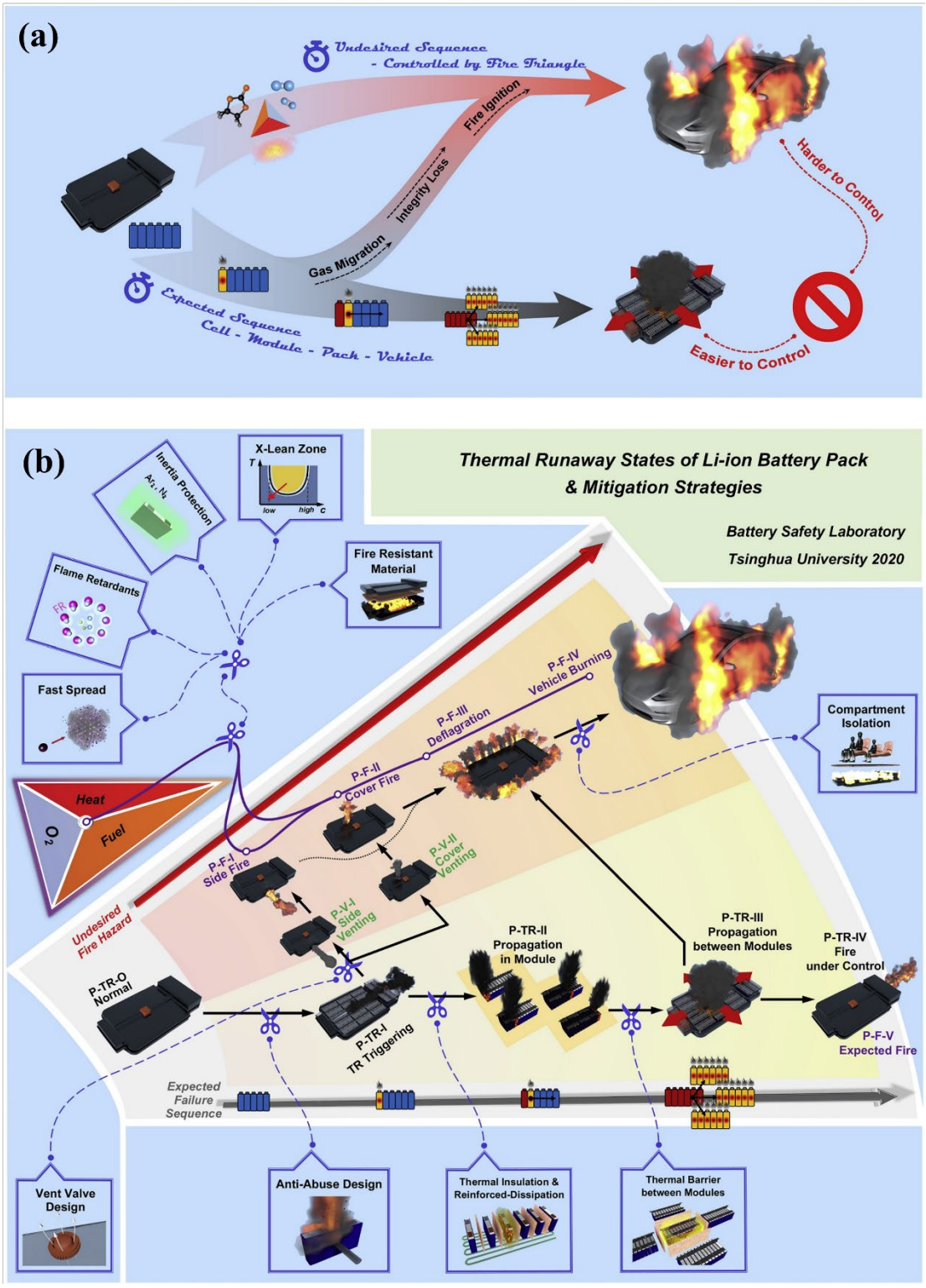

Figure 2.20 TR states of LIB pack and correlated mitigation strategies [186].

ML techniques have already been used in fire modelling [187], safety assessment [188] and fire prediction [189]. Yamanaka et al. [190] introduced a framework for performing multi-objective optimisation using ML methods at a reasonable computational cost. An analysis of the relationship between descriptors and predictors confirms a high correlation between fire spread and negative electrode active material diameter. Battery fire safety applied ML methods for mitigation and control is a potential direction that should be encouraged for the future direction.

2.7 Chapter Summary

Owing to the global interest in clean energy, electrification and net zero emissions, there is a rapid usage increase of battery systems with LIB systems being one of the largest applications. With overwhelming public expectations and more complex application scenarios, LIBs are experiencing unprecedented challenges including concerns regarding thermal resilience, fire and explosion risks.

This chapter aims at bringing new insights into the further application of ML in the field of battery thermal safety, shown in Figure 2.21. The emphasis was made on the three mostly used ML models including ANN, CNN, and LSTM. This chapter firstly introduced battery thermal models. After that, considering the application of ML techniques, this chapter reviewed two major topics: battery thermal management and

battery system safety. The following are the conclusive summaries that were drawn based on this literature review:

ANN, CNN and LSTM are three major ML models used in state-of-the-art publications for battery thermal stability and resilience studies. Due to multivariate analysis function, high precision, and excellent data noise tolerance, ANN is advantageous for parameters optimisation contributing to better and highly efficient BTMs design. CNN is utilised for pattern recognition in scenarios with thermal images involved in BTMs. LSTM leverages sequential or times series data and can be served a role in temperature prediction, monitoring, and early fire diagnostics and prevention.

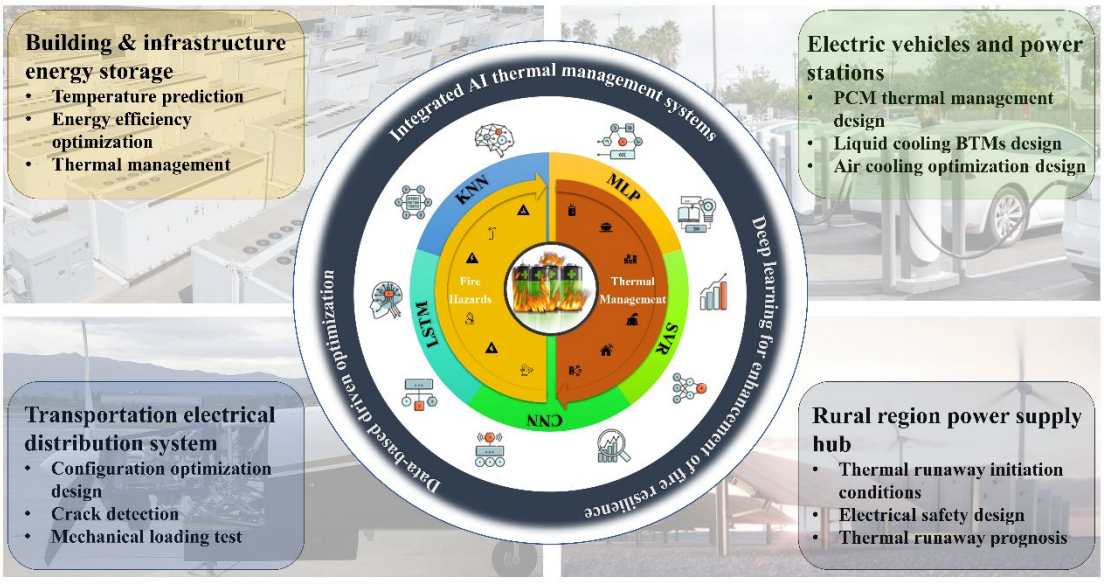

Figure 2.21 Summary of ML techniques potential applications.

Owing to the dramatic influence of the input data on the training process and output, the aforementioned ML models have their respective areas of expertise. Due to its high noise

tolerance, ANN is more suitable for experimental data with noise data. While for the numerical data, dimensionality and training time are two crucial factors in choosing. When it comes to temperature prediction or thermal hazards diagnosis with time series, LSTM is the first option to establish models, but vanishing gradients may appear owing to long series. Furthermore, DT technique, as a relatively new technology, is also applied in battery safety and BTMs. It shows great potential for computation power, data storage capability, and reliability of real-time simulation and responsiveness.

In general, these models were used in the thermal safety issue, but further development is imperative with a more flexible combination and more advanced models. Chapter 3 will introduce the methodology applied in this thesis with the related theory and formulations. The following two chapters will demonstrate the detailed applications of the integrated ANN-CFD framework in this thesis. Chapter 4 will present the analysis of the forced air-cooling directions (axial and radial of the battery cell) and various ambient environment pressures, while Chapter 5 will focus on the investigation of battery pack configuration, the ambient temperature, and the natural ventilation velocity based on the proposed framework.

Chapter 3 Methodology

3.1 General Description

In Chapter 1 and Chapter 2, the numerical modelling techniques and machine learning approaches have been demonstrated and reviewed. This chapter presents all the related models and methods for simulating and evaluating battery performances. As the multiple components comprise a single LIB cell, capturing all the physics and reactions in one model is difficult. Many numerical models focused on a specific character. For example, electrochemical performance is required for electrodes, and thermal stability is essential for the separator. Also, battery cells can work under various modes, such as single cells, battery modules, and battery packs. As per the previous review in Chapter 2, a single cell can be used for a small portable device, and the battery module can be applied for EVs and infrastructure energy storage systems. The thermal analysis for various working scenarios can be simulated through numerical models. Numerical simulations have advantages in delivering battery behaviour insights effectively and low-costly. CFD is a practical tool to study different thermal fluid dynamic parameters and simulate multiple physics fields with varying working domains. In this chapter, the three-dimensional

thermo-electrochemical battery model is introduced to characterise multiple parameters and performances during the battery working process. Moreover, machine learning technique, especially the MLP model, is adopted to find complex interrelations between various properties, and an integrated modelling framework is proposed. The mathematical theory of the governing equations of physical quantities is explained, including mass, momentum, and energy. The formulations of the electrochemical, thermal, and turbulence models are also discussed.

3.2 CFD Model

CFD is mainly dedicated to fluids in motion and how the fluid flow behaviour influences processes, including heat transfer and possibly chemical reactions in combusting flows [88]. Mathematical equations are applied to describe the fluid motion by physical characterisation, usually in partial differential form and called governing equations. CFD modelling is fundamentally based on the governing equations of fluid dynamics. These equations represent the mathematical statement of the conservation laws of physics. Also, the CFD model stands for the basic description of the fluid flow processes [191]. The appropriate numerical form of the physical boundary condition depends on the mathematical form of the governing equations and the numerical algorithm used [192]. Generally, the governing equations include mass, momentum, and energy conservation, which are expressed below:

Mass is conserved for the fluid, and the mass conservation equation:

$$\rho_a \left(\frac{\partial}{\partial t} + \nabla \vec{v} \right) = 0 \tag{3.1}$$

Based on Newton's second law, the momentum change rate equals the sum of forces acting on the fluid. The momentum conservation equation:

$$\frac{\partial (\rho_a \vec{v})}{\partial t} + \nabla (\rho_a \vec{v} \vec{v}) = -\nabla P_a \tag{3.2}$$

From the first law of thermodynamics, the rate of change of energy equals the sum of the heat added to and the rate of work done on the fluid. The energy conservation equation:

$$\frac{\partial \left(\rho_a C_{pa} T_a \right)}{\partial t} + \nabla \cdot \left(\rho_a C_{pa} \vec{v} T_a \right) = \nabla \cdot (K_a \nabla T_a) \tag{3.3}$$

These governing equations are used for computational procedures in finite difference or finite volume methods. In these equations, ρ, C_p, T, P, and K stand for the density, specific heat, temperature, pressure, and heat conductivity coefficient, respectively. The subscript a denotes the cooling air.

For the battery cell, the governing equations also can be applied. More specifically, the energy equation can be written as follows:

$$\rho_b C_{pb} \frac{\partial T}{\partial t} = \nabla \cdot (K_b \nabla T) + q \tag{3.4}$$

where q represents the heat generation rate per unit volume of a single battery, and the subscript b denotes the battery cell.

Moreover, the CFD methodology provides a numerical solution for turbulence flow. Compared to the other two-equation models, the k-ω model is the model of choice in the sublayer of the boundary layer, which demonstrates the advantage of treatment of low Reynolds number applications near the wall. However, it does not work well for

simulating the free stream flow as it tends to be dependent on an assumed value of ω [193]. The shear-stress transport k-ω model was suggested by Menter [194], which is a hybrid model that blends the advantages of both the standard k-ε model (the mainstream flow) and the k-ω model (near wall region). The shear-stress transport k-ω model has been widely used and was chosen to simulate the turbulence flow during the battery pack cooling process. The k-ω model has improved the accuracy of the turbulence model for predicting free shear flows. The major two components, turbulence kinetic energy k and the specific dissipation rate ω, are calculated from the following transport equations [195]:

$$\frac{\partial}{\partial t}(\rho k) + \frac{\partial}{\partial x_i}(\rho k u_i) = \frac{\partial}{\partial x_j}\left(\Gamma_k \frac{\partial k}{\partial x_j}\right) + G_k - Y_k + S_k + G_b \tag{3.5}$$

$$\frac{\partial}{\partial t}(\rho \omega) + \frac{\partial}{\partial x_i}(\rho \omega u_i) = \frac{\partial}{\partial x_j}\left(\Gamma_\omega \frac{\partial \omega}{\partial x_j}\right) + G_\omega - Y_\omega + D_\omega + S_\omega + G_{\omega b} \tag{3.6}$$

where G_k represents the production of turbulence kinetic energy. G_ω represents the generation of specific dissipation rate ω. Γ is the effective diffusivity and is calculated by the following equations (3.7) – (3.8). Y and S represent the dissipation, and user-defined source terms, respectively. D_ω stands for the cross-diffusion term. Moreover, G_b and $G_{\omega b}$ account for buoyancy terms. All the terms are calculated by the CFD software during the simulation process:

$$\Gamma_k = \mu + \frac{\mu_t}{\sigma_k} \tag{3.7}$$

$$\Gamma_\omega = \mu + \frac{\mu_t}{\sigma_\omega} \tag{3.8}$$

where σ_k and σ_ω are the turbulent Prandtl numbers for turbulence kinetic energy k and the specific dissipation rate ω, respectively, as well as the turbulent viscosity, μ_t, is calculated by k and ω. The normal model constants are σ_k=2.0 and σ_ω=2.0.

In Equations 3.5 and 3.6, the exact equation for the production of turbulence kinetic energy G_k and the production of specific dissipation rate G_ω are defined as follows.

$$\mathrm{G}_k = -\rho\overline{u_i{}'u_j{}'}\frac{\partial u_j}{\partial x_i} \tag{3.9}$$

$$\mathrm{G}_\omega = \alpha\frac{\omega}{k}G_k \tag{3.10}$$

where the coefficient α is given by Equation 3.11.

$$\alpha = \frac{\alpha_\infty}{\alpha^*}\left(\frac{\alpha_0 + Re_t/R_\omega}{1 + Re_t/R_\omega}\right) \tag{3.11}$$

where the constant α^* and Re_t are calculated by the below equations, and R_ω=2.95. In addition, in the high Reynolds number form of the k-ω model, α=α_∞=0.52, and α^*=α^*_∞=1.

$$Re_t = \frac{\rho k}{\mu\omega} \tag{3.12}$$

$$\alpha^* = \alpha^*_\infty\left(\frac{\alpha^*_0 + Re_t/R_\omega}{1 + Re_t/R_\omega}\right) \tag{3.13}$$

$$\alpha^*_0 = \frac{\beta_i}{3} \tag{3.14}$$

$$\beta_i = 0.072 \tag{3.15}$$

Also, the constant α^* is the coefficient that damps the turbulent viscosity and causes a low-Reynolds number correction. β_i is the constant.

3.2.1 Electrochemical battery model

The electrochemical model applied in Chapters 4 and 5 could be seen as a lumped version of a single particle model [196], simulating the transport of intercalated lithium in one of the electrodes. The single particle model predicts the temperature distribution and voltage changes in a single LIB cell during galvanostatic operations. The simplification of this model can be conducted when the battery is mainly controlled by the diffusion process in one of the electrodes only. The model is based on a complete model of a LIB working process cycle [85]. In this model, the lumped battery interfaces are utilised, and the battery cell voltage E_{cell} is calculated by applying time-dependent cell current I_{cell}. Additionally, the single battery cell is modelled by ohmic, exchange current and concentration losses. The battery open circuit voltage (OVC) is required, which has a relationship with battery state-of-charge (SOC).

The electrochemical model can represent the LIB performance, considering the internal migration of the lithium ion movements during the charging and discharging process. With an understanding of electrochemical mechanisms, the physical quantities, including voltage and current, can be fully described. The three-dimensional thermo-electrochemical model built in this section is based on a typical cylindrical $LiFePO_4$/Carbon power battery, considering the physical and electrical conservations, as well as thermal principles and electrochemical kinetics. The electrochemical reactions of common LIBs can be described as the following Equations (3.16) - (3.18), where M stands

for a metal, which is used as a cathode material such as cobalt or nickel, and *C* is recognised as the anode material [197].

The reaction at the positive electrode is described as:

$$LiMO_2 \leftrightarrow Li_{1-x}MO_2 + xLi^+ + xe^- \tag{3.16}$$

The chemical reaction at the negative electrode is expressed as:

$$C + xLi^+ + xe^- \leftrightarrow Li_xC \tag{3.17}$$

The overall reaction can be presented as:

$$LiMO_2 + C \leftrightarrow Li_{1-x}MO_2 + Li_xC \tag{3.18}$$

During the discharging process, lithium is oxidized from Li to Li^+, and the released lithium ions migrate through the electrolyte medium to the cathode. As stated in Equation (3.18), the reaction can be run reverse to recharge the cell.

Figure 3.1 demonstrates the working process of a typical LIB, and the fundamental cell unit is considered a sandwich structure, including the positive electrode, the separator, the negative electrode, and the current collectors located at both electrodes. The metal tab is joined at each correlated current collector and electrode. The separator is located between the cathode and anode, a porous polymer membrane to prevent physical contact of electrodes. The electrolyte is the medium that enables the ion transport mechanism between electrodes. It requires specific working conditions, such as significant ion conductivity, low-set electrical conductivity, extended temperature range of operation, thermo-dynamically stability at a certain range of voltages, environmentally friendly, etc.

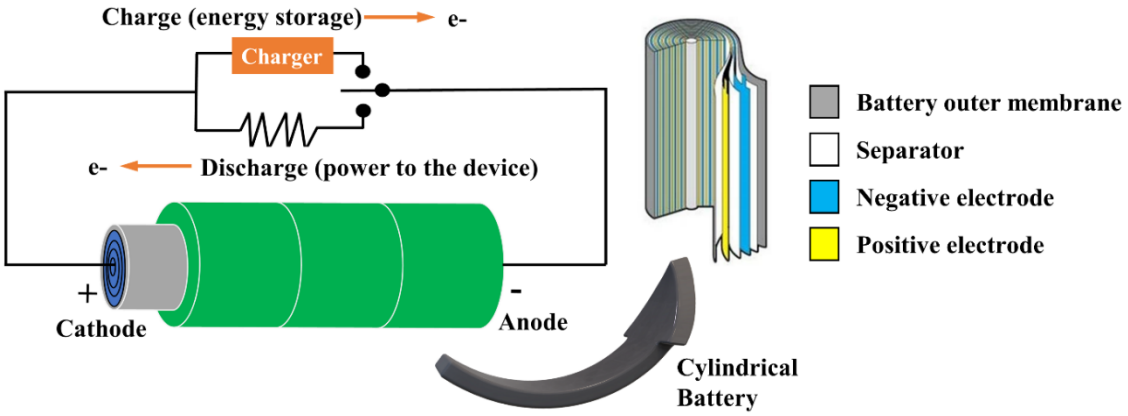

Figure 3.1 The principle of operation for a typical LIB and its structure.

Each electrode and separator are impregnated with electrolyte, achieving transportation of lithium ions. The material parameters for the electrolyte refer to a plasticised ethylene carbonate/dimethyl carbonate (EC/DMC) electrolyte remaining in a polymer matrix. Therefore, the stated electrolyte volume fraction points to this model's total liquid electrolyte and polymer matrix volume fractions. In this model, the potential losses η_{IR} due to ohmic and charge transfer processes are given as follows:

$$\eta_{IR} = \eta_{IR,1C} \frac{I_{cell}}{I_{1C}} \tag{3.19}$$

where $\eta_{IR,1C}$ represents the potential losses under the 1C current. The 1C current I_{1C} means that the discharge current will discharge the entire battery in one hour, and it is calculated as:

$$I_{1C} = \frac{Q_{cell,0}}{3600\ \mathrm{s}} \tag{3.20}$$

The overpotential associated with ohmic losses inside the cell, η_{ohm} (V), is calculated by:

$$\eta_{ohm} = R_{ohm} I_{cell} \tag{3.21}$$

The SOC is defined by the battery current [198], shown as:

$$\frac{\mathrm{dSOC}}{\mathrm{dt}} = \frac{I_{cell}}{Q_{cell,0}} \tag{3.22}$$

Waag et al. [199] demonstrated that the accuracy of state-of-power assessment models could be improved by bringing in a non-linear value in the current-voltage dependency. The dimensionless charge exchange current J_0 is introduced to calculate the activation overpotential inside the battery, η_{act} (V), given as:

$$\eta_{act} = \frac{2rT}{F} asinh\left(\frac{I_{cell}}{2J_0 I_{1C}}\right) \tag{3.23}$$

Other voltage losses are caused by diffusion in an idealised particle or by applying a resistor-capacitor pair. Wang et al. [200] concluded that adding a stemming from a diffusion impedance can improve power prediction. In this section, with the assumption that only one of the electrodes affect the potential loss on the cell level, just one particle is considered. The diffusion of a dimensionless SOC variable is calculated for a 1D geometry with a dimensionless spatial variable X between 0 and 1 using spherical symmetry, given as:

$$\tau \frac{\partial SOC}{\partial t} = -\nabla \cdot (-\nabla SOC) \tag{3.24}$$

The interval stands for an average particle of the electrode controlling the battery, where ranging from 0 to 1 representing from the centre to the surface of the particle.

Then, the boundary conditions of the limitation positions are as follows:

$$\nabla SOC = 0|_{X=0} \tag{3.25}$$

$$\nabla SOC = \frac{\tau I_{cell}}{Q_{cell,0} d}\Big|_{X=1} \tag{3.26}$$

where *d* equals 3 for spherical particles. The surface SOC is identified at the surface of the particle. The average SOC is described by integrating over the volume of the particle, appropriately considering spherical coordinates, and is defined as:

$$SOC_{aver} = \frac{\int_0^1 SOC 4 \prod X^2 \, dX}{\int_0^1 4 \prod X^2 \, dX} = 3 \int_0^1 SOC X^2 dX \tag{3.27}$$

The lumped potential losses associated with concentration overpotential are shown as,

$$\eta_{conc} = E_{ocv}(SOC_{surf}) - E_{ocv}(SOC_{aver}) \tag{3.28}$$

Ultimately, the battery cell voltage E_{cell} is defined as:

$$E_{cell} = E_{ocv}(SOC_{aver}) + \eta_{ohm} + \eta_{act} + \eta_{conc} \tag{3.29}$$

Replacing the expression for η_{conc}, E_{cell} can also be defined as:

$$E_{cell} = E_{ocv}(SOC_{surf}) + \eta_{ohm} + \eta_{act} \tag{3.30}$$

For the lumped battery interface model, Arrhenius expression is applied to model each battery cylinder, with temperature-dependent ohmic, exchange current, and diffusion time-constant parameters. Applying axial symmetry to the model is because some simplification can be achieved for a spirally wound cylindrical battery. For example, the heat conduction in the spiral direction can be neglected. Furthermore, rather than modelling the heat conduction in each layer of the wound sheets in the radial direction (e.g., in each positive electrode layer, each separator layer, and so on), the wound sheets are modelled as one active battery material domain. These approximations are reasonable

for spiral wound battery cells cooled by natural convection [201, 202]. The thermal model also accounts for the conservation laws, which applies Navier–Stokes equations to characterise the flow behaviour [203, 204], including conservation of mass, conservation of momentum and conservation of energy.

A cylindrical coordinate system is introduced to solve the orthotropic thermal conductivity in the combination cell material. Since the cylindrical battery has a spiral winding structure, the thermal conductivity of the electrolyte is anisotropic. Considering the enthalpy equation and the temperature equation, the energy conservation for incompressible fluid can be simplified to:

$$\rho C_p \frac{\partial T}{\partial t} + \rho C_p \boldsymbol{v} \cdot \nabla T = \nabla \cdot (k \nabla T) + H \tag{3.31}$$

where H represents the domain and boundary heat sources based on the sum of irreversible heat, such as Joule heating (charge transport in the electrolyte and the solid conductor materials) and activation losses (overpotentials in the electrode reactions), and reversible heat in an electrochemistry interface (entropy changes in the electrode reactions).

3.2.2 Thermal battery model

In this study, the thermal model is based on a previous two-dimensional axial symmetry approach, simulated by the Heat Transfer in Solids module. A spirally wound type of battery is chosen for this simulation, and the simplification of the heat conduction can be

achieved along the spiral direction. Moreover, instead of simulating the heat conduction in each layer along the radial direction, the wound sheets are acted as a combination cell material domain. These approximations are understandable for spiral wound battery cells cooled under natural convection. The model configuration comprises three connection sections: 1) Battery outer can; 2) A combination cell material domain; 3) Central axis (mandrel where the battery cell sheets are wound). The geometry of the model is shown in Figure 3.2.

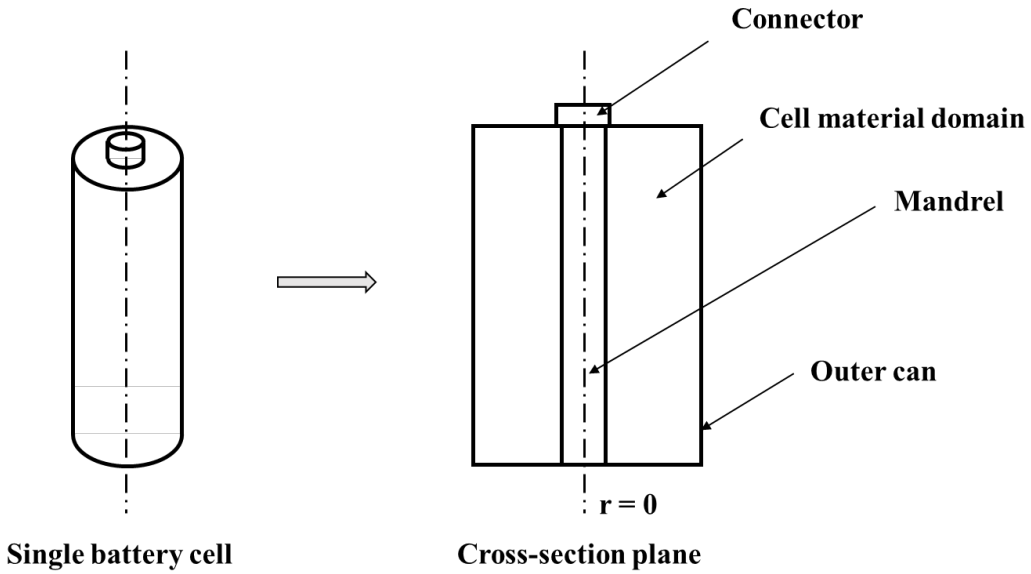

Figure 3.2 Configuration of the applied thermal model for a cylindrical LIB.

For this model, several equations and parameters are considered. Considering the anisotropic thermal conductivities in this model and differences among various directions [205], the thermal conductivities along the radial path, $\kappa_{T,r}$, and along the cylinder length direction, $\kappa_{T,ang}$, are defined separately as follows:

$$\kappa_{T,r} = \frac{\sum L_i}{\sum L_i / \kappa_{T,i}} \tag{3.32}$$

$$\kappa_{T,ang} = \frac{\sum L_i \, \kappa_{T,i}}{\sum L_i} \tag{3.33}$$

The density ρ_{batt} and heat capacity $C_{p,batt}$ for the combination cell material domain is defined as stated by the following equations:

$$\rho_{batt} = \frac{\sum L_i \, \rho_i}{\sum L_i} \tag{3.34}$$

$$C_{p,batt} = \frac{\sum L_i \, C_{p,i}}{\sum L_i} \tag{3.35}$$

The heat source produced by the combination cell material domain is identified by employing the Electrochemical Heating Multiphysics coupling module. However, the heat source term in the combination cell material domain is scaled to solve the lack of heat generation in the current collectors and the canister thickness. This mounted heat source is acquired by multiplying two factors of the volumetric heat source from the 1D LIB model. The former factor is the fraction of the total 1D model in which heat is produced. That is the total length value of electrodes and the separator, divided by the total battery length, including the measurements of both current collectors. The latter factor is the fraction of the entire 3D cylindrical battery. The volume in which heat is produced is the cell's total volume, including the homogenized wound layers of the cell material, the centre axis, and the battery case, minus the volume of the outer case and the volume of the battery centre axis. This heat source is then divided by the total volume of the battery cell domain, which is the difference between the whole battery volume and

the centre axis volume. Thereby, the following equation for the 3D heat source is demonstrated:

$$Q_{h,3D} = Q_{h,1D}\frac{L_{neg} + L_{sep} + L_{pos}}{L_{batt}}\frac{((r_{batt} - d_{can})^2 - r^2{}_{mandrel})(h_{batt} - 2d_{can})}{(r^2{}_{batt} - r^2{}_{mandrel})h_{batt}} \tag{3.36}$$

where the subscripts express the specific parts in the battery model, including the total battery (*batt*), negative electrode (*neg*), positive electrode (*pos*), the battery outer can (*can*), and the battery central mandrel (*mandrel*). In addition, Q_h stands for the heat source with subscripts of one-dimensional model (*1D*) and three-dimensional model (*3D*).

For the lumped battery interface model, Arrhenius expression is applied to model each battery cylinder, with temperature-dependent ohmic, exchange current, and diffusion time-constant parameters. The cell battery model and thermal model are coupled by using the average values for the temperature and generated heat, shown in Figure 3.3. The thermal conductivity in the combination cell material domain is anisotropic due to the spiral type of the battery. The orthotropic thermal conductivity in the combination cell material domain is solved by introducing a cylindrical coordinate system in the model. The zero-Mach-number limit of the compressible conservation equations was applied to depict the flow movement and heat transfer. Heat convection, conduction and radiation are considered to model the heat transfer between the battery pack and the ambient environment. The average heat source calculated from the cell model contributes to the temperature equation in fluid domains. Regarding the enthalpy equation and the

temperature equation, the energy conservation for incompressible fluid can be simplified, which is shown in Equation (3.31).

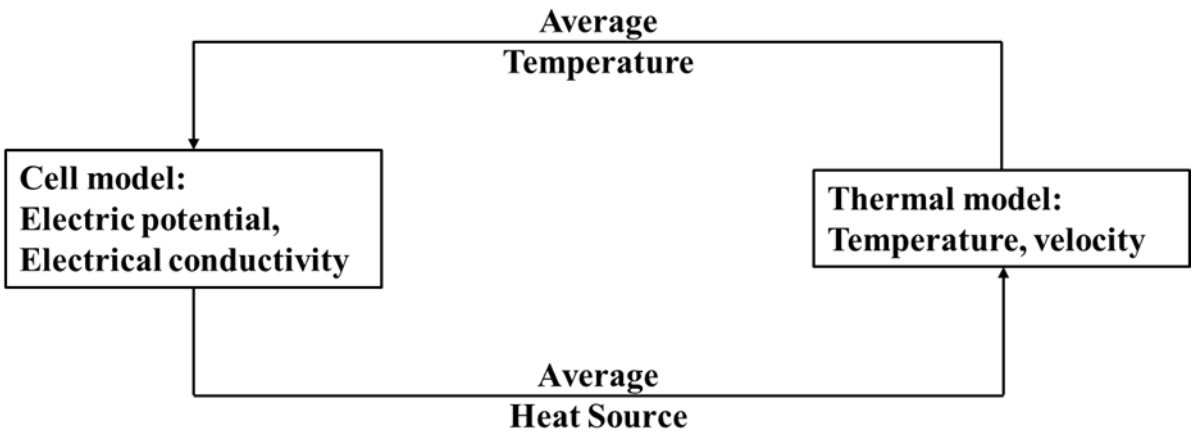

Figure 3.3 Coupling between the cell and thermal model.

3.3 ANN Model

Artificial intelligence has been rapidly developed in recent decades. ANN approach as a popular tool is able to model a wide range of engineering systems contributed by its ability to learn and adapt to find complex interrelations between various properties. This approach is based on the way neurons interacts and function in the human brain. In Chapters 4 and 5, Multi-Layer Perceptron (MLP) model is applied to optimise the operating parameters and ambient conditions based on CFD numerical results. In Chapter 2, a brief introduction to ANN has been demonstrated. This section presents detailed information on the applied ANN model for this study.

The ANN approach for solving problems has seven primary steps, similar to the standard working steps of neural networks, including collecting data, creating the network, configuring the network, initialising the weights and biases, training the network, validating the network, and using the network. These steps are also applied in this thesis.

Multi-Layer Perceptron (MLP) is one of the most popular ANNs, which utilises a supervised training process using examples of data with known outputs [156]. A hidden layer in an ANN is a layer in the middle of input layers and output layers, where artificial neurons take in a set of weighted inputs and generate outputs through an activation function. The initial inputs are external data, such as images, values and documents. The ultimate outcomes complete the task, such as identifying an object from a snap.

An ANN model has five main components: inputs, summation functions, weights, activation functions, and outputs, as shown in Figure 3.4. The network is constructed by connecting the result of specific neurons to the input of other neurons, generating a directed, weighted graph. The weights and the functions that compute the activation can be adjusted by a procedure called learning, which is controlled by a learning rule or training method. The summation function (denoted by *E*) is a function that calculates the net inputs expressed as [206, 207]:

$$E = \sum_{j=1}^{n} w_{ij} x_j + w_{bi} \tag{3.37}$$

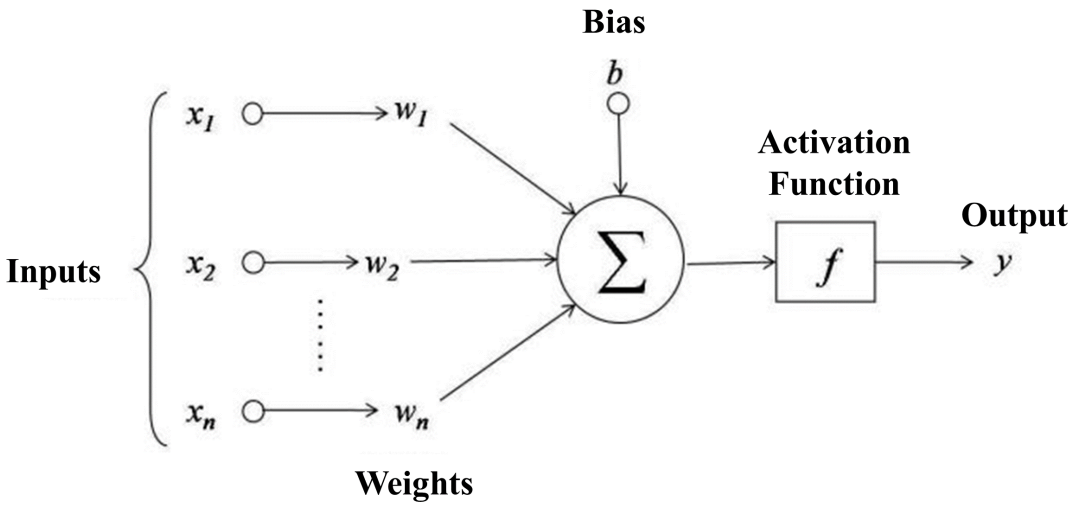

Figure 3.4 A typical multilayer perceptron neural network architecture.

The activation function of a node formulated the output of that node, or "neuron," specified an input or set of inputs. The activation function provides a curvilinear interrelation between the input and output layers. Commonly used activation functions are the threshold function, step activation function, sigmoid function and hyperbolic tangent function [208, 209]. The logistics sigmoid function is adopted in this study and is given by:

$$f(E) = \frac{1}{1 + e^{-E}} \tag{3.38}$$

The number of hidden neurons determined by the formulation according to neural network design [210, 211] is given by:

$$N_h = \frac{N_s}{\left(\alpha(N_i + N_o)\right)} \tag{3.39}$$

where α is a scaling factor ranging from 2-10. In this study, α is prescribed as 2 to achieve an optimal solution without overfitting, and ten hidden neurons were applied in the ANN model.

Compared to a single-layer network, the MLP can be used for arbitrary classification problems [212]. On the other hand, some limitations of MLP also exist, such as underfitting or overfitting. Early stopping and retraining are also applied to ensure the generalisation of MLP. The MLP algorithm has been widely used in various engineering applications with the advantages of fast convergence and strong versatility. In this thesis, to solve nonlinear functions and value optimisation, the optimal function is fitted by the backpropagation networks learning algorithm. As shown in Figure 3.5, the ANN training procedure is demonstrated and explained. The network learns about internal characteristics and structures by comparing the output processed from the input with the target. Moreover, the training process is reflected in adjusting the connection weights of the neural network, and the network weights should gradually converge to the target value. The iteration of the training algorithms can be written as:

$$X_{k+1} = X_k - \beta_k g_k \tag{3.40}$$

where X_k is the vector of the current weight and bias, β_k is the learning rate, and g_k is the current gradient. The iteration stops until the network comes to converge.

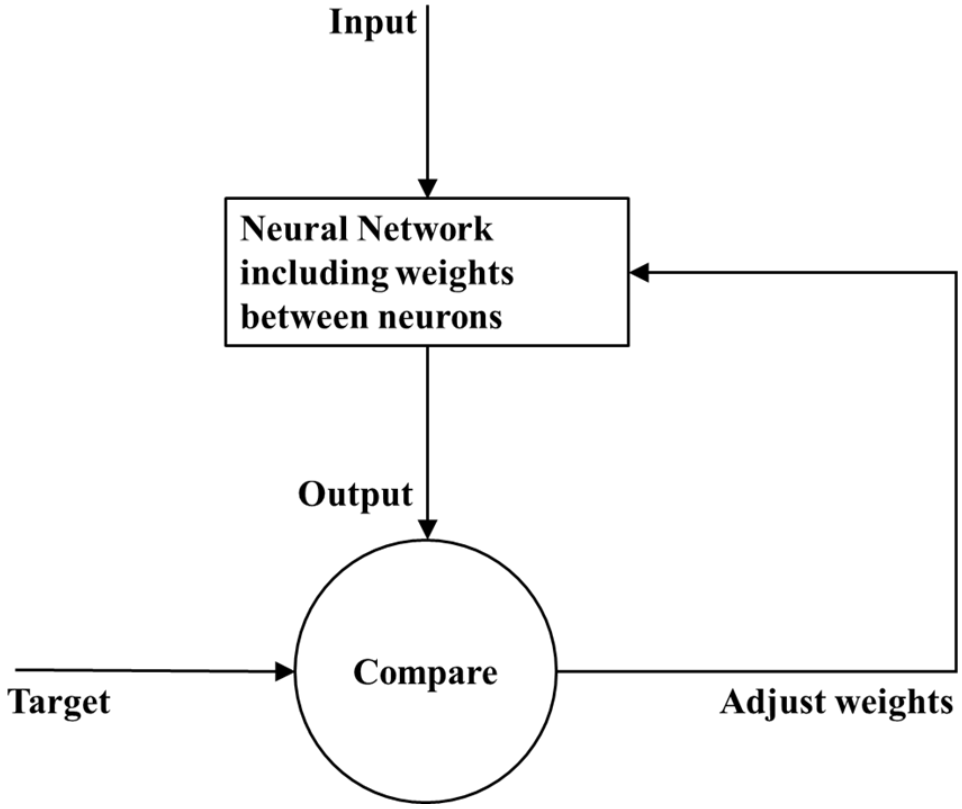

Figure 3.5 Neural network training procedure.

In this section, the training function updates weight and bias values based on the Levenberg-Marquardt optimization. The training stops when the maximum number of epochs is reached or the maximum time is exceeded. After training the data, the validation should be carried out. Firstly, the network performance should be checked, which was the second argument returned from the training function, including the value of the performance function, the magnitude of the gradient, etc. After that, a regression plot is created to validate the network, demonstrating the relationship between the outputs of the network and the targets. The regression plots show the training, validation and testing data, proving the network is sufficiently accurate.

In addition, there are different ways to improve the training and validation results. First of all, the network can be initialised and trained multiple times; different network parameters may produce different solutions each time. On the other hand, increasing the number of hidden neurons (no more than 20) is another method to improve the training results due to the increased flexibility for the network can generate more parameters to optimise. Moreover, applying a different training function may produce different results as well. Finally, using more training data is more likely to result in a better functioning network.

The validation results of the applied ANN model will be demonstrated in sections 4.3.5 and 5.3.2. Various parameters of battery operating and working conditions are considered in this thesis. By viewing the evaluation of the battery cooling performances, the maximum temperature of the battery pack and the temperature difference among the battery pack are selected as the outputs of the ANN model. To study the battery operation conditions and other ambient conditions, these parameters are set as the inputs from the numerical cases in a specific range. The detailed numerical data and optimisation results will be demonstrated and discussed in Chapters 4 and 5. The overall optimisation flowchart is shown in Figure 3.6.

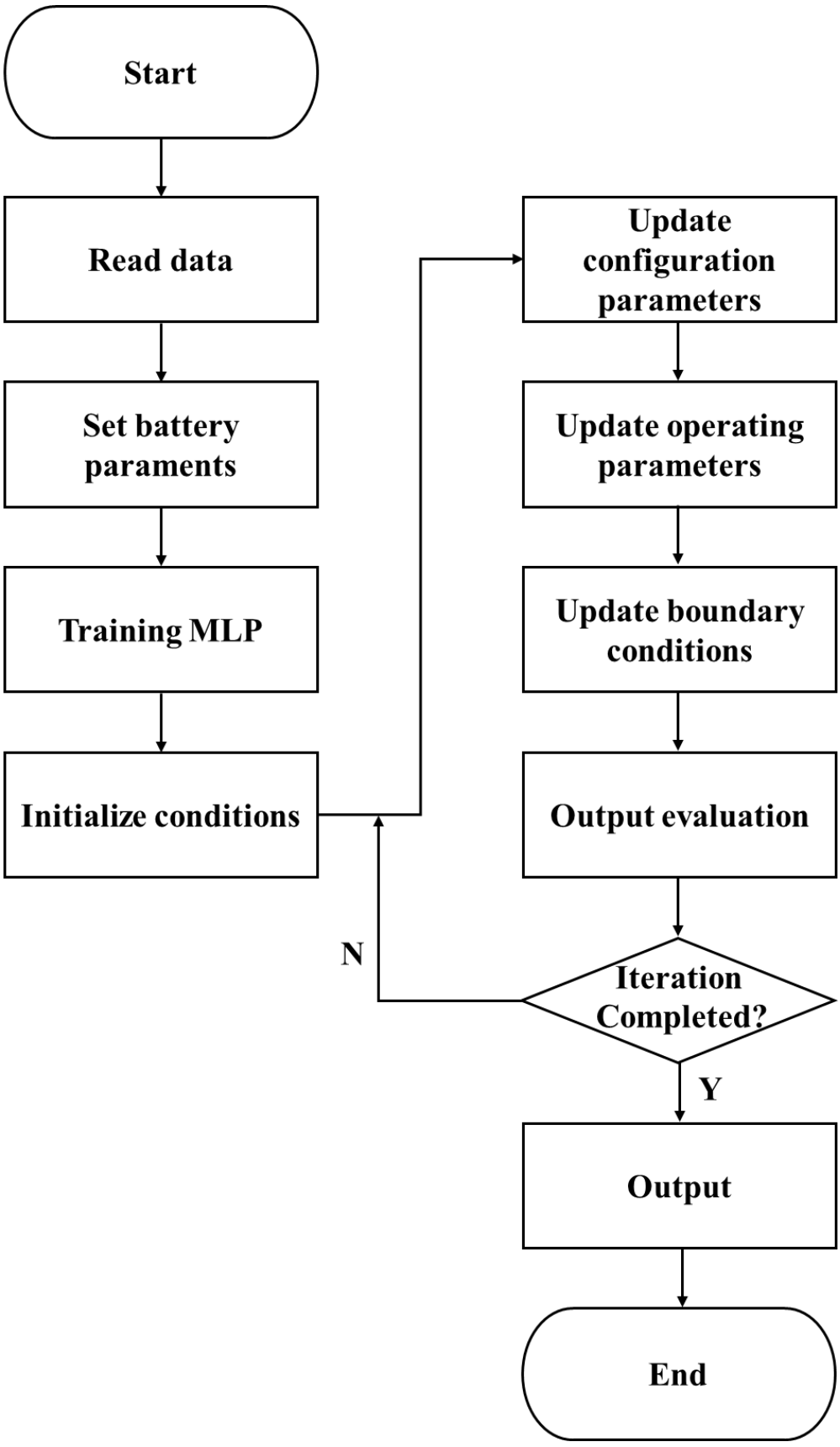

Figure 3.6 The flowchart of MLP optimisation algorithm.

3.4 Chapter Summary

In this chapter, all the numerical methodologies involved in this thesis were demonstrated. The electrochemical battery model and thermal battery model were introduced. A three-dimensional thermo-electrochemical was established using the CFD framework. Based on the fundamentals of fluid dynamics and thermal dynamics, three conservations were considered, including mass, momentum, and energy. The connection between the battery and thermal models was explained as well. After that, the commonly used ANN model in machine learning techniques was introduced. The architecture of the typical ANN model was demonstrated, and the activation function was shown, as well as the expression of the determination function of the hidden layer. The overall working process of the ANN model was demonstrated at last. The training and validation results were presented in the following chapters.

Chapter 4 Lithium-ion Battery Thermal Management Systems and Cooling Systems

This chapter includes the contents from a published journal article [131]: **Li, A.**, Yuen, A. C. Y., Wang, W., Weng, J., & Yeoh, G. H. (2022). Numerical investigation on the thermal management of lithium-ion battery system and cooling effect optimisation. *Applied Thermal Engineering*, 215, 118966. with modifications and reorders to better fit the structure of this thesis.

4.1 General Description

On the basis of the literature review in Chapter 2, the widespread application of lithium-ion batteries as the practice facility of energy storage has come alongside many unforeseen fire safety and thermal runaway issues that leads to increasing research interests. A comprehensive understanding of the thermal features of battery packs and the heat exchange process of energy storage systems is imperative. In this chapter, a three-dimensional thermo-electrochemical model has been developed to simulate the detailed temperature distribution of battery packs applying the methodology in Chapter 3. The numerical analysis of the cooling effect with both natural and forced air ventilation

configurations is compared as well. Moreover, the ANN model was coupled with the CFD simulation results to perform an optimisation of a specific configuration battery system considering configuration dimensions and operating conditions simultaneously. The ANN model builds a relationship between battery spacing and ambient cooling properties. It was found that the changing of ambient pressure creates a larger temperature drop under forced air cooling than that under natural ventilation. The optimum design for the battery pack can decrease the maximum temperature and the temperature difference by 1.94% and 17%, respectively. Overall, the present modelling framework presents an innovative approach to utilising high-fidelity CFD numerical results as inputs for establishing ANN training dataset, potentially enhancing the state-of-art thermal management of lithium-ion battery systems and reducing the risks of thermal runaway and fire outbreaks.

4.2 Introduction

In the previous chapters, the background of LIB has been introduced, and a better understanding of the battery thermal behaviour should address the unforeseen fire safety concerns. When compared to other kinds of batteries, LIB shows less thermal stability, which may drive thermal runaway, and many accidents have happened in recent years [213, 214]. Once a thermal runaway happens, it is easy to propagate from one cell to the whole energy system, while it is difficult to be detected and isolated. Therefore, it is crucial to investigate the LIB thermal runaway process by accurately monitoring and

predicting temperature dynamics during thermal propagation and implementing effective methods to prevent LIB fire accidents and improve fire safety.

Pioneer researches demonstrate that an overtemperature causes thermal runaway, then the heat is accumulated, and other exothermic chemical reactions are triggered [215]. There are two major focal points of thermal management in battery systems, which are handling the charge/discharge cycle and governing the battery heat growth [216]. Usually, the latter has a close relationship with the former. Air cooling of the battery system has been studied intensively as the most traditional cooling approach and is widely applied in the commercial field [217]. The following research works further addressed the advantages and shortcomings of the air-based cooling BTMs, which have been introduced in Section 1.1. Tong et al. [218] established a 2D dimensional thermo-electrochemical coupled model to study the thermal behaviour of forced air cooling with various operation parameters, containing air inlet velocity, cell configuration, cell-to-cell distance and presence of reversal airflow. Yang et al. [219] presented a study of the thermal capability of axial flow air cooling for LIB. Factors including power consumption, space efficiency and temperature uniformity were assessed. Saw et al. [220] numerically studied the thermal capabilities of the battery pack with different air mass flow rates, and the interrelationship between the Nu number and Re number was deduced and validated. Moreover, the proposed method provides an easy way to assess the thermal performance of the LIB pack. E et al. [221] applied a numerical study on the various air cooling plans by shifting the inlet and outlet location, and the application of the baffle plate was considered as well. A parametric study on forced air cooling for the thermal behaviour of

the LIB pack was demonstrated by Lu et al. [222]. It also concluded that packing more batteries along the flow direction is appropriate for battery cooling requirements. Li et al. [223] proposed a complete method to form an efficient air-cooling system, which improved the thermal performance of the battery module. Although the performance of the air cooling method has been investigated and optimised, the optimised parameters were achieved by a trade-off in a specific consideration. Few studies focus on a wider balance of multiple parameters simultaneously and provide a particular solution for various LIB working scenarios, especially for different pressure conditions. Severino et al. [224] proposed a battery thermal management system design to achieve several goals, including cost reduction, increasing lifetime and capacity, and higher safety, using a novel Multi-Objective Particle Swarm Optimisation approach. Furthermore, battery thermal management is affected by many cooling conditions, which benefit the working performance, safety performance and lifecycle of LIBs [225-227]. With the wide application of the LIB energy storage system, the ambient environment also plays an important role in the LIB thermal performance, such as LIB applied on plateau, aircraft, and spacecraft. Chen et al. [228] carried out an experimental investigation to evaluate the fire risks of LIB at various ambient pressures. Liu et al. [229] analysed the effect of pressure and pile sizes on battery thermal runaway. Wang et al. [230] found that with the lower ambient pressure, a longer thermal runaway trigger time and a lower maximum battery surface temperature will achieve. Compared to other cooling methods, the ambient pressure directly affects the air cooling efficiency and the occurrence and

development of LIB fires. Pressure influences on the cooling performance can be further studied, and comprehensive optimisation can be achieved.

With the blowout development of computer science, machine learning, which is able to construct the relationship between the driving factors, has been widely applied in many fields, such as industry and agriculture. The application of machine learning gives us confidence in battery thermal management investigation and optimisation. Qian et al. [231] applied a Bayesian neural network to optimise cell arrangement to enhance the cooling performance of the battery pack. However, pioneering studies have proved the potential of applying a machine learning approach to LIB thermal management problems. The ambient pressure effect on the cooling performance has not been fully addressed. Moreover, the battery spacing and other parameters, such as the cooling direction and the ambient pressure, should be considered simultaneously to enhance battery thermal performance further. ANN model is able to characterise the interrelation between inputs and outputs by using a collection of interconnected nodes (perceptron). The combination of ANN and CFD models for battery research is still relatively new. Hence, the approach with coupling thermo-electrochemical model and ANN model is proposed to analyse the LIB cooling performance and optimise the LIB configuration design by enhancing the fire performance. Figure 4.1 illustrates the schematic figure of the proposed model in this research.

To this end, the battery temperature distributions of the battery pack should be analysed, which can also be represented as a prediction at the early stage of the LIB thermal runaway. Furthermore, a better understanding of thermal behaviour can be achieved with

the numerical analysis of different cooling directions. In this chapter, the following points are addressed:

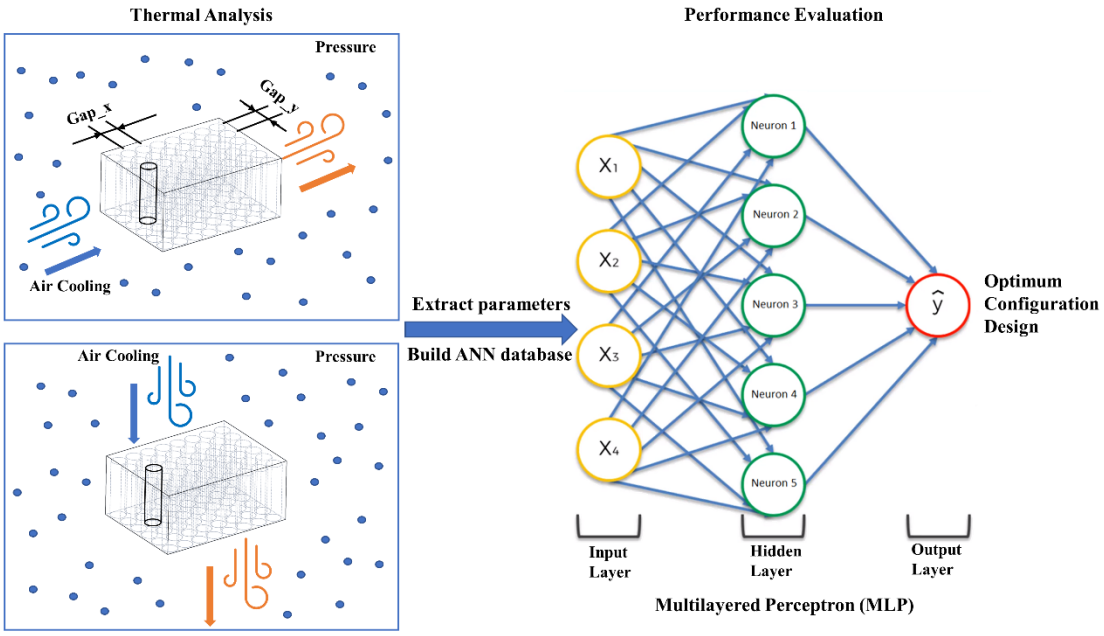

Figure 4.1 Schematic of the proposed approach with coupling thermo-electrochemical model and ANN model.

(i) Develop a 3D thermo-electrochemical model to capture the temperature distribution of both single-cell and LIB packs under normal working conditions.

(ii) Analyse the LIB pack thermal behaviour under various working conditions, including cell space, ambient pressure, and cooling air directions.

(iii) Coupled thermo-electrochemical model with the ANN model to optimise the LIB energy storage system configuration design and improve the cooling efficiency.

The outline of this chapter is summarized as follows: Section 4.3 demonstrates the numerical setup, simulation results with validation, and optimisation results. Finally, Section 4.4 summarises the numerical analysis of this section.

4.3 Results and Discussions

4.3.1 Thermo-electrochemical model setups

The three-dimensional thermo-electrochemical model built in this work is based on a battery pack with 48 cylindrical cells, as shown in Figure 4.2. The battery space is defined by Gap_x and Gap_y. The dimensions of every single cell are 70 mm (height) and 21 mm (diameter). In describing batteries, C-rate is applied to express discharge current, which measures the rate at where a battery is discharged relative to its maximum capacity. The nominal capacity for each cylindrical cell is 4 Ah, and the nominal voltage is 3.6 V. Each cell also has two terminals on both electrodes with dimensions of 3 mm (terminal radius) and 1mm (terminal thickness). The cylindrical cells are connected by aluminium strips. The connection type of this battery pack is coupling two cells in parallel. Then the coupled pairs are connected in series. The height and depth of serial connectors are 1 mm and 2 mm, while the dimensions of parallel connectors are 0.5 mm in height and 1 mm in width. The other parameters of the LIB are listed in Table 4.1.

Table 4.1 Parameters of the single cell applied in the LIB pack.

Parameter	Value	Description
C_rate	4	C rate
κT_batt_ang	30[W/m/K]	Thermal conductivity, in plane
κT_batt_r	1[W/m/K]	Thermal conductivity, cross plane
Ea_eta1C	24[kJ/mol]	Activation energy
Ea_J0	-59[kJ/mol]	Activation energy
Ea_Tau	24[kJ/mol]	Activation energy
T0	20[°C]	Reference temperature
J0_0	0.85	J0 at reference temperature
tau_0	1000[s]	tau at reference temperature
eta_1C	4.5[mV]	eta_1C at reference temperature
rho_batt	2000[kg/m^3]	Battery density
Cp_batt	1400[J/kg/K]	Battery heat capacity
ht	30[W/m^2/K]	Heat transfer coefficient
T_init	20[°C]	Initial/external temperature

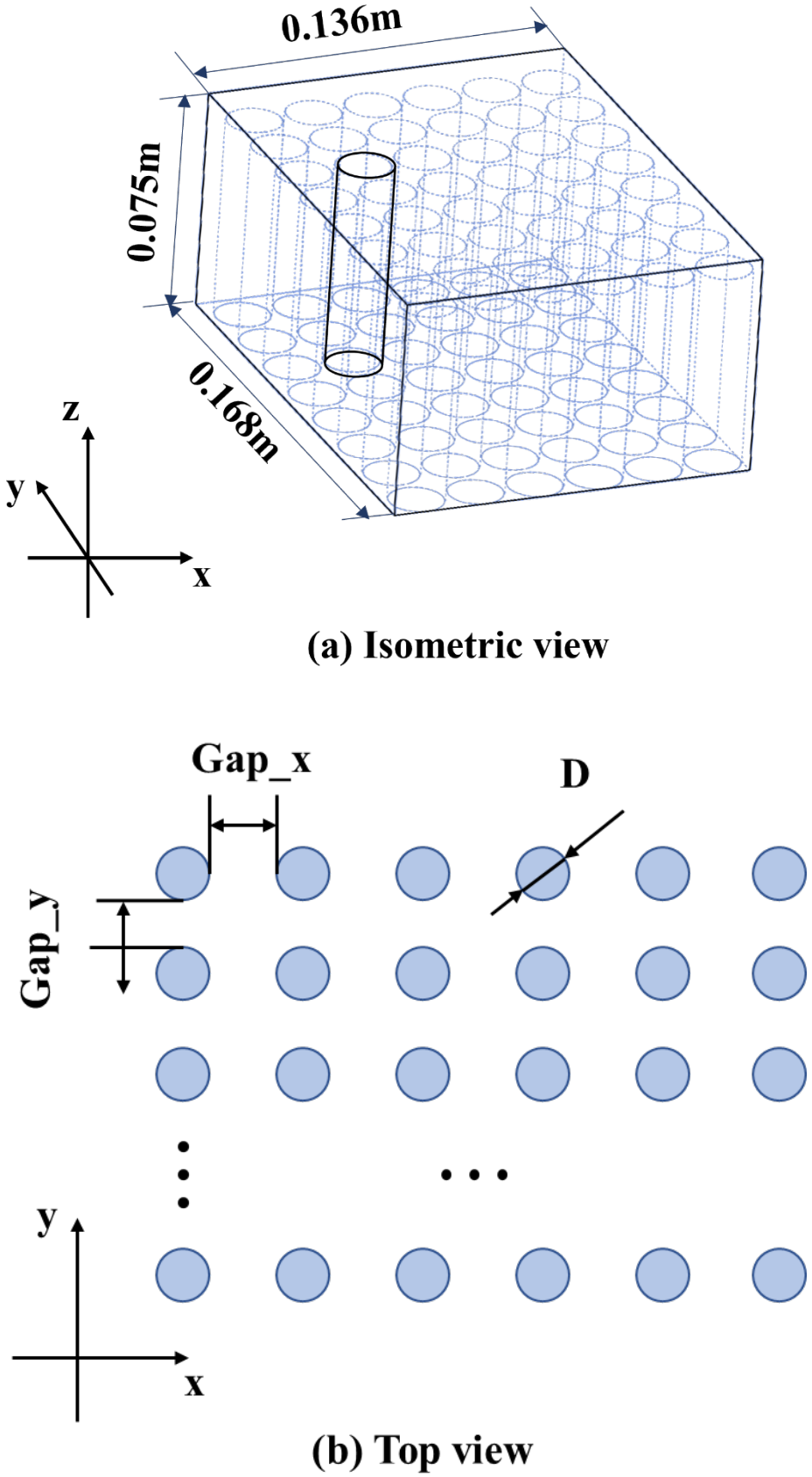

Figure 4.2 Schematic of the LIB pack configuration.

As the model described in Section 3.2.2, the lumped battery interface is applied to model each battery cell with temperature-dependent ohmic, exchange current and diffusion time-constant parameters. With the assumptions and cell nominal capacity, the generated heat is simulated by the thermos-electrochemical model according to Arrhenius expressions.

4.3.2 Model validation

In this section, a finite element based industrial software, COMSOL Multiphysics 5.5, was chosen to solve the three-dimensional thermal-electrochemical model. The mesh was generated by the default mesh module and solutions for mesh independence were examined. For battery variables, the MUMPS time-dependent solver was applied, and for heat transfer variables, the PARDISO solver was chosen. The validation of the electrochemical model is on the basis of a Type 38120 battery cell with a nominal voltage of 3.2 V and capacity of 10 Ah, as well as the thickness of the cathode, the separator and the anode are 91 μm, 40 μm and 142 μm, respectively. The positive electrode is made of iron phosphate ($LiFePO_4$) and the active material particles of amorphous carbon (LiC_6) are applied to the negative electrode. The electrolyte is a mixture of lithium hexafluorophosphate ($LiPF_6$), which is dissolved in a nonaqueous liquid mixture of ethylene carbonate (EC) and dimethyl carbonate (DMC) with a proportion of 1:2. The base case of the thermal model is a cylindrical 18650 LIB. The dimensions of the thermal model include the working battery material domain, which is the wound layers of battery

material with a height of 65 mm and 9 mm radius; the mandrel represents the nylon isolator next to the wounded battery material layers with about 2 mm radius; steel connector of the battery located on the top of the cell with the thickness of 3 mm. The battery pack investigation for the three-dimensional thermo-electrochemical model is modelled by 21,700 battery cylinders with the same nominal capacity and voltage as the single cell of the battery pack.

A fully charged state is set for the initial condition of the LIB. The discharge cycle is simulated, and the various discharge currents are modelled as well. Figure 4.3 demonstrates the simulation results of the 1C discharge rate agree well with the experimental results [93] during the entire discharge process. It can be seen that when the battery voltage decreases to 3 V, the discharge process ends. Before the discharge capacity is over 8 Ah, the maximum error of the working voltage is 2.94%. When the discharge capacity increases, the deviations of the working voltage are more significant due to an uneven reaction current density distribution over the porous electrodes, leading to electrolyte transport limitations and potential drops. Yet, the results around the end of discharge have slight differences caused by thermodynamic data, battery design, and the single particle assumption.

As mentioned in the thermal method, the thermal model applied in this work was similar to the two-dimensional thermal model. The single battery cell forms the battery pack consisting of a matrix of batteries. The two-dimensional thermal model has been validated by Parthasarathy et al. [201]. In the current work, the single battery three-dimensional was tested under the k-epsilon turbulence model. Mesh independence verification was

performed to avoid the grid number and mesh quality impacting the simulation results. The total number of meshes is about 43,486 elements chosen for the validation case, considering the efficiency and accuracy. The most appropriate grid amount for the battery pack simulation is around 211,907 elements. The grid independent study is applied to analyse the suitability of the grid and to estimate the numerical errors in the simulation. A more detailed grid independent study is described in Section 5.3.1.

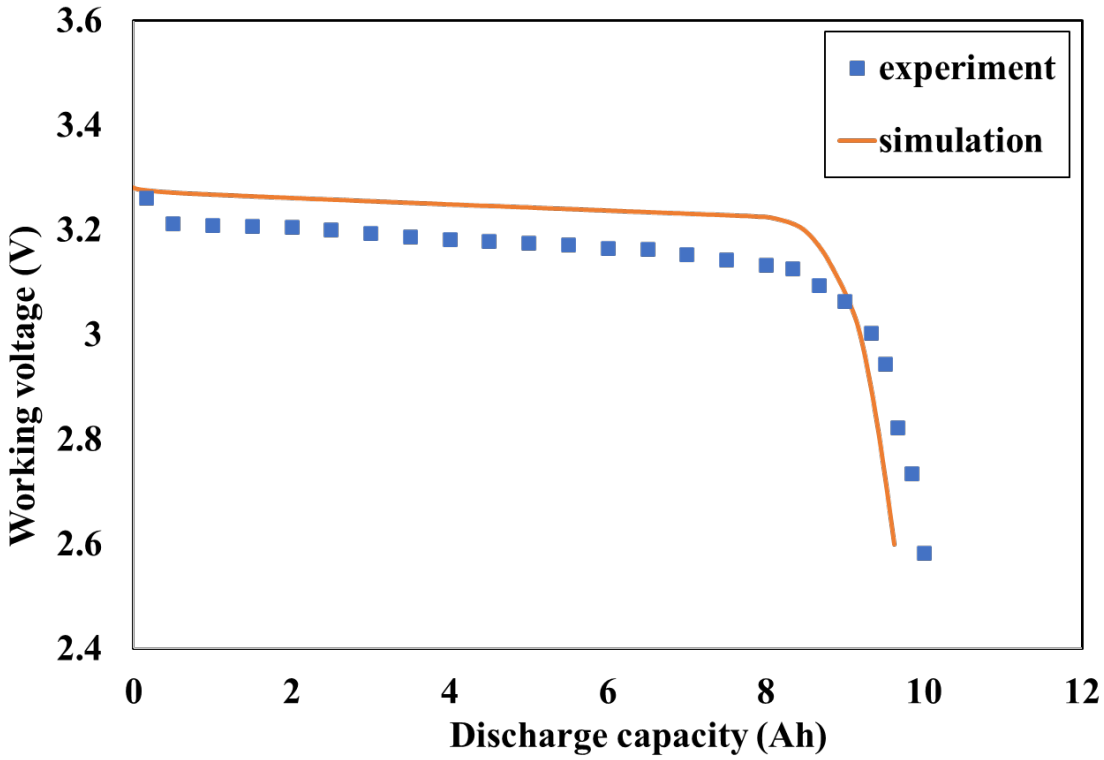

Figure 4.3 Comparison results of working voltage during 1C discharge under natural convection conditions.

Figure 4.4 demonstrates the contour of the battery temperature distribution and airflow streamlines. This usage of the Nonisothermal Flow Multiphysics feature in a one-way coupled study to compute fluid properties, energy, and electrochemistry features shows

one necessary simplification that is potentially applied in battery thermal models. This model can replicate the detailed battery temperature distribution, and the internal and external temperature during the battery working process can be simulated. On the one hand, different types of battery cells can be simulated by changing the battery materials. On the other hand, the same battery cells with various operating conditions can be investigated by changing the boundary conditions.

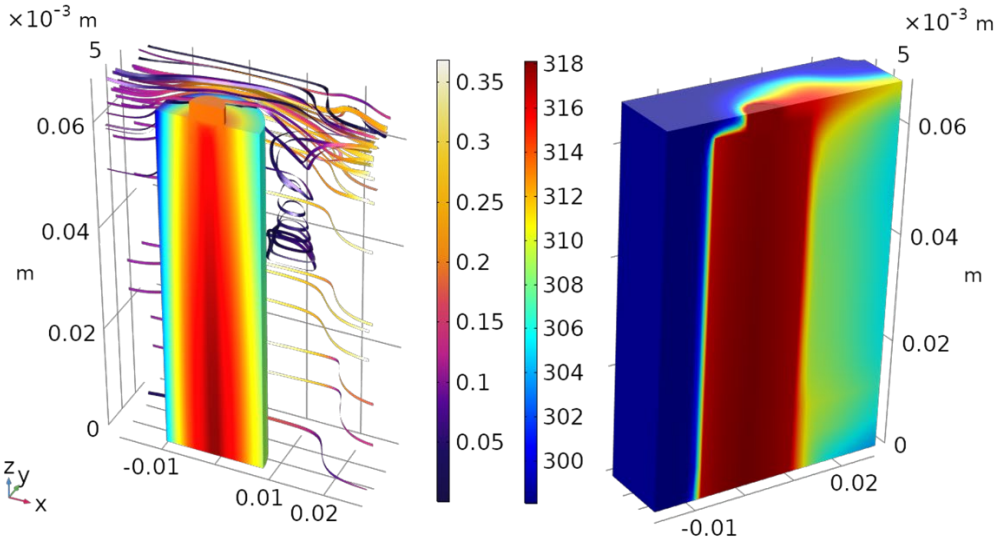

Figure 4.4 (a) Temperature contour of battery cell with velocity streamline at t=1500s; (b) Temperature contour of the whole flow domain.

4.3.3 Simulation results under various pressure conditions

Based on the prementioned battery pack setting, the thermal behaviour of the battery pack has been investigated under various cell spacing configurations and different ambient pressure. Meanwhile, the cooling performance of the battery pack is also evaluated. The battery pack spacing is investigated by this lumped battery model to furtherly understand

the thermal behaviour and cooling performance of the LIB pack. The battery spacing is determined by the previous experimental study by Lopez et al. [232]. The gap along the X-axis direction has been defined with three scenarios, including a 0 m gap (no gap), 0.01 m gap (half diameter of a single cell) and 0.02 m (one single cell, equal to the diameter of a cell). For the y-direction, the scenario setups are the same. Moreover, the ambient pressure is also studied, ranging from 0.2 bar to 1.4 bar.

Under natural ventilation, 63 cases have been investigated. Considering the reliability, consistency, lifespan and other battery performance, the maximum temperature and the temperature difference among the battery pack were extracted from all the cases. Figure 4.5 demonstrated the maximum temperature trending on the left column, and the right column presented the temperature difference. Comparing the maximum temperature trend, ambient pressure has a slight influence on the temperature change. With the pressure decrease, the maximum temperature shows a reverse trend under the current cooling scenario. Since the heat transfer coefficient and heat dispersion rate are increased via the ambient pressure increase, the heat exchange and battery cooling process are enhanced at higher temperatures, and the maximum temperature will be decreased at relatively high pressure.

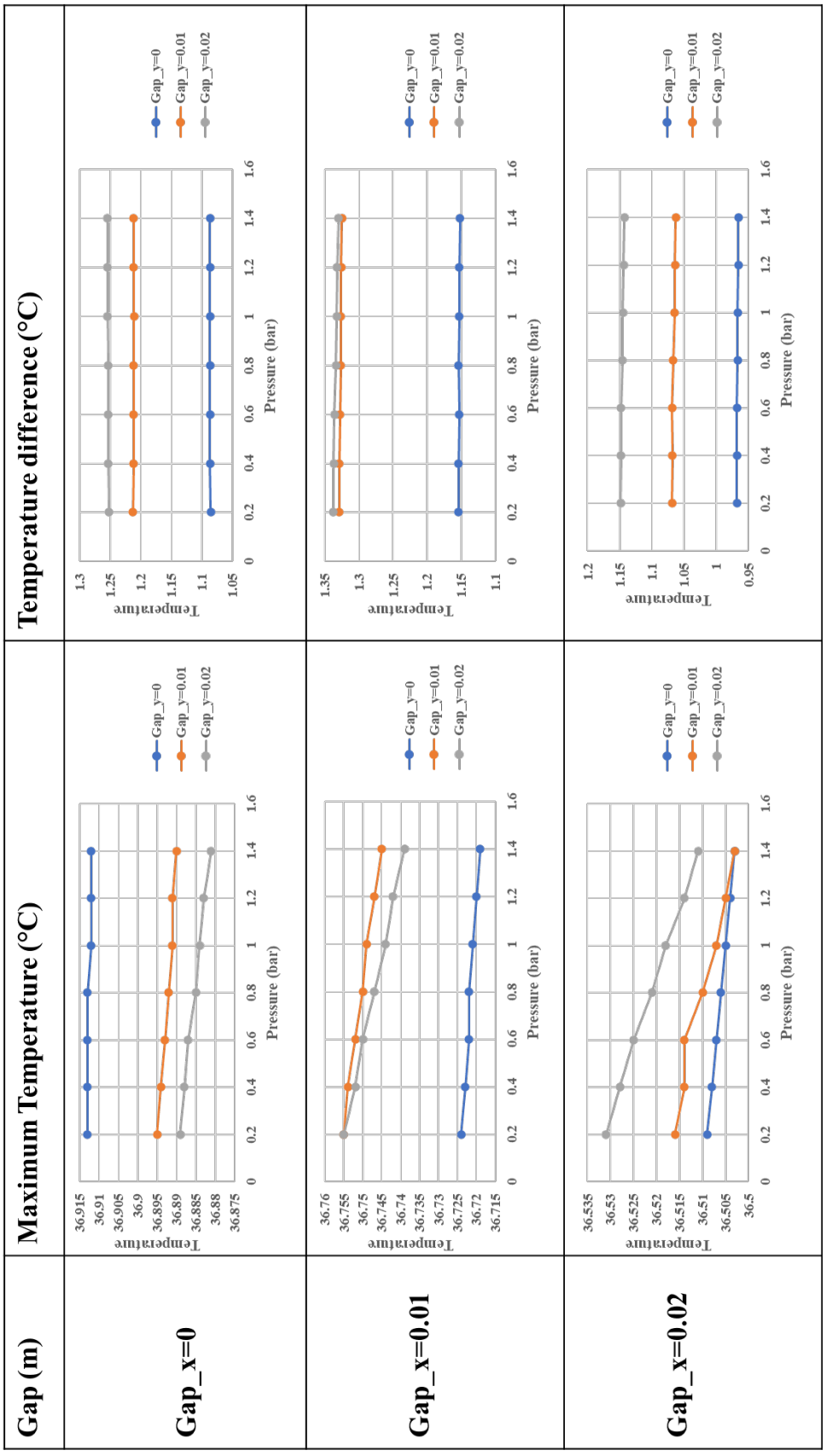

Figure 4.5 Comparison results of maximum temperature and temperature difference under various operation conditions.

Figure 4.6 showed the whole 63 cases plots of the maximum temperature and temperature difference of the battery pack under natural ventilation. From Figure 4.6 (a), the X-direction gap significantly influences the maximum temperature compared to the influence of the Y-direction gap. Also, the X gap of 0.01 m and Y gap of 0.01 m show a better cooling performance than the other two cases with the same X gap value. Along the X direction, the maximum temperature is decreased by increasing the battery gap, shown in Figure 4.6 (a). Since the battery pack is assumed with an X-direction air velocity, the change of the Y-direction gap does not affect the temperature difference much. From the battery spacing point of view, the middle choice is the optimal one by saving the overall battery pack volume. Figure 4.6 (b) illustrates that both direction gaps have a similar effect on the temperature difference under natural ventilation. Considering both performances, the X gap of 0.01m gains a good cooling performance with less space wasting.

(a)

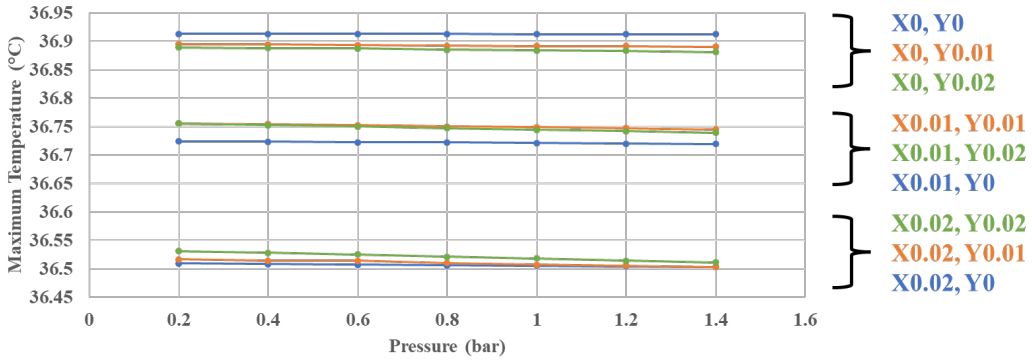

(b)

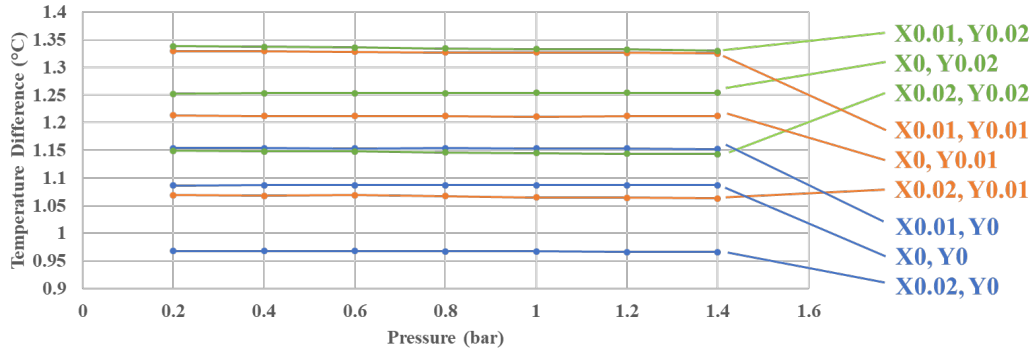

Figure 4.6 Maximum temperature and temperature difference plots of 63 cases.

4.3.4 Simulation results under various air cooling directions

With the establishment of the three-dimensional thermo-electrochemical model, simulation results indicate the thermal behaviour of LIB by the detailed temperature configuration. In order to improve the cooling efficiency and fire safety of LIB packs. Forced air cooling was introduced and compared with natural cooling. The forced air is applied to the battery pack from top to bottom with a constant velocity. In the previous section. Sixty-three cases have been built. In this section, another 63 cases have been completed with the same operating conditions and different cooling approaches. Figure 8 compared the simulation results of two air cooling methods. Figures 4.7 (a) and (b) showed the surface temperature distribution under the discharge time of 0.2 h. The maximum temperature of the natural ventilation is slightly higher than the forced air method, which is about 0.652 °C and the temperature difference increases from 1.087 °C to 2.978 °C. Figures 4.7 (c) and (d) demonstrated the streamline of the temperature gradient for both methods. It can be concluded that natural ventilation performs a

relatively average temperature distribution, while forced air cooling takes away more heat generated from the battery working process.

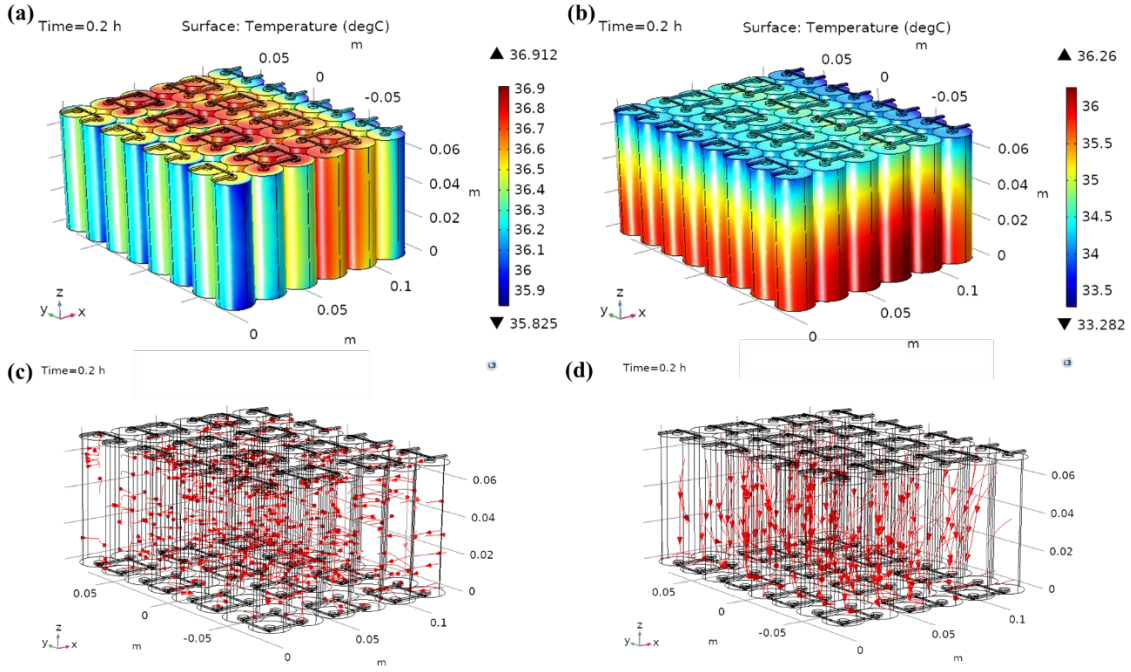

Figure 4.7 Simulation results of temperature distribution contour and temperature gradient streamline for natural ventilation (a) & (c) and forced air cooling (b) & (d).

The influence of battery pack configuration on thermal management and cooling performance has also been discussed between natural ventilation and forced air cooling. As mentioned, the battery spacing combination group is nine, which equals three types of X-direction gap multiplied by 3 types of Y-direction gap. The maximum temperature and temperature difference of nine groups with the same operating conditions were compared, shown in Figure 4.8. From Figure 4.8 (a) and (b), it is easy to find that the increase of the battery gap has a better impact on the drop of maximum temperature for forced air cooling. Comparing Figure 4.8 (c) and (d), the temperature distribution of natural ventilation is

more average. Also, for forced air cooling, the growth of the battery gap will increase the temperature difference, which means the stability of the battery pack can be affected. Although the maximum temperature was decreased, the design of battery spacing should be considered more carefully and comprehensively. Under forced ventilation, the heat transfer from top to bottom is ineffective because the battery height (Y-direction) is too short for sufficient heat exchange. Thus, only the top side of the battery gets cooled. Cooling along the X-direction is preferable for a more economical and balanced design.

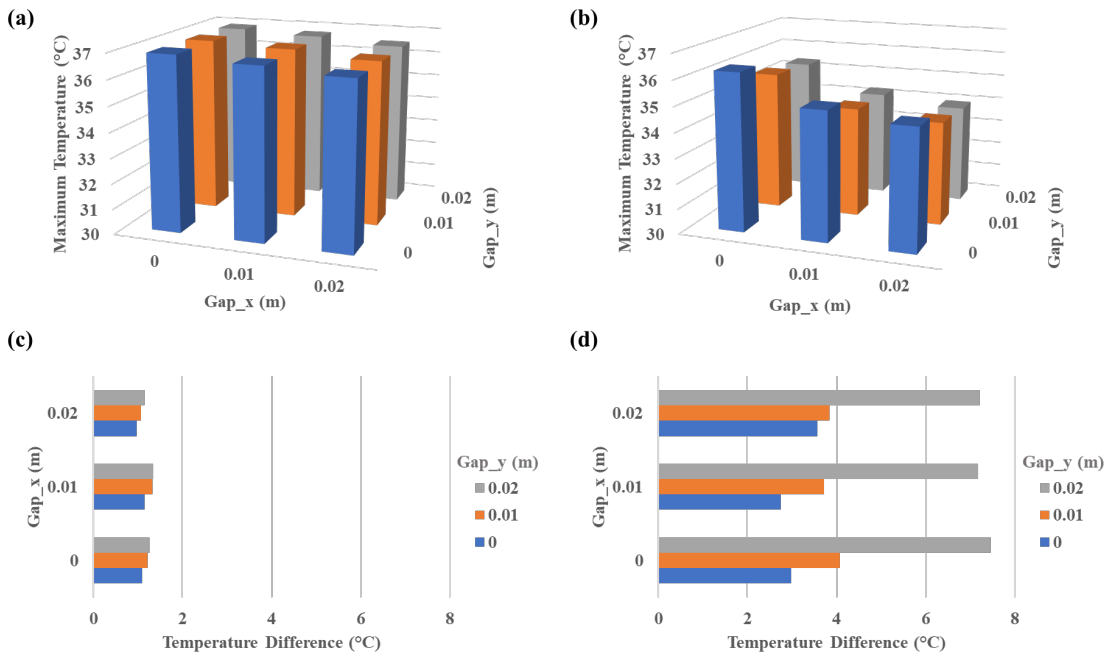

Figure 4.8 Comparison results of maximum temperature and temperature difference for natural ventilation (a) & (c) and forced air cooling (b) & (d).

Moreover, the influence of the ambient pressure on the battery's thermal behaviour and cooling efficiency is also studied. Figure 4.9 compared the simulation results of temperature and temperature differences under different ambient pressures for natural

ventilation and forced air cooling. The chosen 21 cases combine seven ambient pressures to multiply three Y-direction gap groups under the same X-direction gap. The trend of changing the X-direction gap under the same Y-direction gap is similar. From Figure 4.9, it is clear to conclude that the ambient pressure has more impact on the forced air cooling situations compared to the natural ventilation scenarios. Under forced air cooling, the heat transfer between LIB cells and cooling air is much more than that between cells, which can be affected by ambient pressure change, while the temperature is more average by natural ventilation.

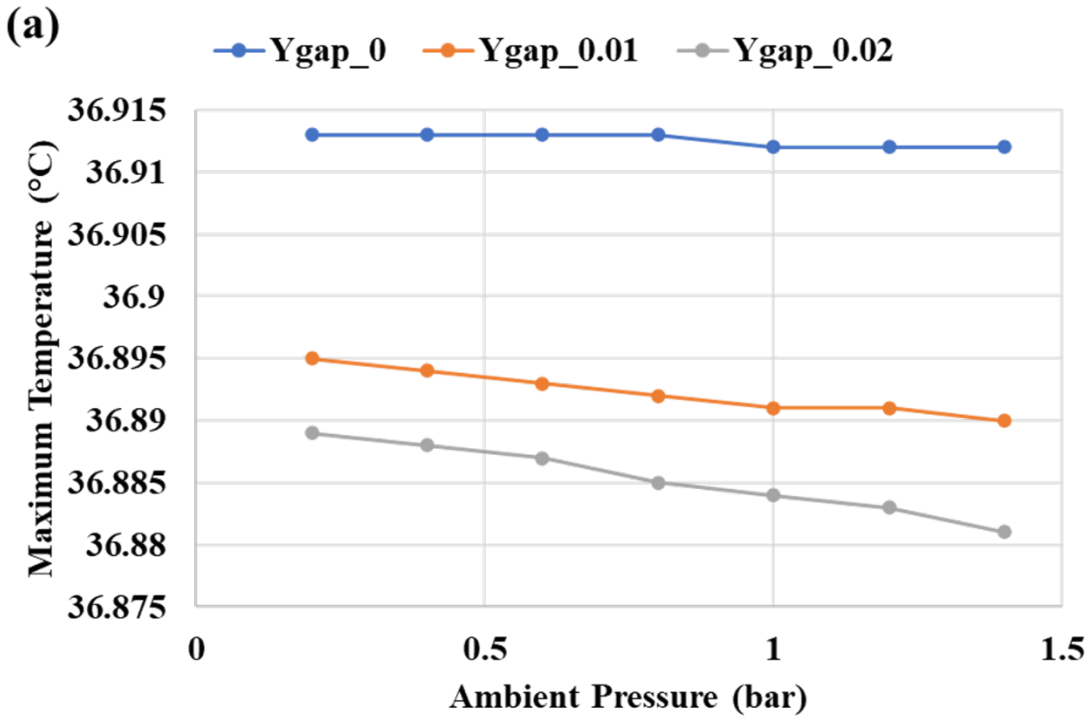

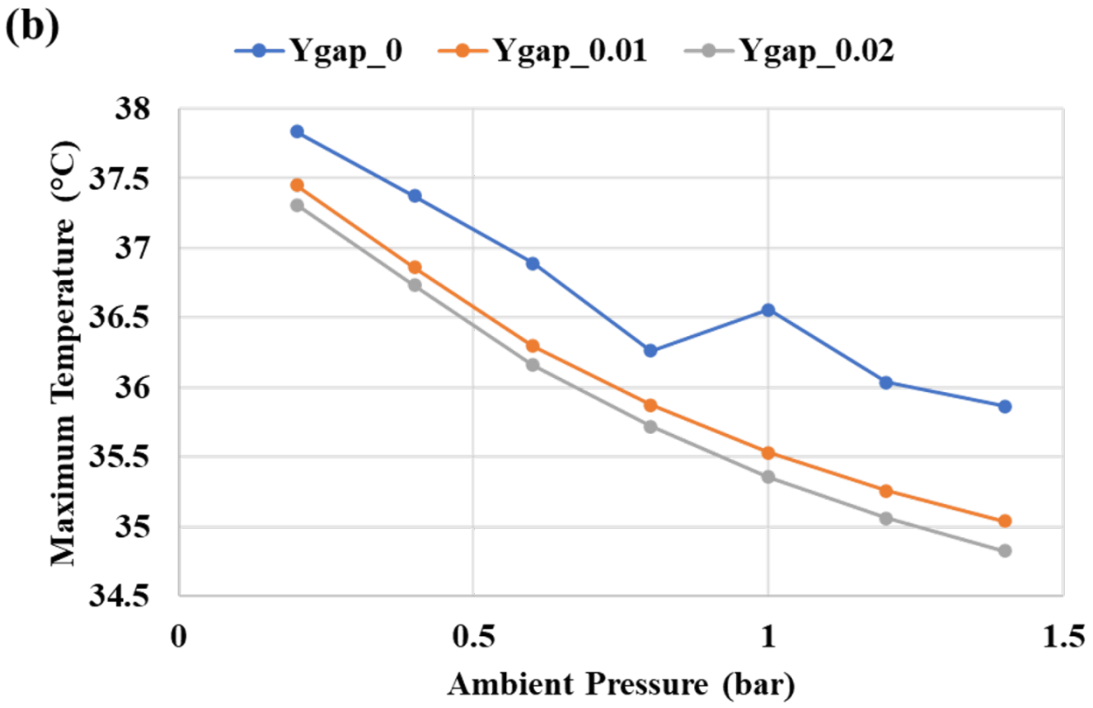
(b)
Ygap_0
Ygap_0.01
Ygap_0.02
Maximum Temperature (°C)
38
37.5
37
36.5
36
35.5
35
34.5
0
0.5
1
1.5
Ambient Pressure (bar)

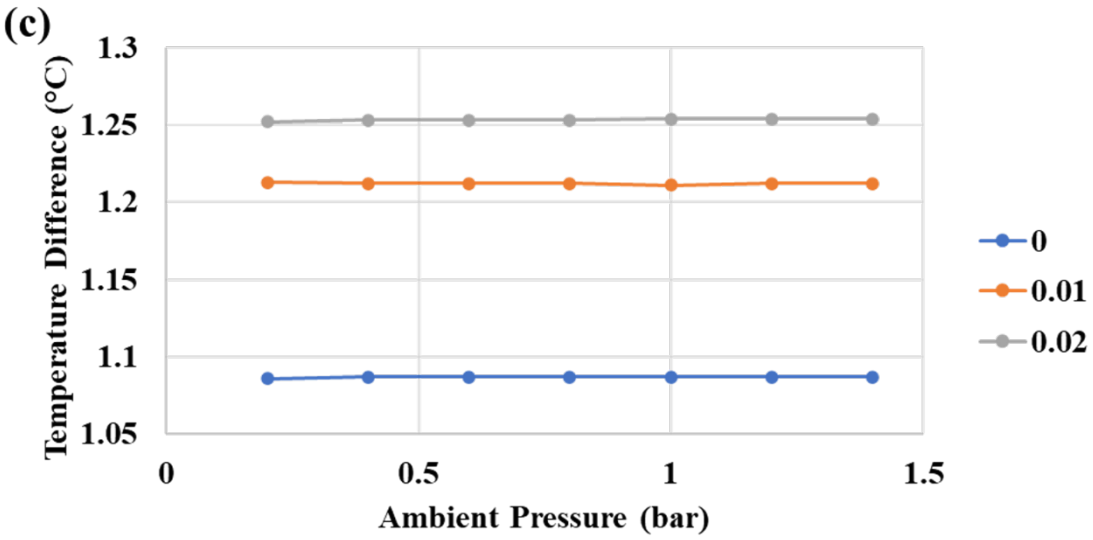
(c)
Temperature Difference (°C)
1.3
1.25
1.2
1.15
1.1
1.05
0
0.5
1
1.5
Ambient Pressure (bar)
0
0.01
0.02

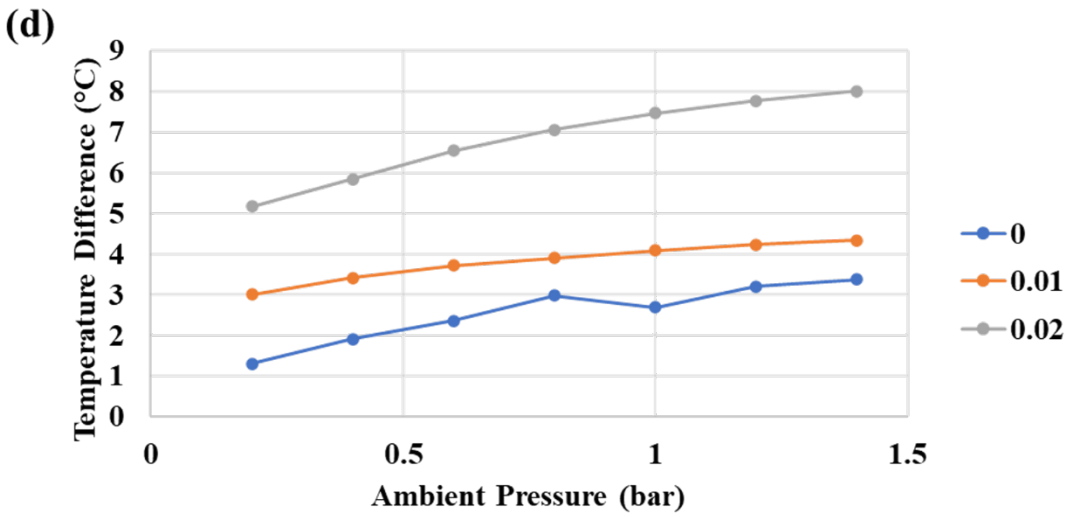

Figure 4.9 Comparison results of maximum temperature and temperature difference under different ambient pressures for natural ventilation (a) & (c) and forced air cooling (b) & (d).

4.3.5 Optimum results coupled MLP model

As mentioned in Chapters 2 and 3, the ANN approach is a convenient and effective way to analyse multiple parameters simultaneously by characterizing the interrelation between inputs and outputs. With the simulation results generated by the thermo-electro model, a dataset can be established. In this section, ambient pressure is a new parameter for the evaluation of battery pack thermal performance. There are 124 cases generated before, which are operated with various heat transfer coefficients and ambient temperature, were also added to the current dataset. The overall dataset consists of 187 cases with seven parameters, divided into five inputs and two outputs, which is shown in Table 4.2.

Table 4.2 Parameter details of the ANN dataset.

Inputs					**Outputs**	
Gap _x	Gap _y	Heat transfer coefficient	Ambient temperature	Ambient pressure	Maximum temperature	Temperature difference
m	m	$W/m^2/K$	°C	bar	°C	°C

The data of seven parameters extracted from the 187 cases formed a database for training the ANN model. MATLAB was applied to train the dataset, generate the function code, and optimise the combination groups. The Levenverg-Marquardt (LM) optimisation approach was applied to train the dataset, which was originally described by Marquardt [233]. This algorithm appears to be the most efficient training algorithm for training moderate-sized feedforward neural networks. The approximation of the Levenberg-Marquardt algorithm is given as follow:

$$x_{m+1} = x_m - [J^T J + \psi I]^{-1} J^T e \tag{4.1}$$

The training process starts from setting aside the samples for validation and testing. In this model, 70% of samples are used to do the training, which is presented to the network to adjust according to its error. Validation and testing samples are 15% each. Validation samples are applied to examine network generalisation and halt training when generalisation stops improving. The testing samples are also important owing to that they can provide an independent measure of network performance. Figure 4.10 illustrates the

whole training results, including the error histogram and regression result. Figure 4.10 (a) demonstrated that the majority of the error lies in the scope of -0.03686 to 0.04011. Figure 4.10 (b-e) present the regression relation between outputs and targets. The training, validation and testing data attained very impressive R values. The coefficient of determination, which is the R square value, can be achieved with the value of 0.99998, 0.99994 and 0.99994, respectively. It is clear that the agreement of the applied ANN model with the built dataset is good, and the prediction accuracy is excellent. The simulation results achieve a good fit with the targets, and the overall fitness is 0.99998. Also, the other prediction errors are less than 1%.

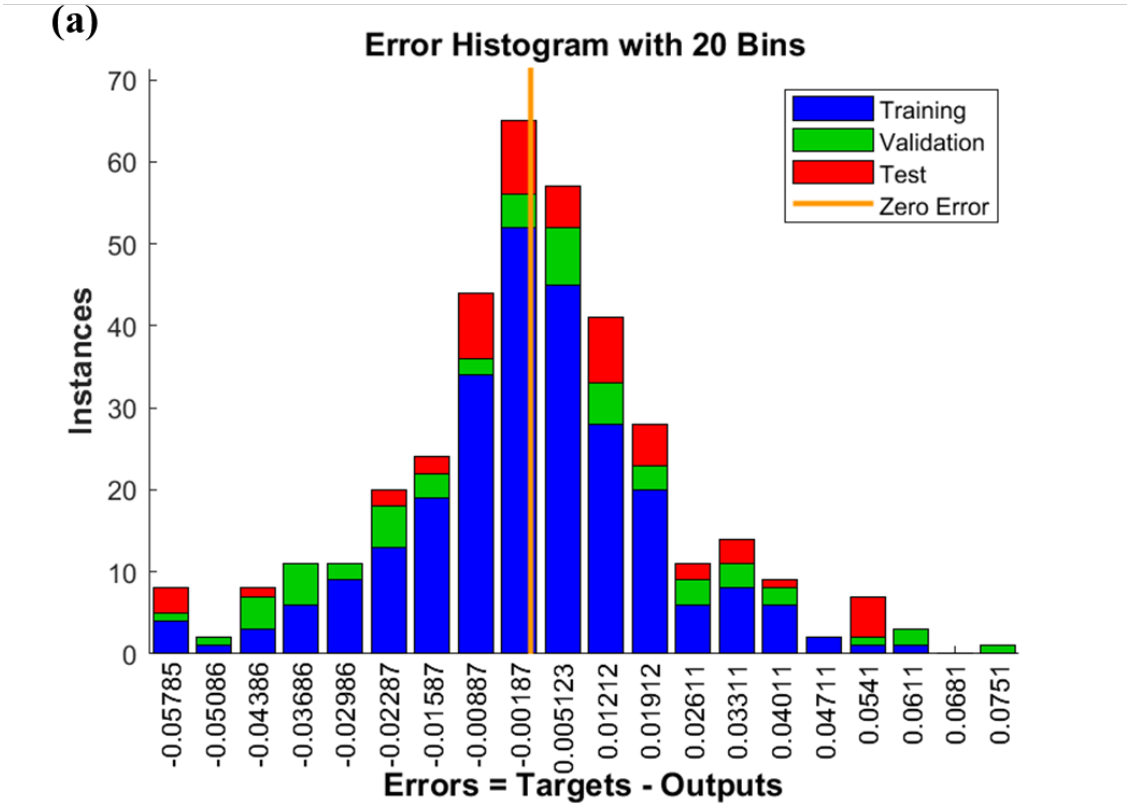

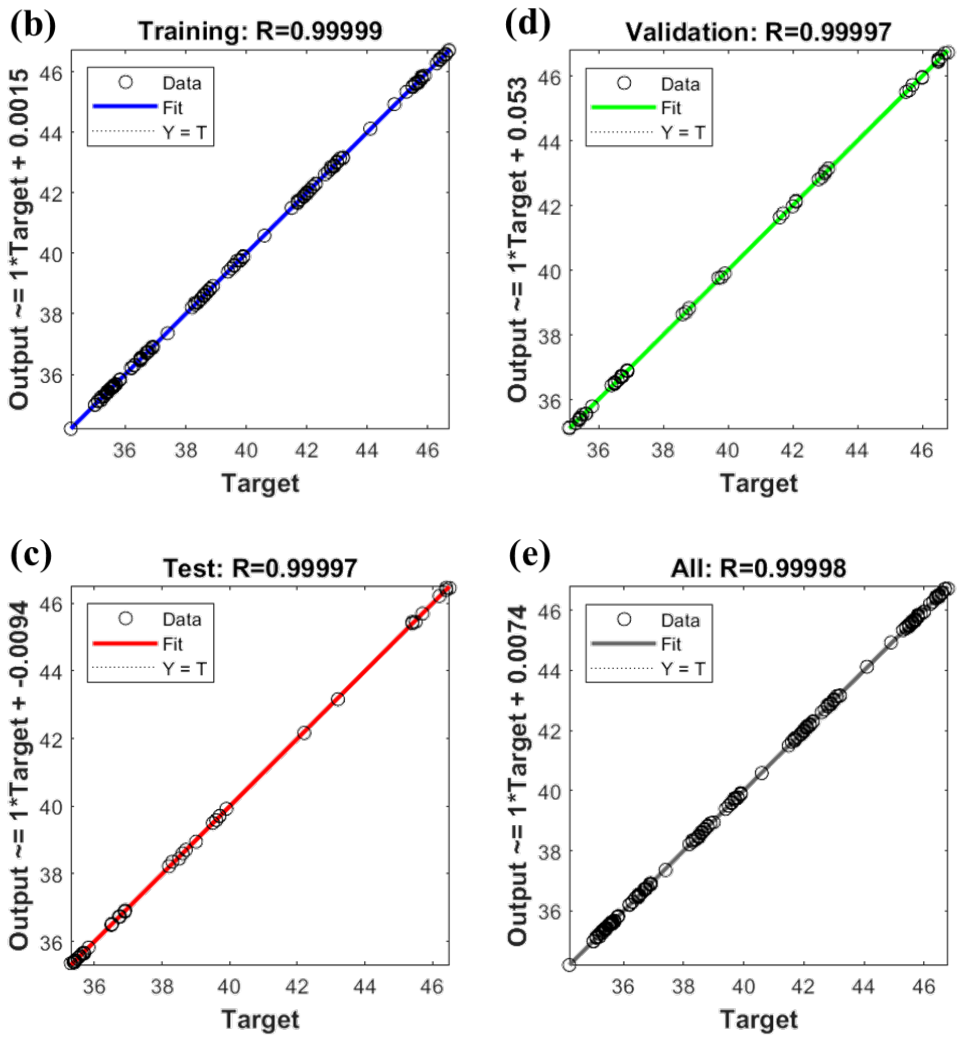

Figure 4.10 (a) Error histogram of the ANN model; (b-e) Regression analysis of the ANN model.

The training results of the ANN model are evaluated by the mean absolute error (MSE). The minimum error for the modelling estimation was determined by the number of nodes per output parameter computation layer set as two. Figure 4.11 demonstrates the validation of the applied ANN model, which is the best validation performance of the model with a very low MSE value attained at epoch 163. Figure 4.12 demonstrates the training process of the ANN model by showing the gradient, mu and validation checks.

The gradient indicates the learning rate and step size of the training process. The gradient showed a continuous drop trend till epoch 169, where mu decreased to 1e-06. A low mu represents the LM methods have a faster and more accurate convergence [233]. The validation check was also depicted in Figure 4.12, and there was no validation fail till epoch 169.

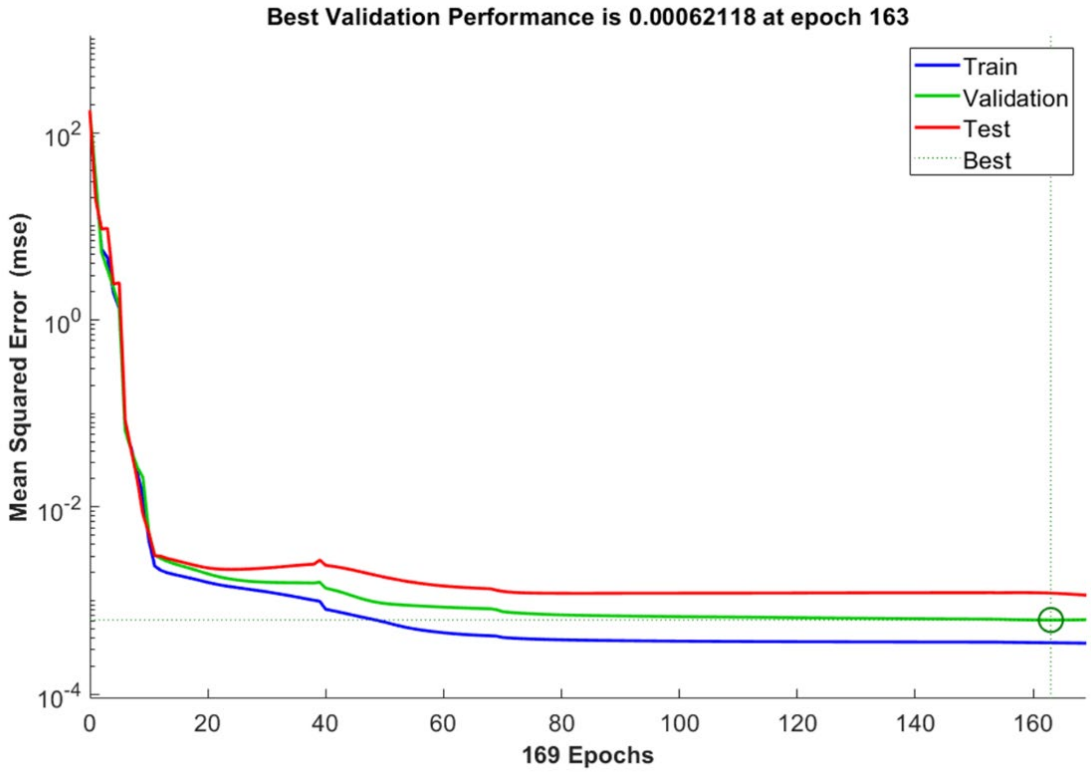

Figure 4.11 Validation performance of the ANN model.

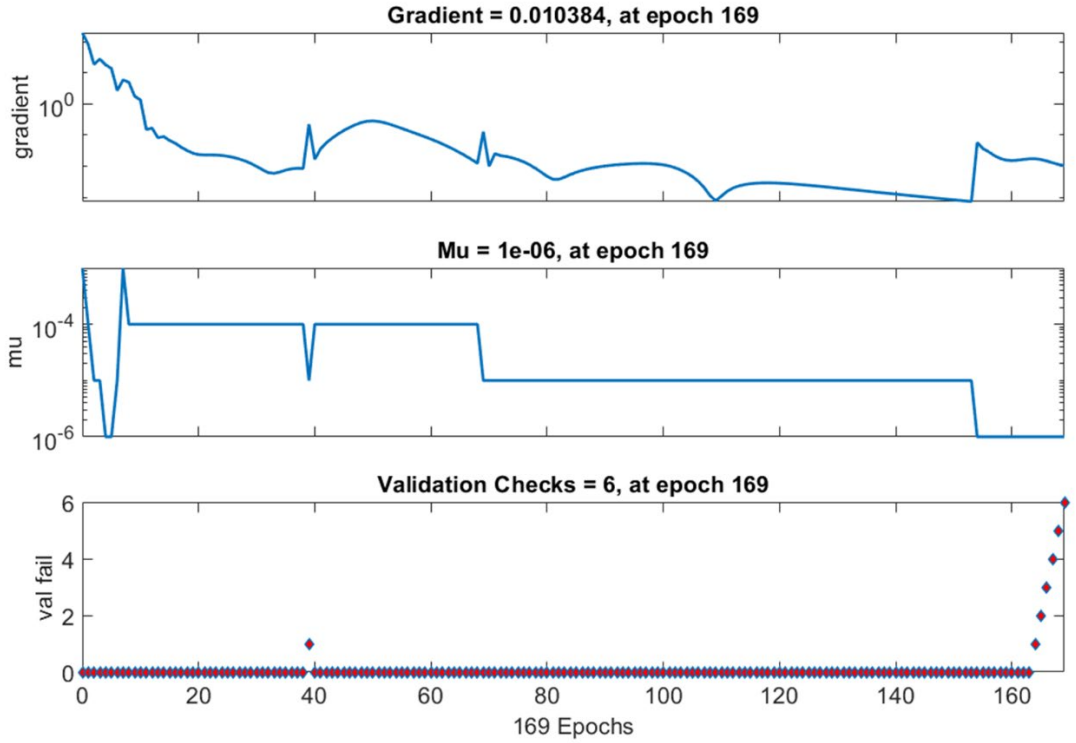

Figure 4.12 Training states of the ANN model.

After training the ANN model, a neural network simulation function can be built. This function can be applied to predict the battery thermal performance under various operating parameters. During the ANN model training, maximum temperature and temperature differences are defined as the outputs. The reason is that these two parameters can indicate the temperature imbalance, which has a huge impact on many battery performances, such as working performance, safety performance and lifecycle of LIBs. The optimisation applied ANN model is to select the optimum case under all the combination groups of operating parameters, including battery spacing at various directions, environmental temperature, ambient pressure and cooling air velocity. The

comprehensive consideration of all the operating conditions can provide a better solution of the battery pack with enhanced performance.

The trained 187 cases demonstrate a range of operating conditions. The extracted seven parameters consist of five inputs and two outputs. Meanwhile, five inputs include configuration dimensions and operating parameters. The inputs with a certain range are divided into 20 internals separately to combine with each other freely. Therefore, 3,200,000 combination groups were generated. The optimum results can be evaluated among these combination groups by comparing the outputs. Figure 3.14 shows the maximum temperature and temperature difference trends from all the potential combination groups generated in MATLAB. From Figure 3.14, the wave peak of the maximum temperature showed a slightly increasing trend, while the peak of the temperature difference had a decrease before an increase. The optimum design for the battery pack can be achieved among these combination groups, and the thermal behaviour and cooling efficiency can be calculated as well. Compared to the base case, the maximum temperature of the optimum case dropped by 1.94% to 36.19 °C. For the temperature difference optimisation, a 17% decrease can be achieved from 0.966 °C to 0.802 °C. Additionally, the ambient pressure was treated as an input in the coupled model, and it can also be treated as a pre-set qualification. Then the rest inputs can be applied in this model for the optimisation design.

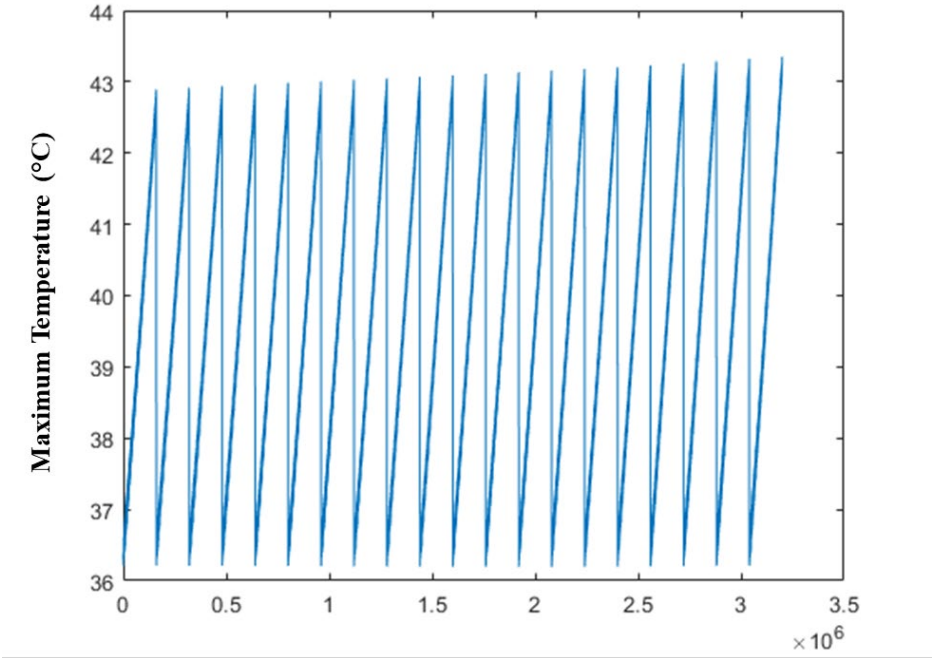

(a)

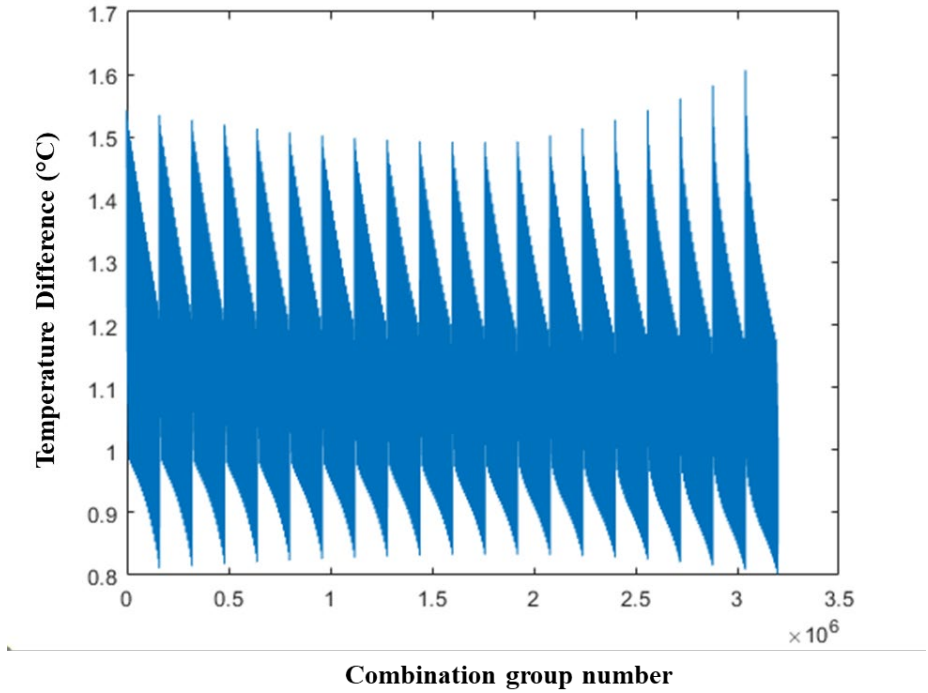

(b)

Figure 4.13 Numerical results of various operation parameter combination groups (a) Maximum temperature; (b) Temperature difference.

4.4 Chapter Summary

In this chapter, a three-dimensional thermo-electrochemical model was developed by coupling a lumped version of a single particle model, and it was coupled with an ANN model to achieve the optimisation design of thermal management for the LIB pack. Also, the different cooling approaches of the LIB pack were compared between natural ventilation and forced air cooling. Moreover, the ambient pressure was considered as an operating parameter and its influence on the battery thermal management were investigated. Compared to natural ventilation, ambient pressure had more influence on forced air cooling. The numerical results of the parametric study were applied to build an ANN dataset to train the ANN model. The relationship among the multiple parameters was built and analysed. The proposed coupled model provided an optimal design by filtering among 3.2 million combination groups. The result indicated that the maximum temperature and the temperature difference can be decreased by the optimal design with the value of 1.94% and 17%, respectively.

A valuable perspective of battery working performance, thermal performance and safety performance was demonstrated. The results provided an effective and efficient way to improve the battery thermal performance, and it also demonstrated the significant advantage of a numerical investigation by optimizing multiple parameters simultaneously. More aspects can be considered with the proposed coupled model in the future. The model can be applied to other battery cooling methods and different battery types can be evaluated and optimised as well. Furthermore, more battery configuration parameters and

operating parameters can be introduced, such as various materials of different battery components, battery cell numbers, connection types, and so force. All the mentioned points can be contributed to forming a comprehensive battery parameter dataset for battery thermal management systems and energy storage system safety. Chapter 5 will assess some other parameters based on this ANN-CFD framework. The optimisation of the configuration design and operating conditions will be presented considering different ambient temperatures and nature ventilation velocity.

Chapter 5 Coupling ANN with CFD for Optimisation Design of Battery Thermal Management Systems

This chapter includes the contents from a published journal article [139]: **Li, A.**, Yuen, A. C. Y., Wang, W., Chen, T. B. Y., Lai, C. S., Yang, W., Wu, W., Chan, Q. N., Kook, S. & Yeoh, G. H. (2022). Integration of Computational Fluid Dynamics and Artificial Neural Network for Optimization Design of Battery Thermal Management System. *Batteries*, *8*(7), 69. with modifications and reorders to better fit the structure of this thesis.

5.1 General Description

As briefly discussed in Chapter 2, many operating parameters and ambient environment conditions affect the performance of the BTMs simultaneously. Chapter 4 studied the different air cooling modes and directions, as well as the influence of the ambient pressure on the cooling performance. In this Chapter, a three-dimensional thermo-electrochemical model coupled with fluid dynamics module has been developed to comprehensively analyse the temperature distribution of battery packs and the heat carried away. The computational fluid dynamics (CFD) simulation results of the lumped battery model were

validated and verified by considering natural ventilation speed and ambient temperature. In the artificial neural networks (ANN) model, the multilayer perceptron was applied to train the numerical outputs and optimal design of the battery setup, achieving a 1.9% decrease in maximum temperature and a 4.5% drop in temperature difference. The simulation results provide a practical compromise in optimizing the battery configuration and cooling efficiency, balancing the layout of the battery system and safety performance. The present modelling framework demonstrates an innovative approach to utilizing high-fidelity electro-thermal/CFD numerical inputs for ANN optimisation, potentially enhancing the state-of-art thermal management and reducing the risks of thermal runaway and fire outbreaks.

5.2 Introduction

As per the previous discussion, temperature plays a critical role in many aspects of the performance of LIBs, including charge acceptance [234], energy capability [235], reliability [236], and so on. However, the abuse of LIB will generate the threat of thermal runaway and overheating. Both positive and negative electrode decomposition are exothermic processes. Also, oxygen can be generated during the decomposition reactions. The generated heat and oxygen are the contributions to the combustion triangle. If the battery experiences harsh working conditions during electric transportation, the generated heat triggers electrodes' decomposition. As a result, the battery potentially faces thermal issues. Suppose the cell temperature is rising over a certain threshold. In that case, a

thermal runaway may turn up, leading to a quick temperature rise and potentially other related undesirable consequences such as the generation of toxic gas and smoke. With the rising battery temperature over a critical point, the other chain exothermic reactions happen. The temperature and pressure in the LIB are cumulated until it exceeds the battery endurance. Eventually, the fire and rupture/explosion are inescapable. Therefore, the thermal management of LIB is essential during the battery working process or battery application. It is also crucial to investigate the LIB thermal runaway process by accurately monitoring and predicting temperature dynamics during thermal propagation and implementing functional methods to improve the cooling efficiency of the battery itself and the battery system.

There are two key topics of concern in battery thermal management: handling the charge/discharge cycle and governing the battery heat growth, which is mentioned in Chapter 4. Many pieces of research focused on the battery thermal management system of EVs have been done [237, 238]. The heat produced during the operating process has been established as the major rise in the working temperature. Model-based investigations promote a theoretical and comprehensive understanding of battery physics beyond what is possible from practical methods only. For example, Kirad and Chaudhari [239] applied numerical models for studying the selection of the battery module spacing with an improvement in cooling performance. Due to the development of computing capability, numerical simulations are gradually applied in battery models, battery components and materials studies, and battery safety engineering [240-242]. Most numerical studies rely on the thermal models, which predict the average surface temperature for a LIB cell [243,

244], and lots of experimental investigations on thermal propagation have been carried out [245, 246]. Nevertheless, to achieve a proper estimation of the thermal behaviour of a battery, many aspects, including the shape, layout, and physical and electrochemical properties, should be illustrated as closely as possible in the simulation. For instance, the asymmetric surface temperature of a battery cell should be considered in the model. The non-uniform temperature distribution in the LIBs leads to an electrical imbalance, lower battery performance, and shorter battery life [247, 248]. Regarding the detailed temperature distribution, an electric-thermal model with the non-uniform feature should be built.

Moreover, battery thermal management systems have been classified in various ways based on different criteria [249, 250]. For example, battery thermal management systems can be branched into three kinds based on various mediums: air-based, liquid-based, and phase change materials-based. Several optimisation studies on the battery thermal management system have been previously done [251-254]. The air-cooling method is considered the most traditional approach and is a favoured option for HEVs and EVs. It is clear that the optimisation of battery packs or systems depends on many parameters, such as geometry structure, coolant properties, operating conditions, and so force. Still, few researchers focus on multiple parameters simultaneously.

As a part of artificial intelligence, machine learning focuses on the study of accuracy improvement by computer algorithms and data to imitate how humans learn [80, 255]. Because LIBs are highly complex, nonlinear systems, applying a probabilistic approach allows for quantification of uncertainty, which positively impacts making decisions in

design and control. ANN model is a kind of model that characterises the interrelation between inputs and outputs by using a collection of interconnected nodes (perceptron). The application of ANN to battery research is still relatively new. Wu et al. [256] generated a design map that fulfils both specific energy and specific power requirements using a systematic approach based on ANN. Feng et al. [257] developed an electrochemical-thermal-neural-network method used for the co-estimation of LIB SOC and state of temperature. However, pioneering studies have highlighted the possibility of using ANN for battery thermal problems. These studies include modelling battery spacing, specific format, and some battery performances. The detailed temperature distribution of LIB and battery pack have not been fully investigated. Besides, the ambient pressure and cooling direction have been studied in Chapter 4. The ambient temperature and natural ventilation should be considered during the battery working process to characterise the thermal behaviour of batteries further and identify the battery fire risks. Therefore, the combination between ANN analysis and the thermo-electrochemical battery model is proposed to investigate further the battery system's cooling efficiency and battery fire safety performance. Figure 5.1 shows the schematic figure of the integrated CFD-ANN model proposed in this study.

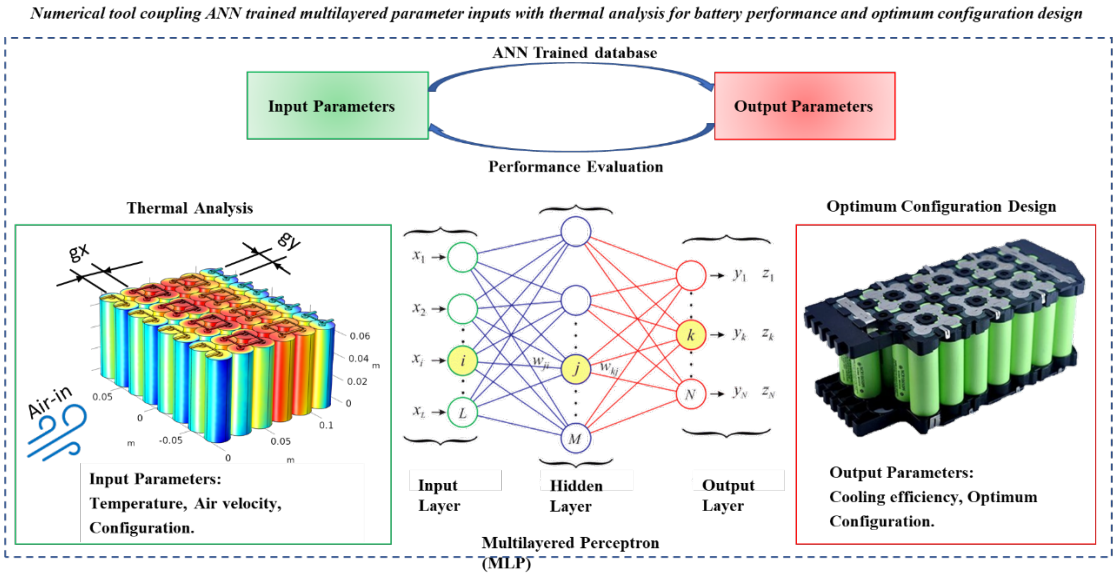

Figure 5.1 Schematic of the proposed CFD-ANN model.

Accordingly, the non-uniform distributions of the battery cell should be investigated for the thermal analysis, which can be treated as a measurement and prediction at the early stage of the LIB thermal runaway fires. Furthermore, with the numerical analysis, a better understanding of battery pack configuration design can be achieved. In this section, the contributions are:

(i) Establishment and development of a three-dimensional thermo-electrochemical model capable of considering temperature distribution of battery packs and heat exchange with the ambient environment.

(ii) Utilise the numerical results to comprehensively describe and predict the battery system's thermal behaviour to improve battery safety during the designing and working stages.

(iii) Coupled the thermo-electrochemical model with the ANN model to optimise

the battery system configuration design and enhance the cooling performance of the battery system.

The outline of this chapter is summarized as follows: Section 5.3 demonstrates the numerical results of the proposed model with validation and verification. Also, the training process and optimisation results are listed in this section. Finally, Section 5.4 presents some conclusions and proposed the future perspectives on this field in the chapter summary section.

5.3 Results and Discussions

As mentioned in Chapter 3, a three-dimensional thermo-electrochemical model has been built. In this section, a corporate software applied finite element, COMSOL Multiphysics 5.5, was employed to study the proposed model. The battery model involves these three steps. At first, a lumped battery model is set up and run for a time-dependent battery current. Then, parameter estimation of the parameters $\eta_{IR,1C}$, τ, and J_0 is demonstrated using experimental data. This is achieved using the Global Least-Squares Objective node in the optimisation interface, combined with the optimisation study step using a Levenberg-Marquardt optimisation solver. Lastly, cell voltage prediction is performed using the optimised lumped parameter values obtained in the previous parameter estimation study compared with experimental data.

5.3.1 Numerical simulation results

The default mesh component was applied for generating the mesh, and mesh independence was examined as well. The MUMPS time-dependent solver was applied for battery variables, and the PARDISO (Parallel Direct Sparse Solver for Cluster) solver was chosen for heat transfer variables. The mesh applied for this study consists of triangular and quadrilateral elements developed by COMSOL Multiphysics 5.5. In order to obtain the thermal behaviour and boundary layer spread, the refined mesh is achieved at the connections of the battery boundary. Mesh independence verification was performed to avoid the grid number and mesh quality impact on the simulation results, shown in Table 5.1. According to Table 5.1, 43,486 elements show reliable and efficient results, and more elements lead to larger computation time. Therefore, the total number of meshes is about 43,486 elements chosen for the validation case, considering the efficiency and accuracy. For the battery pack simulation, the most appropriate grid amount is around 211,907 elements. Subsequently, more simulation results are produced to feed the machine learning model to training.

Table 5.1 Table of mesh independence analysis.

Grid Resolution	Elements Number	Calculation Time	Maximum Electrolyte Temperature
Finer	114273	75.6 min	20.250 °C
Fine	43486	30.5 min	19.829 °C
Normal	23986	18.7 min	19.810 °C
Coarse	9708	10.6 min	18.910 °C

The validation of the electrochemical model and thermal model is established on the Type 38120 battery cell, in which the nominal voltage is 3.2 V and capacity is 10 Ah, as well as the thickness of the cathode, the separator, and the anode are 91 μm, 40 μm and 142 μm, respectively. The type we choose is one of the most commonly used in the current commercial market. It is developed based on physical and electrical conservations, as well as thermal principles and electrochemical kinetics. The battery pack investigation for the three-dimensional thermo-electrochemical model is built by Type 21,700 battery cylinders with a nominal capacity of 4 Ah and a nominal voltage of 3.6 V. The whole air domain is built with 136 mm (X direction) × 168 mm (Y direction) × 75mm (Z direction), and 48 battery cells are assembled in the domain. For the base case, the gap between each cell is zero. The battery cell spacing increases by half the cell diameter and the whole diameter for both X and Y directions. With the changing of the cell gaps, the largest air domain is 245 mm along the X direction and 328 mm in the Y direction. The Z direction keeps the same for all the scenarios. The battery pack is constructed by coupling two cylindrical batteries in parallel. Then the mated battery pairs are connected in series. The geometry and battery parameters are listed in Table 5.2. The geometry specifications are used to build the battery domain for thermal simulations, while the battery parameters are applied for the simulation of the electrochemical model.

Table 5.2 Geometry dimension and electrochemical parameters of the battery cell.

Geometry Parameters			**Battery Parameters**		
d_batt	21 [mm]	Battery diameter	C_rate	4	C rate
			Q_cell	4[A·h]	Battery cell capacity
h_batt	70 [mm]	Battery height	I_1C	Q_cell/1[h]	1C current
			κT_batt_ang	30[W/m/K]	Thermal conductivity, in plane
h_term	1[mm]	Terminal thickness	κT_batt_r	1[W/m/K]	Thermal conductivity, cross plane
			Ea_eta1C	24[kJ/mol]	Activation energy
r_term	3[mm]	Terminal radius	Ea_J0	-59[kJ/mol]	Activation energy
			Ea_Tau	24[kJ/mol]	Activation energy
d_sc	2[mm]	Serial connector depth	T0	20[°C]	Reference temperature
			J0_0	0.85	J0 at reference temperature
h_sc	1[mm]	Serial connector height	tau_0	1000[s]	tau at reference temperature
			eta_1C	4.5[mV]	eta_1C at reference temperature
h_pc	0.5 [mm]	Parallel connector height	rho_batt	2000[kg/m^3]	Battery density
			Cp_batt	1400[J/kg/K]	Battery heat capacity

w_pc	1[mm]	Parallel connector width	ht	30[W/m^2/K]	Heat transfer coefficient
			T_init	20[°C]	Initial/external temperature

The initial battery state is fully charged. The discharge process at different current densities is simulated, and the discharge curves during the process are demonstrated. The battery capacity under various discharge rates is built through the modelling. The simulation will be stopped when the cell potential decreases under 3 V, which is the state of end-of-discharge. The simulation result of the nominal discharge current density representing case 1C, is shown in Figure 5.2 (a). The numerical result shows a good agreement with the experiment data. Meanwhile, there are a few deviations in the usual discharge voltage plateau related to thermodynamic analytics and battery prototypes. The thermal model is validated, and the results are shown in Figure 5.2 (b). The experimental data is extracted from the surface of the battery along the axis to track the surface temperature development. The simulation results in the same location of the testing point have similar growth trends. The slight difference between the experimental and numerical results is because of the temperature rise of the experiment due to the local ohmic heat generation, where the electrical contact resistance among the connectors and terminals of the battery.

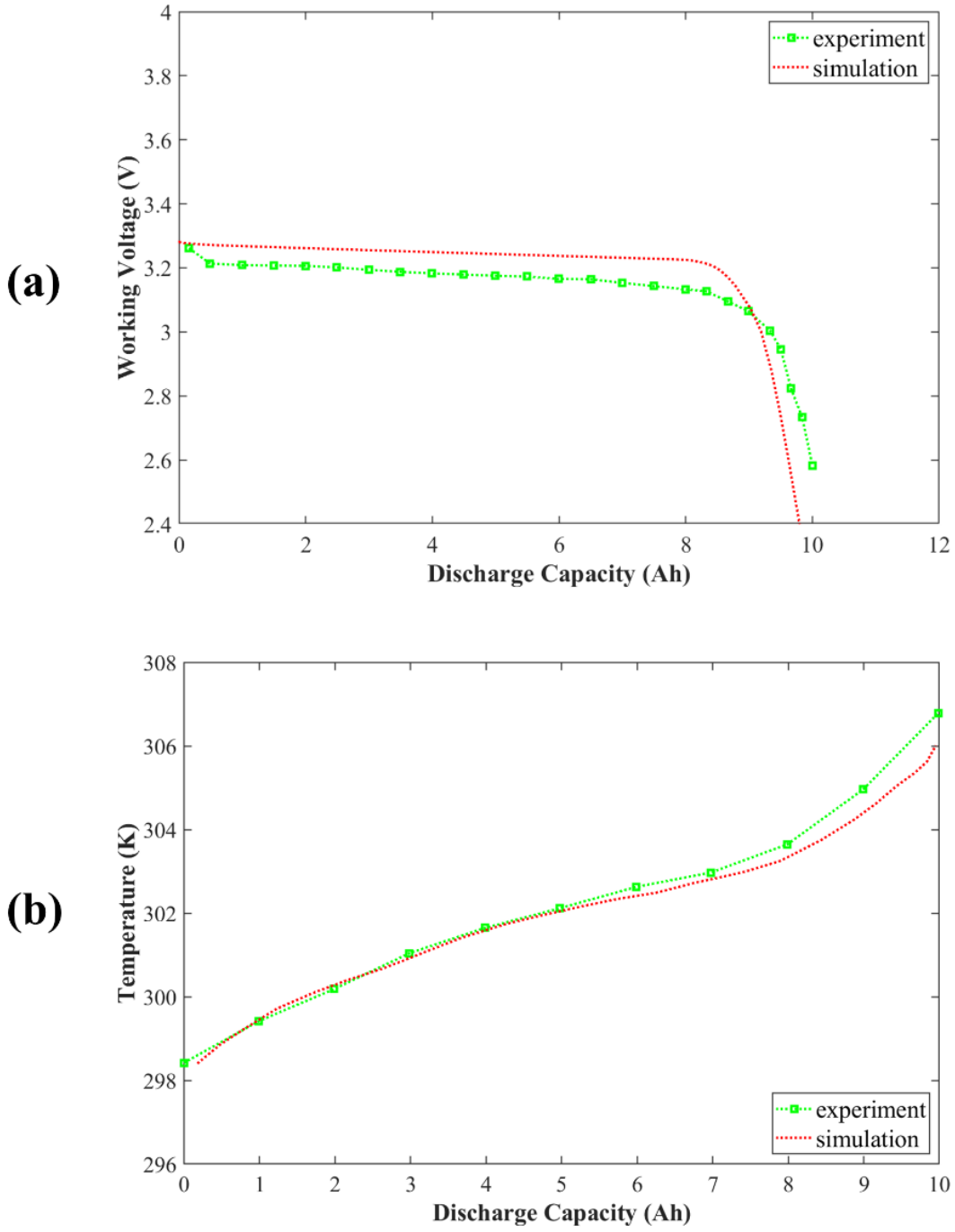

Figure 5.2 Comparison of numerical results of (a) working voltage and (b) temperature with experimental results [93] during 1C galvanostatic discharge under natural convection conditions.

Considering the electrochemical performance, the current flows inside the battery cell and battery pack remain similar due to applying a single particle model. The Single

Particle Battery interface answers for solid diffusion in the electrode particles and the intercalation reaction kinetics. A lumped solution resistance term is used for covering the ohmic potential drop inside the electrolyte. The cell capacity is specified through fractional volumes of both electrodes in the battery. The individual electrode operational state-of-charges are used to identify the initial charge distribution in the battery. The temperature contour and heat flux streamline of the proposed battery pack shows the temperature distribution of the whole battery pack during its working process by the proposed thermo-electrochemical model. The maximum temperature of the battery's innermost parts is around 2 °C higher than the outermost parts. It also provides the temperature difference of the whole battery pack. With the utilization of this lumped model, the broad temperature distribution of battery cell surfaces can be represented. Besides, the heat flux generated inside the battery cell can be simulated, as well as the heat exchange between battery surfaces and the ambient cooling air can be simulated numerically.

Through the numerical study for the whole battery pack, the configuration setup of the battery pack is also investigated. The two-dimensional parameters are defined by different directions with various gaps, which are no gap (0 m), half of a cell (0.01 m) and one cell (0.02 m). Through permutation and combination, nine sets of collocations are formed. Figure 5.3 shows that all the battery cells are constructed together with various gap setups among the parallel-coupled battery pairs, which are the first 9 cases. The gap enhances the convective and conductive between battery cells and ambient air from the battery safety perspective, improving battery pack cooling efficiency and fire safety.

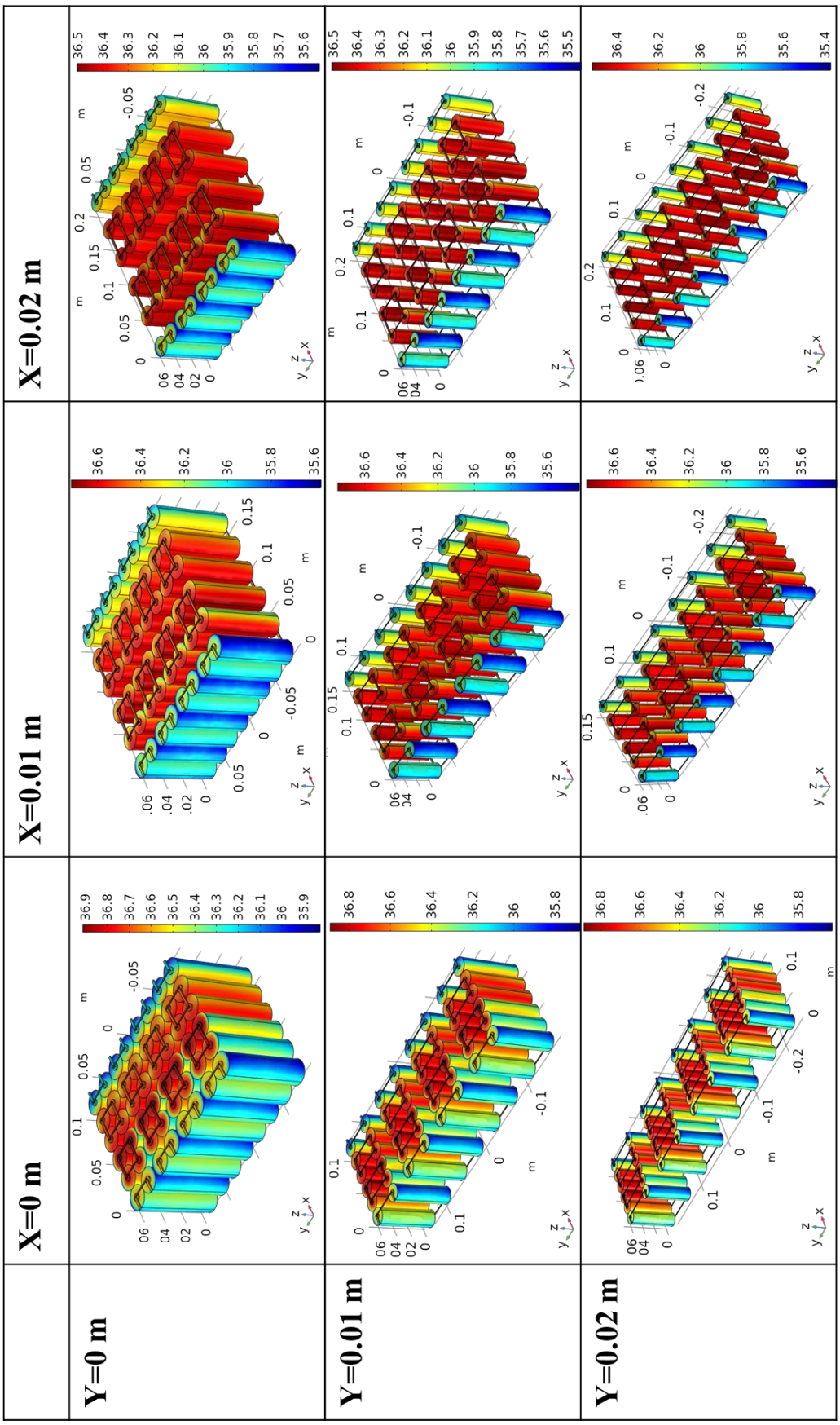

Figure 5.3 Temperature contours of different battery pack configurations.

To further understand the battery temperature distribution, air velocity and ambient environment are considered as well. Buoyancy forces cause natural convection as a consequence of density changes ascribed to temperature differences in the fluid. At heating, the fluid will get up because of the density variation in the boundary layer. Meanwhile, the cooler fluid, which will heat and increase, will replace the raised fluid. This continuous phenomenon is named free or natural convection. Thus, this study selected four sets of air velocities. Moreover, the temperature difference (The difference between the highest and the lowest temperature of the battery pack) and maximum temperature (The maximum temperature of a battery cell) are also considered. Figure 5.4 plots the maximum temperature and temperature difference profiles under various operating conditions, where the geometry conditions remain the same. From Figure 5.4 (a) and (c), air velocity positively impacts decreasing the maximum temperature and temperature difference. Under the same ambient temperature, shown in Figure 5.4 (b), increasing the air velocity can enhance the cooling efficiency, but the drop in maximum temperature is not much. Figure 5.4 (c), cases with air velocity of 4 m/s achieve 36%, which is the maximum percentage of temperature difference drop compared to other cases in this configuration. It is demonstrated that when the minimum values of maximum temperature and temperature difference are reached, the format set up is the best and optimisation results.

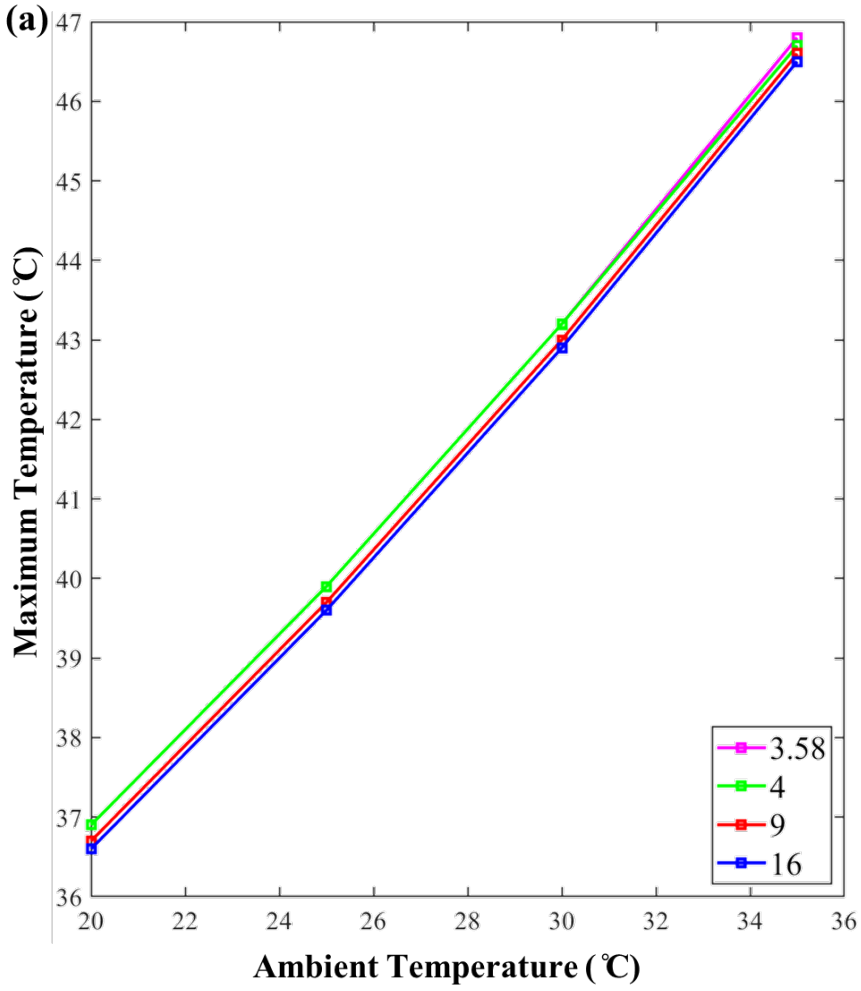
(a)
Maximum Temperature (℃)
Ambient Temperature (℃)
3.58
4
9
16

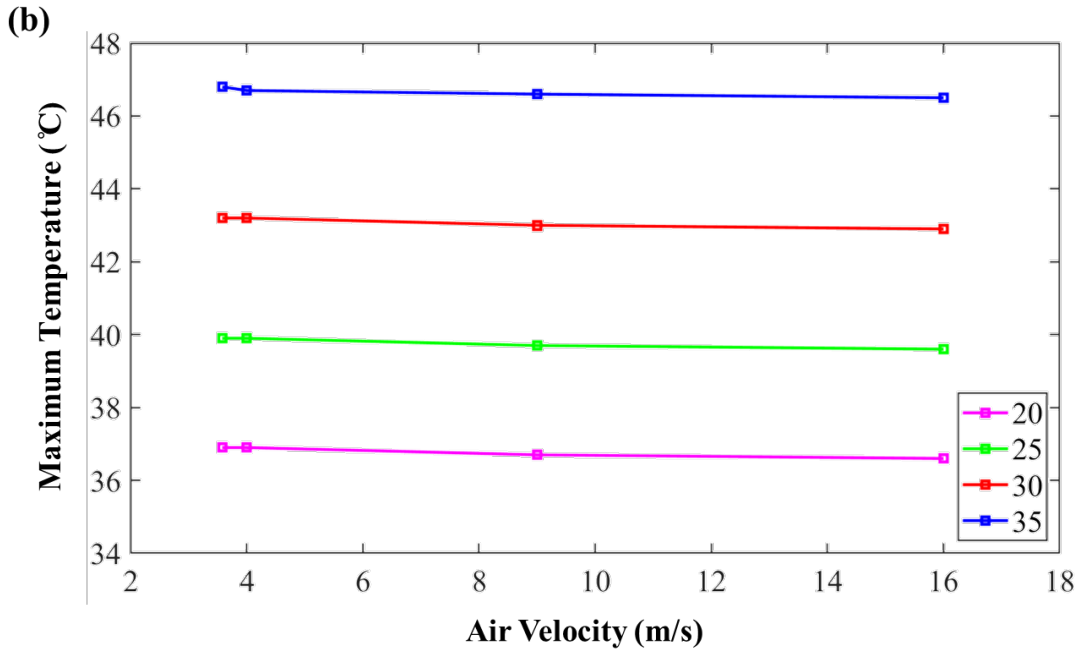
(b)
Maximum Temperature (℃)
Air Velocity (m/s)
20
25
30
35

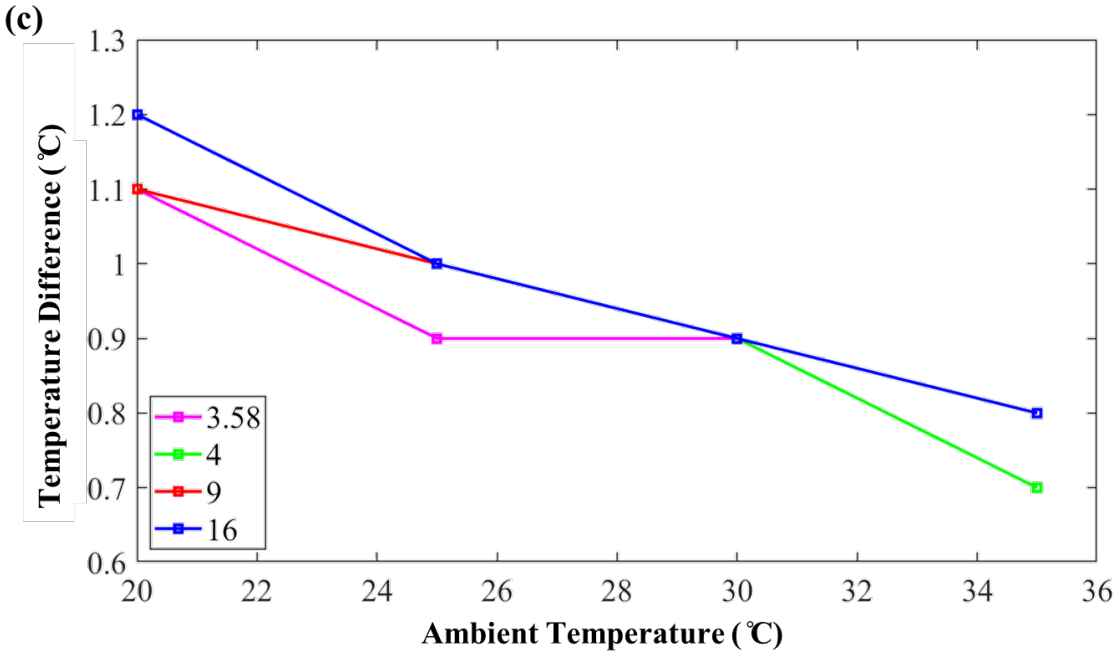

Figure 5.4 The profile of maximum temperature (a, b) and temperature difference (c) under various operation conditions.

5.3.2 Training and results analysis

In this study, the multilayer perceptron (MLP) neural network was applied. It is one of the most competitive types of ANN for regression in various research fields. Because this approach shows a considerable capability for universal approximation, it is regularly applied to model quite highly complex and disordered phenomena. As mentioned previously, the ANN utilises the battery thermal distribution simulation dataset obtained through numerical simulations of a typical battery pack configuration on two cylindrical batteries in parallel and six-coupled battery pairs in series. In summary, it consists of 130 data sets of six parameters (four inputs and two outputs) prepared for the training and testing of the ANN. The detailed inputs and outputs of each dataset are illustrated in Table

5.3. Note that the heat transfer coefficient was replaced with the air velocity more effectively presentative by the ANN. It is possible to extend the ANN model to predictions on other heat transfer methods not considered in the datasets by analysing their coolant velocity. The heat transfer coefficient of air can be estimated to:

$$h_t = 10.45 - v - 10v^{1/2} \tag{5.1}$$

where h_t represents the heat transfer coefficient, and v is the relative speed between the object's exterior and air. This equation is empirical and can be applied to the velocity range from 2 to 20 m/s [258].

Table 5.3 Details of the inputs and outputs for the ANN model.

	Inputs				Outputs	
Parameters	X_Gap	Y_Gap	Air velocity	Ambient temperature	Maximum temperature	Temperature difference
Units	m	m	m/s	°C	°C	°C
Range	0-0.02	0-0.02	30-39.96	20-30	-	-

The proposed ANN model has been trained using the Levenberg-Marquardt (LM) optimisation technique [259]. The LM method based on Levenberg [260] and Marquardt [261] combines Newton's method and gradient descent. It is one of the most efficient training algorithms for neural network modelling [262]. Generally, this algorithm demands more storage space but less time. The training process will be terminated spontaneously when generalisation ends improving, as represented by a growth of the

mean square error of the validation samples. In the LM method, the Hessian matrix can be approximated as:

$$Hf = Jf^T Jf \tag{5.2}$$

The gradient is given by:

$$\nabla f = Jf^T e \tag{5.3}$$

where *Jf* is the Jacobian matrix and *e* is the vector of a network error.

The LM working function or the fitness function is based on the mean square error (MSE) between the network output and the target output:

$$F = MSE = \frac{1}{N}\sum_{i=1}^{N}\left(R_{i,network} - R_{i,target}\right)^2 \tag{5.4}$$

where N is the number of datasets, $R_{i,network}$ is the network output and $R_{i,target}$ is the target output from the simulation data. The number of hidden neurons has been mentioned in Equation (3.32) from the previous chapter, and the configuration structure of the proposed ANN model is shown in Figure 5.5.

Figure 5.6 demonstrates the ANN regression results, and it plots the regression relation between the physical outputs and the targets, which indicates that this ANN model has achieved a good fit with the training datasets. From Figure 5.7, the error histogram plot shows that most errors reside in the range of −0.03688 to 0.0292. The majority of the predictions had a root mean square (RMS) error of approximately 0.088%, with around 10% of the predictions within ± 25% RMS error. The ANN was successfully trained with an overall R (fitness) of 0.999, with most prediction errors within 1% RMS error. In future

works, the ANN model can be further refined to achieve even higher reliability and accuracy. This can be done by adding more simulation results considering a wider range of configurations or applying more advanced ANN training techniques.

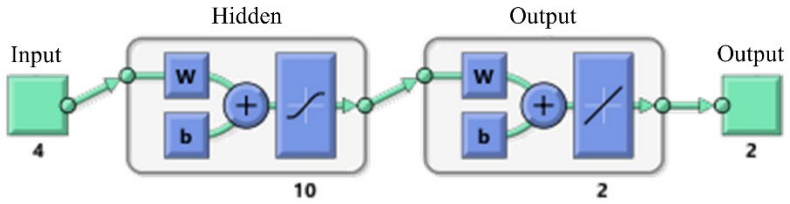

Figure 5.5 The configuration structure of the proposed ANN model.

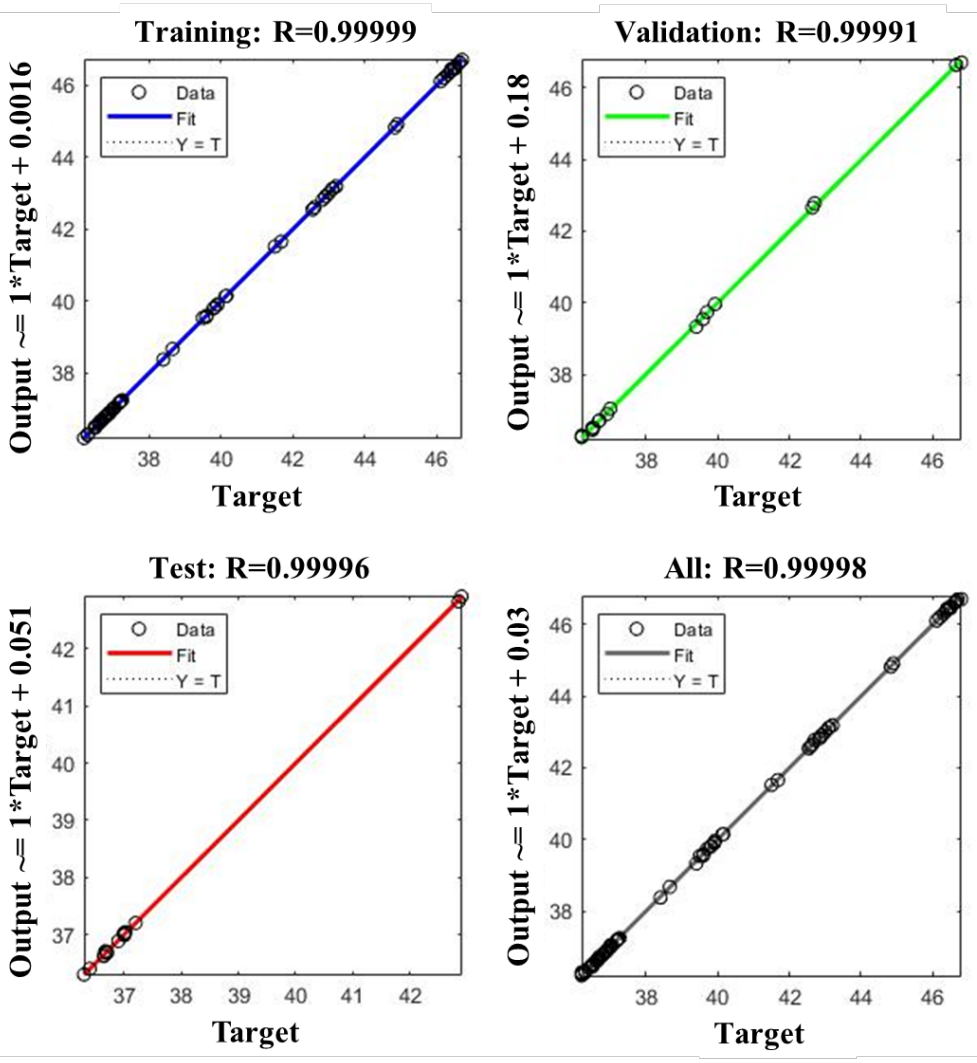

Figure 5.6 Regression results of ANN model.

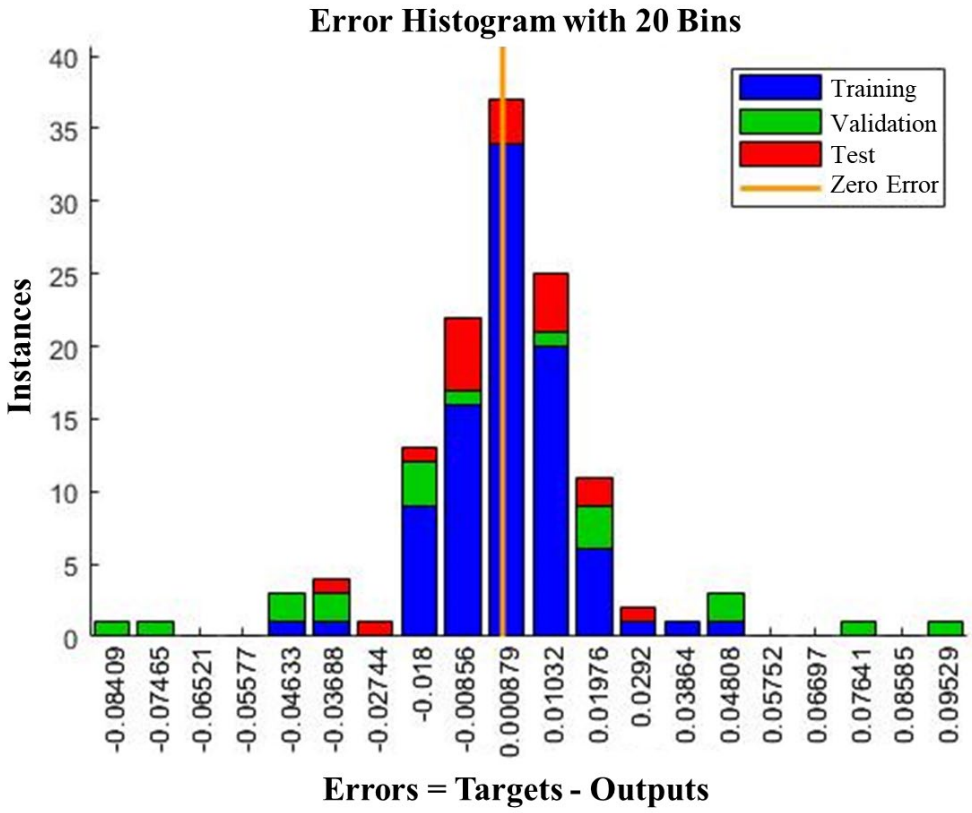

Figure 5.7 RMS error histogram of the ANN model predictions.

5.3.3 Optimisation analysis and discussions

The optimisation configuration has been proposed further to investigate the designed system with various working temperatures to improve the battery system's fire safety performance and cooling efficiency. These simulation results have investigated the air velocity and ambient temperature after successfully training the ANN model. A battery pack comprises many single battery cells, and the operation temperature difference for the single battery cell inside the battery pack will be sourced by the temperature imbalance of the battery pack. This will result in the cell's inconsistency and over the normal state during the charge and discharge process, harming battery pack service life.

Consequently, an appropriate battery thermal management system should simultaneously lower the maximum temperature and temperature difference of the battery packs to ensure the reliability and consistency of EVs and HEVs battery performance.

The 6,250,000 groups of structure and operation features are created in MATLAB. Inputs 1 and 2 are the configuration features, and Inputs 3 and 4 are the operating conditions. The CFD-ANN model calculates the optimal combination to achieve the perfect battery performance under the existing case arrangement with the current four inputs and two outputs.

After successful training of the ANN model, four inputs are divided into 50 intervals separately in a specific range. Then, 6,250,000 groups of structure features are processed in MATLAB, and the optimal result can be selected. According to Figure 5.8, the batteries' maximum temperature and temperature difference are greatly affected by the battery configuration and operating conditions, with a fluctuation as high as about 7 °C for the maximum temperature and 1.5 °C for the temperature difference. It can be obtained that the instability of the maximum temperature shows a different trend with the fluctuation of the temperature difference under the current range of various inputs. Therefore, the maximum temperature is chiefly influenced by the battery properties. The temperature difference can be treated as an indicator to evaluate the batter cooling performance of the battery pack.

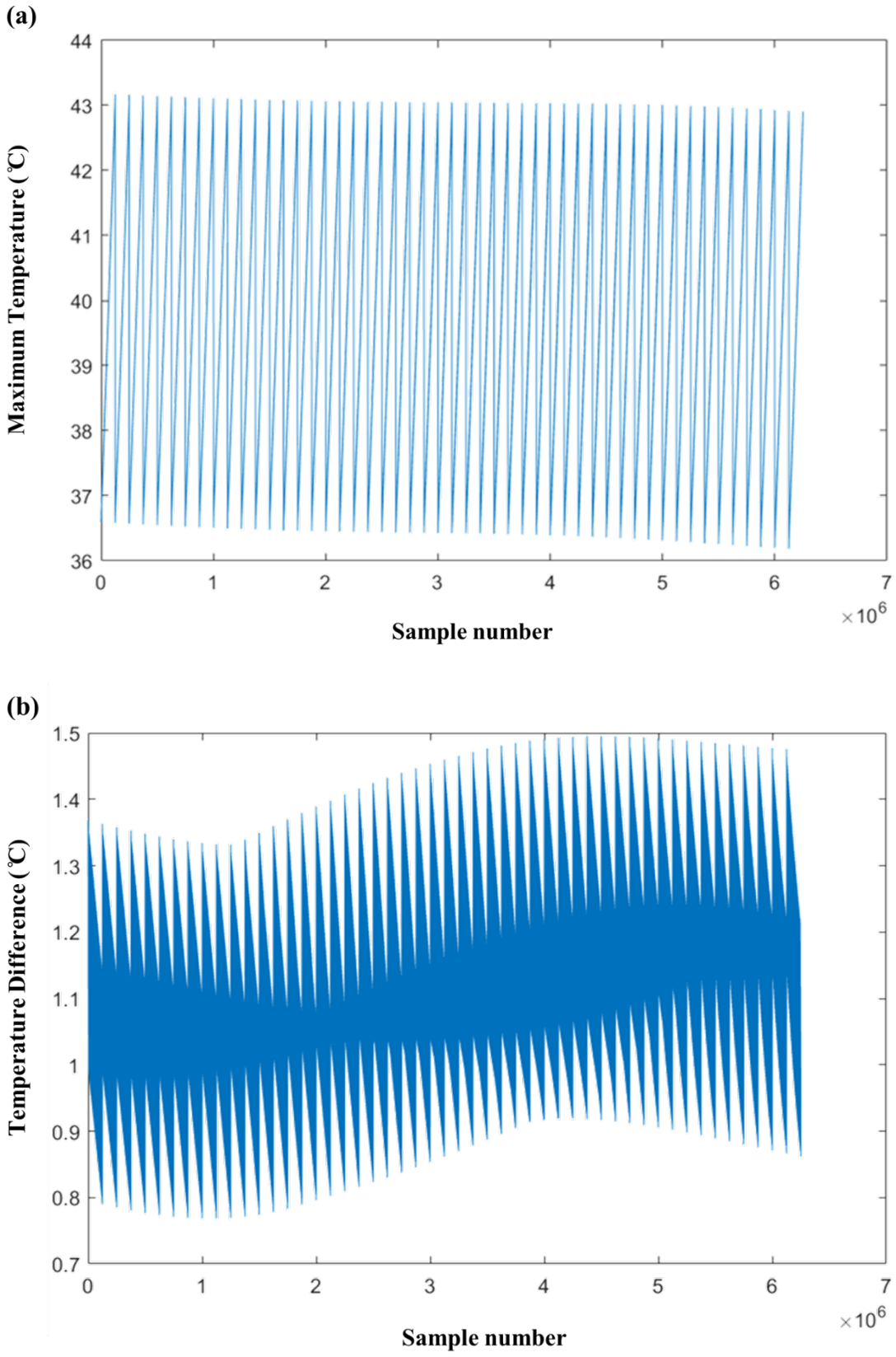

Figure 5.8 (a) Maximum temperature and (b) temperature difference of the battery pack for different input combinations.

From the CFD-ANN model simulation results, the six million sample results are sorted in ascending order of the battery spacing. In order to find the optimal combination, a selection process is set, considering the maximum temperature and temperature difference. Regarding achieving a battery cooling performance, it can be concluded that the optimal case is the 0.02 m X-direction gap and 0.01 m Y-direction gap under 20 °C ambient temperature and the air velocity of 16 m/s. Compared to the original configuration with the same operating conditions, the maximum temperature decreases by 1.9%, which is from 36.9 °C drop to 36.2 °C. The temperature difference drops by 4.5%, compared to the original 1.1 °C temperature difference. The results demonstrated the CFD-ANN model optimisation has improved both the cooling efficiency and battery performance. The proposed framework demonstrates an efficient way to improve the thermal performance of the battery pack by optimizing the configuration under different operating conditions.

5.3.4 Verification of the optimal spacing combination

Within the four input ranges, the ANN model can directly calculate the maximum temperature and the temperature difference. Considering the original 16 cases, the best combination is achieving a maximum temperature of 36.2 °C and a temperature difference of 1.1 °C. With this optimal result, both the maximum temperature and temperature difference are the smallest compared with the other 15 cases. Using the four

inputs from the optimal case, the outputs obtained from the ANN model are maximum temperature (36.2027 °C) and temperature difference (1.119 °C). Compared with the CFD simulation results, the absolute error is 0.019 °C, and the relative error is 1.7%. It can be concluded that this ANN model can provide the optimal configuration combination and enhance the heat dissipation effect of the battery system. Furthermore, the relative error is improved compared to the relative error (1.995%) generated by Qian et al. [231], proving that the proposed framework improves the temperature uniformity of the current battery system.

5.4 Chapter Summary

In this chapter, an optimal design of battery thermal management systems was achieved by applying a three-dimensional thermo-electrochemical model coupled with the ANN model. Utilizing numerical simulations via CFD, different battery pack configurations were investigated in a simulation environment to positively impact cooling efficiency, battery performance, and battery fire safety. The three-dimensional thermo-electrochemical model was introduced to calculate the temperature distribution and validated with the previous experimental data. The numerical case studies were applied to train the proposed ANN model, demonstrating the relationship among geometric parameters, operating conditions and cooling efficiency. The CFD-ANN model compared 6,500,000 combinations with various configurations and boundary conditions. The optimal design for the current battery setup was the case with a 0.02 m X-direction gap

and a 0.01 m Y-direction gap, which lower the maximum temperature and temperature difference by 1.9% and 4.5%.

The results highlighted one significant advantage of numerical simulations. All the pertinent information like structural parameters and operation requirements can be derived from the model. Furthermore, different factors can be simulated and optimised simultaneously in a simulation environment to deliver a constructive perception of the battery's performance and thermal behaviour. In the future, more parameters can be introduced with the current CFD-ANN model, such as electrode materials, electrolyte materials, cell numbers, different coolants, and so force. A universal database of parameters and repercussions for the battery thermal management system can be prepared, which can then be processed by foresight models to make outlooks and predictions of the fire risks of the LIB energy storage system on a set of input variables.

Both Chapters 4 and 5 study the performance of BTMs for the battery pack under normal working conditions. Many different operating parameters and ambient conditions are considered. Nevertheless, the thermal behaviour of the BTMs within some extreme conditions should be also investigated. In the following Chapter 6, the abnormal heat generation will be introduced with an inhouse written user-defined function code to analyse the thermal propagation and heat exchange mechanism, which contributes to comprehensively evaluating the performance of BTMs and improving the safety of battery packs.

Chapter 6 Thermal Propagation Modelling of Abnormal Heat Generation in Various Battery Cell Locations

This chapter includes the contents from a published journal article [263]: **Li, A.**, Yuen, A. C. Y., Wang, W., Weng, J., Lai, C. S., Kook, S. & Yeoh, G. H. (2022). Thermal Propagation Modelling of Abnormal Heat Generation in Various Battery Cell Locations. *Batteries*, *8*(11), 216. with modifications and reorders to better fit the structure of this thesis.

6.1 General Description

In Chapters 4 and 5, the thermal behaviour and cooling performance have been analysed and optimised under normal working conditions. A better understanding of the heat exchange process under extreme conditions will improve a safer design and enhances battery thermal management performance. The heat transfer during serious scenarios, such as battery thermal runaway or abnormal heat generation, provides insight into thermal propagation and cooling efficiency. This chapter proposed a three-dimensional thermal model for the battery pack simulation by applying an in-house model to study the

internal battery thermal propagation effect under the CFD simulation framework. The simulation results were validated with the experimental data. The detailed temperature distribution and heat transfer behaviour were simulated and analysed. The thermal behaviour and cooling performance were compared by changing the abnormal heat generation locations inside the battery pack. The results indicated that various abnormal heat locations disperse heat to the surrounding coolant and other cells. According to the current battery pack setups, the maximum temperature of Row 2 cases can be increased by 2.93%, and the temperature difference was also increased. Overall, a new analytical approach has been demonstrated to investigate several stipulating battery thermal propagation scenarios for enhancing battery thermal performances.

6.2 Introduction

Electrification will be increasingly integrated into our daily lives with the rapid development of energy storage systems. LIBs, one of the most commonly used energy storage units, are now found everywhere owing to their high energy density, high power output, low self-discharge rate and little memory effect. Nevertheless, these advancements also have some counterparts, potentially causing a TR phenomenon due to its less thermal stability. Many LIB fires happened in the recent decade [264, 265], and battery safety has become an essential topic for the development of LIBs. Due to different energy demands, battery cells are usually packed in series or parallel to work as a battery pack or a battery system. Considering the performance of LIBs, the operating temperature

range stays from 15℃ to 40℃ based on battery types [266], while the temperature difference is under 5℃. In order to keep the most suitable working temperature range and avoid thermal issues, such as battery cell dissimilarity [267], gradual ageing effects [268], etc., BTMs become an essential component for battery packs or systems [269]. In practical situations, some improper conditions, such as mechanical, electrical, and thermal abuse, cause an abnormal temperature. The exothermic reaction occurs when the battery temperature is over a specific value, leading to heat cumulation. Afterwards, the other chain reactions are triggered with more heat and gas, resulting in battery fire and explosion. This process is considered a battery TR.

Based on various TR trigger conditions, overheating initiation can be generated by different situations: a) cooling systems fail to control the temperature, b) internal defects, such as short-circuiting, generate heat and transfer to adjacent cells, c) external heat leads to unexpected high temperature. Many research works have been done for the TR investigation. Goupil et al. [270] analysed the influence of the heating rate on the outgassing and cell casing temperature, as well as the comparison of produced flame and released smoke. The results showed that a high heating rate leads to a more violent TR, while it does not affect maximum cell and outgassing temperature too much. Chen et al. [271] applied the t^2 fire principle to numerically predict the fire hazard and total heat release. The ignition time difference parameter was also investigated for the application of battery fire analysis. Huang et al. [272] studied the feature of battery TR under a different SOC. The safe, critical, and hazardous regions were defined based on the

response to thermal behaviour. The TR mechanism is still the current research focus in battery thermal safety.

In most scenarios, a single cell TR will propagate to the neighbour cells, accelerating the heat cumulations and leading to a serious situation. Therefore, effective and efficient BTMs keep the battery or battery systems working under a suitable condition and provide a fire-safe environment before the TR occurs. Depending on the cooling medium, BTMs can be categorized into several types, air cooling BTMs [273, 274], liquid cooling BTMs [275-277], heat pipe cooling BTMs [278-280], phase change material (PCM) cooling BTMs [281-284], and hybrid cooling BTMs [285-287]. The performance and effectiveness of the BTMs play an important role in battery thermal safety.

Compared to other cooling BTMs, air cooling BTMs are one of the most suitable cooling methods due to their relatively low cost of manufacturing and maintenance, simple configuration, high reliability, etc. Numerous studies have been done in this area from both experimental and numerical perspectives. Lopez et al. [232] focused on experimental elucidation and analysis of various LIB module configurations. The TR propagation has been characterised, and the safe practices were achieved by increasing the inner cell spacing. With the development of computer science, the CFD technique has become a mature and effective tool to analyse many perspectives of battery studies, such as the single battery thermo-electrochemical performance [288-290], each component of the battery cell [291, 292], multi-scale multi-domain thermal analysis [293], the battery pack/module overall performances [294-296], etc. Behi et al. [297] compared natural ventilation and forced-air cooling based on a battery module consisting of cylindrical cells.

Also, a comparison among natural ventilation air cooling, forced-air cooling, heat pipe, and heat pipe with copper sheets was demonstrated. The numerical results show that the heat pipe with copper sheets provides the most excellent maximum temperature and the best temperature uniformity of the battery module. Tang et al. [298] built an electrochemical-thermal model to optimise the structural design of the battery module. In addition, various modes of heat transfer were investigated during the TR propagation. Heat conduction is the primary heat transfer mode for the direct-connect cell mode, while heat radiation is the primary mode for the indirect-connect cell mode. Wang et al. [299] built air-based BTMs with uneven cell spacing configurations. A neural-network-based model presented the multi-objective optimisation, and the results showed that the energy consumption was reduced to 41.19% of the original layout. Chen et al. [300] introduced three novel schemes, hollow spoiler prisms, added PCM, and fins, to enhance the heat transfer capacity and safety of a battery pack. The numerical comparison results showed that compared to the conventional air cooling system, all the proposed three schemes improved the cooling performance, where the case with a fin and PCM filled spoiler prism demonstrated the best result and prevented the TR propagation among battery cells. Yang et al. [301] investigated the battery cooling performance of the reverse-layered stagger-arranged battery pack configuration using CFD simulations and optimised the temperature distribution by adding a spoiler. The maximum temperature of the battery pack decreased by 1.85 K compared to the one without a spoiler. Zhai et al. [302] proposed an experimental-based Domino prediction model to predict the TR propagation path and probability. Meanwhile, the thermal analysis of three different trigger TR battery

locations was demonstrated, and the whole TR propagation process was divided into four stages.

The cell TR or abnormal heat generation is an essential factor for BTMs. It also affects the temperature distribution of the whole battery system, which links to the battery energy density. Additionally, understanding the TR occurrence reduces the risks of battery fires. In essence, the in-depth characterisation of battery internal thermal propagation and heat transfer behaviours are key to fully realise the effectiveness of BTMs and improving the battery performance without sacrificing safety risks. Figure 6.1 demonstrates a brief schematic picture of the whole idea for this chapter. This section aims to investigate the influence of different TR cell locations on TR propagation based on the forced-air cooling BTMs. Based on previous research works and the aforementioned research motivations, the key objectives of this chapter are constructed as follows:

(i) A three-dimensional thermal model with an in-house written code will be developed, and the detailed temperature distribution will be replicated by CFD simulations.

(ii) The numerical results will be validated against the previous experimental results, and more scenarios with various conditions will be presented and compared.

(iii) The heat transfer mechanism will be analysed, and this will provide insight into the design of BTMs and the improvement of battery safety.

(iv) The potential application of this work and the future perspectives will be presented.

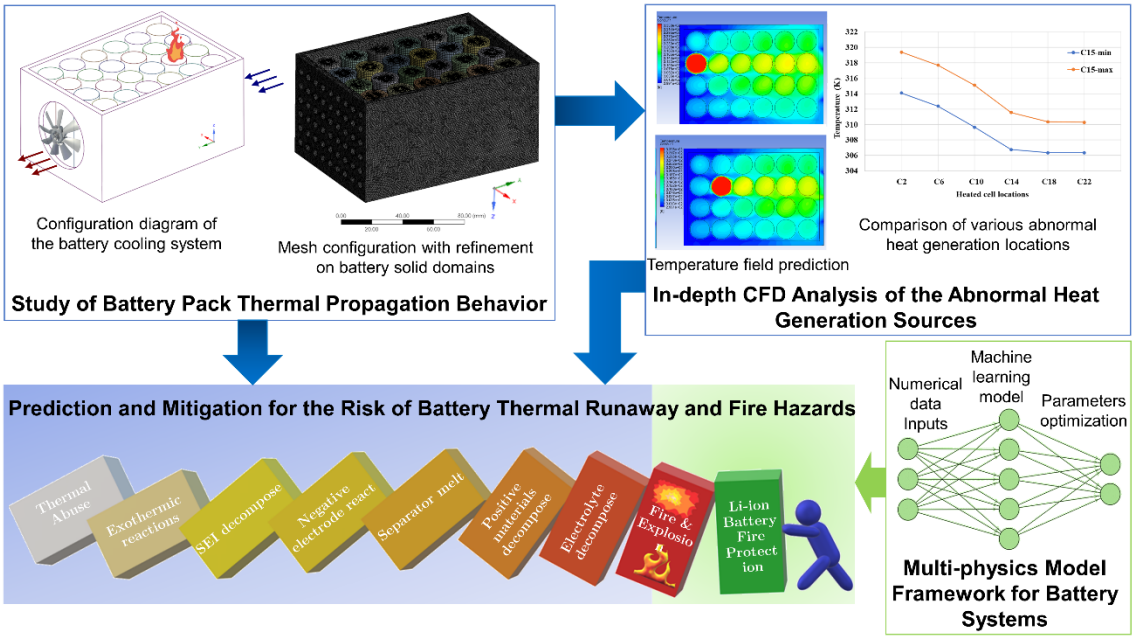

Figure 6.1 Schematic picture of the structure of this chapter.

This chapter is constructed as follows. The overall numerical model framework is introduced in Section 6.3, and the model validation and verification are described as well. After that, the numerical analysis and results are exhibited in Section 6.4. In section 6.5, the chapter summary is demonstrated.

6.3 Model Configuration

6.3.1 Model description

In this section, the commercial CFD software (ANSYS-Fluent) with an in-house written code is employed to simulate the battery thermal behaviour and replicate the temperature distribution across the battery pack. A battery pack with 24 × 18,650 cells was utilised, which uses air cooling BTMs by a fan located at the outlet, shown in Figure 6.2. The

experiments were carried out by Behi. et al. [297] under the case with cell spacing of 2 mm and air velocity of 2 m/s. The battery pack comprises 24 cylindrical cells in parallel-series connection, and 54 holes (6 rows × 9 columns) were embedded in the inlet surface. The configuration is aligned with the experiment setup to validate the simulation results with the experimental data. The whole battery pack is set as 130 mm × 90 mm × 70 mm, and the diameter of each inlet hole is 5 mm, which is one-tenth of the suction fan diameter designed by Behi et al. [297]. Besides, the main parameters of the single battery cell, the ventilation fan and the outer polyvinyl chloride (PVC) case are summarized in Table 6.1, respectively.

Table 6.1 Parameters and properties of the battery cell, ventilation fan and outer case.

Parameters of battery cell		**Parameters of ventilation fan**		**Parameters of outer case**	
Specific heat capacity	1200 [J/kg/K]	Outlet diameter	50 mm	Specific heat capacity	600 [J/kg/K]
Density	2722 [kg/m^3]	Inlet air temperature	299.15 K	Density	100 [kg/m^3]
Anisotropic thermal conductivities	k_r = 0.2 [W/m/K], k_z = 37.6 [W/m/K]	Pack size (length × width × height)	130 mm × 90 mm × 70 mm	Thermal conductivities	0.1 [W/m/K]

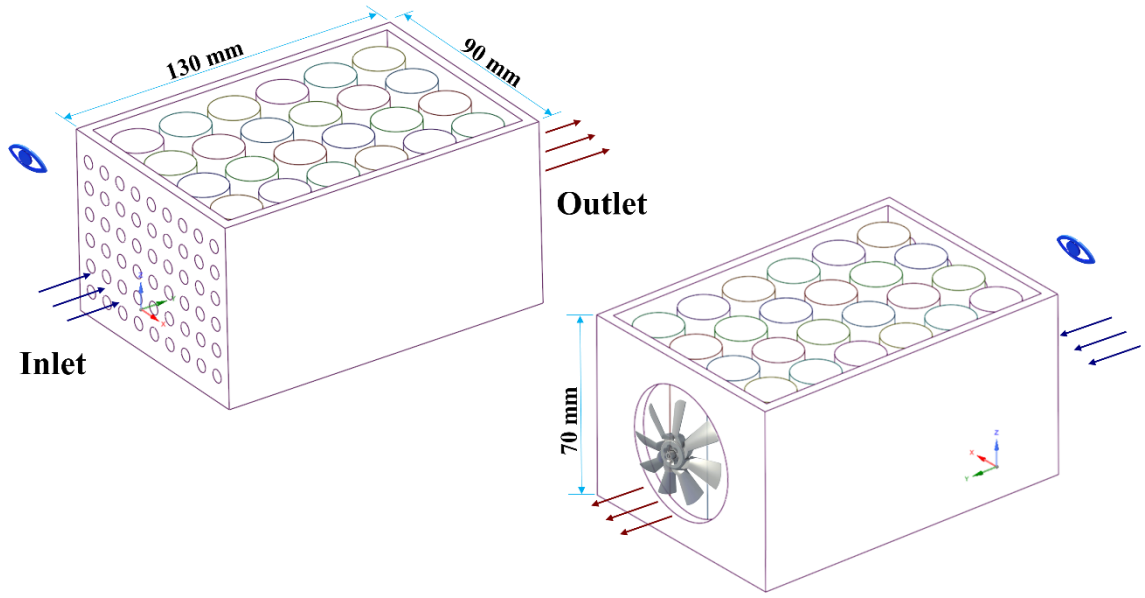

Figure 6.2 Schematic figure of the battery pack with 24 18,650 cells.

6.3.2 Model verification and validation

Typically, the cooling performance of the BTMs is evaluated by three index parameters: the maximum temperature, temperature difference and energy consumption [299]. To validate the numerical results of this work, the experimental data generated by Behi et al. [297] is chosen. The simulation configuration is the same as the experiment setup, which consists of a 24 cells battery pack, a polyvinyl chloride (PVC) case and a cooling fan, shown in Figure 6.1. The testing point of the K-type thermocouple is designated at the specific position, which is the position of cell 5 (C5) and cell 15 (C15), shown in Figure 6.3. The thermocouples were calibrated, and the accuracy and uncertainty were evaluated by Behi et al. [297] during the experimental data collection.

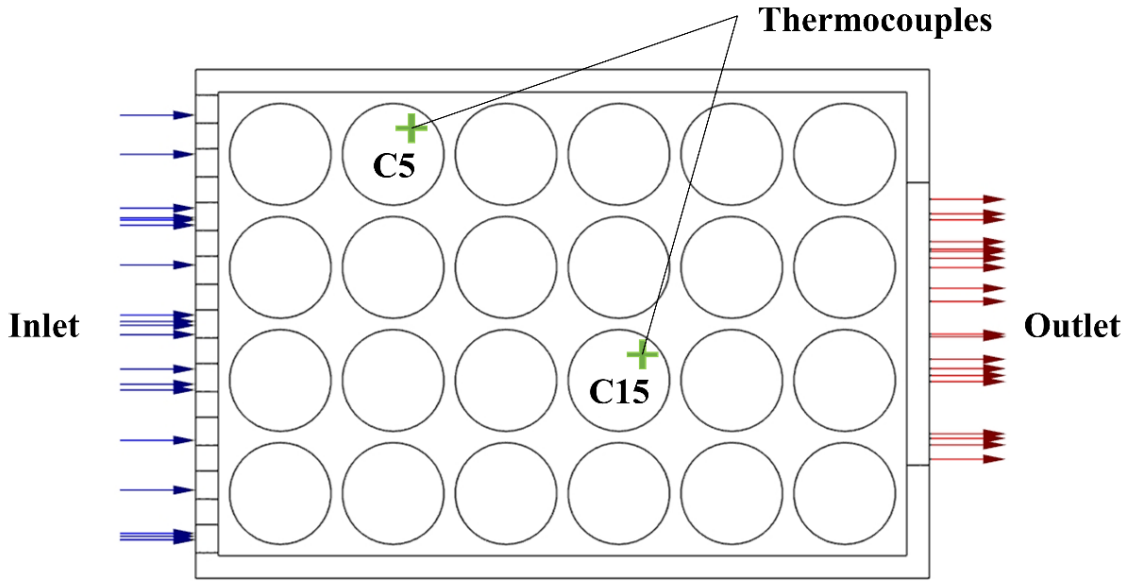

Figure 6.3 Schematic figure of thermocouple testing point.

Under normal working conditions, the battery pack completed the discharge cycle with a 1.5 C discharge rate, which could be considered a heat source equal to 48,750 W/m^3. The air inlet velocity is 2 m/s with coupled boundary conditions among air-battery and air-PVC case interfaces. The boundary walls are specified as adiabatic non-slip walls. The second-order upwind spatial discretization is applied for pressure, momentum, energy, turbulent kinetic energy and specific dissipation rate.

To achieve a credible CFD solution, mesh independence analysis is required to quantify the numerical errors and uncertainties. Based on the experimental layout, the geometry of the whole battery pack was built, and the computational region was mapped by an unstructured mesh, shown in Figure 6.4 (a). The maximum volume temperature and the surface weighted average temperature specified by C5 and C15 under various mesh

element sizes to evaluate the mesh independence were illustrated in Figure 6.4 (b). Compared to the different grid size and element numbers, it is observed that the maximum volume temperature and the surface weighted average temperature of both cells stabilizes when the grid amount reaches 1.99 million. Hence, the medium element number of 1.99 million grids is applied for this battery pack simulation.

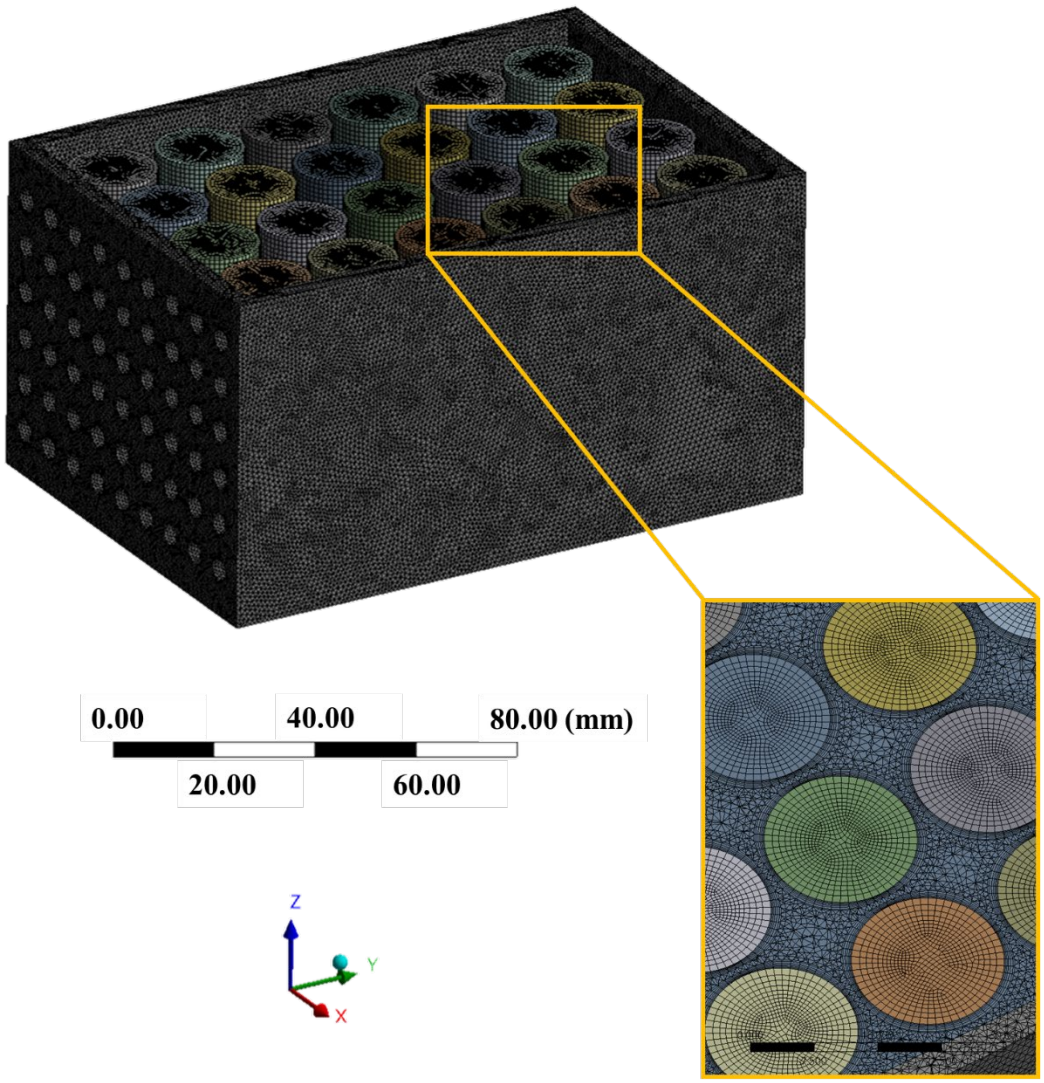

(a)

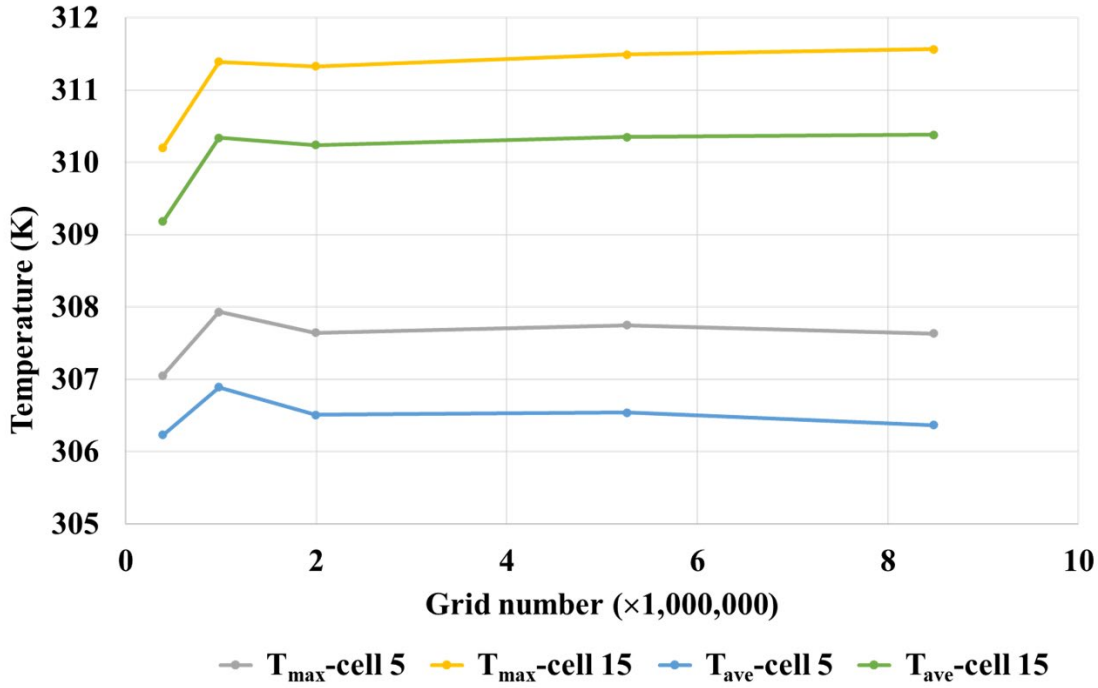

(b)

Figure 6.4 (a) Schematic of the computational domain and mesh; (b) Mesh independence analysis.

As shown in Figure 6.3, the experimental temperature data was collected from the testing points and used to validate the numerical results. Validation of the CFD model means validating the numerical calculations by establishing a range of physical conditions obtained from the calculations and performing comparisons of the results from the CFD code with experiments that span the range of conditions. The comparison between the experimental data (black) and predicted temperature from the CFD model (red) is presented in Figure 6.5 (a), which demonstrates that the numerical results achieve an acceptable agreement with the experimental data. The relative error between the experimental and numerical results is approximately less than 0.3%. Thus, the error is

acceptable, and the numerical model can capture the thermal behaviour and demonstrate proper prediction for the current setups.

Based on this setup, the overall thermal behaviour of the battery pack can be replicated by the CFD simulation. Figure 6.5 (b) shows the temperature distribution of the cross-section plane for the whole computational domain. It is easy to conclude that the cooling effect drops due to the heat exchange upstream when the cooling air goes through the battery pack. The cooling effect near the inlet is better than that next to the outlet. Additionally, the whole battery pack is symmetry along the moving direction of the cooling air, and the battery temperature of the upper row is slightly lower than the middle row. To be easily identified, the upper row is defined as Row 1, where C5 is located. Similarly, the row with C15 is named Row 3. The middle row between Rows 1 and 3 is defined as Row 2.

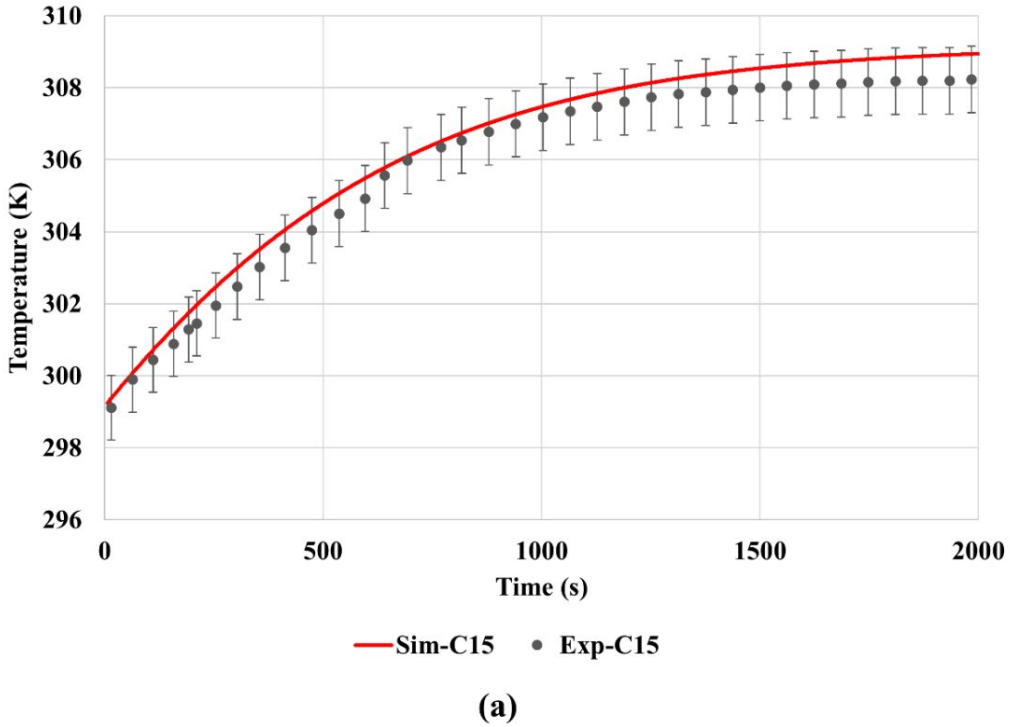

(a)

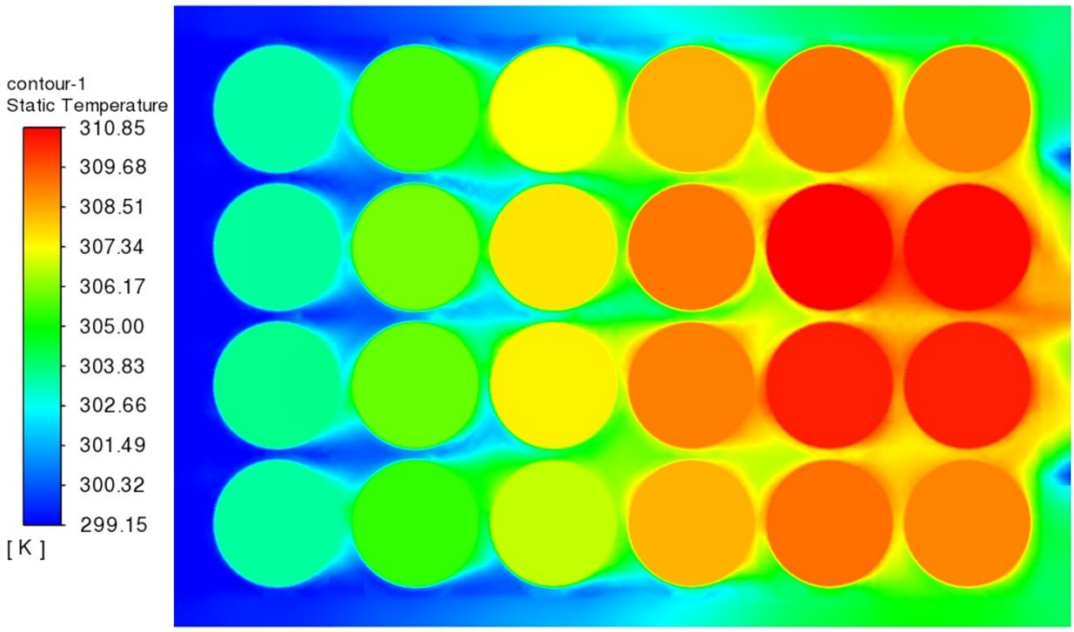

(b)

Figure 6.5 (a) Numerical model validation, the error bar is 0.3%; (b) Temperature distribution in the cross-section plane.

6.4 Results and Discussions

6.4.1 Applied extreme heat to the model

During the thermal runaway propagation, extra heat is generated due to complex exothermic reactions, and the temperature of the thermal runaway cell will increase dramatically. This feather was captured experimentally by Lopez. et al. [232]. Based on the experimental data, we applied an in-house written user-defined function to replicate the temperature change of the thermal runaway cell. By using this code in the previously validated model, the current case successfully simulates the scenario with a cell

experiencing thermal runaway. The case layout is the same as the pre-mentioned case, and an abnormal heat generation is applied in cell 6, shown in Figure 6.6 (a).

The heat propagation inside the battery pack under the addition of abnormal heat generation was presented in Figure 6.6 (b). Compared to Figure 6.5 (b), the added abnormal heat generation increased the maximum temperature with the value of 12 K. Additionally, the temperature difference also increased from 11.7 K to 23.3 K, which changed the original temperature distribution of the force-air cooling case.

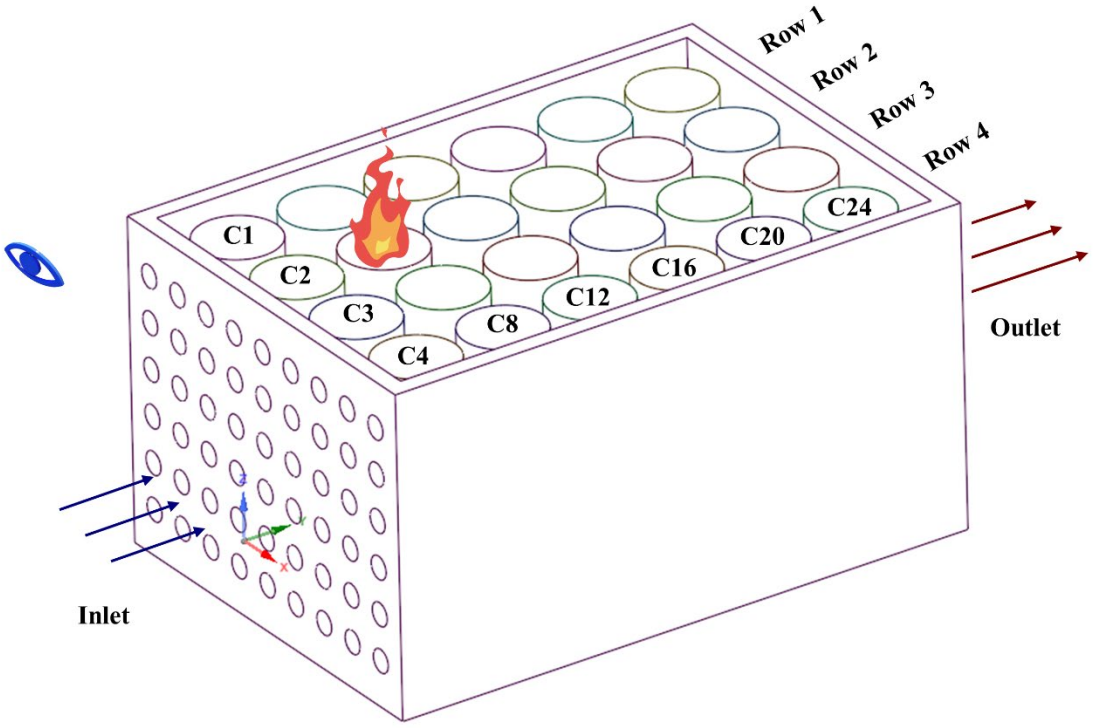

(a)

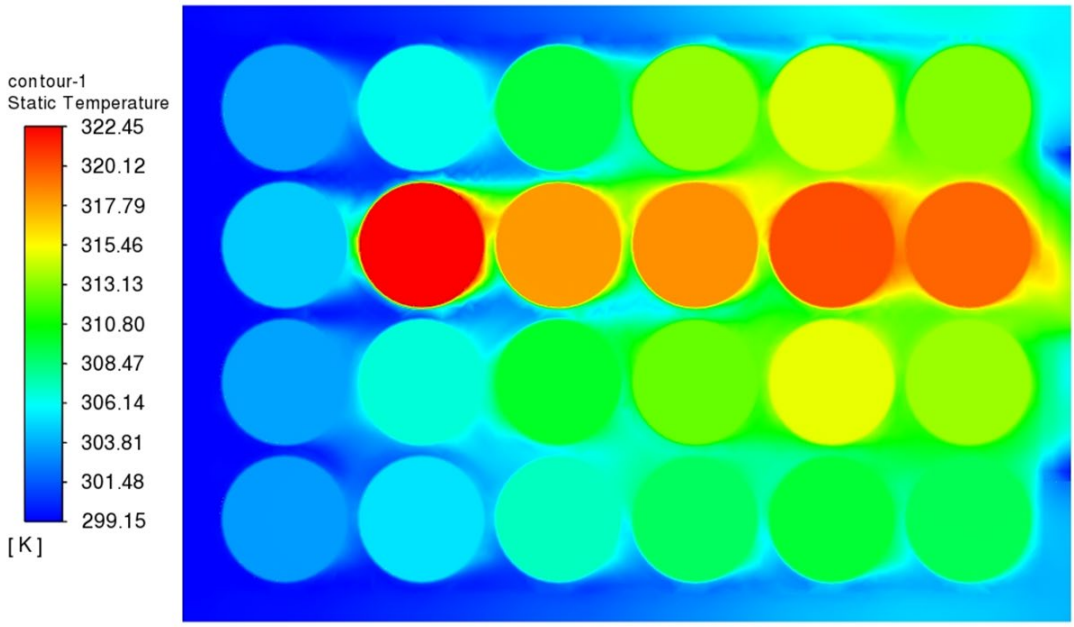

(b)

Figure 6.6 (a) Schematic figure of the battery with a thermal runaway cell; (b) Temperature distribution in the cross-section plane under this scenario.

The temperature contours of the various vertical cross-section planes along each row are demonstrated in Figure 6.7. It is easy to know that the temperature distribution along the vertical cross-section planes is followed the heat exchange mechanism. The temperature distribution at the horizontal cross-section, the top view of the battery pack, demonstrates a similar behaviour. Therefore, the top-view temperature contours will be further investigated in the section.

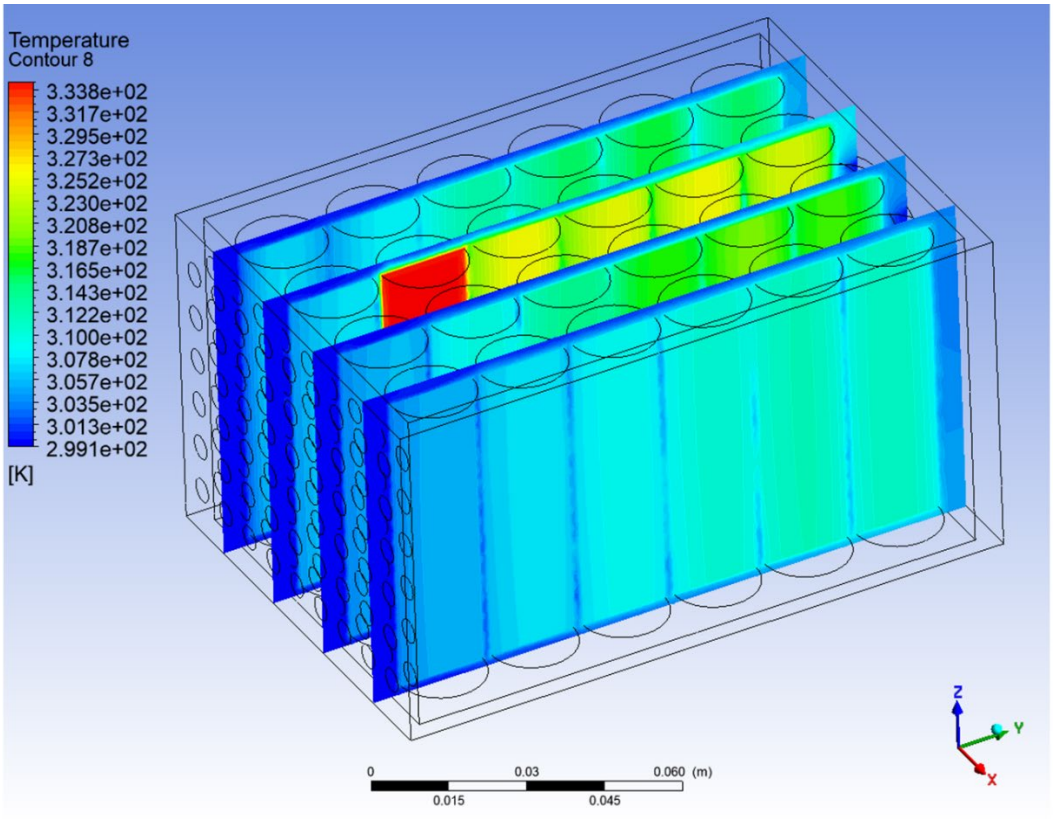

(a)

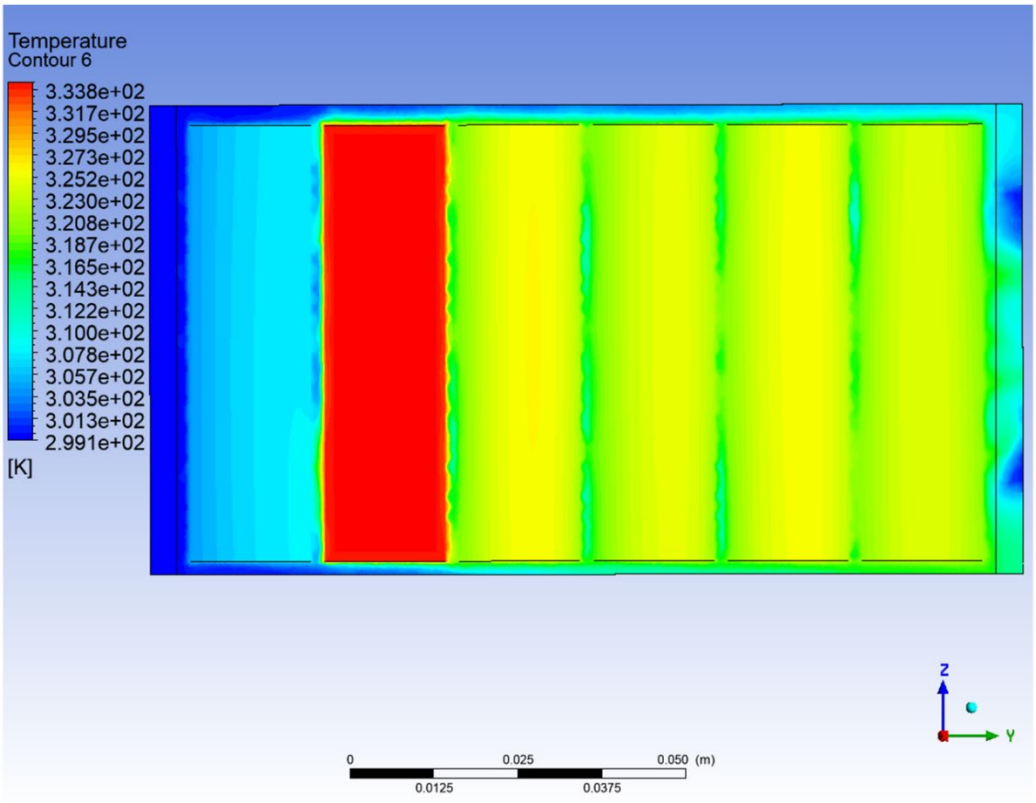

(b)

Figure 6.7 The temperature distribution of the different rows' vertical cross-section under C6 conditions,

(a) The whole pack; (b) Row 2.

In this case, the abnormal heat generation is applied, and the neighbouring cell temperature is calculated and compared with the experimental data extracted from Lopez. et al. [232]. The comparison results between the numerical and experimental data are demonstrated in Figure 6.8, indicating a satisfactory agreement. The error of the maximum temperature for the neighbouring cell is less than 1 K. Therefore, this case can be further expanded to analyse the heat transfer mechanism under the abnormal heat generation scenarios.

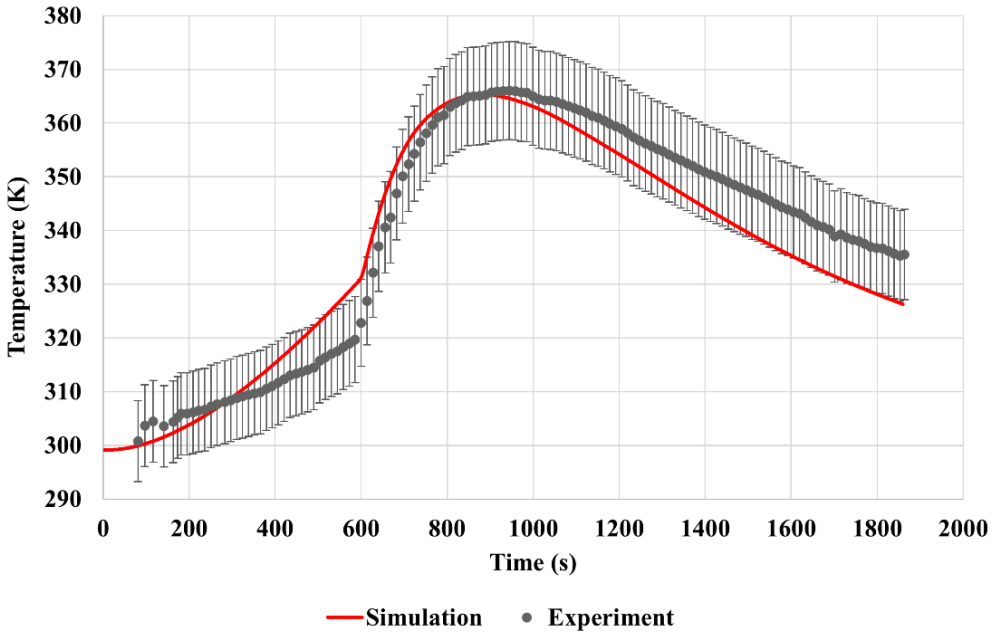

Figure 6.8 Comparison between the numerical and experimental data for a temperature change of the neighbouring cell. The error bar is 2.5%.

6.4.2 Different abnormal heat generation locations

Many previous studies focused on the design feature, such as channel configuration and coolant properties, to investigate the thermal behaviour of the battery pack and the cooling process. Different thermal runaway locations play an essential role in battery heat transfer and battery safety. Moreover, the heat propagation also affects the trigger of the thermal runaway for neighbouring battery cells, which determines whether the abnormal heat generation transfer to a severe battery fire or explosion. Experimental study on this point will cover an expensive expense, and it is hard to compare with various conditions. Hence, numerical investigation demonstrates an effective and efficient way to carry out the comparison study. It is safer and less polluted than heating or burning real battery cells and packs.

The current battery pack configuration from the top view of the battery pack consists of six cells in a row, the longitudinal direction along the forced-air cooling path, and four cells in a column, which is the transverse direction. Therefore, the battery pack can be treated as a symmetry set up along the air velocity direction, as shown in Figure 6.6 (a). The battery cell is arranged from up to bottom and left to right, with serial numbers from one to twenty-four. The total four rows can be divided into two rows near the outer case wall (Rows 1 & 4), and another two in the middle (Rows 2 & 3). Also, the top half with Row 1 & 2 can be mirrored to the bottom half with Rows 3 & 4.

With the application of the in-house written user-defined function code, abnormal heat generation can be applied to the battery pack directly. The comparison of the various

locations along the same row can be observed. For Row 2, the abnormal heat generation was applied from C2 (the nearest cell located to the air inlet) to C22 (the nearest cell located to the air outlet). The temperature distribution is shown in Figure 6.9. The applied abnormal heat generation was controlled as a thermal runaway in a single cell, but the heat did not trigger the thermal runaway of adjacent cells. The heat propagation was shown that the abnormal heat was transferred to the adjacent cell most along the longitudinal direction due to the forced-air cooling.

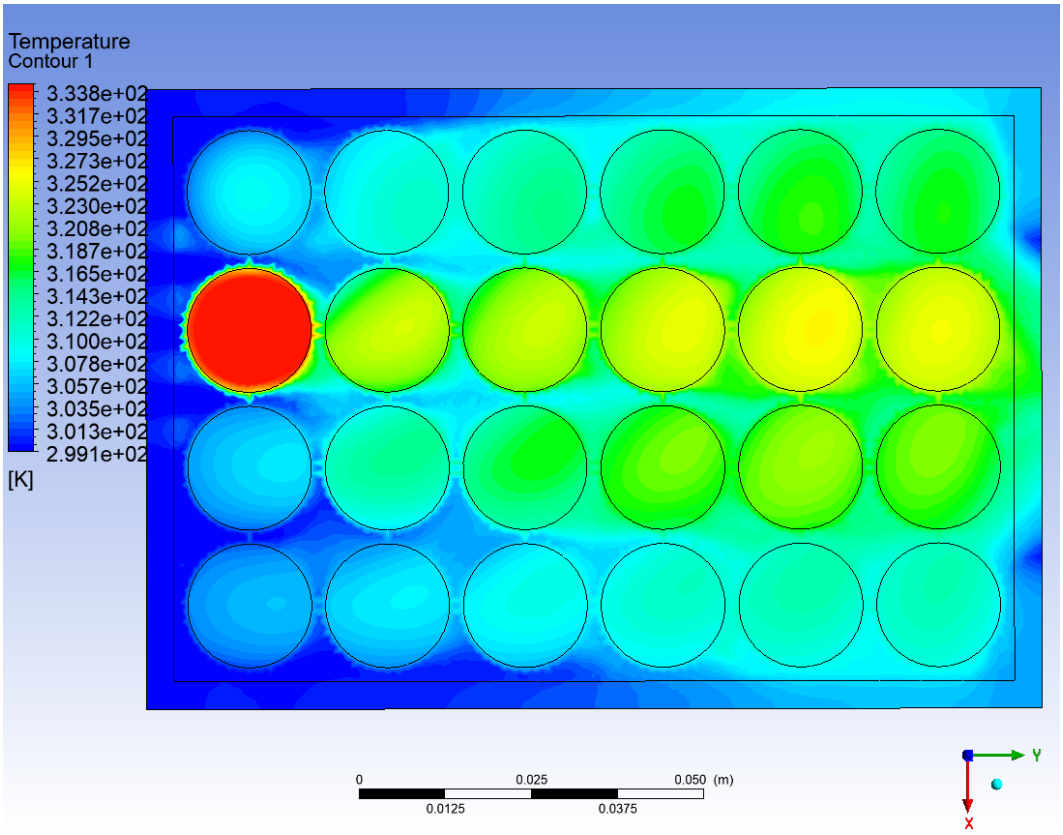

(a)

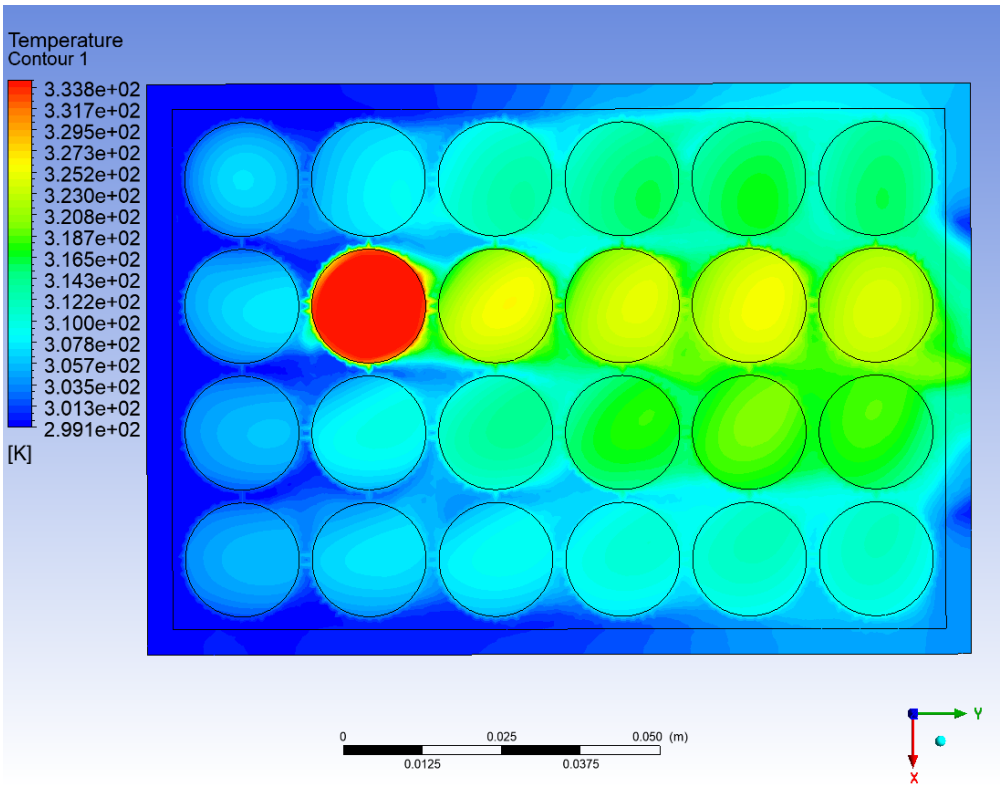
Temperature
Contour 1
3.338e+02
3.317e+02
3.295e+02
3.273e+02
3.252e+02
3.230e+02
3.208e+02
3.187e+02
3.165e+02
3.143e+02
3.122e+02
3.100e+02
3.078e+02
3.057e+02
3.035e+02
3.013e+02
2.991e+02
[K]
0
0.025
0.050 (m)
0.0125
0.0375
Y
X

(b)

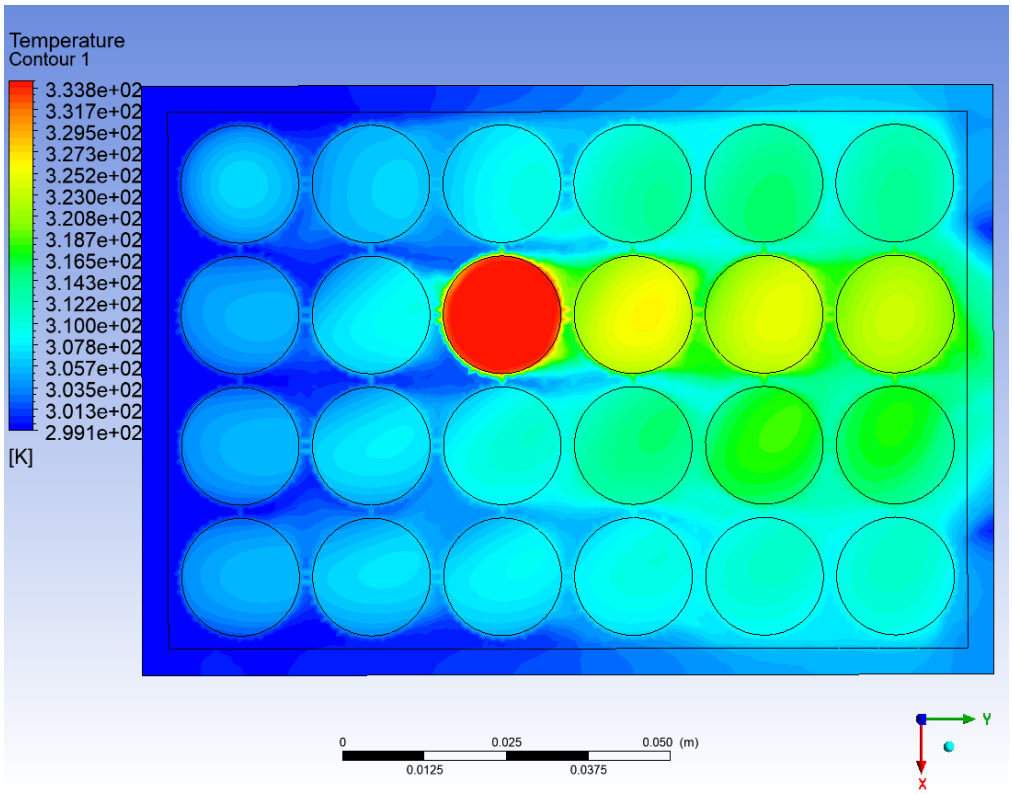
Temperature
Contour 1
3.338e+02
3.317e+02
3.295e+02
3.273e+02
3.252e+02
3.230e+02
3.208e+02
3.187e+02
3.165e+02
3.143e+02
3.122e+02
3.100e+02
3.078e+02
3.057e+02
3.035e+02
3.013e+02
2.991e+02
[K]
0
0.025
0.050 (m)
0.0125
0.0375
Y
X

(c)

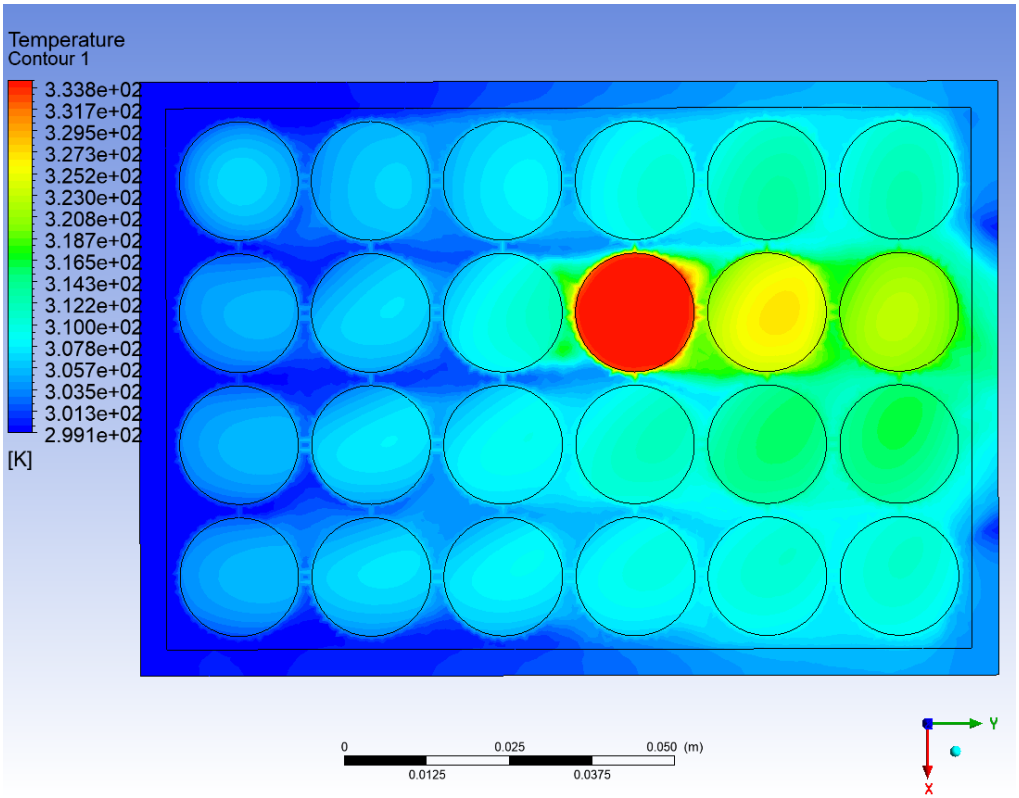
Temperature
Contour 1
3.338e+02
3.317e+02
3.295e+02
3.273e+02
3.252e+02
3.230e+02
3.208e+02
3.187e+02
3.165e+02
3.143e+02
3.122e+02
3.100e+02
3.078e+02
3.057e+02
3.035e+02
3.013e+02
2.991e+02
[K]
0
0.025
0.050 (m)
0.0125
0.0375
Y
X

(d)

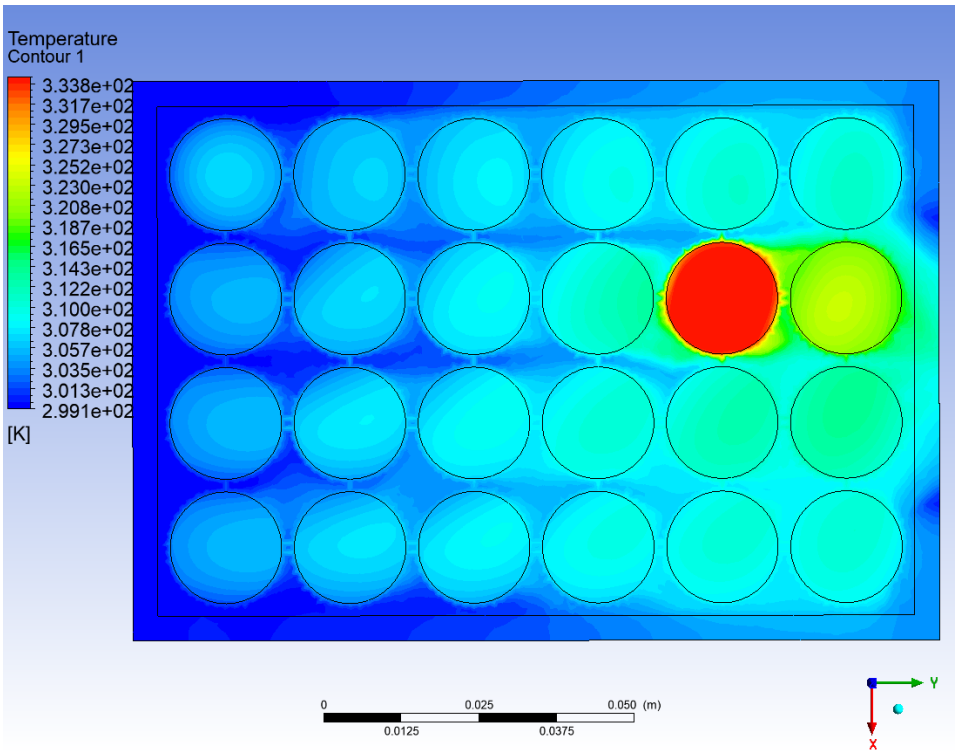
Temperature
Contour 1
3.338e+02
3.317e+02
3.295e+02
3.273e+02
3.252e+02
3.230e+02
3.208e+02
3.187e+02
3.165e+02
3.143e+02
3.122e+02
3.100e+02
3.078e+02
3.057e+02
3.035e+02
3.013e+02
2.991e+02
[K]
0
0.025
0.050 (m)
0.0125
0.0375
Y
X

(e)

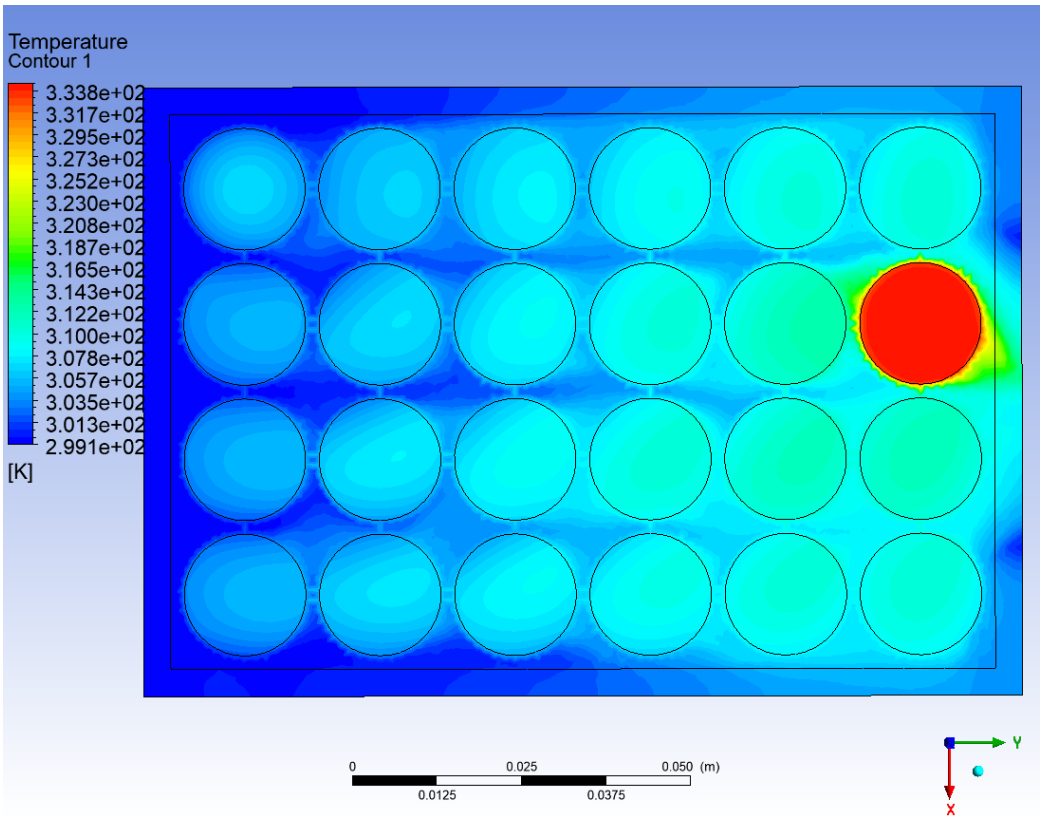

(f)

Figure 6.9 Comparison of the temperature distributions among the applied abnormal heat generation on different cells in Row 2.

Due to the forced-air cooling, the abnormal heat was pushed to one dimension. For example, the case on the right of the top line showed that the cooling was efficient for the first two columns since the cooling air had not been heated up by the thermal runaway cell. Moreover, the location of the thermal runaway or abnormal heat generation affected the BTMs performance related to the maximum temperature and temperature difference. The thermal runaway cell not only heated the adjacent cells but also heated the cooling air, reducing the cooling performance of the downstream cells. From Figure 6.9, it is easy to find that the cells located upstream of the cell with abnormal heat generation were

similar to the base case without extra heat. The temperature of the downstream cells was increased due to the abnormal heat generation, and the temperature difference was also increased.

According to the various locations of the thermal runaway cell, the maximum and minimum temperatures of C15 were compared and demonstrated in Figure 6.10. C15 is the cell in the same column as C14 and is also in Row 3. It can be concluded that the temperature of C15 was stabilized since the thermal runaway cell moved downstream of itself. Also, both the maximum and minimum temperatures increased by 9.1 K and 7.7 K, respectively, which illustrates that when abnormal heat is generated, or thermal runaway occurs, at the early stage, which is before the thermal runaway is triggered of adjacent cells, the increasing temperature is due to the cooling air was heated up and the cooling efficiency was reduced. Compared to cases C2 and C22, the maximum temperature was increased by 2.93%, and the minimum temperature was increased by 2.52%.

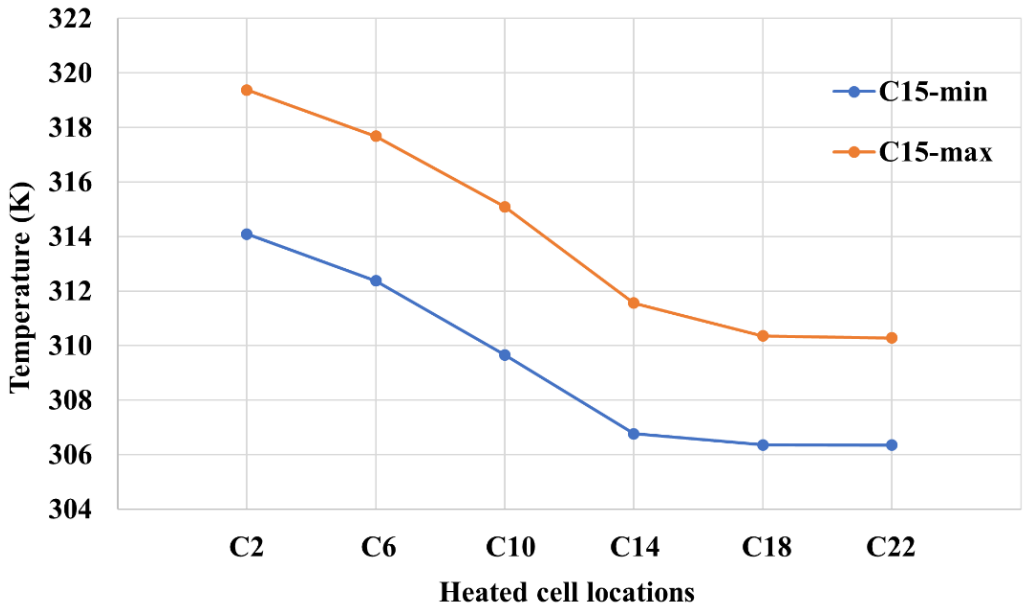

Figure 6.10 Temperature changes of cell 15 among the applied abnormal heat generation on different cells

in Row 2.

For Row 1, the thermal behaviour was similar to the Row 2 scenarios, shown in Figure 6.11. The demonstrated cases have abnormal heat generation at C5, C13 and C21. Considering the temperature change of C15, Row 2 (C6, C14, C22) has more influence on the temperature change than Row 1 (C5, C13, C21), and C15 is closer to Row 2. Additionally, comparing the C5 case with C13 and C21, the corner temperature is higher, which is the same reason that the cooling air was heated up and the cooling performance is not enough for the corner cell.

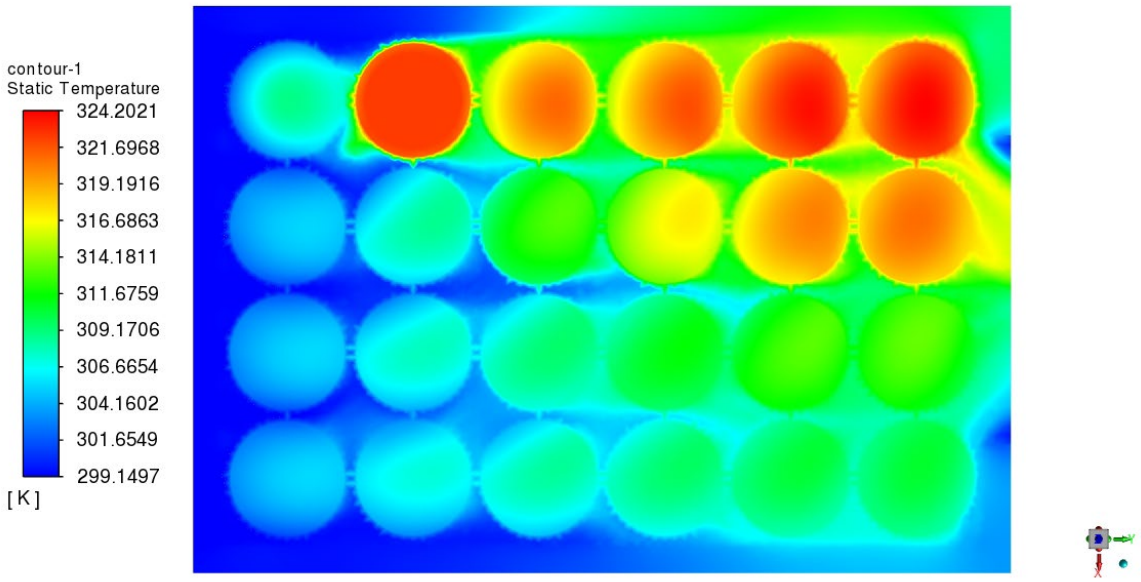

(a)

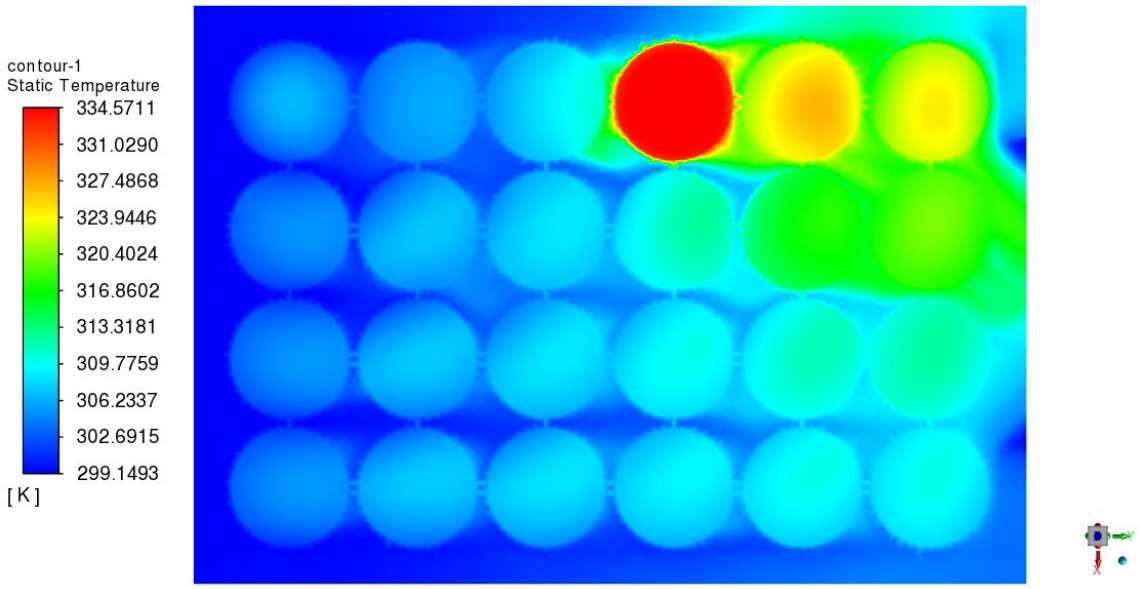

(b)

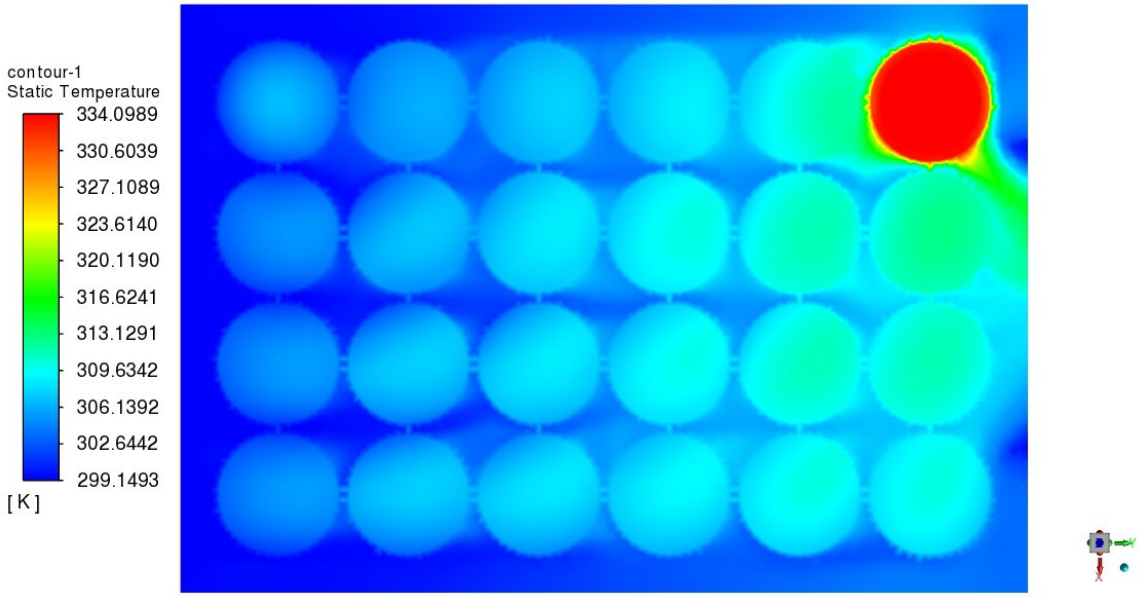

(c)

Figure 6.11 Comparison of the temperature distributions among the applied abnormal heat generation on different cells in Row 1.

6.4.3 Further discussions

The numerical analysis of this chapter not only can be linked to battery thermal management but also can be applied to the early detection analysis of battery fire risks. From the external of the battery cell, the abnormal heat generation should be cooled down to reduce the temperature imbalance, which can further extend the life span of the battery system. On the other hand, abnormal heat generation can be linked to the battery material development, which can be an indicator to evaluate the performance of the battery materials and enhance the fire resilience of different batteries. A better understanding of the abnormal heat generation mechanism will contribute to constructing a comprehensive battery safety analysing tool to predict the potential battery fire risk and deliver efficient battery thermal management solutions. Also, by coupling this numerical model with other models, i.e., ANN model, an intelligent battery alerting system can be further developed.

6.5 Chapter Summary

This chapter developed a three-dimensional thermal model for the battery pack simulation by applying an in-house written code by ANSYS Fluent. The detailed temperature distribution of the whole battery pack was demonstrated under normal operating conditions and severe conditions, such as thermal runaway or abnormal heat generation. After validating both scenarios, the comparison study of various extreme heat locations was carried out. The heat transfer mechanism inside the battery pack was investigated. The battery cell with abnormal heat generation not only increases the temperature of

adjacent cells but also can heat the cooling air and leads to relatively poor cooling performance. Take Row 2 cases as an example, the maximum temperature can be increased by 2.93%, and the cell temperature unbalancing was also increased.

The results highlighted one significant advantage of the numerical analysis, which is the capability to simulate severe scenarios and ease of comparison with many different setups. The proposed model can be further applied to battery performance evaluation and optimisation design. For future perspectives, more parameters can be involved and analysed at the same time. Moreover, these numerical results can be built as a dataset for coupling with machine learning techniques, such as artificial neural networks, to comprehensively enhance both the battery cell/pack and the BTMs performance simultaneously, as well as improve the safety of the battery and energy storage system.

Chapter 7 Conclusions and Future Works

7.1 Conclusions

Nowadays, the increasing popularity of lithium-ion battery systems, particularly in electric vehicles and energy storage systems, has gained broad research interest regarding performance optimisation, thermal stability, and fire safety. With the emerging electrification taking place across different industry sectors, the critical aspect of containing and isolating lithium-ion battery (LIB) fires as well as other fires resulting from the auxiliary electrical systems, has heightened focus on the increasing dangers associated with the use of electrification technologies. Moreover, due to the complex chemical reactions, the potential loss of fortune and the injury of people from battery fires, a comprehensive investigation of the thermal behaviour and heat exchange process of the battery system is paramount. In addition, assessing battery safety and studying thermal behaviour by carrying out battery fire tests is not only costly and dangerous, but also it generates toxic gases or pollution. Therefore, to address these limitations, this thesis focuses on building a high-fidelity computational approach for analysing thermal behaviour, improving the cooling efficiency of the battery thermal management system,

and enhancing the fire safety performance of the battery system. Chapter 1 briefly introduced the background of the LIB and battery fires. The knowledge gap in the battery thermal model and battery thermal management system (BTMs) evaluation was elaborated. The aims and objectives of this research work were also demonstrated. The outline structure of this thesis was also presented.

An extensive literature review was performed on the current machine learning (ML) assisted advanced BTMs in Chapter 2. The ML models applied in BTMs and battery system safety were summarised. The artificial neuron network (ANN) approach, with the advancements of multivariate analysis function, high precision, and excellent data noise tolerance, was found to be advantageous for parameter optimisation contributing to better and highly efficient BTMs design. Other techniques, such as convolutional neural networks (CNN), Long short-term memory (LSTM), etc., were also introduced and reviewed. The corresponding gaps in the existing methods demonstrated the motivation for this thesis.

In Chapter 3, a comprehensive methodology demonstration was provided to explain all the involved numerical models. The computational fluid dynamics (CFD) modelling technique was introduced with the fundamental knowledge of conservation laws at the beginning. After that, the battery structure and basic electrochemical reactions were described. The electrochemical model was presented, including the lumped battery model. Then, the thermal model was elaborated, and the coupling between the battery cell model and the thermal model was also explained. In addition, a detailed description of the ANN model was delivered in this chapter as well. All the applied equations in this research

work were presented. The coupling and optimisation processes were explained by flowcharts.

A three-dimensional thermo-electrochemical model was developed to simulate the detailed temperature distribution of battery packs in Chapter 4 with the description of the conservation laws and other scalar properties governing the fluid motion and heat transfer. The model was validated with the experimental data, and the agreement agreed well. With the application of this model, the scenarios with different ambient pressures were set up and analysed. It was found that changing ambient pressure created a more significant temperature drop under forced air cooling than natural ventilation. Moreover, cases with various air-cooling directions were also studied. With the application of the ANN model, the relationship between the cooling direction and the ambient pressure was built, and an optimal combination was demonstrated, where the maximum temperature was dropped by 1.94%, and the temperature difference could be decreased by 17%.

Next, the thermal behaviour of the battery pack was further investigated by the three-dimensional thermo-electrochemical model. The integrated CFD-ANN framework was applied to the influence of natural ventilation speed and ambient temperature on the thermal performance of the battery pack. The optimisation design based on the CFD-ANN framework considered multiple nonlinear parameters simultaneously, which contributed to analysing and predicting the performance of BTMs. The simulation results provided a practical pathway to optimise the battery configuration and cooling efficiency, balancing the layout of the battery system and safety performance, as well as achieving a 1.9% decrease in maximum temperature and a 4.5% drop in temperature difference.

Additionally, the ANN model established through CFD simulation results can accurately describe the relationship between the configuration dimensions and operating conditions, with a relative error as low as 1.727%.

Since the battery thermal runaway involved thermal abuse conditions during the battery working process, an extreme situation such as abnormal heat generation was further investigated. A three-dimensional thermal model for the battery pack simulation by applying an in-house model to study the internal battery thermal propagation effect under the CFD simulation framework was delivered in Chapter 6. The thermal behaviour and cooling performance were compared by changing the abnormal heat generation locations inside the battery pack. The results indicated that various abnormal heat locations disperse heat to the surrounding coolant and other cells, and the maximum temperature of outer row cases could be increased by 2.93% based on the current battery pack layout.

With the advancement summarised above, this thesis brought great contribution in numerical solutions of analysing and predicting the battery or battery pack thermal performance, as well as evaluating BTMs performance and optimising the configuration of the battery storage system. In particular, the proposed integrated CFD-ANN framework not only balanced the operating parameter and ambient conditions simultaneously, but also enhanced the cooling performance and mitigates the fire risk of the battery storage system. On the other hand, the current data sets were built based on the cylindrical battery cell with an air-cooling system. Further, various battery types (i.e., prismatic cell and pouch cell) and different cooling methods (i.e., liquid cooling, PCM cooling and hybrid cooling system) can be considered to build a more extensive battery data set. Also, for the

current cylindrical type of battery, other sizes can be involved to provide a comprehensive insight for the battery system design. This proposed integration framework has proven to be a useful numerical tool for performance-based battery storage system designs and future real-time fire detection alarm systems.

7.2 Suggestions for Future Works

Because of the prevailing and new fire risks, there is a demand and a need to develop an integrated system approach that uniquely and holistically tackles the critical areas of fire prevention, protection, intervention, and risk management and mitigation to not only effectively eliminate or minimise the exposure of battery energy storage systems to fire threats but also better transform and promote safe industry operations.

While the industry applications for LIB are still relatively new, there is room for further improvement and unrevealed new technological explorations, such as thermally stable components, smart material design, safety monitoring BTMs, battery system safety design model, thermal management system, battery safety evaluation system, etc. While researchers are developing new energy materials with high energy density, fast electric cycle speed, and excellent longevity, the safety perspective, if not more important, is crucial as well. Researchers are expected to collaborate and develop future LIBs or BTMs with guaranteed overall safety performance. CFD models can be further applied to the battery design and risk predictions, i.e., a battery monitoring system can be coupled with CFD simulations to reproduce the real time battery performance and predict potential fire

risks. The abnormal heat generation can be predicted and analysed for an early warning of battery failure. The potential directions of ML applied in BTMs are listed in the following: a) ML techniques, such as ANN, CNN, LSTM, support vector regression (SVR), digital twin (DT), and so force, can be further investigated for LIB and BTMs optimal design, risk prediction, fault diagnosis, and hazard mitigation; b) Multiphysics numerical simulations can be coupled to build more performance-oriented datasets for ML training; c) Other potential ML methods can be included for improving LIB safety research with various data types and amounts; d) ML techniques can be further applied to other energy storage systems for improving the performance and mitigating the potential risks.

In addition, since the development of each battery component with high performances is undergoing, such as separator, electrolyte, and electrodes, the investigation of new materials and performances is mainly based on experiments. Numerical simulations can provide reliable results compared to experiments and contribute to studying the mechanism of some effects. Meanwhile, numerical simulations provide an efficient and economical way to develop better batteries or battery systems. Furthermore, the integration of multi-domain multi-scale models, including ML, CFD, and molecular dynamics (MD), has the potential to study the all-inclusive coupled internal/external phenomena of LIB fires. With increase understanding from the numerical investigation, a smart material design and intelligent BTMs can be further developed.

In the longer term, these further works shall benefit battery safety research by contributing a comprehensive and multifunctional model for practical applications in battery energy storage design.

References

[1] J. B. Goodenough, "Energy storage materials: a perspective," *Energy Storage Materials,* vol. 1, pp. 158-161, 2015.

[2] Q. Wang, B. Mao, S. I. Stoliarov, and J. Sun, "A review of lithium ion battery failure mechanisms and fire prevention strategies," *Progress in Energy and Combustion Science,* vol. 73, pp. 95-131, 2019.

[3] A. Yoshino, "The Birth of the Lithium-Ion Battery," *Angew Chem Int Edit,* vol. 51, no. 24, pp. 5798-5800, 2012.

[4] S. Santhanagopalan, K. Smith, J. Neubauer, G.-H. Kim, A. Pesaran, and M. Keyser, *Design and analysis of large lithium-ion battery systems*. Artech House, 2014.

[5] M. Wakihara, "Recent developments in lithium ion batteries," *Materials Science and Engineering: R: Reports,* vol. 33, no. 4, pp. 109-134, 2001.

[6] G. E. Blomgren, "The development and future of lithium ion batteries," *Journal of The Electrochemical Society,* vol. 164, no. 1, p. A5019, 2016.

[7] J. Kim, J. Oh, and H. Lee, "Review on battery thermal management system for electric vehicles," *Applied thermal engineering,* vol. 149, pp. 192-212, 2019.

[8] F. Global, "Property Loss Prevention Data Sheets 5-28," 2021. Accessed: 05/11/2022. [Online]. Available: https://fireprotectionsupport.nl/wp-content/uploads/2021/07/FMDS0528.pdf

[9] Y. Fu, S. Lu, K. Li, C. Liu, X. Cheng, and H. Zhang, "An experimental study on burning behaviors of 18650 lithium ion batteries using a cone calorimeter," *Journal of Power Sources,* vol. 273, pp. 216-222, 2015.

[10] F. Larsson, P. Andersson, P. Blomqvist, A. Lorén, and B.-E. Mellander, "Characteristics of lithium-ion batteries during fire tests," *Journal of Power Sources,* vol. 271, pp. 414-420, 2014.

[11] P. Ribière, S. Grugeon, M. Morcrette, S. Boyanov, S. Laruelle, and G. Marlair, "Investigation on the fire-induced hazards of Li-ion battery cells by fire calorimetry," *Energy & Environmental Science,* vol. 5, no. 1, pp. 5271-5280, 2012.

[12] T. Wu, H. Chen, Q. Wang, and J. Sun, "Comparison analysis on the thermal runaway of lithium-ion battery under two heating modes," *Journal of hazardous materials,* vol. 344, pp. 733-741, 2018.

[13] F. Larsson and B.-E. Mellander, "Abuse by external heating, overcharge and short circuiting of commercial lithium-ion battery cells," *Journal of The Electrochemical Society,* vol. 161, no. 10, p. A1611, 2014.

[14] M.-S. Wu, P.-C. J. Chiang, J.-C. Lin, and Y.-S. Jan, "Correlation between electrochemical characteristics and thermal stability of advanced lithium-ion batteries in abuse tests—short-circuit tests," *Electrochimica acta,* vol. 49, no. 11, pp. 1803-1812, 2004.

[15] A. Friesen, F. Horsthemke, X. Mönnighoff, G. Brunklaus, R. Krafft, M. Börner, T. Risthaus, M. Winter, and F. M. Schappacher, "Impact of cycling at low temperatures on the safety behavior of 18650-type lithium ion cells: Combined study of mechanical and thermal abuse testing accompanied by post-mortem analysis," *Journal of power sources,* vol. 334, pp. 1-11, 2016.

[16] J. Lin, X. Liu, S. Li, C. Zhang, and S. Yang, "A review on recent progress, challenges and perspective of battery thermal management system," *International Journal of Heat and Mass Transfer,* vol. 167, p. 120834, 2021.

[17] H. Sun and R. Dixon, "Development of cooling strategy for an air cooled lithium-ion battery pack," *Journal of Power Sources,* vol. 272, pp. 404-414, 2014.

[18] Y. Fan, Y. Bao, C. Ling, Y. Chu, X. Tan, and S. Yang, "Experimental study on the thermal management performance of air cooling for high energy density cylindrical lithium-ion batteries," *Applied Thermal Engineering,* vol. 155, pp. 96-109, 2019.

[19] X. Peng, C. Ma, A. Garg, N. Bao, and X. Liao, "Thermal performance investigation of an air-cooled lithium-ion battery pack considering the inconsistency of battery cells," *Applied Thermal Engineering,* vol. 153, pp. 596-603, 2019.

[20] Z. Shang, H. Qi, X. Liu, C. Ouyang, and Y. Wang, "Structural optimization of lithium-ion battery for improving thermal performance based on a liquid cooling system," *International Journal of Heat and Mass Transfer,* vol. 130, pp. 33-41, 2019.

[21] E. Jiaqiang, D. Han, A. Qiu, H. Zhu, Y. Deng, J. Chen, X. Zhao, W. Zuo, H. Wang, and J. Chen, "Orthogonal experimental design of liquid-cooling structure on the cooling effect of a liquid-cooled battery thermal management system," *Applied Thermal Engineering,* vol. 132, pp. 508-520, 2018.

[22] C. Menale, F. D'Annibale, B. Mazzarotta, and R. Bubbico, "Thermal management of lithium-ion batteries: An experimental investigation," *Energy,* vol. 182, pp. 57-71, 2019.

[23] Y. Lv, D. Zhou, X. Yang, X. Liu, X. Li, and G. Zhang, "Experimental investigation on a novel liquid-cooling strategy by coupling with graphene-modified silica gel for the thermal management of cylindrical battery," *Applied Thermal Engineering,* vol. 159, p. 113885, 2019.

[24] A. Alihosseini and M. Shafaee, "Experimental study and numerical simulation of a Lithium-ion battery thermal management system using a heat pipe," *Journal of Energy Storage,* vol. 39, p. 102616, 2021.

[25] J. Smith, R. Singh, M. Hinterberger, and M. Mochizuki, "Battery thermal management system for electric vehicle using heat pipes," *International Journal of Thermal Sciences,* vol. 134, pp. 517-529, 2018.

[26] X. Li, J. Zhao, J. Duan, S. Panchal, J. Yuan, R. Fraser, M. Fowler, and M. Chen, "Simulation of cooling plate effect on a battery module with different channel arrangement," *Journal of Energy Storage,* vol. 49, p. 104113, 2022.

[27] C.-V. Hémery, F. Pra, J.-F. Robin, and P. Marty, "Experimental performances of a battery thermal management system using a phase change material," *Journal of Power Sources,* vol. 270, pp. 349-358, 2014.

[28] Q. Huang, X. Li, G. Zhang, J. Zhang, F. He, and Y. Li, "Experimental investigation of the thermal performance of heat pipe assisted phase change material for battery thermal management system," *Applied Thermal Engineering,* vol. 141, pp. 1092-1100, 2018.

[29] J. Zhang, X. Li, G. Zhang, Y. Wang, J. Guo, Y. Wang, Q. Huang, C. Xiao, and Z. Zhong, "Characterization and experimental investigation of aluminum nitride-based composite phase change materials for battery thermal management," *Energy Conversion and Management,* vol. 204, p. 112319, 2020.

[30] N. Joshy, M. Hajiyan, A. R. M. Siddique, S. Tasnim, H. Simha, and S. Mahmud, "Experimental investigation of the effect of vibration on phase change material (PCM) based battery thermal management system," *Journal of Power Sources,* vol. 450, p. 227717, 2020.

[31] A. Lazrak, J.-F. Fourmigué, and J.-F. Robin, "An innovative practical battery thermal management system based on phase change materials: Numerical and experimental investigations," *Applied Thermal Engineering,* vol. 128, pp. 20-32, 2018.

[32] X. Qi, M. O. Sidi, I. Tlili, T. K. Ibrahim, M. A. Elkotb, M. El-Shorbagy, and Z. Li,

"Optimization and sensitivity analysis of extended surfaces during melting and freezing of phase changing materials in cylindrical Lithium-ion battery cooling," *Journal of Energy Storage,* vol. 51, p. 104545, 2022.

[33] W. Yang, F. Zhou, H. Zhou, Q. Wang, and J. Kong, "Thermal performance of cylindrical lithium-ion battery thermal management system integrated with mini-channel liquid cooling and air cooling," *Applied Thermal Engineering,* vol. 175, p. 115331, 2020.

[34] R. Wang, Z. Liang, M. Souri, M. Esfahani, and M. Jabbari, "Numerical analysis of lithium-ion battery thermal management system using phase change material assisted by liquid cooling method," *International Journal of Heat and Mass Transfer,* vol. 183, p. 122095, 2022.

[35] D. S. Jang, S. Yun, S. H. Hong, W. Cho, and Y. Kim, "Performance characteristics of a novel heat pipe-assisted liquid cooling system for the thermal management of lithium-ion batteries," *Energy Conversion and Management,* vol. 251, p. 115001, 2022.

[36] S. Lei, Y. Shi, and G. Chen, "A lithium-ion battery-thermal-management design based on phase-change-material thermal storage and spray cooling," *Applied Thermal Engineering,* vol. 168, p. 114792, 2020.

[37] D. K. Sharma and A. Prabhakar, "A review on air cooled and air centric hybrid thermal management techniques for Li-ion battery packs in electric vehicles," *Journal of Energy Storage,* vol. 41, p. 102885, 2021.

[38] Y. Li, Z. Zhou, and W.-T. Wu, "Three-dimensional thermal modeling of Li-ion battery cell and 50 V Li-ion battery pack cooled by mini-channel cold plate," *Applied Thermal Engineering,* vol. 147, pp. 829-840, 2019.

[39] U. Morali, "A numerical and statistical implementation of a thermal model for a lithium-ion battery," *Energy,* vol. 240, p. 122486, 2022.

[40] X. Hu, W. Liu, X. Lin, and Y. Xie, "A comparative study of control-oriented thermal models for cylindrical Li-ion batteries," *IEEE Transactions on Transportation Electrification,* vol. 5, no. 4, pp. 1237-1253, 2019.

[41] C. Bibin, M. Vijayaram, V. Suriya, R. S. Ganesh, and S. Soundarraj, "A review on thermal issues in Li-ion battery and recent advancements in battery thermal management system," *Materials Today: Proceedings,* vol. 33, pp. 116-128, 2020.

[42] V. Q. Dao, M.-C. Dinh, C. S. Kim, M. Park, C.-H. Doh, J. H. Bae, M.-K. Lee, J. Liu, and Z. Bai, "Design of an effective State of Charge estimation method for a lithium-ion battery pack using extended kalman filter and artificial neural network," *energies,* vol. 14, no. 9, p. 2634, 2021.

[43] J. Meng, M. Ricco, G. Luo, M. Swierczynski, D.-I. Stroe, A.-I. Stroe, and R. Teodorescu, "An overview and comparison of online implementable SOC estimation methods for lithium-ion battery," *IEEE Transactions on Industry Applications,* vol. 54, no. 2, pp. 1583-1591, 2017.

[44] A. Garg, S. Singh, W. Li, L. Gao, X. Cui, C. T. Wang, X. Peng, and N. Rajasekar, "Illustration of experimental, machine learning, and characterization methods for study of performance of Li-ion batteries," *International Journal of Energy Research,* vol. 44, no. 12, pp. 9513-9526, 2020.

[45] P. Cicconi, M. Germani, and D. Landi, "Modeling and thermal simulation of a PHEV battery module with cylindrical LFP cells," *World Electric Vehicle Journal,* vol. 6, no. 1, pp. 175-185, 2013.

[46] J. Cen, Z. Li, and F. Jiang, "Experimental investigation on using the electric vehicle air conditioning system for lithium-ion battery thermal management," *Energy for sustainable development,* vol. 45, pp. 88-95, 2018.

[47] Z. Lu, X. Yu, L. Wei, F. Cao, L. Zhang, X. Meng, and L. Jin, "A comprehensive experimental study on temperature-dependent performance of lithium-ion battery," *Applied Thermal Engineering,* vol. 158, p. 113800, 2019.

[48] L. Zhang, Q. Duan, X. Meng, K. Jin, J. Xu, J. Sun, and Q. Wang, "Experimental investigation on intermittent spray cooling and toxic hazards of lithium-ion battery thermal runaway," *Energy Conversion and Management,* vol. 252, p. 115091, 2022.

[49] A. Li, A. C. Y. Yuen, W. Wang, I. M. De Cachinho Cordeiro, C. Wang, T. B. Y. Chen, J. Zhang, Q. N. Chan, and G. H. Yeoh, "A Review on Lithium-Ion Battery Separators towards Enhanced Safety Performances and Modelling Approaches," *Molecules,* vol. 26, no. 2, p. 478, Jan 18 2021.

[50] A. Li, J. Weng, A. C. Y. Yuen, W. Wang, H. Liu, E. W. M. Lee, J. Wang, S. Kook, and G. H. Yeoh, "Machine learning assisted advanced battery thermal management system: A state-of-the-art review," *Journal of Energy Storage,* vol. 60, p. 106688, 2023/04/01/ 2023.

[51] L. Zhang, X. Hu, Z. Wang, J. Ruan, C. Ma, Z. Song, D. G. Dorrell, and M. G. Pecht, "Hybrid electrochemical energy storage systems: An overview for smart grid and electrified vehicle applications," *Renewable and Sustainable Energy Reviews,* vol. 139, p. 110581, 2021.

[52] H. Dai, B. Jiang, X. Hu, X. Lin, X. Wei, and M. Pecht, "Advanced battery management strategies for a sustainable energy future: Multilayer design concepts and research trends," *Renewable and Sustainable Energy Reviews,* vol. 138, p. 110480, 2021.

[53] Y. Yang, S. Bremner, C. Menictas, and M. Kay, "Battery energy storage system size determination in renewable energy systems: A review," *Renewable and Sustainable Energy Reviews,* vol. 91, pp. 109-125, 2018.

[54] M. Armand, P. Axmann, D. Bresser, M. Copley, K. Edström, C. Ekberg, D. Guyomard, B. Lestriez, P. Novák, and M. Petranikova, "Lithium-ion batteries–Current state of the art and anticipated developments," *Journal of Power Sources,* vol. 479, p. 228708, 2020.

[55] Y. Li, M. Vilathgamuwa, B. Xiong, J. Tang, Y. Su, and Y. Wang, "Design of minimum cost degradation-conscious lithium-ion battery energy storage system to achieve renewable power dispatchability," *Applied Energy,* vol. 260, p. 114282, 2020.

[56] T. Chen, Y. Jin, H. Lv, A. Yang, M. Liu, B. Chen, Y. Xie, and Q. Chen, "Applications of lithium-ion batteries in grid-scale energy storage systems," *Transactions of Tianjin University,* vol. 26, no. 3, pp. 208-217, 2020.

[57] C. S. Lai, Y. Jia, Z. Xu, L. L. Lai, X. Li, J. Cao, and M. D. McCulloch, "Levelized cost of electricity for photovoltaic/biogas power plant hybrid system with electrical energy storage degradation costs," *Energy conversion and management,* vol. 153, pp. 34-47, 2017.

[58] C. Roe, X. Feng, G. White, R. Li, H. Wang, X. Rui, C. Li, F. Zhang, V. Null, and M. Parkes, "Immersion cooling for lithium-ion batteries–A review," *Journal of Power Sources,* vol. 525, p. 231094, 2022.

[59] B. Xu, J. Lee, D. Kwon, L. Kong, and M. Pecht, "Mitigation strategies for Li-ion battery thermal runaway: A review," *Renewable and Sustainable Energy Reviews,* vol. 150, p. 111437, 2021.

[60] J. Cao, Z. Ling, S. Lin, Y. He, X. Fang, and Z. Zhang, "Thermochemical heat storage system for preventing battery thermal runaway propagation using sodium acetate trihydrate/expanded graphite," *Chemical Engineering Journal,* vol. 433, p. 133536, 2022.

[61] X. Feng, M. Ouyang, X. Liu, L. Lu, Y. Xia, and X. He, "Thermal runaway mechanism of lithium ion battery for electric vehicles: A review," *Energy Storage Materials,* vol. 10, pp. 246-267, 2018.

[62] P. Jindal and J. Bhattacharya, "understanding the thermal runaway behavior of Li-ion batteries through experimental techniques," *Journal of The Electrochemical Society,* vol. 166, no. 10, p. A2165, 2019.

[63] C. Jin, Y. Sun, H. Wang, X. Lai, S. Wang, S. Chen, X. Rui, Y. Zheng, X. Feng, and H. Wang, "Model and experiments to investigate thermal runaway

characterization of lithium-ion batteries induced by external heating method," *Journal of Power Sources,* vol. 504, p. 230065, 2021.

[64] X. Wu, K. Song, X. Zhang, N. Hu, L. Li, W. Li, L. Zhang, and H. Zhang, "Safety issues in lithium ion batteries: Materials and cell design," *Frontiers in Energy Research,* vol. 7, p. 65, 2019.

[65] Z. Jiang, H. Li, Z. Qu, and J. Zhang, "Recent progress in lithium-ion battery thermal management for a wide range of temperature and abuse conditions," *International Journal of Hydrogen Energy,* 2022.

[66] J. Weng, Q. Huang, X. Li, G. Zhang, D. Ouyang, M. Chen, A. C. Y. Yuen, A. Li, E. W. M. Lee, and W. Yang, "Safety Issue on PCM-based Battery Thermal Management: Material Thermal Stability and System Hazard Mitigation," *Energy Storage Materials,* 2022.

[67] S. Rashidi, N. Karimi, B. Sunden, K. C. Kim, A. G. Olabi, and O. Mahian, "Progress and challenges on the thermal management of electrochemical energy conversion and storage technologies: Fuel cells, electrolysers, and supercapacitors," *Progress in Energy and Combustion Science,* vol. 88, p. 100966, 2022.

[68] A. G. Li, A. C. West, and M. Preindl, "Towards unified machine learning characterization of lithium-ion battery degradation across multiple levels: A critical review," *Applied Energy,* vol. 316, p. 119030, 2022.

[69] H. Rauf, M. Khalid, and N. Arshad, "Machine learning in state of health and remaining useful life estimation: Theoretical and technological development in battery degradation modelling," *Renewable and Sustainable Energy Reviews,* vol. 156, p. 111903, 2022.

[70] S. Anastasi, M. Madonna, and L. Monica, "Implications of embedded artificial intelligence-machine learning on safety of machinery," *Procedia Computer Science,* vol. 180, pp. 338-343, 2021.

[71] N. Zhao and F. You, "Sustainable power systems operations under renewable energy induced disjunctive uncertainties via machine learning-based robust optimization," *Renewable and Sustainable Energy Reviews,* vol. 161, p. 112428, 2022.

[72] A. Yuen, T. Chen, C. Wang, W. Wei, I. Kabir, J. Vargas, Q. Chan, S. Kook, and G. Yeoh, "Utilising genetic algorithm to optimise pyrolysis kinetics for fire modelling and characterisation of chitosan/graphene oxide polyurethane composites," *Composites Part B: Engineering,* vol. 182, p. 107619, 2020.

[73] Y. Liu, O. C. Esan, Z. Pan, and L. An, "Machine learning for advanced energy

materials," *Energy and AI,* vol. 3, p. 100049, 2021.

[74] A. C. Y. Yuen, T. B. Y. Chen, I. M. D. C. Cordero, H. Liu, A. Li, W. Yang, S. C. P. Cheung, Q. N. Chan, S. Kook, and G. H. Yeoh, "Developing a solid decomposition kinetics extraction framework for detailed chemistry pyrolysis and combustion modelling of building polymer composites," *Journal of Analytical and Applied Pyrolysis,* vol. 163, p. 105500, 2022.

[75] M. Andersson, M. Streb, J. Y. Ko, V. L. Klass, M. Klett, H. Ekström, M. Johansson, and G. Lindbergh, "Parametrization of physics-based battery models from input–output data: A review of methodology and current research," *Journal of Power Sources,* vol. 521, p. 230859, 2022.

[76] J. Liu, F. Tavakoli, S. M. Sajadi, M. Z. Mahmoud, B. Heidarshenas, and H. Ş. Aybar, "Numerical evaluation and artificial neural network modeling of the effect of oval PCM compartment dimensions around a triple lithium-ion battery pack despite forced airflow," *Engineering Analysis with Boundary Elements,* vol. 142, pp. 71-92, 2022.

[77] S. Yalçın, S. Panchal, and M. S. Herdem, "A CNN-ABC model for estimation and optimization of heat generation rate and voltage distributions of lithium-ion batteries for electric vehicles," *International Journal of Heat and Mass Transfer,* vol. 199, p. 123486, 2022.

[78] M. Li, C. Dong, R. Wang, X. Yu, Q. Xiao, and H. Jia, "Synthetic thermal convolutional-memory network for the lithium-ion battery behaviour diagnosis against noise interruptions," *IET Energy Systems Integration,* 2022.

[79] Y. Gao, Y. Matsunami, S. Miyata, and Y. Akashi, "Operational optimization for off-grid renewable building energy system using deep reinforcement learning," *Applied Energy,* vol. 325, p. 119783, 2022.

[80] F. Jaliliantabar, R. Mamat, and S. Kumarasamy, "Prediction of lithium-ion battery temperature in different operating conditions equipped with passive battery thermal management system by artificial neural networks," *Materials Today: Proceedings,* vol. 48, pp. 1796-1804, 2022.

[81] O. Kalkan, A. B. Colak, A. Celen, K. Bakirci, and A. S. Dalkilic, "Prediction of experimental thermal performance of new designed cold plate for electric vehicles' Li-ion pouch-type battery with artificial neural network," *Journal of Energy Storage,* vol. 48, p. 103981, 2022.

[82] L. Jiang, Z. Deng, X. Tang, L. Hu, X. Lin, and X. Hu, "Data-driven fault diagnosis and thermal runaway warning for battery packs using real-world vehicle data," *Energy,* vol. 234, p. 121266, 2021.

[83] T. F. Fuller, M. Doyle, and J. Newman, "Simulation and optimization of the dual lithium ion insertion cell," *Journal of the Electrochemical Society,* vol. 141, no. 1, p. 1, 1994.

[84] M. Doyle, T. F. Fuller, and J. Newman, "Modeling of galvanostatic charge and discharge of the lithium/polymer/insertion cell," *Journal of the Electrochemical society,* vol. 140, no. 6, p. 1526, 1993.

[85] M. Doyle, J. Newman, A. S. Gozdz, C. N. Schmutz, and J. M. Tarascon, "Comparison of modeling predictions with experimental data from plastic lithium ion cells," *Journal of the Electrochemical Society,* vol. 143, no. 6, p. 1890, 1996.

[86] D. E. Stephenson, E. M. Hartman, J. N. Harb, and D. R. Wheeler, "Modeling of particle-particle interactions in porous cathodes for lithium-ion batteries," *Journal of the Electrochemical Society,* vol. 154, no. 12, p. A1146, 2007.

[87] I. V. Thorat, D. E. Stephenson, N. A. Zacharias, K. Zaghib, J. N. Harb, and D. R. Wheeler, "Quantifying tortuosity in porous Li-ion battery materials," *Journal of Power Sources,* vol. 188, no. 2, pp. 592-600, 2009.

[88] J. Tu, G. H. Yeoh, and C. Liu, *Computational fluid dynamics: a practical approach*. Butterworth-Heinemann, 2018.

[89] U. S. Kim, C. B. Shin, and C.-S. Kim, "Effect of electrode configuration on the thermal behavior of a lithium-polymer battery," *Journal of Power Sources,* vol. 180, no. 2, pp. 909-916, 2008.

[90] U. S. Kim, J. Yi, C. B. Shin, T. Han, and S. Park, "Modelling the thermal behaviour of a lithium-ion battery during charge," *Journal of Power Sources,* vol. 196, no. 11, pp. 5115-5121, 2011.

[91] U. S. Kim, C. B. Shin, and C.-S. Kim, "Modeling for the scale-up of a lithium-ion polymer battery," *Journal of Power Sources,* vol. 189, no. 1, pp. 841-846, 2009.

[92] J. Yi, U. S. Kim, C. B. Shin, T. Han, and S. Park, "Modeling the temperature dependence of the discharge behavior of a lithium-ion battery in low environmental temperature," *Journal of Power Sources,* vol. 244, pp. 143-148, 2013.

[93] M. Xu, Z. Zhang, X. Wang, L. Jia, and L. Yang, "Two-dimensional electrochemical–thermal coupled modeling of cylindrical LiFePO4 batteries," *Journal of power sources,* vol. 256, pp. 233-243, 2014.

[94] X. Cheng, N. Shi, Y. Li, and S. Wang, "Engineering-Oriented Modeling for Thermal Behaviors of 18650 Li-ion Batteries," *Energy Procedia,* vol. 105, pp. 4757-4762, 2017.

[95] F. Larsson, J. Anderson, P. Andersson, and B.-E. Mellander, "Thermal modelling of cell-to-cell fire propagation and cascading thermal runaway failure effects for lithium-ion battery cells and modules using fire walls," *Journal of the electrochemical society,* vol. 163, no. 14, p. A2854, 2016.

[96] G.-H. Kim, A. Pesaran, and R. Spotnitz, "A three-dimensional thermal abuse model for lithium-ion cells," *Journal of Power Sources,* vol. 170, no. 2, pp. 476-489, 2007.

[97] T. Hatchard, D. MacNeil, A. Basu, and J. Dahn, "Thermal model of cylindrical and prismatic lithium-ion cells," *Journal of The Electrochemical Society,* vol. 148, no. 7, pp. A755-A761, 2001.

[98] G.-H. Kim, K. Smith, K.-J. Lee, S. Santhanagopalan, and A. Pesaran, "Multi-domain modeling of lithium-ion batteries encompassing multi-physics in varied length scales," *Journal of the electrochemical society,* vol. 158, no. 8, pp. A955-A969, 2011.

[99] J. Yi, B. Koo, and C. B. Shin, "Three-dimensional modeling of the thermal behavior of a lithium-ion battery module for hybrid electric vehicle applications," *Energies,* vol. 7, no. 11, pp. 7586-7601, 2014.

[100] X. Feng, X. He, M. Ouyang, L. Lu, P. Wu, C. Kulp, and S. Prasser, "Thermal runaway propagation model for designing a safer battery pack with 25 Ah LiNixCoyMnzO2 large format lithium ion battery," *Applied Energy,* vol. 154, pp. 74-91, 2015.

[101] S. Chen, C. Wan, and Y. Wang, "Thermal analysis of lithium-ion batteries," *Journal of power sources,* vol. 140, no. 1, pp. 111-124, 2005.

[102] C. Lin, S. Xu, G. Chang, and J. Liu, "Experiment and simulation of a LiFePO4 battery pack with a passive thermal management system using composite phase change material and graphite sheets," *Journal of Power Sources,* vol. 275, pp. 742-749, 2015.

[103] S. Abada, M. Petit, A. Lecocq, G. Marlair, V. Sauvant-Moynot, and F. Huet, "Combined experimental and modeling approaches of the thermal runaway of fresh and aged lithium-ion batteries," *Journal of Power Sources,* vol. 399, pp. 264-273, 2018.

[104] L. Cai and R. E. White, "Mathematical modeling of a lithium ion battery with thermal effects in COMSOL Inc. Multiphysics (MP) software," *Journal of Power Sources,* vol. 196, no. 14, pp. 5985-5989, 2011.

[105] Y. Xie, W. Li, Y. Yang, and F. Feng, "A novel resistance-based thermal model for lithium-ion batteries," *International Journal of Energy Research,* vol. 42, no. 14,

pp. 4481-4498, 2018.

[106] K. Fang, D. Mu, S. Chen, B. Wu, and F. Wu, "A prediction model based on artificial neural network for surface temperature simulation of nickel–metal hydride battery during charging," *Journal of power sources,* vol. 208, pp. 378-382, 2012.

[107] H. Li, Q. Duan, C. Zhao, Z. Huang, and Q. Wang, "Experimental investigation on the thermal runaway and its propagation in the large format battery module with Li (Ni1/3Co1/3Mn1/3) O2 as cathode," *Journal of hazardous materials,* vol. 375, pp. 241-254, 2019.

[108] D. Ouyang, J. Liu, M. Chen, J. Weng, and J. Wang, "An experimental study on the thermal failure propagation in lithium-ion battery pack," *Journal of The Electrochemical Society,* vol. 165, no. 10, p. A2184, 2018.

[109] H. Sun, H. V. Burton, and H. Huang, "Machine learning applications for building structural design and performance assessment: state-of-the-art review," *Journal of Building Engineering,* vol. 33, p. 101816, 2021.

[110] L. Wang, E. W. Lee, S. A. Hussian, A. C. Y. Yuen, and W. Feng, "Quantitative impact analysis of driving factors on annual residential building energy end-use combining machine learning and stochastic methods," *Applied Energy,* vol. 299, p. 117303, 2021.

[111] M. Meuwly, "Machine learning for chemical reactions," *Chemical Reviews,* vol. 121, no. 16, pp. 10218-10239, 2021.

[112] A. Dogan and D. Birant, "Machine learning and data mining in manufacturing," *Expert Systems with Applications,* vol. 166, p. 114060, 2021.

[113] L. Benos, A. C. Tagarakis, G. Dolias, R. Berruto, D. Kateris, and D. Bochtis, "Machine learning in agriculture: A comprehensive updated review," *Sensors,* vol. 21, no. 11, p. 3758, 2021.

[114] X. A. Wang, J. Tang, and M. Whitty, "DeepPhenology: Estimation of apple flower phenology distributions based on deep learning," *Computers and Electronics in Agriculture,* vol. 185, p. 106123, 2021.

[115] T. M. Mitchell, "Does machine learning really work?," *AI magazine,* vol. 18, no. 3, pp. 11-11, 1997.

[116] G. L. Hart, T. Mueller, C. Toher, and S. Curtarolo, "Machine learning for alloys," *Nature Reviews Materials,* vol. 6, no. 8, pp. 730-755, 2021.

[117] B. Mahesh, "Machine learning algorithms-a review," *International Journal of Science and Research (IJSR).[Internet],* vol. 9, pp. 381-386, 2020.

[118] M. Bertolini, D. Mezzogori, M. Neroni, and F. Zammori, "Machine Learning for industrial applications: A comprehensive literature review," *Expert Systems with Applications,* vol. 175, p. 114820, 2021.

[119] I. H. Sarker, "Machine learning: Algorithms, real-world applications and research directions," *SN Computer Science,* vol. 2, no. 3, pp. 1-21, 2021.

[120] Y.-c. Wu and J.-w. Feng, "Development and application of artificial neural network," *Wireless Personal Communications,* vol. 102, no. 2, pp. 1645-1656, 2018.

[121] F. Zhang and L. J. O'Donnell, "Support vector regression," in *Machine Learning*: Elsevier, 2020, pp. 123-140.

[122] Q. Quan, Z. Hao, H. Xifeng, and L. Jingchun, "Research on water temperature prediction based on improved support vector regression," *Neural Computing and Applications,* pp. 1-10, 2020.

[123] A. J. Smola and B. Schölkopf, "A tutorial on support vector regression," *Statistics and computing,* vol. 14, no. 3, pp. 199-222, 2004.

[124] A. Oppermann. "Artificial Intelligence vs. Machine Learning vs. Deep Learning." https://builtin.com/artificial-intelligence/ai-vs-machine-learning (accessed 10/06, 2022).

[125] G. Van Houdt, C. Mosquera, and G. Nápoles, "A review on the long short-term memory model," *Artificial Intelligence Review,* vol. 53, no. 8, pp. 5929-5955, 2020.

[126] G. O. Sahinoglu, M. Pajovic, Z. Sahinoglu, Y. Wang, P. V. Orlik, and T. Wada, "Battery state-of-charge estimation based on regular/recurrent Gaussian process regression," *IEEE Transactions on Industrial Electronics,* vol. 65, no. 5, pp. 4311-4321, 2017.

[127] Y. Wang, R. Xu, C. Zhou, X. Kang, and Z. Chen, "Digital twin and cloud-side-end collaboration for intelligent battery management system," *Journal of Manufacturing Systems,* vol. 62, pp. 124-134, 2022.

[128] W. Li, M. Rentemeister, J. Badeda, D. Jöst, D. Schulte, and D. U. Sauer, "Digital twin for battery systems: Cloud battery management system with online state-of-charge and state-of-health estimation," *Journal of energy storage,* vol. 30, p. 101557, 2020.

[129] W. Wang, J. Wang, J. Tian, J. Lu, and R. Xiong, "Application of digital twin in smart battery management systems," *Chinese Journal of Mechanical Engineering,* vol. 34, no. 1, pp. 1-19, 2021.

[130] P. K. Koorata and N. Chandrasekaran, "Numerical investigation of cooling performance of a novel air-cooled thermal management system for cylindrical Li-ion battery module," *Applied Thermal Engineering,* vol. 193, p. 116961, 2021.

[131] A. Li, A. C. Y. Yuen, W. Wang, J. Weng, and G. H. Yeoh, "Numerical investigation on the thermal management of lithium-ion battery system and cooling effect optimization," *Applied Thermal Engineering,* p. 118966, 2022.

[132] H. Behi, M. Behi, D. Karimi, J. Jaguemont, M. Ghanbarpour, M. Behnia, M. Berecibar, and J. Van Mierlo, "Heat pipe air-cooled thermal management system for lithium-ion batteries: High power applications," *Applied Thermal Engineering,* vol. 183, p. 116240, 2021.

[133] P. Ping, Y. Zhang, D. Kong, and J. Du, "Investigation on battery thermal management system combining phase changed material and liquid cooling considering non-uniform heat generation of battery," *Journal of Energy Storage,* vol. 36, p. 102448, 2021.

[134] Z. Liu, X. Liu, H. Meng, L. Guo, and Z. Zhang, "Numerical analysis of the thermal performance of a liquid cooling battery module based on the gradient ratio flow velocity and gradient increment tube diameter," *International Journal of Heat and Mass Transfer,* vol. 175, p. 121338, 2021.

[135] J. Cao, M. Luo, X. Fang, Z. Ling, and Z. Zhang, "Liquid cooling with phase change materials for cylindrical Li-ion batteries: an experimental and numerical study," *Energy,* vol. 191, p. 116565, 2020.

[136] J. Weng, C. Xiao, X. Yang, D. Ouyang, M. Chen, G. Zhang, E. L. Waiming, R. K. K. Yuen, and J. Wang, "An energy-saving battery thermal management strategy coupling tubular phase-change-material with dynamic liquid cooling under different ambient temperatures," *Renewable Energy,* vol. 195, pp. 918-930, 2022.

[137] K. Liu, K. Li, Q. Peng, Y. Guo, and L. Zhang, "Data-driven hybrid internal temperature estimation approach for battery thermal management," *Complexity,* vol. 2018, 2018.

[138] L. Shui, F. Chen, A. Garg, X. Peng, N. Bao, and J. Zhang, "Design optimization of battery pack enclosure for electric vehicle," *Structural and Multidisciplinary Optimization,* vol. 58, no. 1, pp. 331-347, 2018.

[139] A. Li, A. C. Y. Yuen, W. Wang, T. B. Y. Chen, C. S. Lai, W. Yang, W. Wu, Q. N. Chan, S. Kook, and G. H. Yeoh, "Integration of Computational Fluid Dynamics and Artificial Neural Network for Optimization Design of Battery Thermal Management System," *Batteries,* vol. 8, no. 7, p. 69, 2022.

[140] M. K. Tran, S. Panchal, V. Chauhan, N. Brahmbhatt, A. Mevawalla, R. Fraser, and

M. Fowler, "Python-based scikit-learn machine learning models for thermal and electrical performance prediction of high-capacity lithium-ion battery," *International Journal of Energy Research,* vol. 46, no. 2, pp. 786-794, 2022.

[141] J. Kleiner, M. Stuckenberger, L. Komsiyska, and C. Endisch, "Advanced Monitoring and Prediction of the Thermal State of Intelligent Battery Cells in Electric Vehicles by Physics-Based and Data-Driven Modeling," *Batteries,* vol. 7, no. 2, p. 31, 2021.

[142] A. Afzal, J. K. Bhutto, A. Alrobaian, A. Razak Kaladgi, and S. A. Khan, "Modelling and Computational Experiment to Obtain Optimized Neural Network for Battery Thermal Management Data," *Energies,* vol. 14, no. 21, p. 7370, 2021.

[143] J. Kleiner, M. Stuckenberger, L. Komsiyska, and C. Endisch, "Real-time core temperature prediction of prismatic automotive lithium-ion battery cells based on artificial neural networks," *Journal of Energy Storage,* vol. 39, p. 102588, 2021.

[144] S. Arora, W. Shen, and A. Kapoor, "Neural network based computational model for estimation of heat generation in LiFePO4 pouch cells of different nominal capacities," *Computers & Chemical Engineering,* vol. 101, pp. 81-94, 2017.

[145] F. Kolodziejczyk, B. Mortazavi, T. Rabczuk, and X. Zhuang, "Machine learning assisted multiscale modeling of composite phase change materials for Li-ion batteries' thermal management," *International Journal of Heat and Mass Transfer,* vol. 172, p. 121199, 2021.

[146] M. Y. Wang, W. F. Hu, Y. F. Jiang, F. Su, and Z. Fang, "Internal temperature prediction of ternary polymer lithium-ion battery pack based on CNN and virtual thermal sensor technology," *International Journal of Energy Research,* vol. 45, no. 9, pp. 13681-13691, Jul 2021.

[147] S. Zhu, C. He, N. Zhao, and J. Sha, "Data-driven analysis on thermal effects and temperature changes of lithium-ion battery," *Journal of Power Sources,* vol. 482, p. 228983, 2021.

[148] G. Huang, P. Zhao, and G. Zhang, "Real-Time Battery Thermal Management for Electric Vehicles Based on Deep Reinforcement Learning," *IEEE Internet of Things Journal,* vol. 9, no. 15, pp. 14060-14072, 2022.

[149] X. Lin, X. Zhang, L. Liu, and M. Yang, "Optimization investigation on air phase change material based battery thermal management system," *Energy Technology,* vol. 9, no. 7, p. 2100060, 2021.

[150] I. Mokashi, A. Afzal, S. A. Khan, N. A. Abdullah, M. H. B. Azami, R. Jilte, and O. D. Samuel, "Nusselt number analysis from a battery pack cooled by different fluids and multiple back-propagation modelling using feed-forward networks,"

International Journal of Thermal Sciences, vol. 161, p. 106738, 2021.

[151] Z. Xu, J. Xu, Z. Guo, H. Wang, Z. Sun, and X. Mei, "Design and Optimization of a Novel Microchannel Battery Thermal Management System Based on Digital Twin," *Energies,* vol. 15, no. 4, p. 1421, 2022.

[152] V. Talele, P. Thorat, Y. P. Gokhale, and V. Mathew, "Phase change material based passive battery thermal management system to predict delay effect," *Journal of Energy Storage,* vol. 44, p. 103482, 2021.

[153] S. Su, W. Li, Y. Li, A. Garg, L. Gao, and Q. Zhou, "Multi-objective design optimization of battery thermal management system for electric vehicles," *Applied Thermal Engineering,* vol. 196, p. 117235, 2021.

[154] Y. Shi, S. Ahmad, H. Liu, K. T. Lau, and J. Zhao, "Optimization of air-cooling technology for LiFePO4 battery pack based on deep learning," *Journal of Power Sources,* vol. 497, p. 229894, 2021.

[155] X. Tang, Q. Guo, M. Li, C. Wei, Z. Pan, and Y. Wang, "Performance analysis on liquid-cooled battery thermal management for electric vehicles based on machine learning," *Journal of Power Sources,* vol. 494, p. 229727, 2021.

[156] S. Chen, N. Bao, A. Garg, X. Peng, and L. Gao, "A fast charging–cooling coupled scheduling method for a liquid cooling-based thermal management system for lithium-ion batteries," *Engineering,* vol. 7, no. 8, pp. 1165-1176, 2021.

[157] J. Park and Y. Kim, "Supervised-learning-based optimal thermal management in an electric vehicle," *IEEE Access,* vol. 8, pp. 1290-1302, 2019.

[158] A. Nazari, S. Kavian, and A. Nazari, "Lithium-Ion Batteries' Energy Efficiency Prediction Using Physics-Based and State-of-the-Art Artificial Neural Network-Based Models," *Journal of Energy Resources Technology,* vol. 142, no. 10, 2020.

[159] A. A. Hussein and A. A. Chehade, "Robust artificial neural network-based models for accurate surface temperature estimation of batteries," *IEEE Transactions on Industry Applications,* vol. 56, no. 5, pp. 5269-5278, 2020.

[160] E. Bulut, E. İ. Albak, G. Sevilgen, and F. Öztürk, "Prediction and optimization of the design decisions of liquid cooling systems of battery modules using artificial neural networks," *International Journal of Energy Research,* vol. 46, no. 6, pp. 7293-7308, 2022.

[161] Q.-K. Wang, Y.-J. He, J.-N. Shen, Z.-F. Ma, and G.-B. Zhong, "A unified modeling framework for lithium-ion batteries: An artificial neural network based thermal coupled equivalent circuit model approach," *Energy,* vol. 138, pp. 118-132, 2017.

[162] S. Aphale, J. Tope, N. Gharte, S. Lulla, A. Sahasrabuddhe, and J. Shah, "A neural

network approach towards development of computational model for performance estimation of commercial lithium ion batteries," in *2018 2nd Borneo International Conference on Applied Mathematics and Engineering (BICAME)*, 2018: IEEE, pp. 7-11.

[163] M. Aykol, P. Herring, and A. Anapolsky, "Machine learning for continuous innovation in battery technologies," *Nature Reviews Materials,* vol. 5, no. 10, pp. 725-727, 2020.

[164] P. Sun, R. Bisschop, H. Niu, and X. Huang, "A review of battery fires in electric vehicles," *Fire technology,* vol. 56, no. 4, pp. 1361-1410, 2020.

[165] P. Victor Chombo, Y. Laoonual, and S. Wongwises, "Lessons from the electric vehicle crashworthiness leading to battery fire," *Energies,* vol. 14, no. 16, p. 4802, 2021.

[166] M. Ghiji, V. Novozhilov, K. Moinuddin, P. Joseph, I. Burch, B. Suendermann, and G. Gamble, "A review of lithium-ion battery fire suppression," *Energies,* vol. 13, no. 19, p. 5117, 2020.

[167] Z. Khan, Z. Khan, and A. Ghafoor, "A review of performance enhancement of PCM based latent heat storage system within the context of materials, thermal stability and compatibility," *Energy conversion and management,* vol. 115, pp. 132-158, 2016.

[168] B. E. Jebasingh and A. V. Arasu, "A detailed review on heat transfer rate, supercooling, thermal stability and reliability of nanoparticle dispersed organic phase change material for low-temperature applications," *Materials Today Energy,* vol. 16, p. 100408, 2020.

[169] J. Luo, D. Zou, Y. Wang, S. Wang, and L. Huang, "Battery thermal management systems (BTMs) based on phase change material (PCM): A comprehensive review," *Chemical Engineering Journal,* vol. 430, p. 132741, 2022.

[170] D. H. Doughty and E. P. Roth, "A general discussion of Li ion battery safety," *The Electrochemical Society Interface,* vol. 21, no. 2, p. 37, 2012.

[171] J. Weng, C. Xiao, D. Ouyang, X. Yang, M. Chen, G. Zhang, R. K. K. Yuen, and J. Wang, "Mitigation effects on thermal runaway propagation of structure-enhanced phase change material modules with flame retardant additives," *Energy,* vol. 239, p. 122087, 2022.

[172] V. Ruiz, A. Pfrang, A. Kriston, N. Omar, P. Van den Bossche, and L. Boon-Brett, "A review of international abuse testing standards and regulations for lithium ion batteries in electric and hybrid electric vehicles," *Renewable and Sustainable Energy Reviews,* vol. 81, pp. 1427-1452, 2018.

[173] D. Ouyang, M. Chen, Q. Huang, J. Weng, Z. Wang, and J. Wang, "A review on the thermal hazards of the lithium-ion battery and the corresponding countermeasures," *Applied Sciences,* vol. 9, no. 12, p. 2483, 2019.

[174] N. N. Semenov, *Some Problems in Chemical Kinetics and Reactivity, Volume 2*. Princeton University Press, 2017.

[175] A. Kriston, A. Podias, I. Adanouj, and A. Pfrang, "Analysis of the effect of thermal runaway initiation conditions on the severity of thermal runaway—Numerical simulation and machine learning study," *Journal of the Electrochemical Society,* vol. 167, no. 9, p. 090555, 2020.

[176] W. Li, J. Zhu, Y. Xia, M. B. Gorji, and T. Wierzbicki, "Data-driven safety envelope of lithium-ion batteries for electric vehicles," *Joule,* vol. 3, no. 11, pp. 2703-2715, 2019.

[177] M. Seo, T. Goh, M. Park, and S. W. Kim, "Detection of Internal Short Circuit for Lithium-ion Battery Using Convolutional Neural Networks with Data Pre-processing," 2019.

[178] L. Petrich, D. Westhoff, J. Feinauer, D. P. Finegan, S. R. Daemi, P. R. Shearing, and V. Schmidt, "Crack detection in lithium-ion cells using machine learning," *Computational Materials Science,* vol. 136, pp. 297-305, 2017.

[179] D. P. Finegan, J. Zhu, X. Feng, M. Keyser, M. Ulmefors, W. Li, M. Z. Bazant, and S. J. Cooper, "The application of data-driven methods and physics-based learning for improving battery safety," *Joule,* vol. 5, no. 2, pp. 316-329, 2021.

[180] S. Lee, S. Han, K. H. Han, Y. Kim, S. Agarwal, K. S. Hariharan, B. Oh, and J. Yoon, "Diagnosing various failures of lithium-ion batteries using artificial neural network enhanced by likelihood mapping," *Journal of Energy Storage,* vol. 40, p. 102768, 2021.

[181] S. Ding, C. Dong, T. Zhao, L. Koh, X. Bai, and J. Luo, "A meta-learning based multimodal neural network for multistep ahead battery thermal runaway forecasting," *IEEE Transactions on Industrial Informatics,* vol. 17, no. 7, pp. 4503-4511, 2020.

[182] R. Yang, R. Xiong, W. Shen, and X. Lin, "Extreme learning machine-based thermal model for lithium-ion batteries of electric vehicles under external short circuit," *Engineering,* vol. 7, no. 3, pp. 395-405, 2021.

[183] O. Ojo, H. Lang, Y. Kim, X. Hu, B. Mu, and X. Lin, "A neural network based method for thermal fault detection in lithium-ion batteries," *IEEE Transactions on Industrial Electronics,* vol. 68, no. 5, pp. 4068-4078, 2020.

[184] D. Li, P. Liu, Z. Zhang, L. Zhang, J. Deng, Z. Wang, D. G. Dorrell, W. Li, and D. U. Sauer, "Battery Thermal Runaway Fault Prognosis in Electric Vehicles Based on Abnormal Heat Generation and Deep Learning Algorithms," *IEEE Transactions on Power Electronics,* 2022.

[185] A. Garg, J. Mou, S. Su, and L. Gao, "Reconfigurable battery systems: Challenges and safety solutions using intelligent system framework based on digital twins," *IET Collaborative Intelligent Manufacturing,* 2022.

[186] X. Feng, D. Ren, X. He, and M. Ouyang, "Mitigating thermal runaway of lithium-ion batteries," *Joule,* vol. 4, no. 4, pp. 743-770, 2020.

[187] S. Eskandari, M. Amiri, N. Sãdhasivam, and H. R. Pourghasemi, "Comparison of new individual and hybrid machine learning algorithms for modeling and mapping fire hazard: a supplementary analysis of fire hazard in different counties of Golestan Province in Iran," *Natural Hazards,* vol. 104, no. 1, pp. 305-327, 2020.

[188] C. Worrell, L. Luangkesorn, J. Haight, and T. Congedo, "Machine learning of fire hazard model simulations for use in probabilistic safety assessments at nuclear power plants," *Reliability Engineering & System Safety,* vol. 183, pp. 128-142, 2019.

[189] L. Surya, "Risk Analysis Model That Uses Machine Learning to Predict the Likelihood of a Fire Occurring at A Given Property," *International Journal of Creative Research Thoughts (IJCRT), ISSN,* pp. 2320-2882, 2017.

[190] T. Yamanaka, Y. Takagishi, and T. Yamaue, "A framework for optimal safety Li-ion batteries design using physics-based models and machine learning approaches," *Journal of The Electrochemical Society,* vol. 167, no. 10, p. 100516, 2020.

[191] A. R. Sharma, C. S. Sai, A. Kumar, R. V. J. Reddy, D. Danyharsha, and R. Jilte, "Three-dimensional CFD study on heat dissipation in cylindrical lithium-ion battery module," *Materials Today: Proceedings,* vol. 46, pp. 10964-10968, 2021.

[192] W. Li, A. Garg, N. Wang, L. Gao, M. L. Le Phung, and V. M. Tran, "Computational Fluid Dynamics-Based Numerical Analysis for Studying the Effect of Mini-Channel Cooling Plate, Flow Characteristics, and Battery Arrangement for Cylindrical Lithium-Ion Battery Pack," *Journal of Electrochemical Energy Conversion and Storage,* vol. 19, no. 4, p. 041003, 2022.

[193] F. R. Menter, "Performance of popular turbulence model for attached and separated adverse pressure gradient flows," *AIAA journal,* vol. 30, no. 8, pp. 2066-2072, 1992.

[194] F. Menter, "Zonal two equation kw turbulence models for aerodynamic flows,"

in *23rd fluid dynamics, plasmadynamics, and lasers conference*, 1993, p. 2906.

[195] F. R. Menter, "Two-equation eddy-viscosity turbulence models for engineering applications," *AIAA journal,* vol. 32, no. 8, pp. 1598-1605, 1994.

[196] M. Guo, G. Sikha, and R. E. White, "Single-particle model for a lithium-ion cell: Thermal behavior," *Journal of The Electrochemical Society,* vol. 158, no. 2, p. A122, 2010.

[197] S. Megahed and B. Scrosati, "Lithium-ion rechargeable batteries," *Journal of Power Sources,* vol. 51, no. 1-2, pp. 79-104, 1994.

[198] H. Ekström, B. Fridholm, and G. Lindbergh, "Comparison of lumped diffusion models for voltage prediction of a lithium-ion battery cell during dynamic loads," *Journal of Power Sources,* vol. 402, pp. 296-300, 2018.

[199] W. Waag, C. Fleischer, and D. U. Sauer, "Adaptive on-line prediction of the available power of lithium-ion batteries," *Journal of Power Sources,* vol. 242, pp. 548-559, 2013.

[200] S. Wang, M. Verbrugge, J. S. Wang, and P. Liu, "Power prediction from a battery state estimator that incorporates diffusion resistance," *Journal of Power Sources,* vol. 214, pp. 399-406, 2012.

[201] P. M. Gomadam, R. E. White, and J. W. Weidner, "Modeling heat conduction in spiral geometries," *Journal of the Electrochemical Society,* vol. 150, no. 10, p. A1339, 2003.

[202] G. Xu, Y. Zhang, S. Lou, J. Gu, and X. Huang, "Prediction and prevention of over-temperature risk of Li-ion power batteries based on the critical heat transfer coefficient and intervention time," *Applied Thermal Engineering,* p. 118100, 2022.

[203] A. Yuen, G. H. Yeoh, S. C. Cheung, Q. Chan, T. B. Y. Chen, W. Yang, and H. Lu, "Numerical study of the development and angular speed of a small-scale fire whirl," *Journal of computational science,* vol. 27, pp. 21-34, 2018.

[204] A. C. Y. Yuen and G. H. Yeoh, "Numerical simulation of an enclosure fire in a large test hall," *Computational Thermal Sciences: An International Journal,* vol. 5, no. 6, 2013.

[205] S.-C. Chen, Y.-Y. Wang, and C.-C. Wan, "Thermal analysis of spirally wound lithium batteries," *Journal of the Electrochemical Society,* vol. 153, no. 4, p. A637, 2006.

[206] P. D. Wasserman, *Neural computing: theory and practice*. Van Nostrand Reinhold Co., 1989.

[207] S. I. Gallant and S. I. Gallant, *Neural network learning and expert systems*. MIT press, 1993.

[208] B. Raheli, M. T. Aalami, A. El-Shafie, M. A. Ghorbani, and R. C. Deo, "Uncertainty assessment of the multilayer perceptron (MLP) neural network model with implementation of the novel hybrid MLP-FFA method for prediction of biochemical oxygen demand and dissolved oxygen: a case study of Langat River," *Environmental Earth Sciences,* vol. 76, no. 14, pp. 1-16, 2017.

[209] M. Chen, U. Challita, W. Saad, C. Yin, and M. Debbah, "Artificial neural networks-based machine learning for wireless networks: A tutorial," *IEEE Communications Surveys & Tutorials,* vol. 21, no. 4, pp. 3039-3071, 2019.

[210] K. G. Sheela and S. N. Deepa, "Review on methods to fix number of hidden neurons in neural networks," *Mathematical Problems in Engineering,* vol. 2013, 2013.

[211] D. Hunter, H. Yu, M. S. Pukish III, J. Kolbusz, and B. M. Wilamowski, "Selection of proper neural network sizes and architectures-A comparative study," *IEEE Transactions on Industrial Informatics,* vol. 8, no. 2, pp. 228-240, 2012.

[212] M. T. Hagan, H. B. Demuth, and M. Beale, *Neural network design*. PWS Publishing Co., 1997.

[213] Y. Chen, Y. Kang, Y. Zhao, L. Wang, J. Liu, Y. Li, Z. Liang, X. He, X. Li, and N. Tavajohi, "A review of lithium-ion battery safety concerns: The issues, strategies, and testing standards," *Journal of Energy Chemistry,* vol. 59, pp. 83-99, 2021.

[214] M. Chen, O. Dongxu, J. Liu, and J. Wang, "Investigation on thermal and fire propagation behaviors of multiple lithium-ion batteries within the package," *Applied Thermal Engineering,* vol. 157, p. 113750, 2019.

[215] Q. Wang, P. Ping, X. Zhao, G. Chu, J. Sun, and C. Chen, "Thermal runaway caused fire and explosion of lithium ion battery," *Journal of power sources,* vol. 208, pp. 210-224, 2012.

[216] A. H. Akinlabi and D. Solyali, "Configuration, design, and optimization of air-cooled battery thermal management system for electric vehicles: A review," *Renewable and Sustainable Energy Reviews,* vol. 125, p. 109815, 2020.

[217] H. Liu, Z. Wei, W. He, and J. Zhao, "Thermal issues about Li-ion batteries and recent progress in battery thermal management systems: A review," *Energy conversion and management,* vol. 150, pp. 304-330, 2017.

[218] W. Tong, K. Somasundaram, E. Birgersson, A. S. Mujumdar, and C. Yap, "Thermo-electrochemical model for forced convection air cooling of a lithium-

ion battery module," *Applied Thermal Engineering,* vol. 99, pp. 672-682, 2016.

[219] T. Yang, N. Yang, X. Zhang, and G. Li, "Investigation of the thermal performance of axial-flow air cooling for the lithium-ion battery pack," *International Journal of Thermal Sciences,* vol. 108, pp. 132-144, 2016.

[220] L. H. Saw, Y. Ye, A. A. Tay, W. T. Chong, S. H. Kuan, and M. C. Yew, "Computational fluid dynamic and thermal analysis of Lithium-ion battery pack with air cooling," *Applied energy,* vol. 177, pp. 783-792, 2016.

[221] E. Jiaqiang, M. Yue, J. Chen, H. Zhu, Y. Deng, Y. Zhu, F. Zhang, M. Wen, B. Zhang, and S. Kang, "Effects of the different air cooling strategies on cooling performance of a lithium-ion battery module with baffle," *Applied Thermal Engineering,* vol. 144, pp. 231-241, 2018.

[222] Z. Lu, X. Yu, L. Wei, Y. Qiu, L. Zhang, X. Meng, and L. Jin, "Parametric study of forced air cooling strategy for lithium-ion battery pack with staggered arrangement," *Applied Thermal Engineering,* vol. 136, pp. 28-40, 2018.

[223] W. Li, M. Xiao, X. Peng, A. Garg, and L. Gao, "A surrogate thermal modeling and parametric optimization of battery pack with air cooling for EVs," *Applied Thermal Engineering,* vol. 147, pp. 90-100, 2019.

[224] B. Severino, F. Gana, R. Palma-Behnke, P. A. Estévez, W. R. Calderón-Muñoz, M. E. Orchard, J. Reyes, and M. Cortés, "Multi-objective optimal design of lithium-ion battery packs based on evolutionary algorithms," *Journal of Power Sources,* vol. 267, pp. 288-299, 2014.

[225] G. Offer, Y. Patel, A. Hales, L. B. Diaz, and M. Marzook, "Cool metric for lithium-ion batteries could spur progress," ed: Nature Publishing Group, 2020.

[226] M.-K. Tran, C. Cunanan, S. Panchal, R. Fraser, and M. Fowler, "Investigation of Individual Cells Replacement Concept in Lithium-Ion Battery Packs with Analysis on Economic Feasibility and Pack Design Requirements," *Processes,* vol. 9, no. 12, p. 2263, 2021.

[227] C. Akkaldevi, S. D. Chitta, J. Jaidi, S. Panchal, M. Fowler, and R. Fraser, "Coupled Electrochemical-Thermal Simulations and Validation of Minichannel Cold-Plate Water-Cooled Prismatic 20 Ah LiFePO4 Battery," *Electrochem,* vol. 2, no. 4, pp. 643-663, 2021.

[228] M. Chen, J. Liu, Y. He, R. Yuen, and J. Wang, "Study of the fire hazards of lithium-ion batteries at different pressures," *Applied Thermal Engineering,* vol. 125, pp. 1061-1074, 2017.

[229] Y. Liu, H. Niu, Z. Li, J. Liu, C. Xu, and X. Huang, "Thermal runaway

characteristics and failure criticality of massive ternary Li-ion battery piles in low-pressure storage and transport," *Process Safety and Environmental Protection,* vol. 155, pp. 486-497, 2021.

[230] H. Wang, Z. Du, L. Liu, Z. Zhang, J. Hao, Q. Wang, and S. Wang, "Study on the thermal runaway and its propagation of lithium-ion batteries under low pressure," *Fire technology,* vol. 56, no. 6, pp. 2427-2440, 2020.

[231] X. Qian, D. Xuan, X. Zhao, and Z. Shi, "Heat dissipation optimization of lithium-ion battery pack based on neural networks," *Applied Thermal Engineering,* vol. 162, p. 114289, 2019.

[232] C. F. Lopez, J. A. Jeevarajan, and P. P. Mukherjee, "Experimental analysis of thermal runaway and propagation in lithium-ion battery modules," *Journal of the electrochemical society,* vol. 162, no. 9, p. A1905, 2015.

[233] K. Purohit, S. Srivastava, V. Nookala, V. Joshi, P. Shah, R. Sekhar, S. Panchal, M. Fowler, R. Fraser, and M.-K. Tran, "Soft sensors for state of charge, state of energy and power loss in formula student electric vehicle," *Applied System Innovation,* vol. 4, no. 4, p. 78, 2021.

[234] C. Zhang, J. Jiang, Y. Gao, W. Zhang, Q. Liu, and X. Hu, "Charging optimization in lithium-ion batteries based on temperature rise and charge time," *Applied energy,* vol. 194, pp. 569-577, 2017.

[235] G. Dong and J. Wei, "Determination of the load capability for a lithium-ion battery pack using two time-scale filtering," *Journal of Power Sources,* vol. 480, p. 229056, 2020.

[236] Q. Xia, Z. Wang, Y. Ren, D. Yang, B. Sun, Q. Feng, and C. Qian, "Performance reliability analysis and optimization of lithium-ion battery packs based on multiphysics simulation and response surface methodology," *Journal of Power Sources,* vol. 490, p. 229567, 2021.

[237] M. Al-Zareer, I. Dincer, and M. A. Rosen, "Novel thermal management system using boiling cooling for high-powered lithium-ion battery packs for hybrid electric vehicles," *Journal of power sources,* vol. 363, pp. 291-303, 2017.

[238] M. Al-Zareer, I. Dincer, and M. A. Rosen, "Performance assessment of a new hydrogen cooled prismatic battery pack arrangement for hydrogen hybrid electric vehicles," *Energy Conversion and Management,* vol. 173, pp. 303-319, 2018.

[239] K. Kirad and M. Chaudhari, "Design of cell spacing in lithium-ion battery module for improvement in cooling performance of the battery thermal management system," *Journal of Power Sources,* vol. 481, p. 229016, 2021.

[240] M. Shen and Q. Gao, "A review on battery management system from the modeling efforts to its multiapplication and integration," *International Journal of Energy Research,* vol. 43, no. 10, pp. 5042-5075, 2019.

[241] J. Deng, C. Bae, J. Marcicki, A. Masias, and T. Miller, "Safety modelling and testing of lithium-ion batteries in electrified vehicles," *Nature Energy,* vol. 3, no. 4, pp. 261-266, 2018.

[242] I. M. D. C. Cordeiro, H. Liu, A. C. Y. Yuen, T. B. Y. Chen, A. Li, R. F. Cao, and G. H. Yeoh, "Numerical investigation of expandable graphite suppression on metal-based fire," *Heat and Mass Transfer,* pp. 1-17, 2021.

[243] X. Jin, X. Duan, W. Jiang, Y. Wang, Y. Zou, W. Lei, L. Sun, and Z. Ma, "Structural design of a composite board/heat pipe based on the coupled electro-chemical-thermal model in battery thermal management system," *Energy,* vol. 216, p. 119234, 2021.

[244] Z. Wang, W. Fan, and P. Liu, "Simulation of temperature field of lithium battery pack based on computational fluid dynamics," *Energy Procedia,* vol. 105, pp. 3339-3344, 2017.

[245] S. Wilke, B. Schweitzer, S. Khateeb, and S. Al-Hallaj, "Preventing thermal runaway propagation in lithium ion battery packs using a phase change composite material: An experimental study," *Journal of Power Sources,* vol. 340, pp. 51-59, 2017.

[246] Z. An, L. Jia, X. Li, and Y. Ding, "Experimental investigation on lithium-ion battery thermal management based on flow boiling in mini-channel," *Applied Thermal Engineering,* vol. 117, pp. 534-543, 2017.

[247] X. Zhang, Y. Wang, J. Wu, and Z. Chen, "A novel method for lithium-ion battery state of energy and state of power estimation based on multi-time-scale filter," *Applied energy,* vol. 216, pp. 442-451, 2018.

[248] K. Li, J. Yan, H. Chen, and Q. Wang, "Water cooling based strategy for lithium ion battery pack dynamic cycling for thermal management system," *Applied Thermal Engineering,* vol. 132, pp. 575-585, 2018.

[249] R. Zhao, S. Zhang, J. Liu, and J. Gu, "A review of thermal performance improving methods of lithium ion battery: Electrode modification and thermal management system," *Journal of Power Sources,* vol. 299, pp. 557-577, 2015.

[250] J. R. Patel and M. K. Rathod, "Recent developments in the passive and hybrid thermal management techniques of lithium-ion batteries," *Journal of Power Sources,* vol. 480, p. 228820, 2020.

[251] L. Fan, J. Khodadadi, and A. Pesaran, "A parametric study on thermal management of an air-cooled lithium-ion battery module for plug-in hybrid electric vehicles," *Journal of Power Sources,* vol. 238, pp. 301-312, 2013.

[252] T. Wang, K. Tseng, J. Zhao, and Z. Wei, "Thermal investigation of lithium-ion battery module with different cell arrangement structures and forced air-cooling strategies," *Applied energy,* vol. 134, pp. 229-238, 2014.

[253] V. Choudhari, A. Dhoble, and S. Panchal, "Numerical analysis of different fin structures in phase change material module for battery thermal management system and its optimization," *International Journal of Heat and Mass Transfer,* vol. 163, p. 120434, 2020.

[254] S. Chen, X. Peng, N. Bao, and A. Garg, "A comprehensive analysis and optimization process for an integrated liquid cooling plate for a prismatic lithium-ion battery module," *Applied Thermal Engineering,* vol. 156, pp. 324-339, 2019.

[255] T. M. Mitchell, *Machine learning*. 1997.

[256] B. Wu, S. Han, K. G. Shin, and W. Lu, "Application of artificial neural networks in design of lithium-ion batteries," *Journal of Power Sources,* vol. 395, pp. 128-136, 2018.

[257] F. Feng, S. Teng, K. Liu, J. Xie, Y. Xie, B. Liu, and K. Li, "Co-estimation of lithium-ion battery state of charge and state of temperature based on a hybrid electrochemical-thermal-neural-network model," *Journal of Power Sources,* vol. 455, p. 227935, 2020.

[258] E. ToolBox. "Convective Heat Transfer." https://www.engineeringtoolbox.com/convective-heat-transfer-d_430.html (accessed 27/07/2021, 2021).

[259] M. T. Hagan and M. B. Menhaj, "Training feedforward networks with the Marquardt algorithm," *IEEE Trans Neural Netw,* vol. 5, no. 6, pp. 989-93, 1994, doi: 10.1109/72.329697.

[260] K. Levenberg, "A method for the solution of certain non-linear problems in least squares," *Quarterly of applied mathematics,* vol. 2, no. 2, pp. 164-168, 1944.

[261] D. W. Marquardt, "An algorithm for least-squares estimation of nonlinear parameters," *Journal of the society for Industrial and Applied Mathematics,* vol. 11, no. 2, pp. 431-441, 1963.

[262] O. Yetik and T. H. Karakoc, "Estimation of thermal effect of different busbars materials on prismatic Li-ion batteries based on artificial neural networks," *Journal of Energy Storage,* vol. 38, p. 102543, 2021.

[263] A. Li, A. C. Y. Yuen, W. Wang, J. Weng, C. S. Lai, S. Kook, and G. H. Yeoh, "Thermal Propagation Modelling of Abnormal Heat Generation in Various Battery Cell Locations," *Batteries,* vol. 8, no. 11, p. 216, 2022.

[264] L. Kong, C. Li, J. Jiang, and M. G. Pecht, "Li-ion battery fire hazards and safety strategies," *Energies,* vol. 11, no. 9, p. 2191, 2018.

[265] A. C. Y. Yuen, T. B. Y. Chen, A. Li, I. M. De Cachinho Cordeiro, L. Liu, H. Liu, A. L. P. Lo, Q. N. Chan, and G. H. Yeoh, "Evaluating the fire risk associated with cladding panels: An overview of fire incidents, policies, and future perspective in fire standards," *Fire and materials,* vol. 45, no. 5, pp. 663-689, 2021.

[266] S. Arora, "Selection of thermal management system for modular battery packs of electric vehicles: A review of existing and emerging technologies," *Journal of Power Sources,* vol. 400, pp. 621-640, 2018.

[267] N. Yang, X. Zhang, B. Shang, and G. Li, "Unbalanced discharging and aging due to temperature differences among the cells in a lithium-ion battery pack with parallel combination," *Journal of Power Sources,* vol. 306, pp. 733-741, 2016.

[268] W. Yuan, D. Liang, Y. Chu, and Q. Wang, "Aging effect delays overcharge-induced thermal runaway of lithium-ion batteries," *Journal of Loss Prevention in the Process Industries,* vol. 79, p. 104830, 2022.

[269] M. Shahjalal, T. Shams, M. E. Islam, W. Alam, M. Modak, S. B. Hossain, V. Ramadesigan, M. R. Ahmed, H. Ahmed, and A. Iqbal, "A review of thermal management for Li-ion batteries: Prospects, challenges, and issues," *Journal of Energy Storage,* vol. 39, p. 102518, 2021.

[270] V. Goupil, C. Gaya, A. Boisard, and E. Robert, "Effect of the heating rate on the degassing and combustion of cylindrical Li-Ion cells," *Fire Safety Journal,* vol. 133, p. 103648, 2022.

[271] M. Chen, J. Liu, O. Dongxu, S. Cao, Z. Wang, and J. Wang, "A Simplified Analysis to Predict the Fire Hazard of Primary Lithium Battery," *Applied Sciences,* vol. 8, no. 11, p. 2329, 2018.

[272] P. Huang, C. Yao, B. Mao, Q. Wang, J. Sun, and Z. Bai, "The critical characteristics and transition process of lithium-ion battery thermal runaway," *Energy,* vol. 213, p. 119082, 2020.

[273] P. Qin, J. Sun, X. Yang, and Q. Wang, "Battery thermal management system based on the forced-air convection: A review," *ETransportation,* vol. 7, p. 100097, 2021.

[274] X. Li, J. Zhao, J. Yuan, J. Duan, and C. Liang, "Simulation and analysis of air cooling configurations for a lithium-ion battery pack," *Journal of Energy Storage,*

vol. 35, p. 102270, 2021.

[275] Y. Deng, C. Feng, E. Jiaqiang, H. Zhu, J. Chen, M. Wen, and H. Yin, "Effects of different coolants and cooling strategies on the cooling performance of the power lithium ion battery system: A review," *Applied Thermal Engineering,* vol. 142, pp. 10-29, 2018.

[276] Y. Wang, G. Zhang, and X. Yang, "Optimization of liquid cooling technology for cylindrical power battery module," *Applied Thermal Engineering,* vol. 162, p. 114200, 2019.

[277] Y. Yang, W. Li, X. Xu, and G. Tong, "Heat dissipation analysis of different flow path for parallel liquid cooling battery thermal management system," *International Journal of Energy Research,* vol. 44, no. 7, pp. 5165-5176, 2020.

[278] J. Liang, Y. Gan, and Y. Li, "Investigation on the thermal performance of a battery thermal management system using heat pipe under different ambient temperatures," *Energy conversion and management,* vol. 155, pp. 1-9, 2018.

[279] J. Wang, Y. Gan, J. Liang, M. Tan, and Y. Li, "Sensitivity analysis of factors influencing a heat pipe-based thermal management system for a battery module with cylindrical cells," *Applied Thermal Engineering,* vol. 151, pp. 475-485, 2019.

[280] H. Jouhara, N. Serey, N. Khordehgah, R. Bennett, S. Almahmoud, and S. P. Lester, "Investigation, development and experimental analyses of a heat pipe based battery thermal management system," *International Journal of Thermofluids,* vol. 1, p. 100004, 2020.

[281] J. Weng, X. Yang, G. Zhang, D. Ouyang, M. Chen, and J. Wang, "Optimization of the detailed factors in a phase-change-material module for battery thermal management," *International Journal of Heat and Mass Transfer,* vol. 138, pp. 126-134, 2019.

[282] J. Weng, D. Ouyang, X. Yang, M. Chen, G. Zhang, and J. Wang, "Optimization of the internal fin in a phase-change-material module for battery thermal management," *Applied Thermal Engineering,* vol. 167, p. 114698, 2020.

[283] J. Wang, Q. Huang, X. Li, G. Zhang, and C. Wang, "Experimental and numerical simulation investigation on the battery thermal management performance using silicone coupled with phase change material," *Journal of Energy Storage,* vol. 40, p. 102810, 2021.

[284] J. Chen, S. Kang, E. Jiaqiang, Z. Huang, K. Wei, B. Zhang, H. Zhu, Y. Deng, F. Zhang, and G. Liao, "Effects of different phase change material thermal management strategies on the cooling performance of the power lithium ion batteries: A review," *Journal of Power Sources,* vol. 442, p. 227228, 2019.

[285] L. Song, H. Zhang, and C. Yang, "Thermal analysis of conjugated cooling configurations using phase change material and liquid cooling techniques for a battery module," *International Journal of Heat and Mass Transfer,* vol. 133, pp. 827-841, 2019.

[286] J. Li and H. Zhang, "Thermal characteristics of power battery module with composite phase change material and external liquid cooling," *International Journal of Heat and Mass Transfer,* vol. 156, p. 119820, 2020.

[287] K. Chen, J. Hou, M. Song, S. Wang, W. Wu, and Y. Zhang, "Design of battery thermal management system based on phase change material and heat pipe," *Applied Thermal Engineering,* vol. 188, p. 116665, 2021.

[288] E. Immonen and J. Hurri, "Incremental thermo-electric CFD modeling of a high-energy Lithium-Titanate Oxide battery cell in different temperatures: A comparative study," *Applied Thermal Engineering,* vol. 197, p. 117260, 2021.

[289] M. A. P. Estevez, S. Calligaro, O. Bottesi, C. Caligiuri, and M. Renzi, "An electro-thermal model and its electrical parameters estimation procedure in a lithium-ion battery cell," *Energy,* vol. 234, p. 121296, 2021.

[290] T. Mesbahi, R. B. Sugrañes, R. Bakri, and P. Bartholomeüs, "Coupled electro-thermal modeling of lithium-ion batteries for electric vehicle application," *Journal of Energy Storage,* vol. 35, p. 102260, 2021.

[291] X. Cui, S. Chen, M. Xiao, and W. Li, "A computational fluid dynamics coupled multi-objective optimization framework for thermal system design for Li-ion batteries with metal separators," *Journal of Electrochemical Energy Conversion and Storage,* vol. 18, no. 3, 2021.

[292] M. Shiea, A. Querio, A. Buffo, G. Boccardo, and D. Marchisio, "CFD-PBE modelling of continuous Ni-Mn-Co hydroxide co-precipitation for Li-ion batteries," *Chemical Engineering Research and Design,* vol. 177, pp. 461-472, 2022.

[293] A. C. Y. Yuen, I. M. De Cachinho Cordeiro, T. B. Y. Chen, Q. Chen, H. Liu, and G. H. Yeoh, "Multiphase CFD modelling for enclosure fires—A review on past studies and future perspectives," *Experimental and Computational Multiphase Flow,* pp. 1-25, 2021.

[294] M. Falcone, E. Palka Bayard De Volo, A. Hellany, C. Rossi, and B. Pulvirenti, "Lithium-Ion Battery Thermal Management Systems: A Survey and New CFD Results," *Batteries,* vol. 7, no. 4, p. 86, 2021.

[295] P. Jindal, P. Sharma, M. Kundu, S. Singh, D. K. Shukla, V. J. Pawar, Y. Wei, and P. Breedon, "Computational Fluid Dynamics (CFD) analysis of Graphene

Nanoplatelets for the cooling of a multiple tier Li-ion battery pack," *Thermal Science and Engineering Progress,* vol. 31, p. 101282, 2022.

[296] A. Jishnu, A. Garg, S. Shaosen, Y. Su, and B. K. Panigrahi, "A novel procedure combining computational fluid dynamics and evolutionary approach to minimize parasitic power loss in air cooling of Li-ion battery for thermal management system design," *Energy Storage,* vol. 3, no. 1, p. e210, 2021.

[297] H. Behi, D. Karimi, M. Behi, M. Ghanbarpour, J. Jaguemont, M. A. Sokkeh, F. H. Gandoman, M. Berecibar, and J. Van Mierlo, "A new concept of thermal management system in Li-ion battery using air cooling and heat pipe for electric vehicles," *Applied Thermal Engineering,* vol. 174, p. 115280, 2020.

[298] Z. Tang, A. Song, S. Wang, J. Cheng, and C. Tao, "Numerical Analysis of Heat Transfer Mechanism of Thermal Runaway Propagation for Cylindrical Lithium-ion Cells in Battery Module," *Energies,* vol. 13, no. 4, p. 1010, 2020.

[299] Y. Wang, B. Liu, P. Han, C. Hao, S. Li, Z. You, and M. Wang, "Optimization of an air-based thermal management system for lithium-ion battery packs," *Journal of Energy Storage,* vol. 44, p. 103314, 2021.

[300] W. Chen, S. Hou, J. Shi, P. Han, B. Liu, B. Wu, and X. Lin, "Numerical Analysis of Novel Air-Based Li-Ion Battery Thermal Management," *Batteries,* vol. 8, no. 9, p. 128, 2022.

[301] W. Yang, Y. Wang, F. Guo, Y. Bai, and X. Liu, "Optimization study of air-cooled stagger-arranged battery pack with reverse-layered airflow," *Journal of Energy Storage,* vol. 55, p. 105524, 2022.

[302] H. Zhai, H. Li, P. Ping, Z. Huang, and Q. Wang, "An experimental-based Domino prediction model of thermal runaway propagation in 18,650 lithium-ion battery modules," *International Journal of Heat and Mass Transfer,* vol. 181, p. 122024, 2021.